

Summary of the
Bulletin of the
International Seismological Centre

2022

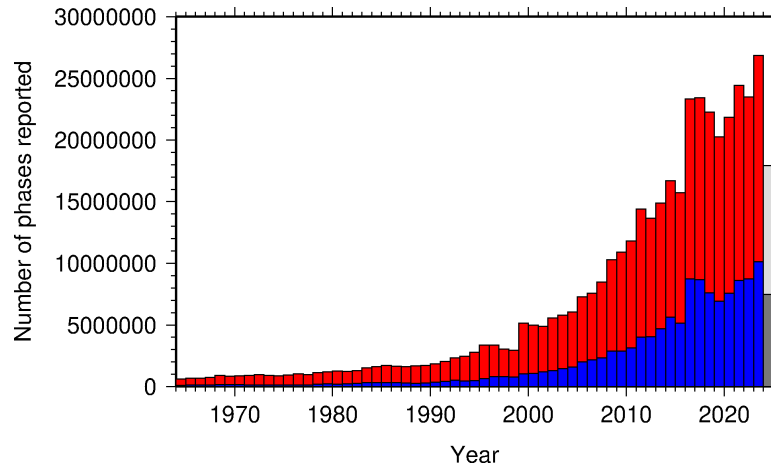
January – June

Volume 59 Issue I

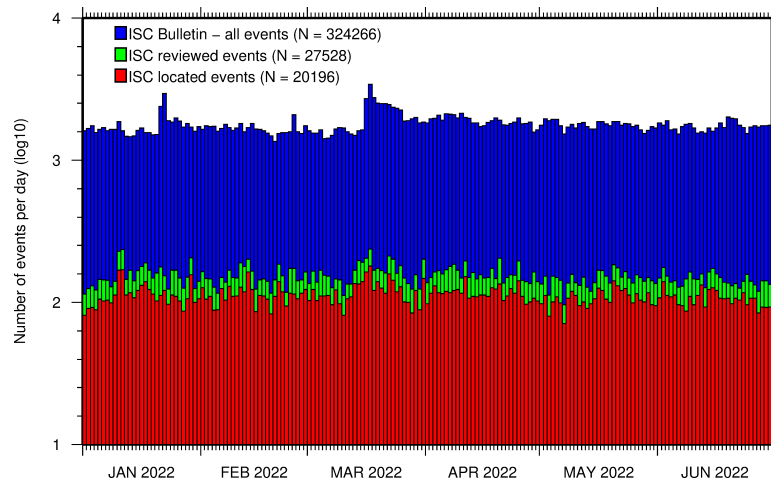
www.isc.ac.uk

ISSN 2309-236X

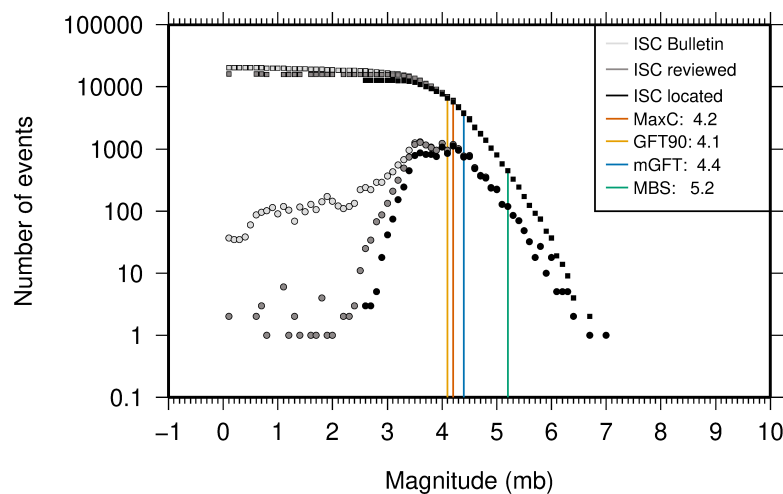
2026



The number of phases (red) and number of amplitudes (blue) collected by the ISC for events each year since 1964. The data in grey covers the current period where data are still being collected before the ISC review takes place and are accurate at the time of publication. See Section 7.3.



The number of events within the Bulletin for the current summary period. The vertical scale is logarithmic. See Section 8.1.



Frequency and cumulative frequency magnitude distribution for all events in the ISC Bulletin, ISC reviewed events and events located by the ISC. The magnitude of completeness (M_C) is shown for the ISC Bulletin. Note: only events with values of m_b are represented in the figure. See Section 8.4.

Summary of the Bulletin of the International Seismological Centre

2022

January - June

Volume 59 Issue I

Produced and edited by:

Kathrin Lieser, James Harris and Dmitry Storchak



Published by
International Seismological Centre

The International Seismological Centre (ISC) is a Charitable Incorporated Organization (CIO) registered with The Charity Commission for England and Wales. Registered charity number: 1188971.

ISC Data Products

<http://www.isc.ac.uk/products/>

ISC Bulletin:

<http://www.isc.ac.uk/iscbulletin/search>

ISC Bulletin and Catalogue monthly files, to the last reviewed month in ISF2 format:

[http://download.isc.ac.uk/isf2/\[bulletin|catalogue\]/yyyy/yyyymm.gz](http://download.isc.ac.uk/isf2/[bulletin|catalogue]/yyyy/yyyymm.gz)

[ftp://www.isc.ac.uk/pub/isf2/\[bulletin|catalogue\]/yyyy/yyyymm.gz](ftp://www.isc.ac.uk/pub/isf2/[bulletin|catalogue]/yyyy/yyyymm.gz)

Datafiles for the ISC data before the rebuild in isf or ffb formats:

[http://download.isc.ac.uk/prerebuild/\[isf|ffb\]/\[bulletin|catalogue\]/yyyy/yyyymm.gz](http://download.isc.ac.uk/prerebuild/[isf|ffb]/[bulletin|catalogue]/yyyy/yyyymm.gz)

[ftp://www.isc.ac.uk/pub/prerebuild/\[isf|ffb\]/\[bulletin|catalogue\]/yyyy/yyyymm.gz](ftp://www.isc.ac.uk/pub/prerebuild/[isf|ffb]/[bulletin|catalogue]/yyyy/yyyymm.gz)

ISC-EHB Bulletin:

<http://www.isc.ac.uk/isc-ehb/search/>

IASPEI Reference Event List (GT bulletin):

<http://www.isc.ac.uk/gtevents/search/>

ISC-GEM Global Instrumental Earthquake Catalogue:

<http://www.isc.ac.uk/iscgem/download.php>

ISC Event Bibliography:

http://www.isc.ac.uk/event_bibliography/bibsearch.php

International Seismograph Station Registry:

<http://www.isc.ac.uk/registries/search/>

Seismological Contacts:

<http://www.isc.ac.uk/projects/seismocontacts/>

Copyright © 2026 by International Seismological Centre

Permission granted to reproduce for personal and educational use only. Commercial copying, hiring, lending is prohibited.

International Seismological Centre

Pipers Lane

Thatcham

RG19 4NS

United Kingdom

www.isc.ac.uk

The International Seismological Centre (ISC) is a Charitable Incorporated Organization (CIO) registered with The Charity Commission for England and Wales. Registered charity number: 1188971.

ISSN 2309-236X

Contents

1	Preface	1
2	The International Seismological Centre	2
2.1	The ISC Mandate	2
2.2	Brief History of the ISC	3
2.3	Former Directors of the ISC and its U.K. Predecessors	5
2.4	Member Institutions of the ISC	6
2.5	Sponsoring Organisations	11
2.6	Data Contributing Agencies	12
2.7	ISC Staff	21
3	Availability of the ISC Bulletin	26
4	Citing the International Seismological Centre	27
4.1	The ISC Bulletin	27
4.2	The Summary of the Bulletin of the ISC	28
4.3	The IASPEI Reference Event List	28
4.4	The ISC-GEM Catalogue	28
4.5	The ISC-EHB Dataset	29
4.6	The ISC Event Bibliography	30
4.7	International Registry of Seismograph Stations	30
4.8	Seismological Dataset Repository	30
5	Operational Procedures of Contributing Agencies	31
5.1	From Analogue to Digital: Evolution of Morocco’s Seismic Network and Its Implications for Seismotectonic Studies	31
5.1.1	Introduction	31
5.1.2	Regional Tectonic Setting	32
5.1.3	Seismotectonic Characteristics	33
5.1.4	Seismic Monitoring	33
5.1.5	Data Processing	37
5.1.6	Data Availability	38
5.1.7	Conclusions	38
6	Summary of Seismicity, January - June 2022	40

7	Statistics of Collected Data	45
7.1	Introduction	45
7.2	Summary of Agency Reports to the ISC	45
7.3	Arrival Observations	50
7.4	Hypocentres Collected	57
7.5	Collection of Network Magnitude Data	59
7.6	Moment Tensor Solutions	65
7.7	Timing of Data Collection	68
8	Overview of the ISC Bulletin	70
8.1	Events	70
8.2	Seismic Phases and Travel-Time Residuals	79
8.3	Seismic Wave Amplitudes and Periods	84
8.4	Completeness of the ISC Bulletin	86
8.5	Magnitude Comparisons	88
9	The Leading Data Contributors	92
9.1	The Largest Data Contributors	92
9.2	Contributors Reporting the Most Valuable Parameters	95
9.3	The Most Consistent and Punctual Contributors	100
10	Appendix	101
10.1	ISC Operational Procedures	101
10.1.1	Introduction	101
10.1.2	Data Collection	101
10.1.3	ISC Automatic Procedures	102
10.1.4	ISC Location Algorithm	106
10.1.5	Review Process	116
10.1.6	Probabilistic Point Source Model (ISC-PPSM)	118
10.1.7	ISC Standard Waveform Download	118
10.1.8	Automatic amplitude and Period Measurements for ISC Magnitudes Estimations	120
10.1.9	The use of Network Code for Arrivals at the ISC and in ISCLoc	123
10.1.10	History of Operational Changes	125
10.2	IASPEI Standards	126
10.2.1	Standard Nomenclature of Seismic Phases	126
10.2.2	Flinn-Engdahl Regions	134
10.2.3	IASPEI Magnitudes	140
10.2.4	The IASPEI Seismic Format (ISF)	144
10.2.5	Ground Truth (GT) Events	146
10.2.6	Nomenclature of Event Types	148

10.3 Tables	149
11 Glossary of ISC Terminology	167
12 Acknowledgements	171
References	172

1

Preface

Dear Colleague,

This is the first 2022 issue of the Summary of the ISC Bulletin, which remains the most fundamental reason for continued operations at the ISC. This issue covers earthquakes and other seismic events that occurred during the period from January to June 2022. Users can search the ISC Bulletin on the ISC website. The monthly Bulletin files are available from the ISC ftp site. For instructions, please see the www.isc.ac.uk/iscbulletin/.

This publication contains information on the ISC, its staff, Members, Sponsors and Data providers. It offers analysis of the data contributed to the ISC by many seismological agencies worldwide as well as analysis of the data in the ISC Bulletin itself. This issue also includes seismological standards and procedures used by the ISC in its operations.

I would like to reiterate here that all ISC hypocenter solutions (1964-present) are now based on the ak135 velocity model and all ISC magnitudes (1964-present) are based on the latest robust procedures.

As part of the series covering the Data Reporters to the ISC, we included an invited article from Morocco's National Centre for Scientific and Technical Research (CNRST) on the history, current status and monitoring procedures.

We hope that you find this publication useful in your work. If your home-institution or company is unable, for one reason or another, to support the long-term international operations of the ISC in full by becoming a Member or a Sponsor, then, please, consider subscribing to this publication by contacting us at admin@isc.ac.uk.

With kind regards to our Data Contributors, Members, Sponsors and users,

Dr Dmitry A. Storchak
Director
International Seismological Centre (ISC)

The ISC is a Charitable Incorporated Organization (CIO) registered with The Charity Commission for England and Wales. Registered charity number: 1188971.

2

The International Seismological Centre

2.1 The ISC Mandate

The International Seismological Centre (ISC) was set up in 1964 with the assistance of UNESCO as a successor to the International Seismological Summary (ISS) to carry forward the pioneering work of Prof. John Milne, Sir Harold Jeffreys and other British scientists in collecting, archiving and processing seismic station and network bulletins and preparing and distributing the definitive summary of world seismicity.

Under the umbrella of the International Association of Seismology and Physics of the Earth Interior (IASPEI/IUGG), the ISC has played an important role in setting international standards such as the International Seismic Bulletin Format (ISF), the IASPEI Standard Seismic Phase List (SSPL) and both the old and New IASPEI Manual of the Seismological Observatory Practice (NMSOP-2) (<https://doi.org/10.2312/GFZ.NMSOP-2>).

The ISC has contributed to scientific research and prominent scientists such as John Hodgson, Eugene Herrin, Hal Thirlaway, Jack Oliver, Anton Hales, Ola Dahlman, Shigeji Suehiro, Nadia Kondorskaya, Vit Karnik, Stephan Müller, David Denham, Bob Engdahl, Adam Dziewonski, John Woodhouse and Guy Masters all considered it an important duty to serve on the ISC Executive Committee and the Governing Council.

The main mission of the ISC is to maintain:

- the ISC **Bulletin** – the longest continuous definitive summary of World seismicity (collaborating with 150 seismic networks and data centres around the world). (www.isc.ac.uk/iscbulletin/)
- the International Seismographic Station Registry (**IR**, jointly with the World Data Center for Seismology, Denver). (www.isc.ac.uk/registries/)
- the IASPEI Reference Event List (Ground Truth, **GT**, jointly with IASPEI). (www.isc.ac.uk/gtevents/)

These are fundamentally important tasks. Bulletin data produced, archived and distributed by the ISC for almost 60 years are the definitive source of such information and are used by thousands of seismologists worldwide for seismic hazard estimation, for tectonic studies and for regional and global imaging of the Earth's structure. Key information in global tomographic imaging is derived from the analysis of ISC data. The ISC Bulletin served as a major source of data for such well known products as the ak135 global 1-D velocity model and the ISC-EHB (*Engdahl et al.*, 2020; 1998; *Weston et al.*, 2018) and Centennial (*Engdahl and Villaseñor*, 2002) catalogues. It presents an important quality-control benchmark for the Comprehensive Nuclear-Test-Ban Treaty Organization (CTBTO). The ISC Bulletin is a cornerstone of

the ISC-GEM Global Instrumental Reference Earthquake Catalogue for Global Earthquake risk Model (GEM).

The ISC Bulletin contains over 12 million seismic events: earthquakes, chemical and nuclear explosions, mine blasts and mining induced events. Over 2 million of them are regional and teleseismically recorded events that have been reviewed by the ISC analysts. The ISC Bulletin contains approximately 450 million individual seismic station readings of arrival times, amplitudes, periods, SNR, slowness and azimuth, reported by approximately 32,000 seismic stations currently registered in the IR. Over 16,000 stations have contributed to the ISC Bulletin in recent years. This number includes the numerous sites of the USArray. The IASPEI GT List currently contains 80,000 events for which latitude, longitude and depth of origin are known with high confidence (to 5 km or better) and seismic signals were recorded at regional and/or teleseismic distances.

2.2 Brief History of the ISC

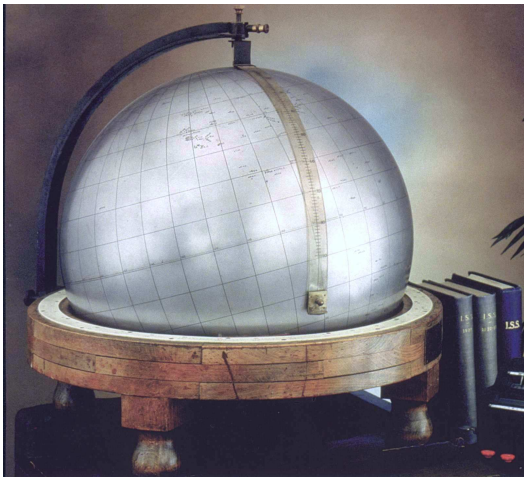


Figure 2.1: *The steel globe bearing positions of early seismic stations was used for locating positions of earthquakes for the International Seismological Summaries.*

(BCIS).

Following Milne's death in 1913, Seismological Bulletins of the BAAS were continued under Prof. H.H. Turner, later based at Oxford University. Upon formal post-war dissolution of the International Association of Seismology in 1922 the newly founded Seismological Section of the International Union of Geodesy and Geophysics (IUGG) set up the International Seismological Summary (ISS) to continue at Oxford under Turner, to produce the definitive global catalogues from the 1918 data-year onwards, under the auspices of IUGG and with the support of the BAAS.

ISS production, led by several professors at Oxford University, and Sir Harold Jeffreys at Cambridge University, continued until it was superseded by the ISC Bulletin, after the ISC was formed in Edinburgh in 1964 with Dr P.L. Willmore as its first director.

During the period 1964 to 1970, with the help of UNESCO and other international scientific bodies, the ISC was reconstituted as an international non-governmental body, funded by interested institutions from various countries. Initially there were supporting members from seven countries, now there are 80, and member institutions include national academies, research foundations, government departments and research institutes, national observatories and universities. Each member, contributing a minimum unit of subscription or more, appoints a representative to the ISC's Governing Council, which meets every two years to decide the ISC's policy and operational programme. Representatives from the International Association of Seismology and Physics of the Earth's Interior also attend these meetings. The Governing Council appoints the Director and a small Executive Committee to oversee the ISC's operations.



Figure 2.2: *ISC building in Thatcham, Berkshire, UK.*

In 1975, the ISC moved to Newbury in southern England to make use of better computing facilities there. The ISC subsequently acquired its own computer and in 1986 moved to its own building at Pipers Lane, Thatcham, near Newbury. The internal layout of the new premises was designed for the ISC and includes not only office space but provision for the storage of extensive stocks of ISS and ISC publications and a library of seismological observatory bulletins, journals and books collected over many tens of years.

In 1997 the first set of the ISC Bulletin CD-ROMs was produced (not counting an earlier effort at USGS). The first ISC website appeared in 1998 and the first ISC database was put in day-to-day operations from 2001. Major developments also included the introduction of bar-codes to assist ISC analysts reviewing the ISC Bulletin as well as the introduction of the automatic email data capture system to modernise the data collection at the ISC.

During the 2004-2007 period, in search of financial efficiency, the ISC moved its operations from UNIX to a Linux operating system, and the ORACLE database gave way to the PostgreSQL database management system.

The new ISC seismic event locator, ISCloc, was developed, tested and put into operation by the end of 2010. A stable version of the locator was routinely applied to seismic events from data year 2011 with the Jeffreys-Bullen travel-time tables giving way to the use of the ak135 1D velocity model. During the 2009-2020 period, the ISC Bulletin Rebuild project involved a major general bulletin clean-up, sourcing and integrating 90 previously unavailable datasets from around the world, and re-computation of all ISC hypocentres and magnitudes for the period 1964-2010 followed by analyst review.

During the 2010s, in addition to its two traditional products (the Bulletin of the ISC and the International Seismograph Station Registry(IR)), the ISC developed a number of new datasets and services that were designed to serve the individual needs of different scientific research communities: the ISC-GEM Global Instrumental Earthquake Catalogue, the IASPEI Ground Truth (GT) reference event dataset, the ISC-EHB dataset, the ISC Event Bibliography, the International Contacts in Seismology, and the CTBTO Link to the ISC database.

In 2014, the ISC took over the maintenance of the website of the International Association of Seismology and Physics of the Earth's Interior (IASPEI).

In 2016, a new Visual Bulletin Analysis System (VBAS) revolutionised the work of the ISC Analysts performing manual analysis of the ISC Bulletin by moving it from a paper-based batch-type to a screen-based interactive system.

In April 2020, the ISC was registered as a **Charitable Incorporated Organization** (CIO) with the Charity Commission for England and Wales. The ISC **Constitution**, compliant with UK charity law, was adopted by the ISC Governing Council in May 2020. The **Bye-laws**, fully compliant with the Constitution, provided further details and clarification of exact rules and procedures applicable in the day-to-day operation of the ISC in pursuit of its mission. The Byelaws were adopted by the Governing Council in June 2021 and amended in July 2025.

The ISC **Data Management Policy**, establishing the dynamic character of the ISC data, approach to versioning, and ways of tracking and preserving changes in the ISC database was adopted in July 2023.

The ISC **Data Collection Policy** was adopted in September 2024. It clarified the priority of the ISC to continue the well-established practice of collecting good quality event parameter data from seismic networks and data centres whilst re-confirming the growing practice of the ISC using openly available digital waveform data to constrain event parameters that are not readily available from reporting agencies.

Further ISC products, developed during the 2020s, include the ISC Seismological Dataset Repository, the ISC Electronic Archive of Printed Station / Network Bulletins, and the ISC Station Services that combined the station location data from both the IR and the International Federation of Digital Seismograph Networks (FDSN).

Since 2011, several scientific articles were published by ISC staff that specified the ways individual ISC products were built and maintained for the scientific community's use. All ISC products have been given a digital object identifier (DOI). Ways of appropriate citing of the ISC data have been recommended on the ISC website.

Throughout 2009-2025 a major internal reconstruction of the ISC building in Thatcham was undertaken to allow for more members of staff working in mainstream ISC operations as well as major development projects.

2.3 Former Directors of the ISC and its U.K. Predecessors



John Milne
Publisher of the Shide Circular Reports on Earthquakes
1900-1912



Herbert Hall Turner
Seismological Bulletins of the BAAS
1913-1917
Director of the ISS
1918-1930



Harry Hemley Plaskett
Director of the ISS
1931-1939



Harold Jeffreys
Director of the ISS
1939-1957



Robert Stoneley
Director of the ISS
1957-1960



P.L. (Pat) Willmore
Director of the ISS
1960-1963
Director of the ISC
1964-1970



Edouard P. Arnold
Director of the ISC
1970-1977



Anthony A. Hughes
Director of the ISC
Sep 1977 - Dec 1997



Raymond J. Willemann
Director of the ISC
1998-2003



Avi Shapira
Director of the ISC
2004-2007

2.4 Member Institutions of the ISC

The ISC Constitution and Bye-laws stipulate that any national academy, agency, scientific institution or other non-profit organisation may become a Member of the ISC on payment to the ISC of a sum equal to at least one unit of subscription and the nomination of a voting representative to serve on the ISC's governing body. Membership shall be effective for one year from the date of receipt at the ISC of the annual contribution of the Member and is thereafter renewable for periods of one year.

The ISC is currently supported by its 81 Member Institutions and Award 2414178 from the US National Science Foundation via the University of Oxford and Grant INT004 from the Royal Society in UK.

Figures 2.3 and 2.4 show major sectors to which the ISC Member Institutions belong and proportional

financial contributions that each of these sectors make towards the ISC’s annual budget.

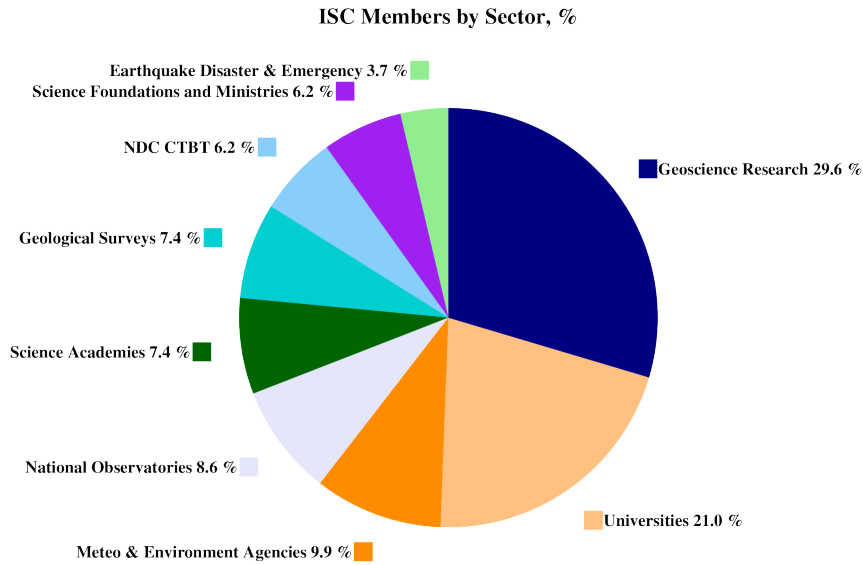


Figure 2.3: Distribution of the ISC Member Institutions by sector during the review of data in this Summary as a percentage of total number of Members.

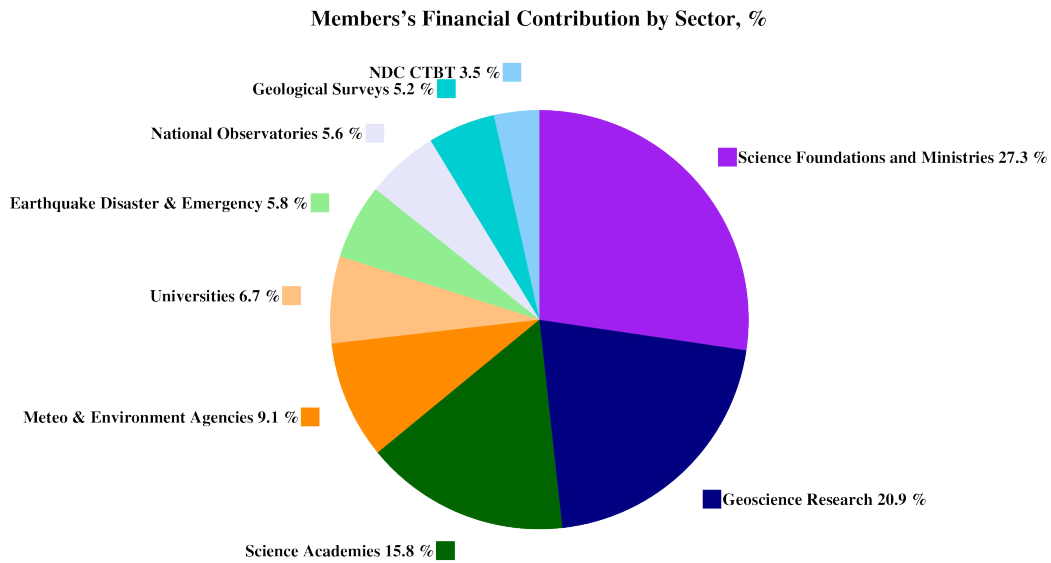


Figure 2.4: Distribution of Member’s financial contributions to the ISC by sector during the review of data in this Summary as a percentage of total annual Member contributions.

There follows a list of all current Member Institutions with a category (1 through 9) assigned according to the ISC Constitution. Each category relates to the number of membership units contributed.



Institute of Geosciences,
Polytechnic University of Tirana
Albania
www.geo.edu.al
Category: 1



Centre de Recherche en Astronomie,
Astrophysique et Géophysique (CRAAG)
Algeria
www.craag.dz
Category: 1



Geoscience Australia
Australia
www.ga.gov.au
Category: 4

 <p>Australian National University earthsciences.anu.edu.au Category: 1</p>	<p>Geophysics, Research School of Earth Sciences, Australian National University Australia earthsciences.anu.edu.au Category: 1</p>	 <p>Federal Ministry of Education, Science and Research www.bmbwf.gv.at Category: 2</p>	<p>Federal Ministry for Education, Science and Research Austria www.bmbwf.gv.at Category: 2</p>	 <p>Centre of Geophysical Monitoring (CGM) of the National Academy of Sciences of Belarus Belarus cgm.by Category: 1</p>	<p>Centre of Geophysical Monitoring (CGM) of the National Academy of Sciences of Belarus Belarus cgm.by Category: 1</p>
 <p>Belgian Science Policy Office (BELSPO) Belgium www.belspo.be Category: 1</p>	<p>Belgian Science Policy Office (BELSPO) Belgium www.belspo.be Category: 1</p>	 <p>Observatório Nacional www.gov.br Category: 1</p>	<p>Observatorio Nacional Brazil www.gov.br Category: 1</p>	 <p>UNIVERSIDADE DE SÃO PAULO</p>	<p>Universidade de São Paulo, Centro de Sismologia Brazil www.sismo.iag.usp.br Category: 1</p>
 <p>UnB</p>	<p>Seismological Observatory, Institute of Geosciences, University of Brasilia Brazil www.obsis.unb.br Category: 1</p>	 <p>NIGGG</p>	<p>National Institute of Geophysics, Geodesy and Geography (NIGGG), Bulgarian Academy of Sciences Bulgaria niggg.bas.bg Category: 1</p>	 <p>CANADA 1842 GEOLOGICAL SURVEY - COMMISSION GÉOLOGIQUE</p>	<p>The Geological Survey of Canada Canada natural-resources.canada.ca Category: 4</p>
 <p>CSN</p>	<p>Centro Sismológico Nacional, Universidad de Chile Chile www.csn.uchile.cl Category: 1</p>	 <p>CHINA EARTHQUAKE ADMINISTRATION</p>	<p>China Earthquake Administration China www.cea.gov.cn Category: 4</p>	 <p>IES 中央研究院 地球科學研究所</p>	<p>Institute of Earth Sciences, Academia Sinica Chinese Taipei www.earth.sinica.edu.tw Category: 1</p>
 <p>GEOLGICAL SURVEY 1950</p>	<p>Geological Survey Department Cyprus www.moa.gov.cy Category: 1</p>	 <p>AKADEMIE VĚD ČESKÉ REPUBLIKY</p>	<p>Institute of Geophysics, Czech Academy of Sciences Czech Republic www.ig.cas.cz Category: 1</p>	 <p>GEUS</p>	<p>Geological Survey of Denmark and Greenland (GEUS) Denmark www.geus.dk Category: 2</p>
 <p>NRIAG</p>	<p>National Research Institute for Astronomy and Geophysics (NRIAG), Cairo Egypt www.nriag.sci.eg Category: 1</p>	 <p>UNIVERSITY OF HELSINKI</p>	<p>The University of Helsinki Finland www.helsinki.fi Category: 2</p>	 <p>GeoAZUR TERRE - Océan - Espace</p>	<p>Géoazur, Université Côte d'Azur France univ-cotedazur.eu Category: 1</p>
 <p>INSU</p>	<p>Institute National des Sciences de l'Univers France www.insu.cnrs.fr Category: 4</p>	 <p>ASNR</p>	<p>Autorité de Sûreté Nucléaire et de Radioprotection (formerly IRSN) France recherche-expertise.asnr.fr Category: 1</p>	 <p>cea</p>	<p>Laboratoire de Détection et de Géophysique/CEA France www-dase.cea.fr Category: 2</p>
 <p>GFZ Helmholtz-Zentrum POTSDAM</p>	<p>GeoForschungsZentrum Potsdam Germany www.gfz.de Category: 2</p>	 <p>BGR</p>	<p>Bundesanstalt für Geowissenschaften und Rohstoffe Germany www.bgr.bund.de Category: 4</p>	 <p>NATIONAL OBSERVATORY OF ATHENS</p>	<p>The Seismological Institute, National Observatory of Athens Greece www.noa.gr Category: 1</p>
 <p>yfi</p>	<p>HUN-REN Institute of Earth Physics and Space Science Hungary epss.hun-ren.hu Category: 1</p>	 <p>Icelandic Met Office</p>	<p>The Icelandic Meteorological Office Iceland www.vedur.is Category: 1</p>	 <p>NATIONAL GEOPHYSICAL RESEARCH INSTITUTE</p>	<p>National Geophysical Research Institute (NGRI), Council of Scientific and Industrial Research (CSIR) India www.ngri.res.in Category: 2</p>



National Centre for
Seismology, Ministry of
Earth Sciences of India
India
www.moes.gov.in
Category: 4



Agency for
Meteorology,
Climatology, and
Geophysics (BMKG)
Indonesia
www.bmkg.go.id
Category: 3



Iraqi Meteorological
Organization and
Seismology
Iraq
meteoseism.gov.iq
Category: 1



Dublin Institute for
Advanced Studies
Ireland
www.dias.ie
Category: 1



Soreq Nuclear Research
Centre (SNRC)
Israel
www.gov.il
Category: 1



Geological Survey of
Israel
Israel
www.gov.il
Category: 1



Istituto Nazionale di
Oceanografia e di
Geofisica Sperimentale
Italy
www.ogs.trieste.it
Category: 1



Istituto Nazionale di
Geofisica e
Vulcanologia
Italy
www.ingv.it
Category: 3



University of the West
Indies at Mona
Jamaica
www.mona.uwi.edu
Category: 1



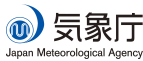
National Institute of
Polar Research (NIPR)
Japan
www.nipr.ac.jp
Category: 1



Japan Agency for
Marine-Earth Science
and Technology
(JAMSTEC)
Japan
www.jamstec.go.jp
Category: 2



Earthquake Research
Institute, University of
Tokyo
Japan
www.eri.u-tokyo.ac.jp
Category: 3



The Japan
Meteorological Agency
(JMA)
Japan
www.jma.go.jp
Category: 5



Centro de Investigación
Científica y de
Educación Superior de
Ensenada (CICESE)
Mexico
www.cicese.edu.mx
Category: 1

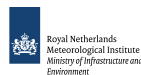


Institute of Geophysics,
National University of
Mexico
Mexico
www.igeofcu.unam.mx
Category: 1



National Centre for
Scientific and Technical
Research (CNRST)
Morocco

Category: 1



The Royal Netherlands
Meteorological
Institute (KNMI)
Netherlands
www.knmi.nl
Category: 2



GNS Science
New Zealand
www.gns.cri.nz
Category: 3



The University of
Bergen
Norway
www.uib.no
Category: 2



Stiftelsen NORSAR
Norway
www.norsar.no
Category: 2



Institute of Geophysics,
Polish Academy of
Sciences
Poland
www.igf.edu.pl
Category: 1



Instituto Português do
Mar e da Atmosfera
Portugal
www.ipma.pt
Category: 2



Red Sísmica de Puerto
Rico
Puerto Rico
redsismica.uprm.edu
Category: 1



Korean Meteorological
Administration
Republic of Korea
www.kma.go.kr
Category: 1



National Institute for
Earth Physics
Romania
www.infp.ro
Category: 1



Russian Academy of
Sciences
Russia
www.ras.ru
Category: 5



Saudi Geological
Survey (SGS)
Saudi Arabia
sgs.gov.sa
Category: 2



Earth Observatory of Singapore (EOS), an autonomous Institute of Nanyang Technological University Singapore
earthobservatory.sg
Category: 1



Environmental Agency of Slovenia
Slovenia
www.arso.gov.si
Category: 1



Council for Geoscience South Africa
www.geoscience.org.za
Category: 2



Instituto Geográfico Nacional Spain
www.ign.es
Category: 3



Institute of Marine Sciences (ICM-CSIC) Spain
www.icm.csic.es
Category: 1



Institut Cartogràfic i Geològic de Catalunya (ICGC) Spain
www.icgc.cat
Category: 1



National Defence Research Establishment (FOI) Sweden
www.foi.se
Category: 1



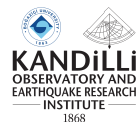
Uppsala Universitet Sweden
www.uu.se
Category: 2



The Swiss Academy of Sciences Switzerland
www.scnat.ch
Category: 2



Disaster and Emergency Management Authority (AFAD) Turkey
www.deprem.gov.tr
Category: 2



Kandilli Observatory and Earthquake Research Institute Turkey
www.koeri.boun.edu.tr
Category: 1



British Geological Survey United Kingdom
www.bgs.ac.uk
Category: 2



AWE Blacknest United Kingdom
www.blacknest.gov.uk
Category: 2



The Royal Society United Kingdom
www.royalsociety.org
Category: 6



Lamont-Doherty Earth Observatory, Columbia Climate School, Columbia University U.S.A.
lamont.columbia.edu
Category: 1



Center for Earthquake Research and Information (CERI), the University of Memphis U.S.A.
www.memphis.edu
Category: 1



Pacific Northwest Seismic Network (PNSN) U.S.A.
www.pnsn.org
Category: 1



Incorporated Research Institutions for Seismology U.S.A.
www.iris.edu
Category: 2



University of Utah Seismograph Stations (UUSS) U.S.A.
quake.utah.edu
Category: 1



The National Science Foundation of the United States. (NSF Award 2414178) U.S.A.
www.nsf.gov
Category: 9



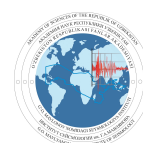
National Earthquake Information Center, U.S. Geological Survey U.S.A.
www.usgs.gov
Category: 1



Alaska Earthquake Center (AEC), University of Alaska Fairbanks U.S.A.
earthquake.alaska.edu
Category: 1



Texas Seismological Network (TexNet), Bureau of Economic Geology, J.A. and K.G. Jackson School of Geosciences, University of Texas at Austin U.S.A.
texnet.beg.utexas.edu
Category: 1



Mavlyanov Institute of Seismology, Academy of Sciences, Republic of Uzbekistan
seismos.uz
Category: 1

In addition the ISC is currently in receipt of grants from the International Data Centre (IDC) of the Preparatory Commission of the Comprehensive Nuclear-Test-Ban Treaty Organization (CTBTO),

Lighthill Risk Network, and USGS.



2.5 Sponsoring Organisations

Article 9.8.1 of the ISC Constitution stipulates that any organisation with an interest in the work of the ISC may at the discretion of the ISC Executive Committee become a Sponsoring Organisation (Sponsor) upon payment of a mutually agreed annual fee. In line with the Article VI of the ISC Bye-laws, the Sponsors are entitled to attend meetings of the ISC Governing Council without a vote.



GeoSIG provides earthquake, seismic, structural, dynamic and static monitoring and measuring solutions. As an ISO Certified company, GeoSIG is a world leader in design and manufacture of a diverse range of high quality, precision instruments for vibration and earthquake monitoring. GeoSIG instruments are at work today in more than 100 countries around the world with well-known projects such as the NetQuakes installation with USGS and Oresund Bridge in Denmark. GeoSIG offers off-the-shelf solutions as well as highly customised solutions to fulfil the challenging requirements in many vertical markets including the following:

- Earthquake Early Warning and Rapid Response (EEWRR)
- Seismic and Earthquake Monitoring and Measuring
- Industrial Facility Seismic Monitoring and Shutdown
- Structural Analysis and Ambient Vibration Testing
- Induced Vibration Monitoring
- Research and Scientific Applications



SARA designs and manufactures seismometers, accelerometers and portable multichannel seismographs for both seismology and applied geophysics. Since 2002 we provided over 5,000 seismic units, 15,000 acceleration transducers and 15,000 geophysical exploration channels, to thousands of professionals and researchers who are using our equipment with success. Providing low-cost instrumentation for developing countries is our main goal. We developed our seismological software SEISMOWIN which provides full support for all international file formats and communication standards like miniSEED, GSE, SeedLink and a number of tools for earthquake location and site assessment. The GEOEXPLORER software suite offers a number of modules for geological surveys.

In 2023 we introduced our new compact broadband seismometer to the market, suitable for surface, posthole and borehole installation, and new versions of our popular SL06 recorder with rack mount housing and ADC with PGA offering 24 or 32 bit streaming.

Visit our web site and download the free tools available at: www.sara.pg.it



Gaiacode is a science based, forward looking, innovative company designing and building the next generation of seismic instrumentation.



MS&AD InterRisk Research & Consulting

MS&AD InterRisk Research & Consulting, Inc. is responsible for the core of risk-related service businesses in the MS&AD group. We provide services which meet various expectations of the clients, including consulting, research and investigation, seminars and publications for risk management in addition to the think-tank functions.

2.6 Data Contributing Agencies

In addition to its Members and Sponsors, the ISC owes its existence and successful long-term operations to its 152 seismic bulletin data contributors. These include government agencies responsible for national

seismic networks, geoscience research institutions, geological surveys, meteorological agencies, universities, national data centres for monitoring the CTBT and individual observatories. There would be no ISC Bulletin available without the regular stream of data that are unselfishly and generously contributed to the ISC on a free basis.



Institute of
Geosciences,
Polytechnic University
of Tirana
Albania
TIR



Centre de Recherche en
Astronomie,
Astrophysique et
Géophysique
Algeria
CRAAG



Instituto Nacional de
Prevención Sísmica
Argentina
SJA



Universidad Nacional
de La Plata
Argentina
LPA



National Survey of
Seismic Protection
Armenia
NSSP



Geoscience Australia
Australia
AUST

Curtin University
Australia
CUPWA



Bundesanstalt für
Geologie, Geophysik,
Klimatologie und
Meteorologie
Austria
VIE



International Data
Centre, CTBTO
Austria
IDC



Republican Seismic
Survey Center of
Azerbaijan National
Academy of Sciences
Azerbaijan
AZER



Royal Observatory of
Belgium
Belgium
UCC



Observatorio San
Calixto
Bolivia
SCB



Republic
Hydrometeorological
Service, Seismological
Observatory, Banja
Luka
Bosnia and
Herzegovina
RHSSO

Botswana Geoscience
Institute
Botswana
BGSI



Instituto Astronomico
e Geofisico
Brazil
VAO



Observatory
Seismological of the
University of Brasilia
Brazil
OSUNB



National Institute of
Geophysics, Geology
and Geography
Bulgaria
SOF



Canadian Hazards
Information Service,
Natural Resources
Canada
Canada
OTT



Centro Sismológico
Nacional, Universidad
de Chile
Chile
GUC



China Earthquake
Networks Center
China
BJI



Institute of Earth
Sciences, Academia
Sinica
Chinese Taipei
ASIES



Central Weather
Bureau (CWB)
Chinese Taipei
TAP



Red Sismológica
Nacional de Colombia
Colombia
RSNC



Sección de Sismología,
Vulcanología y
Exploración Geofísica
Costa Rica
UCR



Seismological Survey of
the Republic of Croatia
Croatia
ZAG



Servicio Sismológico
Nacional Cubano
Cuba
SSNC



Cyprus Geological
Survey Department
Cyprus
NIC



Institute of Geophysics,
Czech Academy of
Sciences
Czech Republic
WBNET



The Institute of
Physics of the Earth
(IPEC)
Czech Republic
IPEC



Institute of Geophysics,
Czech Academy of
Sciences
Czech Republic
PRU



Korea Earthquake
Administration
Democratic People's
Republic of Korea
KEA



Geological Survey of
Denmark and
Greenland
Denmark
DNK



Universidad Autonoma
de Santo Domingo
Dominican Republic
SDD



Observatorio
Sismológico Politécnico
Loyola
Dominican Republic
OSPL



Servicio Nacional de
Sismología y
Vulcanología
Ecuador
IGQ



National Research
Institute of Astronomy
and Geophysics
Egypt
HLW



Servicio Nacional de
Estudios Territoriales
El Salvador
SNET



University of Addis
Ababa
Ethiopia
AAE



Institute of Seismology,
University of Helsinki
Finland
HEL



EOST / RéNaSS
France
STR



Laboratoire de
Détection et de
Géophysique/CEA
France
LDG



Institut de Physique du
Globe de Paris
France
IPGP

Laboratoire de
Géophysique/CEA
French Polynesia
PPT



Institute of Earth
Sciences/ National
Seismic Monitoring
Center
Georgia
TIF



Seismological
Observatory
Berggießhübel, TU
Bergakademie Freiberg
Germany
BRG



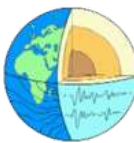
Bundesanstalt für
Geowissenschaften und
Rohstoffe
Germany
BGR



Helmholtz Centre
Potsdam GFZ German
Research Centre For
Geosciences
Germany
GFZ



Alfred Wegener
Institute for Polar and
Marine Research
Germany
AWI



Geophysikalisches
Observatorium Collm
Germany
CLL



National Observatory
of Athens
Greece
ATH



Department of
Geophysics, Aristotle
University of
Thessaloniki
Greece
THE



University of Patras,
Department of Geology
Greece
UPSL



INSIVUMEH
Guatemala
GCG



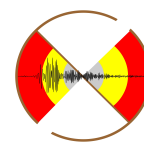
Hong Kong
Observatory
Hong Kong
HKC



HUN-REN Inst of
Earth Physics and
Space Science,
Kövesligethy Radó
Seismo Obs
Hungary
KRSZO



Icelandic
Meteorological Office
Iceland
REY



National Centre for
Seismology of the
Ministry of Earth
Sciences of India
India
NDI



National Geophysical
Research Institute
India
HYB



Badan Meteorologi,
Klimatologi dan
Geofisika
Indonesia
DJA



Tehran University
Iran
TEH



International Institute
of Earthquake
Engineering and
Seismology (IIEES)
Iran
THR



Seismological
Laboratory of
University of Basrah
Iraq
SLUB



Iraqi Meteorological
and Seismology
Organisation
Iraq
ISN



Dublin Institute for
Advanced Studies
Ireland
DIAS



The Geophysical
Institute of Israel
Israel
GII



MedNet Regional
Centroid - Moment
Tensors
Italy
MED_RCMT



Dipartimento per lo
Studio del Territorio e
delle sue Risorse
(RSNI)
Italy
GEN



SARA Electronic
Instrument s.r.l.
Italy
SARA



Istituto Nazionale di
Geofisica e
Vulcanologia
Italy
ROM



Laboratory of Research
on Experimental and
Computational
Seimology
Italy
RISSC



Istituto Nazionale di
Oceanografia e di
Geofisica Sperimentale
(OGS)
Italy
OGS



Jamaica Seismic
Network
Jamaica
JSN



Japan Meteorological
Agency
Japan
JMA



National Research
Institute for Earth
Science and Disaster
Resilience
Japan
NIED



National Institute of
Polar Research
Japan
SYO



Jordan Seismological
Observatory
Jordan
JSO



National Nuclear
Center
Kazakhstan
NNC



Seismological
Experimental
Methodological
Expedition
Kazakhstan
SOME



Institute of Seismology,
Academy of Sciences of
Kyrgyz Republic
Kyrgyzstan
KRNET

Kyrgyz Seismic
Network
Kyrgyzstan
KNET



Latvian Seismic
Network
Latvia
LVSN



National Council for
Scientific Research
Lebanon
GRAL



Geological Survey of
Lithuania
Lithuania
LIT



Macao Meteorological
and Geophysical
Bureau
Macao, China
MCO

Antananarivo
Madagascar
TAN



Geological Survey
Department Malawi
Malawi
GSDM



Instituto de Geofísica
de la UNAM
Mexico
MEX



Centro de Investigación
Científica y de
Educación Superior de
Ensenada
Mexico
ECX



Institute of
Hydrometeorology and
Seismology of
Montenegro
Montenegro
PDG



Centre National de
Recherche
Morocco
CNRM



The Geological Survey
of Namibia
Namibia
NAM



National Seismological
Centre, Nepal
Nepal
DMN



Koninklijk Nederlands
Meteorologisch
Instituut
Netherlands
DBN



Institute of Geological
and Nuclear Sciences
New Zealand
WEL



Central American
Tsunami Advisory
Center
Nicaragua
CATAC



Seismological
Observatory Skopje
North Macedonia
SKO



University of Bergen
Norway
BER



Stiftelsen NORSAR
Norway
NAO



Sultan Qaboos
University
Oman
OMAN



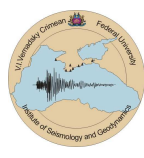
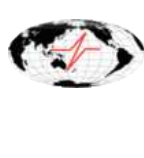
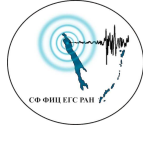
Universidad de Panama
Panama
UPA



Philippine Institute of
Volcanology and
Seismology
Philippines
MAN



Manila Observatory
Philippines
QCP

	Institute of Geophysics, Polish Academy of Sciences Poland WAR		Private Observatory of Pawel Jacek Wiejacz, D.Sc. Poland PJWWP		Instituto Dom Luiz, University of Lisbon Portugal IGIL
	Sistema de Vigilância Sismológica dos Açores Portugal SVSA		Instituto Português do Mar e da Atmosfera, I.P. Portugal INMG		Centre of Geophysical Monitoring of the National Academy of Sciences of Belarus Republic of Belarus BELR
	Inst. of Seismology and Geodynamics, V.I. Vernadsky Crimean Federal University Republic of Crimea CFUSG		Korea Meteorological Administration Republic of Korea KMA		National Institute for Earth Physics Romania BUC
	Federal Center for Integrated Arctic Research Russia FCIAR		Yakutiya Regional Seismological Center, GS SB RAS Russia YARS		Altay-Sayan Branch, Geophysical Survey, Russian Academy of Sciences Russia ASGSR
	Geophysical Survey of Russian Academy of Sciences Russia MOS		Mining Institute of the Ural Branch of the Russian Academy of Sciences Russia MIRAS		North Eastern Regional Seismological Centre, Magadan, GS RAS Russia NERS
	Kamchatka Branch of the Geophysical Survey of the RAS Russia KRSC		Kola Branch, Geophysical Survey, Russian Academy of Sciences Russia KOGSR		Sakhalin Experimental and Methodological Seismological Expedition, GS RAS Russia SKHL
	Baykal Regional Seismological Centre, GS SB RAS Russia BYKL		Republicki seizmoloski zavod Serbia BEO		Geophysical Institute, Slovak Academy of Sciences Slovakia BRA



Slovenian Environment
Agency
Slovenia
LJU



Council for Geoscience
South Africa
PRE



Institut Cartogràfic i
Geològic de Catalunya
Spain
MRB



Instituto Geográfico
Nacional
Spain
MDD



Real Instituto y
Observatorio de la
Armada
Spain
SFS



University of Uppsala
Sweden
UPP



Swiss Seismological
Service (SED)
Switzerland
ZUR



Thai Meteorological
Department
Thailand
BKK



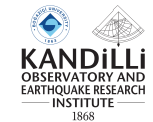
The Seismic Research
Centre
Trinidad and Tobago
TRN



Institut National de la
Météorologie
Tunisia
TUN



Disaster and
Emergency
Management
Presidency
Turkey
AFAD



Kandilli Observatory
and Earthquake
Research Institute
Turkey
ISK



National Earthquake
Information Center
U.S.A.
NEIC



The Global CMT
Project
U.S.A.
GCMT



Texas Seismological
Network, University of
Texas at Austin
U.S.A.
TXNET



Red Sismica de Puerto
Rico
U.S.A.
RSPR



Pacific Northwest
Seismic Network
U.S.A.
PNSN



Pacific Tsunami
Warning Center
U.S.A.
PTWC



Subbotin Institute of
Geophysics, National
Academy of Sciences
Ukraine
SIGU

Main Centre for
Special Monitoring
Ukraine
MCSM



Dubai Seismic Network
United Arab Emirates
DSN



British Geological
Survey
United Kingdom
BGS



Revision and
Continuation of the
EHB project
United Kingdom
ISC-EHB



International
Seismological Centre
Probabilistic Point
Source Model
United Kingdom
ISC-PPSM



International
Seismological Centre
United Kingdom
ISC

Institute of Seismology,
Academy of Sciences,
Republic of Uzbekistan
Uzbekistan
ISU



Fundación Venezolana
de Investigaciones
Sismológicas
Venezuela
FUNV



Goetz Observatory
Zimbabwe
BUL

East African Network
EAF

2.7 ISC Staff

Listed below are the staff (and their country of origin) who were employed at the ISC during the time period when the ISC worked on the data covered by this issue of the Summary.

- Dmitry Storck
- Director
- Russia / United Kingdom



- Lynn Elms
- Administration Officer
- United Kingdom



- James Harris
- Senior System and
Database Administrator
- United Kingdom



- Oliver Rea
- System Administrator
- United Kingdom



- Calum Clague
- Data Collection Officer
- South Africa / United Kingdom



- Domenico Di Giacomo
- Senior Seismologist
- Italy/UK



- Tom Garth
- Seismologist / Senior Developer
- United Kingdom



- Ryan Gallacher
- Seismologist / Developer
- United Kingdom



- Natalia Poiata
- Seismologist / Developer
- Moldova / Romania



- Adrian Armstrong
- Software Engineer
- United Kingdom



- Rosemary Hulin
- Analyst
- United Kingdom



- Blessing Shumba
- Seismologist / Senior Analyst
- Zimbabwe / United Kingdom



- Rebecca Verney
- Analyst
- United Kingdom



- Elizabeth Ayres
- Analyst / Historical Data Officer
- United Kingdom



- Kathrin Lieser
- Analyst Administrator /
Summary Editor / Seismologist
- Germany



- Burak Sakarya
- Seismologist / Analyst
- Turkey



- Rian Harris
- Historical Data Officer
- United Kingdom



- Susana Carvalho
- Historical Data Officer
- Portugal



3

Availability of the ISC Bulletin

The ISC Bulletin is available from the following sources:

- Web searches

The entire ISC Bulletin is available directly from the ISC website via tailored searches.

(www.isc.ac.uk/iscbulletin/search)

- Bulletin search - provides the most verbose output of the ISC Bulletin in ISF or QuakeML.
- Event catalogue - only outputs the prime hypocentre for each event, producing a simple list of events, locations and magnitudes.
- Arrivals - search for arrivals in the ISC Bulletin. Users can search for specific phases for selected stations and events.

- FTP site

The ISC Bulletin is also available to download from the ISC ftp site, which contains the current Bulletin in ISF2 format.

(<ftp://www.isc.ac.uk> and <http://download.isc.ac.uk>)

4

Citing the International Seismological Centre

Data from the ISC should always be cited. This includes use by academic or commercial organisations, as well as individuals. A citation should show how the data were retrieved and may be in one of these suggested forms:

The ISC is named as a valid data centre for citations within American Geophysical Union (AGU) publications. As such, please follow the AGU guidelines when referencing ISC data in one of their journals. The ISC may be cited as both the institutional author of the Bulletin and the source from which the data were retrieved.

4.1 The ISC Bulletin

International Seismological Centre (2026), On-line Bulletin, <https://doi.org/10.31905/D808B830>

The procedures used for producing the ISC Bulletin have been described in a number of scientific articles. Depending on the use of the Bulletin, users are encouraged to follow the citation suggestions below:

a) For current ISC location procedure:

Bondár, I. and D.A. Storchak (2011). Improved location procedures at the International Seismological Centre, *Geophys. J. Int.*, 186, 1220-1244, <https://doi.org/10.1111/j.1365-246X.2011.05107.x>

b) For Rebuilt ISC Bulletin:

Storchak, D.A., Harris, J., Brown, L., Lieser, K., Shumba, B., Verney, R., Di Giacomo, D., Korger, E. I. M. (2017). Rebuild of the Bulletin of the International Seismological Centre (ISC), part 1: 1964–1979. *Geosci. Lett.* (2017) 4: 32. <https://doi.org/10.1186/s40562-017-0098-z>

Storchak, D.A., Harris, J., Brown, L., Lieser, K., Shumba, B., Di Giacomo, D. (2020) Rebuild of the Bulletin of the International Seismological Centre (ISC), part 2: 1980–2010. *Geosci. Lett.* (2020) 7: 18, <https://doi.org/10.1186/s40562-020-00164-6>

c) For principles of the ISC data collection process:

R J Willemann, D A Storchak (2001). Data Collection at the International Seismological Centre, *Seis. Res. Lett.*, 72, 440-453, <https://doi.org/10.1785/gssr1.72.4.440>

d) For interpretation of magnitudes:

Di Giacomo, D., and D.A. Storchak (2016). A scheme to set preferred magnitudes in the ISC Bulletin, *J. Seism.*, 20(2), 555-567, <https://doi.org/10.1007/s10950-015-9543-7>

e) For use of source mechanisms:

Lentas, K., Di Giacomo, D., Harris, J., and Storchak, D. A. (2020). The ISC Bulletin as a comprehensive source of earthquake source mechanisms, *Earth Syst. Sci. Data*, 11, 565-578, <https://doi.org/10.5194/essd-11-565-2020>

Lentas, K. (2018). Towards routine determination of focal mechanisms obtained from first motion P-wave arrivals, *Geophys. J. Int.*, 212(3), 1665–1686. <https://doi.org/10.1093/gji/ggx503>

f) For use of the original (pre-Rebuild) ISC Bulletin as a historical perspective:

Adams, R.D., Hughes, A.A., and McGregor, D.M. (1982). Analysis procedures at the International Seismological Centre. *Phys. Earth Planet. Inter.* 30: 85-93, [https://doi.org/10.1016/0031-9201\(82\)90093-0](https://doi.org/10.1016/0031-9201(82)90093-0)

4.2 The Summary of the Bulletin of the ISC

International Seismological Centre (2026), Summary of the Bulletin of the International Seismological Centre, January - June 2022, 59(I), <https://doi.org/10.31905/DTFN4W76>

4.3 The IASPEI Reference Event List

International Seismological Centre (2026), IASPEI Reference Event (GT) List, <https://doi.org/10.31905/32NSJF7V>

Gallacher, R., Garth, T., Harris, J., Bondár, I., McLaughlin, K., and Storchak, D. A. (2025). Revising the Seismic Ground Truth Reference Event Identification Criteria. *Seismica*, 4(1). <https://doi.org/10.26443/seismica.v4i1.1536>

4.4 The ISC-GEM Catalogue

International Seismological Centre (2026), ISC-GEM Earthquake Catalogue, <https://doi.org/10.31905/d808b825>, 2026.

Depending on the use of the Catalogue, to quote the appropriate scientific articles, as suggested below.

a) For a general use of the catalogue, please quote the following three papers (Storchak et al., 2013; 2015; Di Giacomo et al., 2018):

Storchak, D.A., D. Di Giacomo, I. Bondár, E.R. Engdahl, J. Harris, W.H.K. Lee, A. Villaseñor and P. Bormann (2013). Public Release of the ISC-GEM Global Instrumental Earthquake Catalogue (1900-2009). *Seism. Res. Lett.*, 84, 5, 810-815, <https://doi.org/10.1785/0220130034>

Storchak, D.A., D. Di Giacomo, E.R. Engdahl, J. Harris, I. Bondár, W.H.K. Lee, P. Bormann and A. Villaseñor (2015). The ISC-GEM Global Instrumental Earthquake Catalogue (1900-2009): Introduction, *Phys. Earth Planet. Int.*, 239, 48-63, <https://doi.org/10.1016/j.pepi.2014.06.009>

Di Giacomo, D., E.R. Engdahl and D.A. Storchak (2018). The ISC-GEM Earthquake Catalogue

(1904–2014): status after the Extension Project, *Earth Syst. Sci. Data*, 10, 1877-1899, <https://doi.org/10.5194/essd-10-1877-2018>

b) For use of location parameters, please quote (Bondár et al., 2015):

Bondár, I., E.R. Engdahl, A. Villaseñor, J. Harris and D.A. Storchak, 2015. ISC-GEM: Global Instrumental Earthquake Catalogue (1900-2009): II. Location and seismicity patterns, *Phys. Earth Planet. Int.*, 239, 2-13, <https://doi.org/10.1016/j.pepi.2014.06.002>

c) For use of magnitude parameters, please quote (Di Giacomo et al., 2015a; 2018):

Di Giacomo, D., I. Bondár, D.A. Storchak, E.R. Engdahl, P. Bormann and J. Harris (2015a). ISC-GEM: Global Instrumental Earthquake Catalogue (1900-2009): III. Re-computed MS and mb, proxy MW, final magnitude composition and completeness assessment, *Phys. Earth Planet. Int.*, 239, 33-47, <https://doi.org/10.1016/j.pepi.2014.06.005>

Di Giacomo, D., E.R. Engdahl and D.A. Storchak (2018). The ISC-GEM Earthquake Catalogue (1904–2014): status after the Extension Project, *Earth Syst. Sci. Data*, 10, 1877-1899, <https://doi.org/10.5194/essd-10-1877-2018>

d) For use of station data from historical bulletins, please quote (Di Giacomo et al., 2015b; 2018):

Di Giacomo, D., J. Harris, A. Villaseñor, D.A. Storchak, E.R. Engdahl, W.H.K. Lee and the Data Entry Team (2015b). ISC-GEM: Global Instrumental Earthquake Catalogue (1900-2009), I. Data collection from early instrumental seismological bulletins, *Phys. Earth Planet. Int.*, 239, 14-24, <https://doi.org/10.1016/j.pepi.2014.06.005>

Di Giacomo, D., E.R. Engdahl and D.A. Storchak (2018). The ISC-GEM Earthquake Catalogue (1904–2014): status after the Extension Project, *Earth Syst. Sci. Data*, 10, 1877-1899, <https://doi.org/10.5194/essd-10-1877-2018>

e) For use of direct values of M_0 from the literature, please quote (Lee and Engdahl, 2015):

Lee, W.H.K. and E.R. Engdahl (2015). Bibliographical search for reliable seismic moments of large earthquakes during 1900-1979 to compute MW in the ISC-GEM Global Instrumental Reference Earthquake Catalogue (1900-2009), *Phys. Earth Planet. Int.*, 239, 25-32, <https://doi.org/10.1016/j.pepi.2014.06.004>

4.5 The ISC-EHB Dataset

International Seismological Centre (2026), ISC-EHB Dataset, <https://doi.org/10.31905/PY08W6S3>

Engdahl, E.R., R. van der Hilst, and R. Buland (1998). Global teleseismic earthquake relocation with improved travel times and procedures for depth determination, *Bull. Seism. Soc. Am.*, 88, 3, 722-743. <http://www.bssaonline.org/content/88/3/722.abstract>

Weston, J., Engdahl, E.R., Harris, J., Di Giacomo, D. and Storchack, D.A. (2018). ISC-EHB: Reconstruction of a robust earthquake dataset, *Geophys. J. Int.*, 214, 1, 474-484, <https://doi.org/10.1093/gji/ggy155>

Engdahl, E. R., Di Giacomo, D., Sakarya, B., Gkarlaoui, C. G., Harris, J., and Storchak, D. A. (2020). ISC-EHB 1964-2016, an Improved Data Set for Studies of Earth Structure and Global Seismicity, *Earth and Space Science*, 7(1), e2019EA000897, <https://doi.org/10.1029/2019EA000897>

4.6 The ISC Event Bibliography

International Seismological Centre (2026), On-line Event Bibliography, <https://doi.org/10.31905/EJ3B5LV6>

Also, please reference the following SRL article that describes the details of this service:

Di Giacomo, D., Storchak, D.A., Safronova, N., Ozgo, P., Harris, J., Verney, R. and Bondár, I., 2014. A New ISC Service: The Bibliography of Seismic Events, *Seismol. Res. Lett.*, 85, 2, 354-360, <https://doi.org/10.1785/0220130143>

4.7 International Registry of Seismograph Stations

International Seismological Centre (2026), International Seismograph Station Registry (IR), <https://doi.org/10.31905/EL3FQQ40>

4.8 Seismological Dataset Repository

International Seismological Centre (2026), Seismological Dataset Repository, <https://doi.org/10.31905/6TJZECEY>

The ISC is named as a valid data centre for citations within American Geophysical Union (AGU) publications. As such, please follow the AGU guidelines when referencing ISC data in one of their journals. The ISC may be cited as both the institutional author of the Bulletin and the source from which the data were retrieved.

5

Operational Procedures of Contributing Agencies

5.1 From Analogue to Digital: Evolution of Morocco's Seismic Network and Its Implications for Seismotectonic Studies

Youssef Timoulali, Mohamed Kasmi, Nacer Jabour

National Center for Scientific and Technical Research (CNRST), Rabat, Morocco



Youssef Timoulali



Mohamed Kasmi



Nacer Jabour

Morocco lies at the northwestern margin of the African Plate, where oblique convergence with the Eurasian Plate defines a complex zone of distributed deformation extending from the Azores–Gibraltar region to the western Mediterranean. The country exhibits moderate to significant seismic activity governed by both interplate and intraplate processes. Seismicity is mainly concentrated in the Rif belt, the Middle and High Atlas ranges, and the Atlantic and Mediterranean margins, reflecting the interaction between active plate boundary dynamics and reactivation of inherited crustal structures. This study, presents an overview of the historical development of seismic monitoring in Morocco. It traces the transition from the first analogue instruments to the modern digital broadband network, highlighting key milestones in instrumentation, data processing, and network expansion. The modernisation of the Moroccan seismic network has significantly improved earthquake detection capabilities, location accuracy, and data reliability, thereby enhancing our understanding of regional seismicity and active tectonic processes. The results contribute to refining the seismotectonic framework of Morocco and support ongoing efforts in seismic hazard assessment and risk mitigation.

5.1.1 Introduction

Moroccan seismicity reflects the interplay between Africa–Eurasia convergence and intraplate deformation within the North African margin. The rate of plate convergence, estimated at 4–5 mm/yr (*DeMets et al.*, 2010; *Nocquet*, 2012), is accommodated across several tectonic domains exhibiting distinct stress

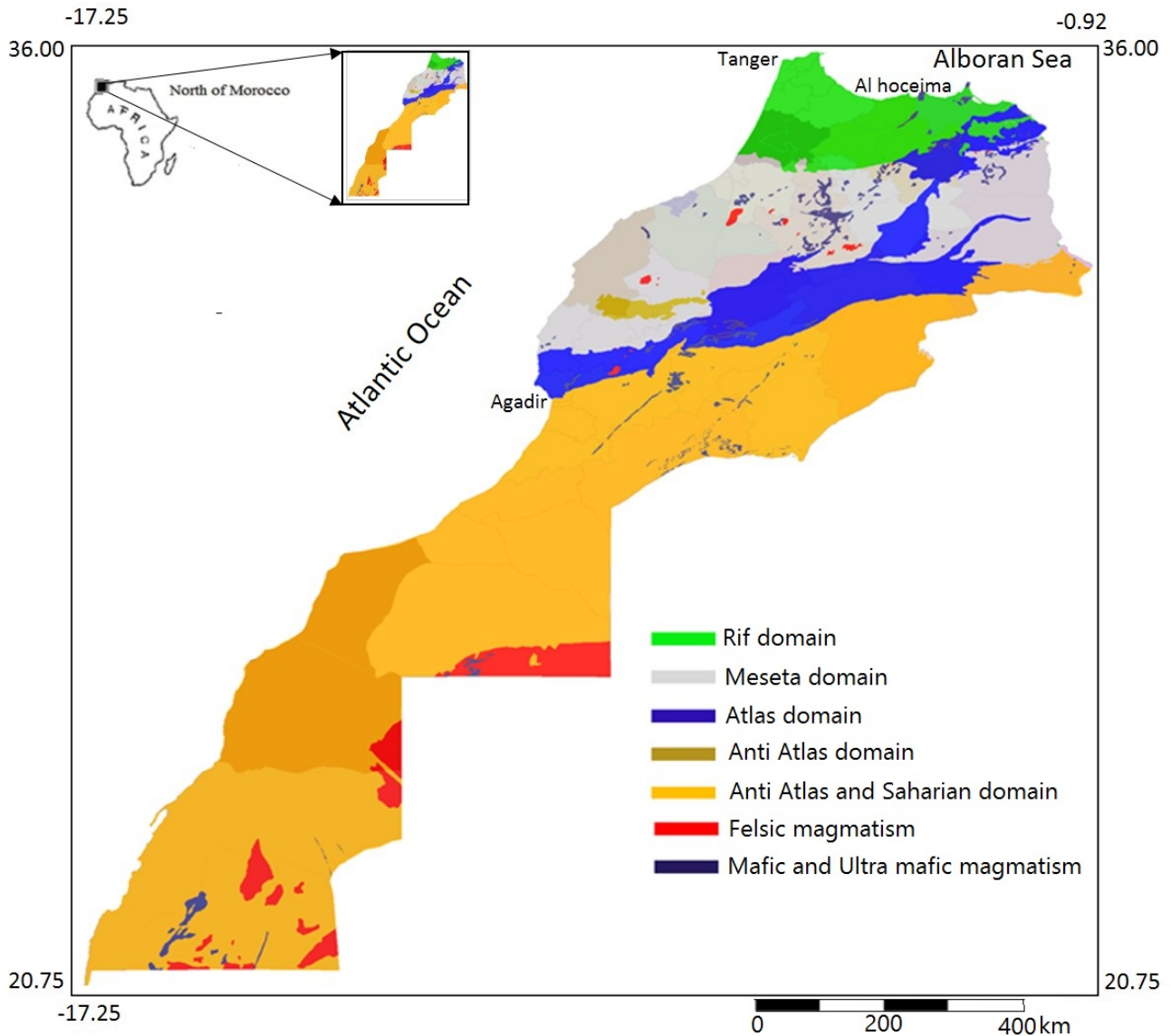


Figure 5.1: The regional location of Morocco in North Africa (top left) and the major tectonic domains (modified after Service Géologique du Maroc (1985)).

regimes and fault kinematics. Although seismic activity is moderate compared to other Mediterranean regions, Morocco has experienced several damaging earthquakes, demonstrating the persistence of active crustal deformation and the potential for significant seismic hazards.

5.1.2 Regional Tectonic Setting

The seismicity of Morocco is primarily distributed across three major tectonic domains: the Rif system, the Atlas system and the Atlantic–Mediterranean margins (Figure 5.1).

- **The Rif Domain:** These northern orogenic belts form part of the Gibraltar Arc system, resulting from the convergence of the African and Alboran domains. Deformation is dominantly compressional to transpressional, expressed through thrust and strike-slip faulting. Major active structures include the Jebha–Al Hoceima–Nador corridor, the Bokkoya Fault System, and the Trans-Alboran

Fault Zone, which have generated destructive events such as the Al Hoceima earthquakes of 1994 and 2004 (M_W 6.0–6.3) (Akoglu *et al.*, 2006).

- **The Atlas Mountains:** The High, Middle, and Anti-Atlas ranges represent an intraplate orogenic system formed by the Cenozoic inversion of Mesozoic extensional basins under the Africa–Eurasia compressional regime. Seismicity within the Atlas is generally moderate (M_W 4–6), but the Al Haouz earthquake of 8 September 2023 (M_W 6.8) revealed the capacity of this belt to produce large crustal earthquakes through the reactivation of deep-seated thrusts within the High Atlas structural block.
- **The Atlantic and Mediterranean Margins:** These margins host offshore fault systems such as the Azores–Gibraltar Transform Zone (AGFZ) and the Southwest Iberian Margin Faults, capable of generating major interplate earthquakes (e.g. the Lisbon event of 1755, M_W 8.5). Although the Moroccan Atlantic margin exhibits lower seismicity, occasional moderate events suggest reactivation of inherited Hercynian structures.

5.1.3 Seismotectonic Characteristics

Moroccan earthquakes are predominantly crustal, with focal depths ranging between 5 and 25 km, and are associated with reverse, strike-slip, or normal faulting mechanisms (Figure 5.2). Focal mechanism solutions indicate a prevailing NW–SE compressional stress orientation, consistent with the Africa–Eurasia convergence direction (Medina, 1995; Stich *et al.*, 2010).

Spatially, seismicity clusters along the northern Rif, the Middle Atlas corridor, and the central High Atlas, while the southern and Saharan domains remain relatively aseismic. Active fault mapping and geodetic investigations have identified key structures such as the Tizi n’Test Fault, Imilchil–Tadighoust Fault, and the South Atlas Front, suggesting the potential for moderate to strong intraplate events (El Mrabet, 1991).

Historically, Morocco has been affected by several destructive earthquakes, including the earthquakes in Fez (1624), Agadir (1960, M_W 5.7) -which caused over 12,000 fatalities- and Al Hoceima (1994, 2004, 2023, M_W 6.3–6.8). These events highlight the recurrence of damaging earthquakes in both plate boundary and intraplate settings, reinforcing the need for continuous seismic monitoring and hazard reassessment.

5.1.4 Seismic Monitoring

The history of seismic monitoring in Morocco dates back to the early twentieth century. In 1906, Montessus de Ballore, one of the pioneering French seismologists, identified the potential seismic hazard affecting North African countries and Spain (Montessus de Ballore, 1906). The first seismic instrument in Morocco was installed in 1937 at the Averroès Observatory, marking the beginning of instrumental seismology in the country. However, the establishment of a structured national seismic monitoring system only gained real momentum following the Agadir earthquake of 29 February 1960 (M_W 5.7), which revealed the need for continuous seismic surveillance and rapid response capabilities.

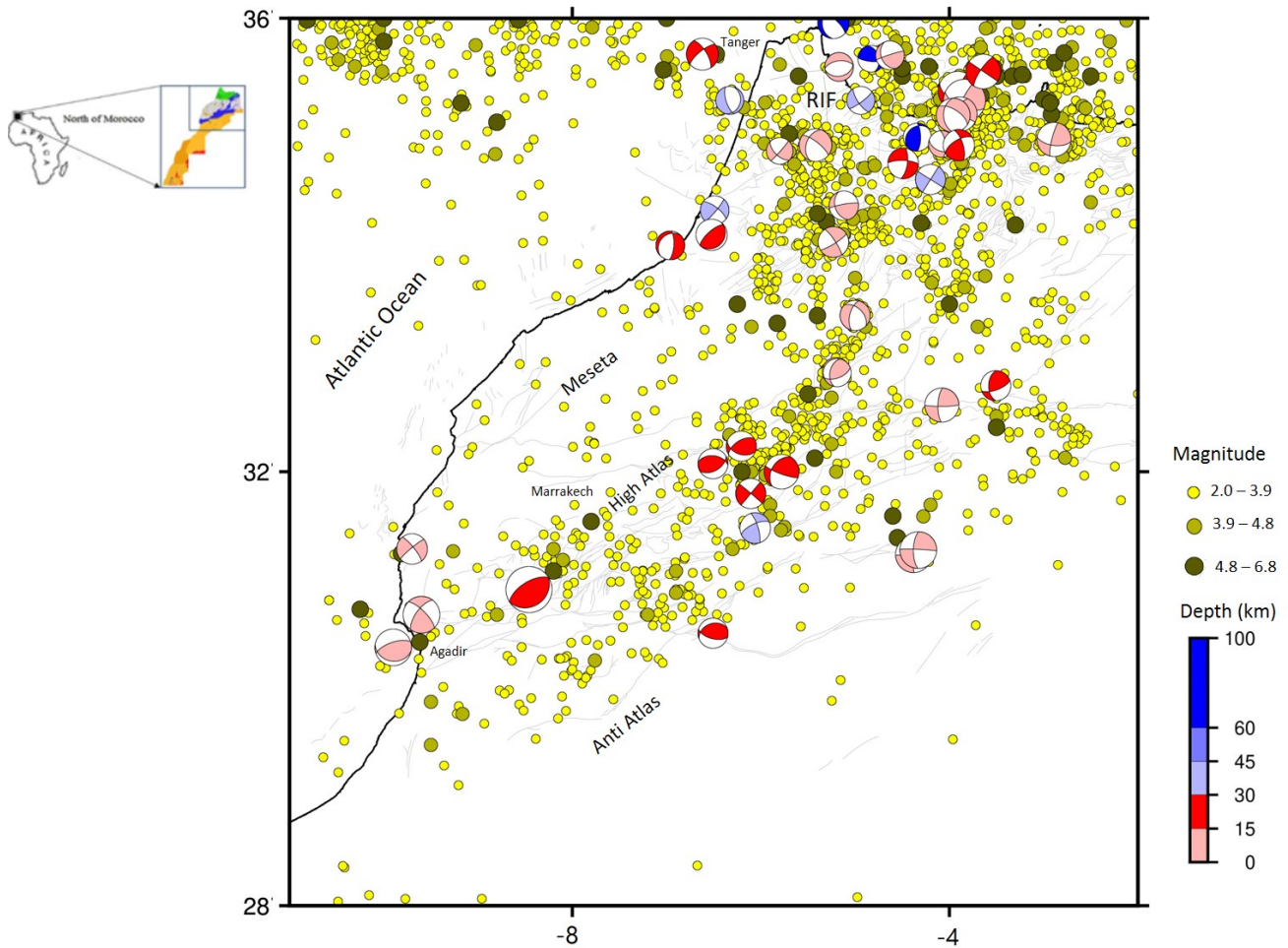


Figure 5.2: Instrumental seismicity from catalogue of CNRST-Morocco and focal mechanisms from Global CMT (Ekström et al., 2012). The compressional quadrants of the focal mechanisms are coloured coded by depth.

During the 1980s, significant progress was achieved with the installation of 15 seismic stations, substantially improving the country’s capacity to detect and locate earthquakes. In 1982, the Council of Arab Ministers of Housing and Urban Development initiated the Program for the Assessment and Mitigation of Earthquake Risk in the Arab Region (PAMERAR), which enabled Morocco to acquire telemetric seismic networks and upgrade its monitoring infrastructure.

Since then, the National Institute of Geophysics (ING), under the National Centre for Scientific and Technical Research (CNRST), has developed three successive generations of observation networks, each incorporating progressively more advanced technologies. These networks have significantly enhanced the precision, reliability, and real-time capabilities of seismic data acquisition, improving both the detection threshold and the rapid determination of earthquake parameters at the national scale.

History of National Seismological Network (1970 – 2012)

The first national seismological network, established during the 1970s by the Geophysics Department of the Scientific Institute of Mohammed V University, consisted of a combination of short- and long-period analogue instruments (Ben Sari, 2004): 14 short-period stations with analogue visible recording;

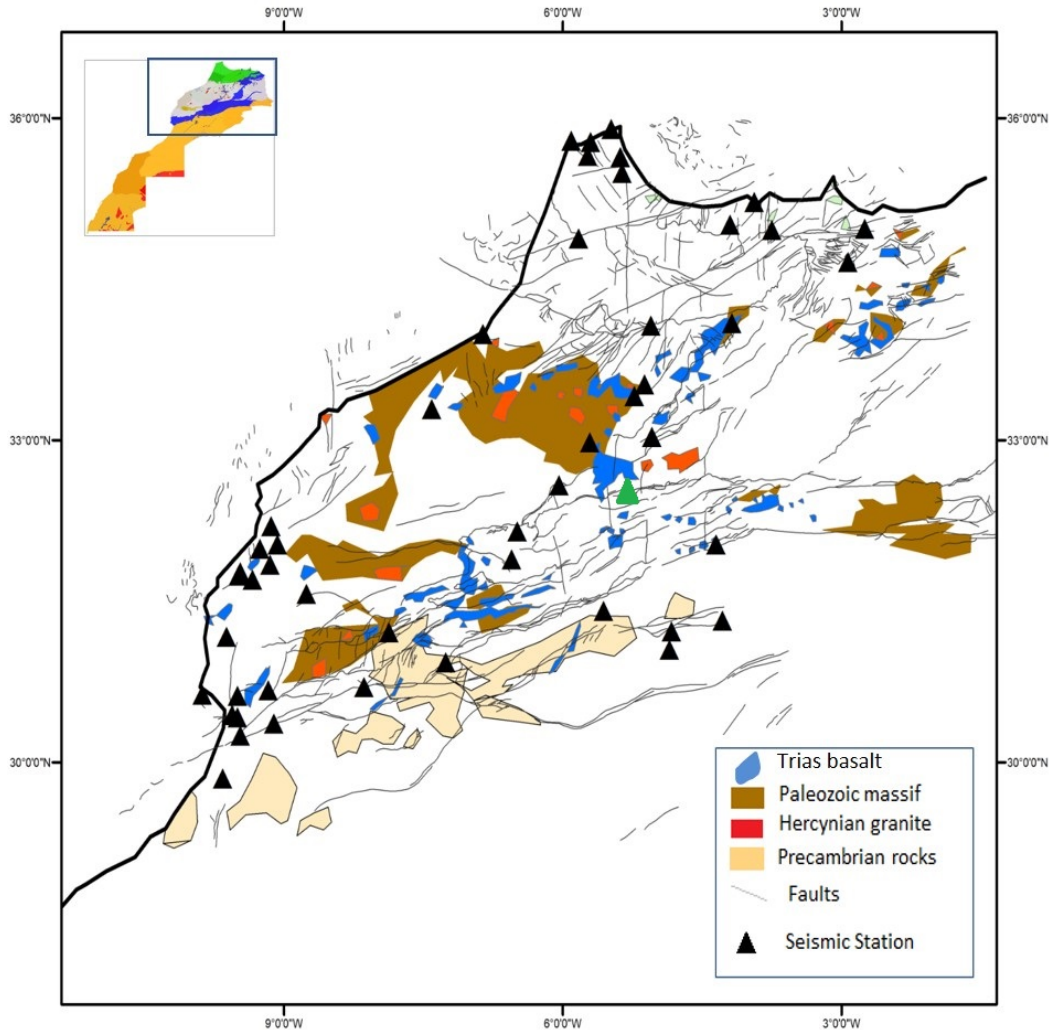


Figure 5.3: The Moroccan analogue seismic network, operated between 1988 and 2012, was deployed across northern Morocco. The green triangle represents the (VBB) observatory located in the Midelt region.

2 short-period stations with analogue magnetic tape recording, offering improved bandwidth; 5 long-period stations with analogue visible recording; 2 accelerographs, one recording on photographic paper and the other on magnetic tape.

Most of these instruments were installed at dam sites, complemented by three observatories located in Averroès (Berrechid region), Ifrane and Tiouine (Ouarzazate region). This early network represented the foundation for modern seismic monitoring in Morocco.

The National Seismic Monitoring and Early Warning Network, established in 1988 by the Laboratory of Geophysics (LAG) under the CNRST, constituted a real-time data acquisition system covering the national territory and adjacent regions. Over 70 seismic instruments were deployed across Morocco, approximately half of which were telemetric stations connected to the central processing facility in Rabat via UHF/VHF radio transmission links (31 in total) and dedicated telephone lines (6 lines) (Figure 5.3).

The telemetric component comprised of 30 short-period stations, each equipped with a vertical component seismograph. In addition, 23 accelerographs and 9 relay stations formed part of the national network.

Data were recorded in both analogue and digital formats for the telemetered network, digitally for accelerographs and portable stations, and analogically for other mobile instruments. Timing synchronisation was ensured by GPS satellite clocks for telemetered stations and accelerographs, and by DCF77 radio time signals for portable systems.

The short-period network (1 Hz) operated on analogue frequency modulation. Data acquisition was conducted at the central observatory in Rabat, which included 31 analogue drum recorders and one digital acquisition unit equipped with two threshold-detection tape readers for data storage.

In regions where telemetered stations could not be installed, a portable seismic network was deployed, consisting of six portable seismographs using thermal-paper recording. For microseismicity investigations and aftershock monitoring, six analogue seismographs and two three-component digital stations were utilized.

Furthermore, 23 accelerographs equipped with three-component sensors had been installed to monitor strong ground motions and hydraulic structures, in collaboration with the Directorate of Hydraulic Infrastructure.

As part of bilateral cooperation between the CNRST and the Istituto Nazionale di Geofisica (INGV), Italy, a Very Broad-Band (VBB) observatory was installed in the Midelt region (Figure 5.3). This observatory represented the latest generation of seismic instrumentation in Morocco at the time, equipped with Streckeisen STS-1 sensors and a 24-bit digitizer. This station was relocated to Rabat and is now operating under the code RTC.

Current National Seismic Network and Future Perspectives

Over the past two decades, Morocco has undertaken significant modernisation efforts to enhance its national seismic monitoring and early warning capabilities. These initiatives aim to improve the spatial coverage, data quality, and real-time transmission of seismic information, thereby supporting both scientific research and disaster risk reduction policies.

The major modernisation phase took place over the period 2012–2025, involving the progressive adoption of satellite-based data transmission. In addition to hardware modernisation, substantial progress has been made in the development of automated data processing and early warning systems. The implementation of real-time algorithms for event detection, location, and magnitude estimation enables rapid generation of preliminary bulletins, supporting emergency response coordination. Data management and analysis capabilities have also been enhanced through the establishment of dedicated computing infrastructure and national databases accessible to researchers and public institutions.

The National Institute of Geophysics (ING), under the National Center for Scientific and Technical Research (CNRST), has progressively upgraded its seismic infrastructure through the integration of digital broadband technology, satellite telemetry (figure 4), and automated data processing systems. A total of 36 seismic stations are presently operational within the network. These include 12 Streckeisen STS-2, 2 Streckeisen STS-2.5, 8 Nanometrics Trillium-240, 4 Kinometrics MBB-2, and 10 short-period Lennartz 3Dlite instruments, ensuring broad frequency coverage and high-quality waveform acquisition across the monitored region.

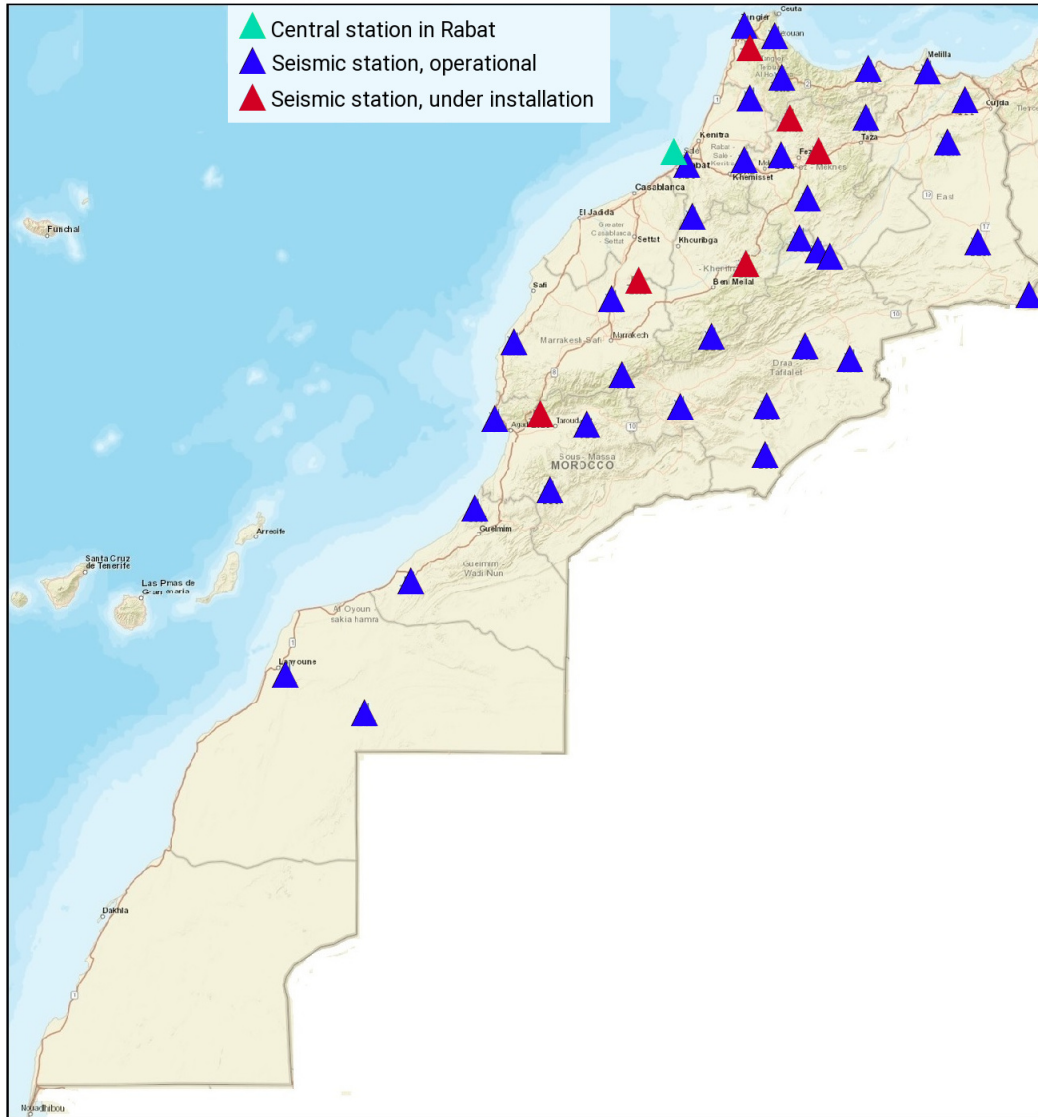


Figure 5.4: The Moroccan digital seismic network has been deployed across the entire national territory, providing comprehensive coverage for seismic monitoring.

5.1.5 Data Processing

A central aspect of the network modernisation is the implementation of the Antelope real-time seismic monitoring system (Boulder Real Time Technologies), which offers comprehensive tools for data acquisition, processing, analysis, archiving, and rapid dissemination of seismic alerts. This system enables the seamless integration of telemetry streams with real-time event detection, hypocentre determination, magnitude estimation, and automatic alert generation, significantly enhancing the operational performance of Morocco’s seismic monitoring system.

Seismic event processing and location are conducted using the IASP91 velocity model as the reference Earth structure, with depth discretisations tailored to the scale of seismicity. For local earthquakes, the model is sampled at depths of 0–30 km at 2 km intervals to achieve higher resolution within the crust. For regional events, a simplified configuration with depth levels at 15 km and 30 km is applied to optimise computation while maintaining adequate accuracy. Magnitude estimation is performed within

the Antelope framework: local magnitudes (ML) are derived from the maximum amplitude recorded by short-period and broadband stations, whereas body-wave (mb) and surface-wave (MS) magnitudes are determined for regional and teleseismic events using standard amplitude–period correction functions.

The transition from analogue to digital acquisition systems has markedly improved the precision and reliability of earthquake detection and localisation, while also facilitating rapid dissemination of seismic alerts to national authorities and civil protection agencies. Recent developments include the installation of Very Broad-Band (VBB) stations and Global Positioning System (GPS) time-synchronized sensors, allowing continuous recording of ground motion across a broad frequency range.

The implementation of satellite-based data transmission, currently underway, represents a major advancement toward a fully digital, real-time monitoring network. Out of 50 planned satellite-linked stations, 36 have already been completed, significantly extending national coverage, particularly in remote and seismically active regions such as the High Atlas and Rif domains.

Parallel efforts have focused on the integration of seismic and accelerometric data to improve the characterisation of strong ground motion and site effects. The expansion of the accelerograph network, notably in urban centres and critical infrastructure sites (e.g., dams, bridges, and industrial facilities), provides essential input for seismic microzonation, structural safety assessment, and the calibration of ground-motion prediction models.

In addition to hardware modernisation, substantial progress has been made in automated data processing and early warning systems using Antelope’s capabilities. Real-time algorithms for event detection, location, and magnitude estimation now allow the generation of rapid bulletins to support emergency response. Data management has also been enhanced through the creation of centralized databases, accessible to researchers and relevant public institutions.

5.1.6 Data Availability

The CNRST provides access to seismic data, including a comprehensive seismic catalogue and bulletins in collaboration with the International Seismological Centre (ISC) and Euro-Mediterranean Seismological Centre (EMSC). Several stations are jointly operated within the Western Mediterranean network, in partnership with the Instituto Geográfico Nacional (IGN) of Spain, Instituto Português do Mar e da Atmosfera (IPMA) of Portugal and Istituto Nazionale di Geofisica e Vulcanologia (INGV) of Italy, through the Mediterranean Very Broadband Seismographic Network (MedNet), in addition one station operates as an auxiliary station of the Comprehensive Nuclear-Test-Ban Treaty Organization (CTBTO).

5.1.7 Conclusions

Moroccan seismicity results from the complex interaction between active plate boundary dynamics and intraplate reactivation of inherited faults. The Rif belt and Atlas Mountains remain the most active zones, while offshore structures along the Azores–Gibraltar–Iberian system are capable of producing large-magnitude events. The occurrence of the 2023 Al Haouz earthquake underscores the seismic potential of the Atlas domain and the importance of continued instrumental observation, seismotectonic research, and hazard reassessment for effective seismic risk management.

References

- Akoglu A. M., Cakir Z. Meghraoui M., Belabes S., El Alami S. O., Ergintav S. and Akyuz H. S. (2006), The 1994 - 2004 Al Hoceima (Morocco) earthquake sequence: Conjugate fault rupture deduced from InSAR, *Earth Planet. Sci. Lett.*, 252(3-4), 467-480, <https://doi.org/10.1016/j.epsl.2006.10.010>.
- Ben Sari, D. (2004), Pr evision et pr evencion des catastrophes naturelles et environnementales: Le Cas du Maroc, *Sciences de la terre*, UNESCO, ISBN 92-3-203980-X.
- DeMets, C., R.G. Gordon and D.F. Argus (2010), Geologically current plate motions, *Geophys. J. Int.*, 181(1), 1–80, <https://doi.org/10.1111/j.1365-246X.2009.04491.x>.
- Ekstr om, G., M. Nettles and A. M. Dziewonski (2012), The global CMT project 2004-2010: Centroid-moment tensors for 13,017 earthquakes, *Phys. Earth Planet. Inter.* 200-201, 1-9, <https://doi.org/10.1016/j.pepi.2012.04.002>.
- El Mrabet, T. (1991), Historical seismicity of Morocco, Third-cycle thesis, Faculty of Human Sciences, Mohammed V University, Rabat, 375 p.
- Medina, F. (1995), Present-day state of stress in northern Morocco from focal mechanism analysis, *J. Struct. Geol.*, 17(7), 1035-1046, [https://doi.org/10.1016/0191-8141\(94\)00123-H](https://doi.org/10.1016/0191-8141(94)00123-H).
- Montessus de Ballore, F. (1906), Les tremblements de terre: g eographie s eismologique, Armand Colin, Paris.
- Nocquet, J.M. (2012), Present-day kinematics of the Mediterranean: A comprehensive overview of GPS results, *Tectonophysics*, 579, 220–242, <https://doi.org/10.1016/j.tecto.2012.03.037>.
- Service G eologique du Maroc (1985), Carte G eologique du Maroc, 1:1,000,000, 260, https://cartes-geoscientifiques.mem.gov.ma/catalogue/pages/cartes_geologiques/index.html
- Stich, D., Mancilla, F. and Morales, J. (2010), Moment tensor inversion for Iberia–Maghreb earthquakes 2005–2008, *Tectonophysics*, 483(3-4), 390-398, <https://doi.org/10.1016/j.tecto.2009.11.006>.

6

Summary of Seismicity, January - June 2022

The period between January and June 2022 produced only 3 earthquakes with $M_W \geq 7$; these are listed in Table 6.1. The largest event in this Summary’s time period was the M_W 7.3 Fukushima–Oki earthquake offshore Japan (2022/03/16 14:36:32.03 (UTC), 37.7061°N, 141.6601°E, 50 km depth, 3684 stations (ISC)). It occurred within the subduction Pacific slab and was one of the largest forearc intraslab earthquakes in Japan, causing four fatalities, leaving over 100 injured and severely damaging local infrastructure (Wang *et al.*, 2022). The Pacific coast of Japan has been struck by four intraslab events with magnitudes larger than 7 in the last two decades. The penultimate occurring only one year and a month before this earthquake. A study by Wang *et al.* (2022) indicates that the generation of these intraslab events is possibly associated with the reactivation of buried hydrated faults that formed at the outer rise and are subducted with the oceanic plate.

The most discussed event in the scientific community during this Summary’s time period, with currently 348 entries in the ISC Event Bibliography (Di Giacomo *et al.*, 2014; International Seismological Centre, 2026), was the enormous Hunga Tonga-Hunga Ha’apai eruption in January that was recorded on seismic stations around the globe (2022/01/15 04:14:46.80 (UTC), 20.5789°S, 175.6555°W, depth fixed to surface, 731 stations (ISC)). The volcanic eruption generated an unparalleled global dataset of a broad range of waves: infrasound waves were detected globally on the International Monitoring System (IMS) (Vergoz *et al.*, 2022), seismometers around the globe recorded seismic as well as air-to-ground coupled waves and even audible sound could be observed as far away as Alaska (about 10,000 km distance) (e.g. Matoza *et al.*, 2022). Most prominent were Lamb waves (atmospheric boundary waves propagating along the Earth’s surface at the speed of sound) that could be observed circling the Earth four times within six days and were comparable in size to the 1883 Krakatoa eruption (Matoza *et al.*, 2022). The Lamb waves contributed to the first arrivals of the generated tsunami waves unexpectedly arriving 2 hours earlier than modelled (Kubota *et al.*, 2022)).

Table 6.1: Summary of the earthquakes of magnitude $M_w \geq 7$ between January and June 2022.

Date	lat	lon	depth	Mw	Flinn-Engdahl Region
2022-03-16 14:36:32	37.71	141.66	49	7.3	Near east coast of eastern Honshu
2022-05-26 12:02:20	-14.87	-70.37	226	7.2	Central Peru
2022-03-31 05:44:00	-22.51	170.55	14	7.0	Southeast of Loyalty Islands

The number of events in this Bulletin Summary categorised by type are given in Table 6.2.

Figure 6.1 shows the number of moderate and large earthquakes in the first half of 2022. The distribution of the number of earthquakes should follow the Gutenberg-Richter law.

Figures 6.2 to 6.5 show the geographical distribution of moderate and large earthquakes in various magnitude ranges.

Table 6.2: Summary of events by type between January and June 2022.

felt earthquake	377
known earthquake	178363
known chemical explosion	10808
known induced event	1292
known landslide	1
known mine explosion	3297
known rockburst	2586
known volcanic event	10
known experimental explosion	112
suspected earthquake	113835
suspected chemical explosion	5306
suspected induced event	60
suspected mine explosion	7661
suspected rockburst	92
suspected experimental explosion	378
suspected ice-quake	134
unknown	89
total	324401

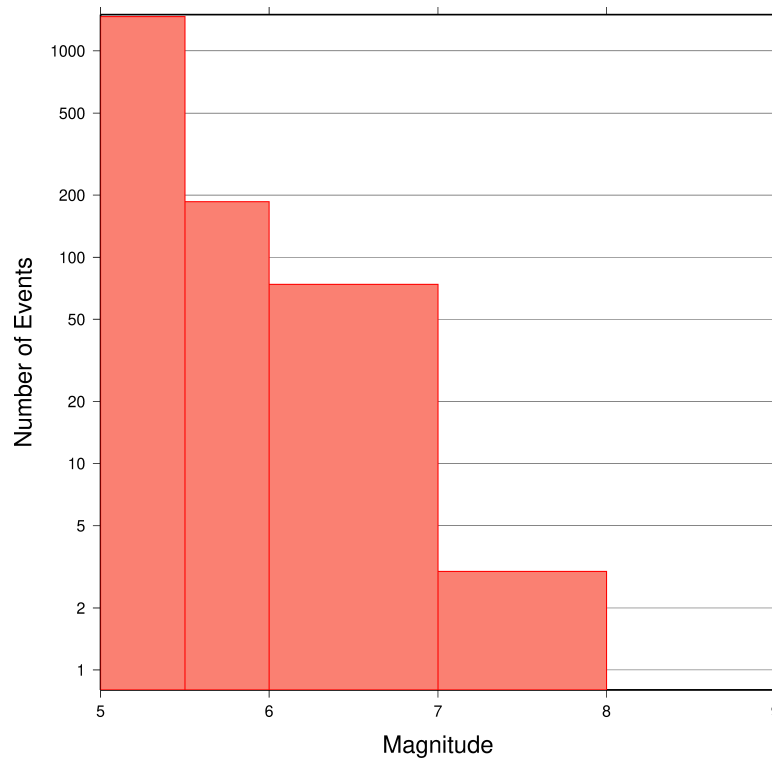


Figure 6.1: Number of moderate and large earthquakes between January and June 2022. The non-uniform magnitude bias here correspond with the magnitude intervals used in Figures 6.2 to 6.5.

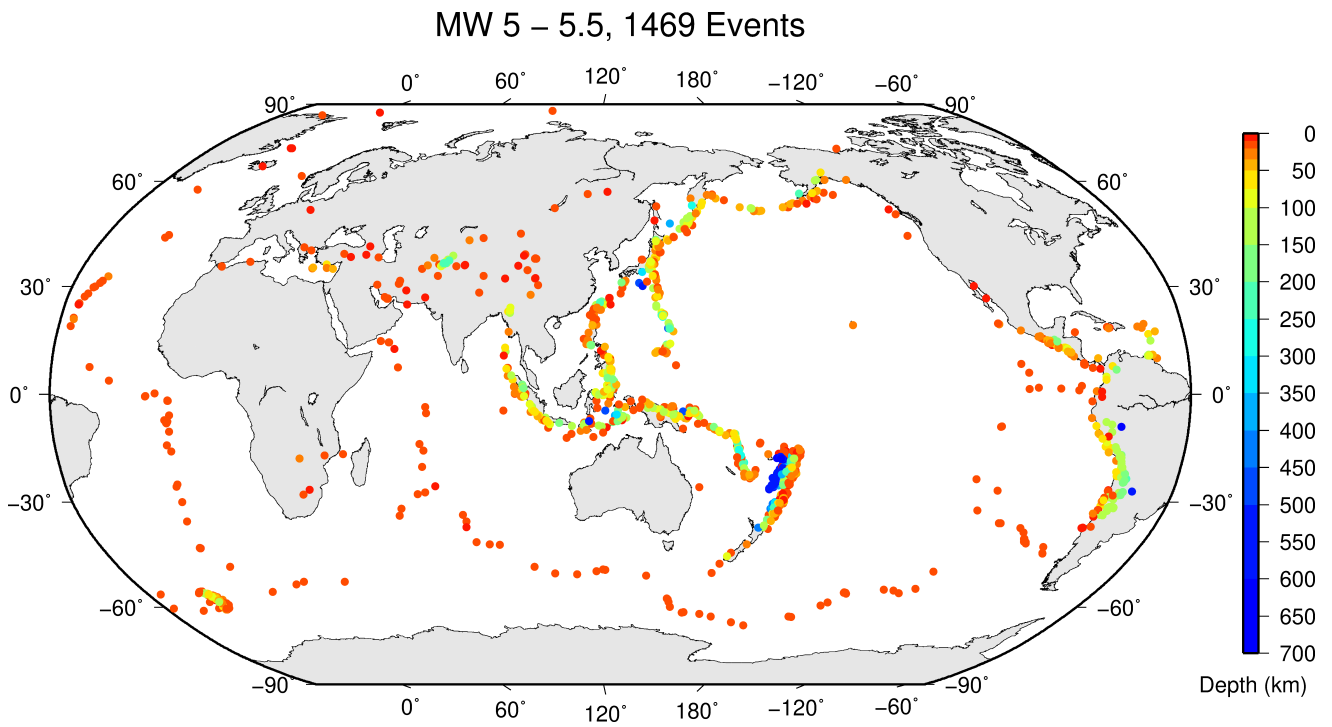


Figure 6.2: Geographic distribution of magnitude 5-5.5 earthquakes between January and June 2022.

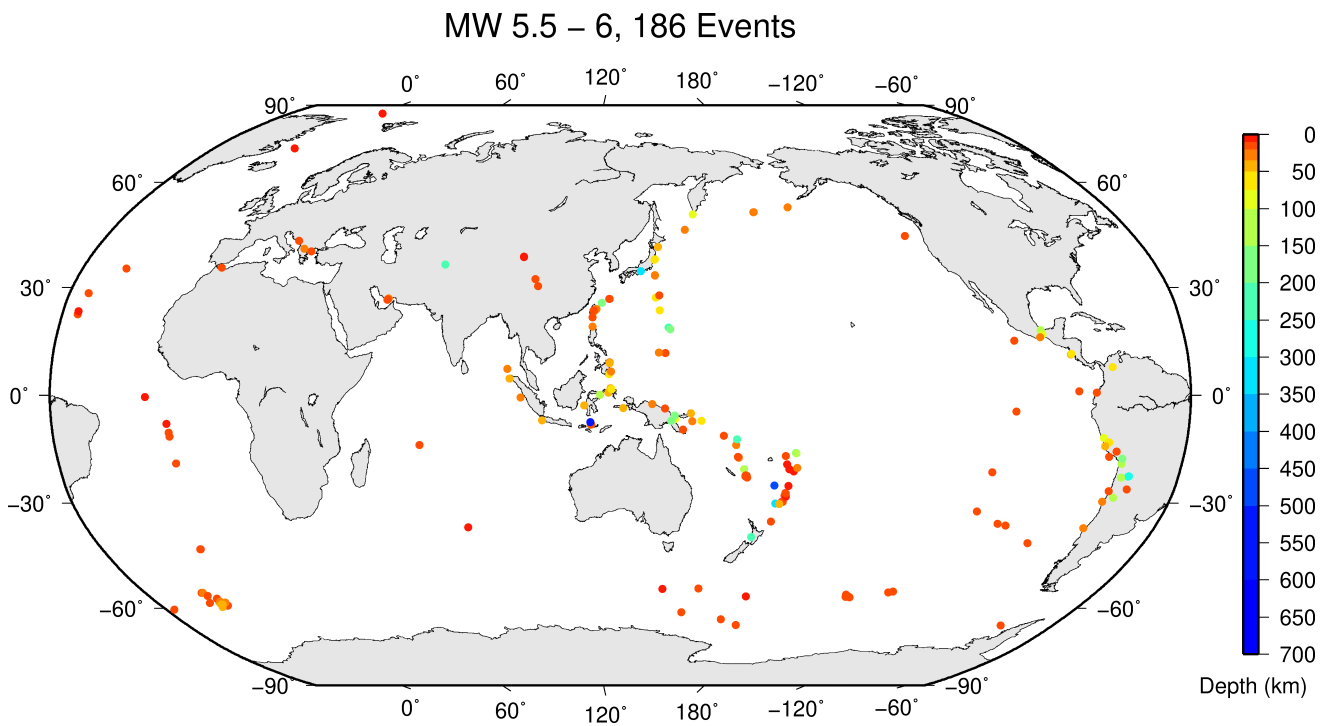


Figure 6.3: Geographic distribution of magnitude 5.5-6 earthquakes between January and June 2022.

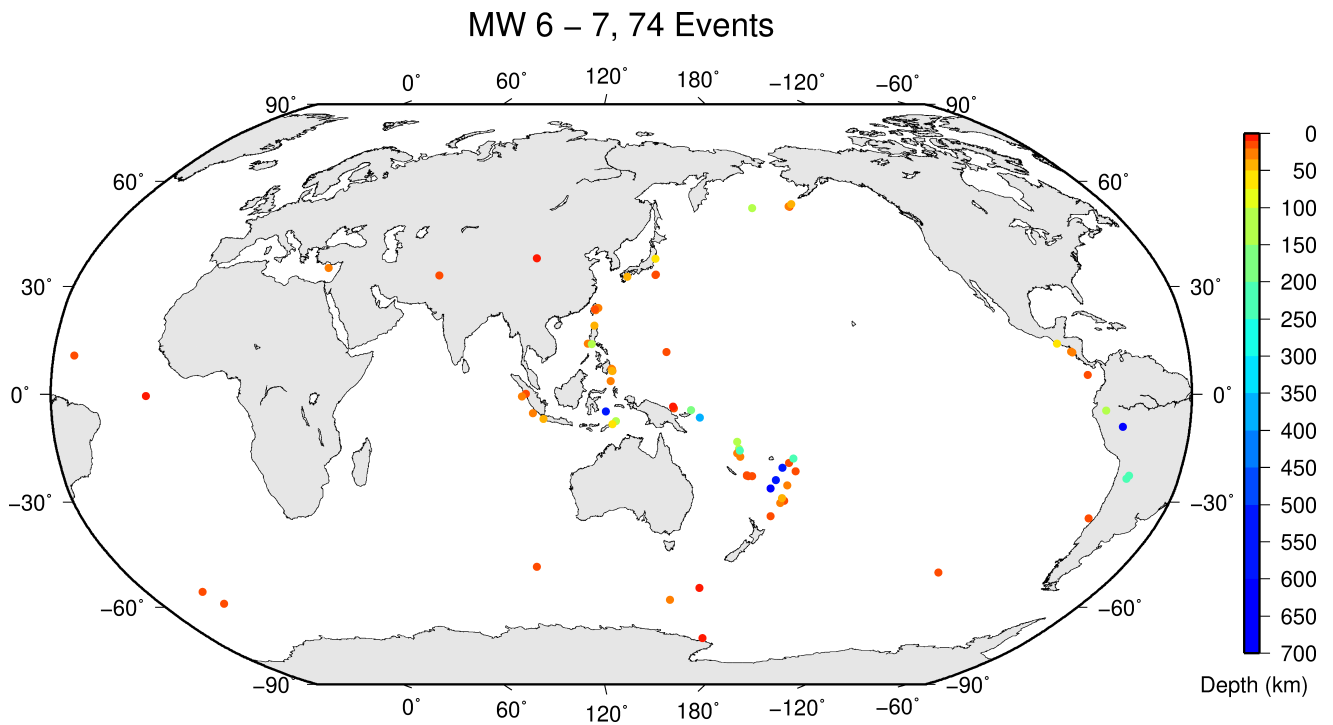


Figure 6.4: Geographic distribution of magnitude 6-7 earthquakes between January and June 2022.

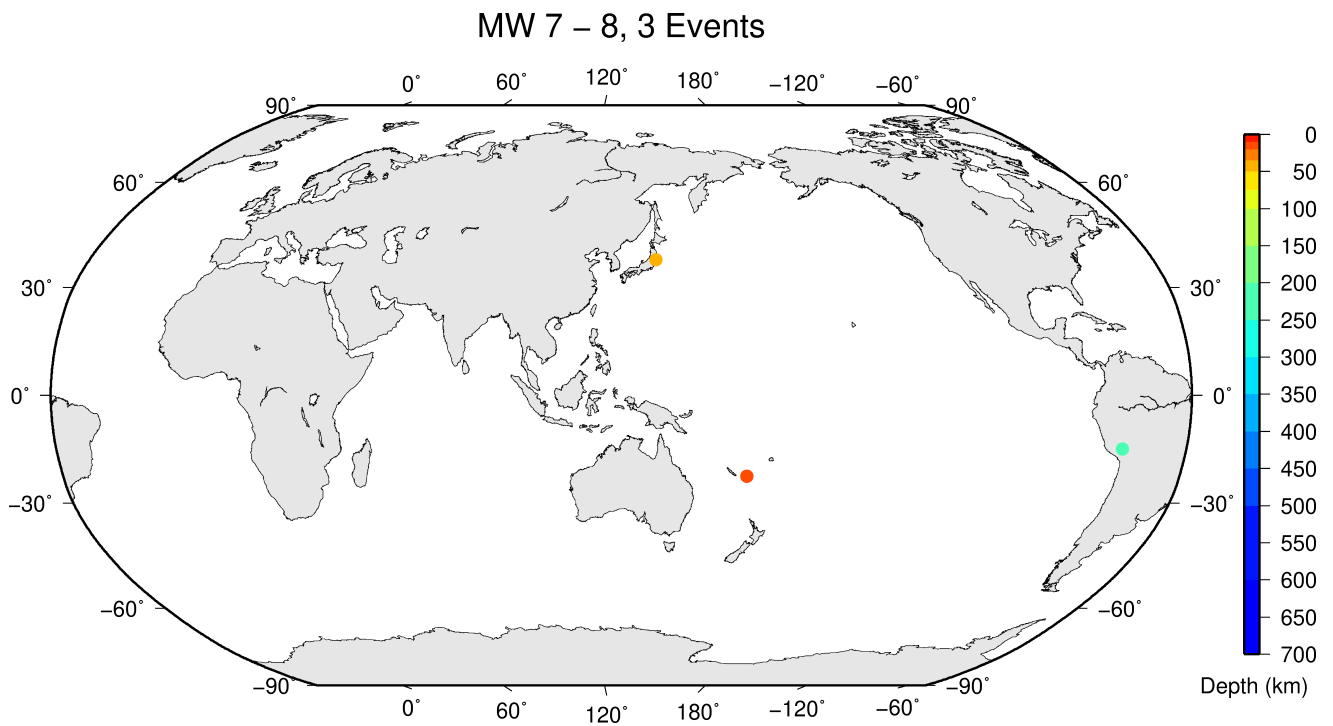


Figure 6.5: Geographic distribution of magnitude 7-8 earthquakes between January and June 2022.

References

- Di Giacomo, D., D.A. Storchak, N. Safronova, P. Ozgo, J. Harris, R. Verney and I. Bondár (2014), A New ISC Service: The Bibliography of Seismic Events, *Seismol. Res. Lett.*, 85(2), 354–360, <https://doi.org/10.1785/0220130143>.
- International Seismological Centre (2026), On-line Event Bibliography, <https://doi.org/10.31905/EJ3B5LV6>.
- Kubota T., T. Saito and K Nishida (2022), Global fast-travelling tsunamis driven by atmospheric Lamb waves on the 2022 Tonga eruption, *Science*, 377, 91–94, <https://doi.org/10.1126/science.abo4364>.
- Matoza, R.S. et al. (2022), Atmospheric waves and global seismoacoustic observations of the January 2022 Hunga eruption, Tonga, *Science*, 377, 95–100, <https://doi.org/10.1126/science.abo7063>.
- Vergoz, J., P. Hupe, C. Listowski, A. Le Pichon, M.A. Garcés, E. Marchetti, P. Labazuy, L. Ceranna, C. Pilger, P. Gaebler, S.P. Näsholm, Q. Brissaud, P. Poli, N. Shapiro, R. De Negri and P. Mialle (2022), IMS observations of infrasound and acoustic-gravity waves produced by the January 2022 volcanic eruption of Hunga, Tonga: A global analysis, *Earth Planet. Sci. Lett.*, 591, <https://doi.org/10.1016/j.epsl.2022.117639>.
- Wang, Z., D. Zhao and X. Chen (2022), Fine Structure of the Subducting Slab and the 2022 M 7.4 Fukushima–Oki Intraslab Earthquake, *Seismol. Res. Lett.*, 94, 17–25, <https://doi.org/10.1785/0220220234>.

7

Statistics of Collected Data

7.1 Introduction

The ISC Bulletin is based on the parametric data reports received from seismological agencies around the world. With rare exceptions, these reports include the results of waveform review done by analysts at network data centres and observatories. These reports include combinations of various bulletin elements such as event hypocentre estimates, moment tensors, magnitudes, event type and felt and damaging data as well as observations of the various seismic waves recorded at seismic stations.

Data reports are received in different formats that are often agency specific. Once an authorship is recognised, the data are automatically parsed into the ISC database and the original reports filed away to be accessed when necessary. Any reports not recognised or processed automatically are manually checked, corrected and re-processed. This chapter describes the data that are received at the ISC before the production of the reviewed Bulletin.

Notably, the ISC integrates all newly received data reports into the automatic ISC Bulletin (available on-line) soon after these reports are made available to ISC, provided it is done before the submission deadline that currently stands at 12 months following an event occurrence.

With data constantly being reported to the ISC, even after the ISC has published its review, the total data shown as collected, in this chapter, is limited to two years after the time of the associated reading or event, i.e. any hypocentre data collected two years after the event are not reflected in the figures below.

7.2 Summary of Agency Reports to the ISC

A total of 152 agencies have reported data for January 2022 to June 2022. The parsing of these reports into the ISC database is summarised in Table 7.1.

Table 7.1: Summary of the parsing of reports received by the ISC from a total of 152 agencies, containing data for this summary period.

	Number of reports
Total collected	10577
Automatically parsed	9404
Manually parsed	1173

Data collected by the ISC consists of multiple data types. These are typically one of:

- Bulletin, hypocentres with associated phase arrival observations.

- Catalogue, hypocentres only.
- Unassociated phase arrival observations.

In Table 7.2, the number of different data types reported to the ISC by each agency is listed. The number of each data type reported by each agency is also listed. Agencies reporting indirectly have their data type additionally listed for the agency that reported it. The agencies reporting indirectly may also have ‘hypocentres with associated phases’ but with no associated phases listed - this is because the association is being made by the agency reporting directly to the ISC. Summary maps of the agencies and the types of data reported are shown in Figure 7.1 and Figure 7.2.

Table 7.2: Agencies reporting to the ISC for this summary period. Entries in bold are for new or renewed reporting by agencies since the previous six-month period.

Agency	Country	Directly or indirectly reporting (D/I)	Hypocentres with associated phases	Hypocentres without associated phases	Associated phases	Unassociated phases	Amplitudes
TIR	Albania	D	1901	21	35999	186	9146
CRAAG	Algeria	D	348	0	3581	0	0
LPA	Argentina	D	0	0	0	1728	0
SJA	Argentina	D	1053	2	46283	0	13578
NSSP	Armenia	D	61	0	1202	0	0
AUST	Australia	D	2517	720	262583	0	253348
CUPWA	Australia	D	82	59	767	9	0
IDC	Austria	D	18528	0	661806	0	562604
VIE	Austria	D	6283	65	64955	3	64292
AZER	Azerbaijan	D	4229	0	46707	0	0
UCC	Belgium	D	1576	0	8785	3	3045
SCB	Bolivia	D	1028	0	15897	0	2666
RHSSO	Bosnia and Herzegovina	D	1551	0	26636	3187	0
BGSI	Botswana	D	389	0	5961	0	1978
OSUNB	Brazil	D	245	1	6708	0	0
VAO	Brazil	D	840	16	17912	0	0
SOF	Bulgaria	D	402	0	5363	1864	0
OTT	Canada	D	1547	49	31129	0	0
PGC	Canada	I OTT	1185	0	21742	0	0
GUC	Chile	D	4624	403	129559	3742	37790
BJI	China	D	1280	0	113413	27791	80659
ASIES	Chinese Taipei	D	0	68	0	0	0
TAP	Chinese Taipei	D	7383	0	550675	0	0
RSNC	Colombia	D	11722	0	361175	137	83054
UCR	Costa Rica	D	489	1	17393	0	0
ZAG	Croatia	D	0	0	0	64170	0
SSNC	Cuba	D	2943	0	69930	10	19123
NIC	Cyprus	D	605	0	16987	0	6462
IPEC	Czech Republic	D	413	0	6126	19170	1995
PRU	Czech Republic	D	4609	0	50774	100	12674
WBNET	Czech Republic	D	86	0	1568	0	1568
KEA	Democratic People's Republic of Korea	D	167	0	1711	0	799
DNK	Denmark	D	2500	1155	36756	23510	8427
OSPL	Dominican Republic	D	1571	0	22063	0	6023
SDD	Dominican Republic	D	545	0	9241	0	3196
IGQ	Ecuador	D	85	0	6047	0	0
HLW	Egypt	D	42	0	713	0	0
SNET	El Salvador	D	6169	325	49002	564	0
EST	Estonia	I HEL	151	19	0	0	0
AAE	Ethiopia	D	444	11	2629	172	490
HEL	Finland	D	6344	1324	171853	0	32354
CSEM	France	I AWI	3826	89	0	0	0
IPGP	France	D	0	121	0	0	0
LDG	France	D	2559	5	52532	4	14804

Table 7.2: (continued)

Agency	Country	Directly or indirectly reporting (D/I)	Hypocentres with associated phases	Hypocentres without associated phases	Associated phases	Unassociated phases	Amplitudes
STR	France	D	6123	0	130068	82	0
PPT	French Polynesia	D	1513	300	9315	37	8015
TIF	Georgia	D	0	101	0	1737	0
AWI	Germany	D	3758	0	12167	115	12199
BGR	Germany	D	563	100	13182	0	4725
BNS	Germany	I BGR	2	22	0	0	0
BRG	Germany	D	0	0	0	1439	542
CLL	Germany	D	2470	0	11722	844	4705
GDNRW	Germany	I BGR	0	3	0	0	0
GFZ	Germany	D	3243	862	233134	0	319878
HLUG	Germany	I BGR	1	2	0	0	0
LEDBW	Germany	I BGR	18	3	0	0	0
ATH	Greece	D	11434	3	532749	0	121776
THE	Greece	D	2799	0	97130	3771	52559
UPSL	Greece	D	0	1	0	0	0
GCG	Guatemala	D	2408	0	29165	57	970
HKC	Hong Kong	D	0	0	0	39	0
KRSZO	Hungary	D	1379	75	22345	0	6523
REY	Iceland	D	31	0	1537	0	0
HYB	India	D	982	1	3381	0	42
NDI	India	D	870	4	30508	1508	7910
DJA	Indonesia	D	6298	0	310266	0	224173
TEH	Iran	D	1325	0	26792	0	9237
THR	Iran	D	77	0	1926	0	696
ISN	Iraq	D	164	0	1774	0	575
SLUB	Iraq	D	3	0	39	49	0
DIAS	Ireland	D	0	0	0	1225	0
GII	Israel	D	2999	0	62175	1	0
GEN	Italy	D	982	0	25204	16	0
MED_RCMT	Italy	D	0	63	0	0	0
OGS	Italy	D	449	0	9285	11388	0
RISSC	Italy	D	9	0	194	0	0
ROM	Italy	D	8363	93	756227	256060	511358
SARA	Italy	D	487	0	4286	0	0
JSN	Jamaica	D	218	0	1927	0	0
JMA	Japan	D	124852	12883	832965	0	17703
NIED	Japan	D	0	809	0	0	0
SYO	Japan	D	0	0	0	702	0
JSO	Jordan	D	1306	2	23778	0	19421
NNC	Kazakhstan	D	8607	0	77831	0	71518
SOME	Kazakhstan	D	3500	146	43306	571	36052
KNET	Kyrgyzstan	D	984	0	7519	0	2920
KRNET	Kyrgyzstan	D	680	0	11178	0	0
LVSN	Latvia	D	90	0	387	0	226
GRAL	Lebanon	D	121	0	1159	936	0
LIT	Lithuania	D	846	847	4614	536	0
MCO	Macao, China	D	0	0	0	22	0
TAN	Madagascar	D	788	1	8259	2	0
GSDM	Malawi	D	0	0	0	185	0
ECX	Mexico	D	1146	0	31000	2	5565
MEX	Mexico	D	13924	151	215262	8	79
PDG	Montenegro	D	774	0	14816	34	6872
CNRM	Morocco	D	6214	0	64835	0	0
NAM	Namibia	D	80	0	1000	0	282
DMN	Nepal	D	1905	0	15459	22	14884
DBN	Netherlands	D	51	1	1317	0	0
WEL	New Zealand	D	10391	79	586562	72342	249070
CATAC	Nicaragua	D	2808	111	107931	1011	0
SKO	North Macedonia	D	0	939	0	8850	2759
BER	Norway	D	3034	1620	56655	4942	9496
NAO	Norway	D	2448	986	7014	0	2245
OMAN	Oman	D	719	0	31367	0	0
UPA	Panama	D	611	0	13496	38	8
ARE	Peru	I RSNC	8	0	257	0	0
MAN	Philippines	D	39	317	4671	24541	1674
QCP	Philippines	D	0	0	0	149	0

Table 7.2: (continued)

Agency	Country	Directly or indirectly reporting (D/I)	Hypocentres with associated phases	Hypocentres without associated phases	Associated phases	Unassociated phases	Amplitudes
PJWWP	Poland	D	114	4	242	2	11
WAR	Poland	D	0	0	0	5892	233
IGIL	Portugal	D	866	70	3123	0	961
INMG	Portugal	D	2707	0	116310	3713	54284
PDA	Portugal	I SVSA	1	0	0	0	0
SVSA	Portugal	D	1465	0	49252	766	29580
BELR	Republic of Belarus	D	0	0	0	25394	7760
CFUSG	Republic of Crimea	D	88	0	2159	20	1308
KMA	Republic of Korea	D	7	0	155	0	0
BUC	Romania	D	426	0	16038	109160	5114
ASGSR	Russia	D	105	5088	4280	0	1287
BYKL	Russia	D	200	0	13960	0	5282
DAGSR	Russia	I MOS	211	168	0	0	0
FCIAR	Russia	D	105	1	1306	104	263
IDG	Russia	I MOS	0	65	0	0	0
IGKR	Russia	I MOS	0	1	0	0	0
KMGSR	Russia	I MOS	0	3	0	0	0
KOGSR	Russia	D	2592	191	19509	28	0
KRSC	Russia	D	466	0	17038	0	0
MIRAS	Russia	D	354	0	4447	0	3651
MOS	Russia	D	2544	6088	278112	0	94934
NEGSR	Russia	I MOS	0	141	0	0	0
NERS	Russia	D	119	0	2180	0	1061
NOGSR	Russia	I MOS	101	127	0	0	0
OBGSR	Russia	I MOS	0	95	0	0	0
SAGSR	Russia	I MOS	0	22	0	0	0
SKHL	Russia	D	1082	1142	21968	2	8797
YAGSR	Russia	I MOS	0	196	0	0	0
YARS	Russia	D	256	1	5172	0	3373
BEO	Serbia	D	1089	0	28489	0	0
BRA	Slovakia	D	5140	0	21449	0	2752
LJU	Slovenia	D	1381	0	17847	3539	6291
PRE	South Africa	D	1903	0	29741	6	8616
MDD	Spain	D	6058	38	143341	0	41063
MRB	Spain	D	1318	0	52400	0	14658
SFS	Spain	D	1032	0	27008	19	0
UPP	Sweden	D	1822	1040	27338	0	0
ZUR	Switzerland	D	468	1	15824	0	6159
BKK	Thailand	D	396	10	5901	0	6165
TRN	Trinidad and Tobago	D	1945	0	34095	35868	0
TUN	Tunisia	D	40	0	233	0	0
AFAD	Turkey	D	9318	0	275309	2	108734
ISK	Turkey	D	9638	0	218288	645	77408
AEIC	U.S.A.	I NEIC	2	3258	100914	0	0
BUT	U.S.A.	I NEIC	0	107	1703	0	0
CERI	U.S.A.	I NEIC	0	90	0	0	0
GCMT	U.S.A.	D	0	2544	0	0	0
HVO	U.S.A.	I NEIC	0	614	22146	0	0
IRIS	U.S.A.	I BGR	4	0	0	0	0
NCEDC	U.S.A.	I NEIC	0	305	26073	0	0
NEIC	U.S.A.	D	21607	8675	1694426	29	851849
PAS	U.S.A.	I NEIC	0	229	21800	0	0
PNSN	U.S.A.	D	0	106	0	0	0
PTWC	U.S.A.	D	177	0	2817	0	0
REN	U.S.A.	I NEIC	0	131	3651	0	0
RSPR	U.S.A.	D	2380	305	45218	0	0
SEA	U.S.A.	I NEIC	0	37	1939	0	0
SLM	U.S.A.	I NEIC	0	0	1114	0	0
TXNET	U.S.A.	D	1315	0	62892	0	22300
UUSS	U.S.A.	I NEIC	0	43	662	0	0
MCSM	Ukraine	D	849	1	40186	20526	43719
SIGU	Ukraine	D	27	27	732	0	292
DSN	United Arab Emirates	D	605	0	8376	0	0

Table 7.2: (continued)

Agency	Country	Directly or indirectly reporting (D/I)	Hypocentres with associated phases	Hypocentres without associated phases	Associated phases	Unassociated phases	Amplitudes
BGS	United Kingdom	D	385	37	13215	2	5862
ISC-PPSM	United Kingdom	D	0	63	0	0	0
EAF	Unknown	D	422	12	3307	6574	2020
ISC-EHB	Unknown	D	0	4363	0	0	0
ISU	Uzbekistan	D	931	0	9352	0	0
FUNV	Venezuela	D	693	2	7137	0	0
BUL	Zimbabwe	D	146	5	997	256	0

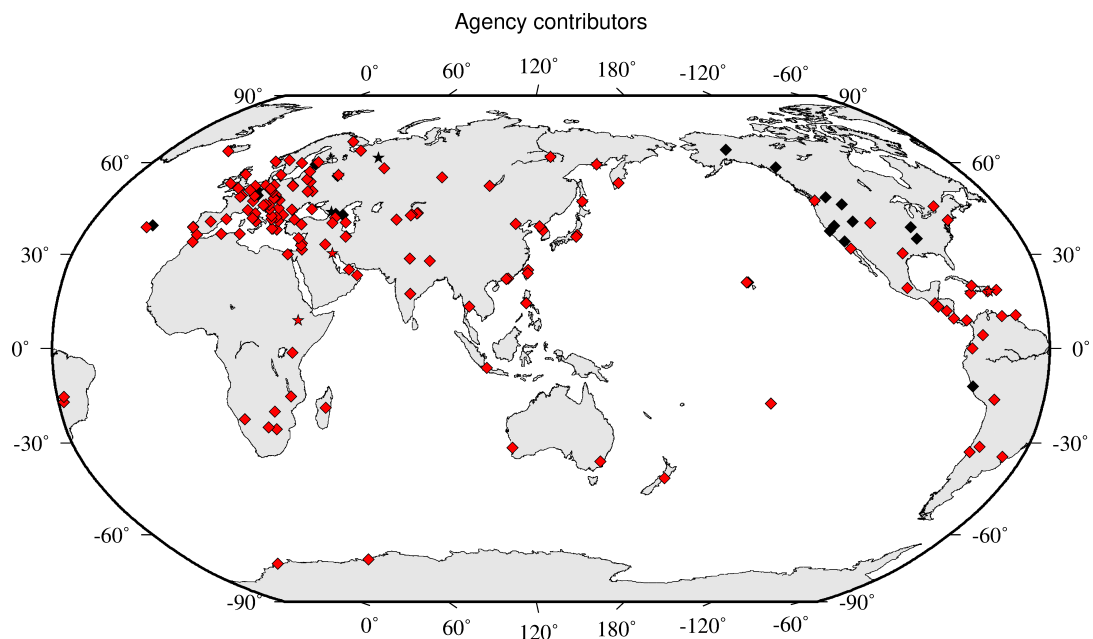


Figure 7.1: Map of agencies that have contributed data to the ISC for this summary period. Agencies that have reported directly to the ISC are shown in red. Those that have reported indirectly (via another agency) are shown in black. Any new or renewed agencies, since the last six-month period, are shown by a star. Each agency is listed in Table 7.2.

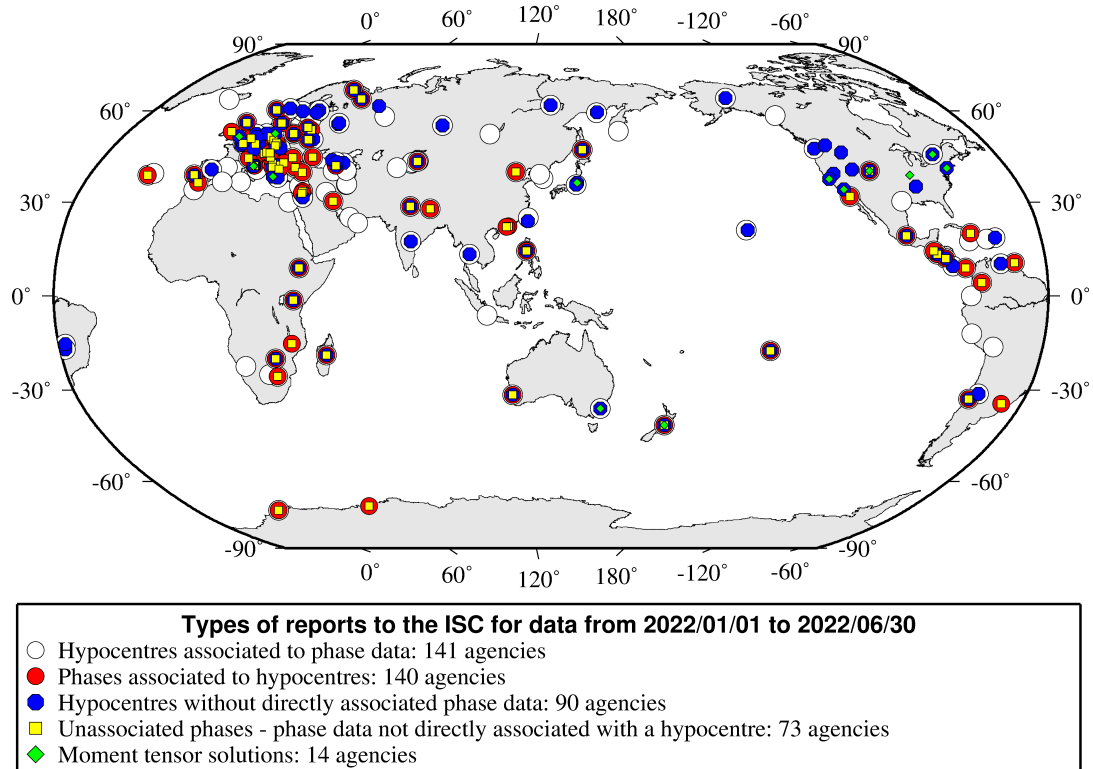


Figure 7.2: Map of the different data types reported by agencies to the ISC. A full list of the data types reported by each agency is shown in Table 7.2.

7.3 Arrival Observations

The collection of phase arrival observations at the ISC has increased dramatically with time. The increase in reported phase arrival observations is shown in Figure 7.3.

The reports with phase data are summarised in Table 7.3. This table is split into three sections, providing information on the reports themselves, the phase data, and the stations reporting the phase data. A map of the stations contributing these phase data is shown in Figure 7.4.

The ISC encourages the reporting of phase arrival times together with amplitude and period measurements whenever feasible. Figure 7.5 shows the percentage of events for which phase arrival times from each station are accompanied with amplitude and period measurements.

Figure 7.6 indicates the number of amplitude and period measurement for each station.

Together with the increase in the number of phases (Figure 7.3), there has been an increase in the number of stations reported to the ISC. The increase in the number of stations is shown in Figure 7.7. This increase can also be seen on the maps for stations reported each decade in Figure 7.8.

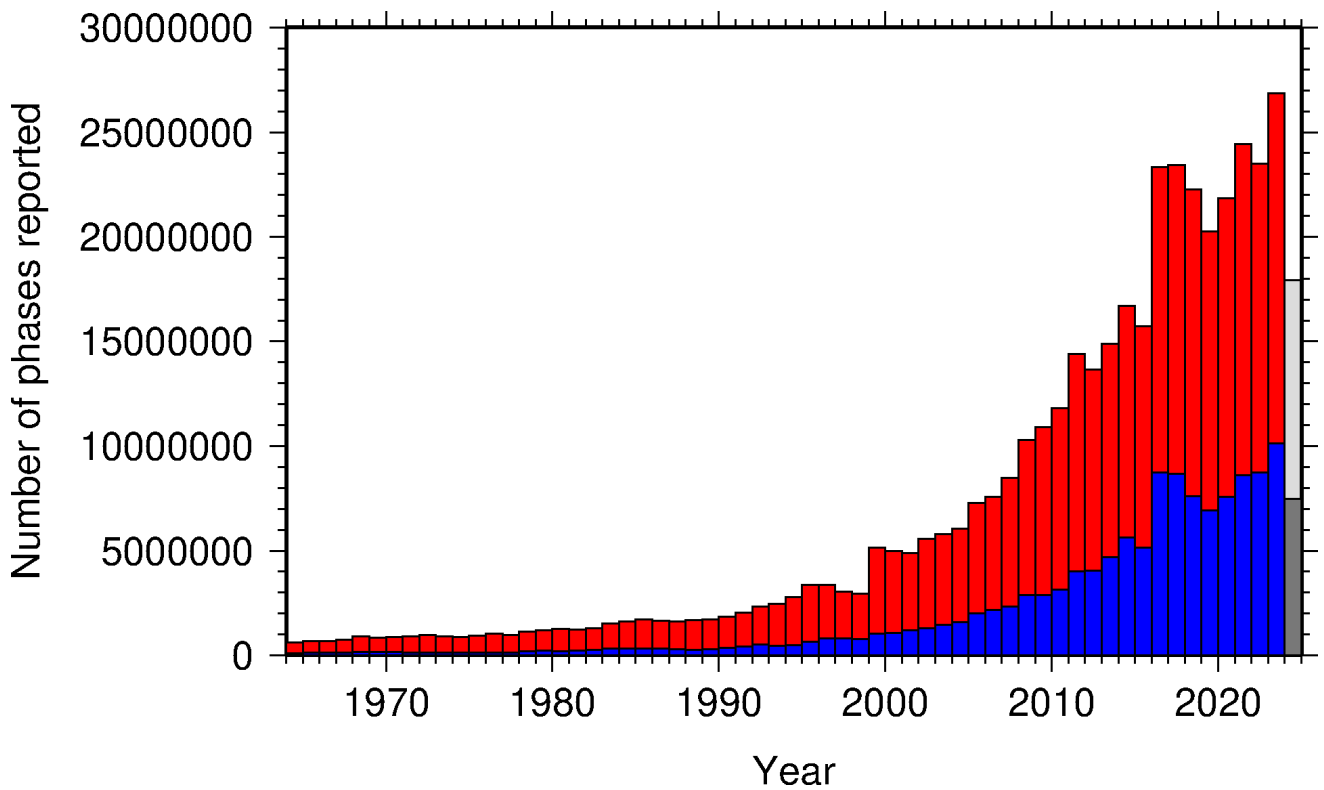


Figure 7.3: Histogram showing the number of phases (red) and number of amplitudes (blue) collected by the ISC for events each year since 1964. The data in grey covers the current period where data are still being collected before the ISC review takes place and is accurate at the time of publication.

Table 7.3: Summary of reports containing phase arrival observations.

Reports with phase arrivals	10099
Reports with phase arrivals including amplitudes	7080
Reports with only phase arrivals (no hypocentres reported)	169
Total phase arrivals received	11359072
Total phase arrival-times received	10102035
Number of duplicate phase arrival-times	779991 (7.7%)
Number of amplitudes received	4362526
Stations reporting phase arrivals	13723
Stations reporting phase arrivals with amplitude data	7569
Max number of stations per report	2939

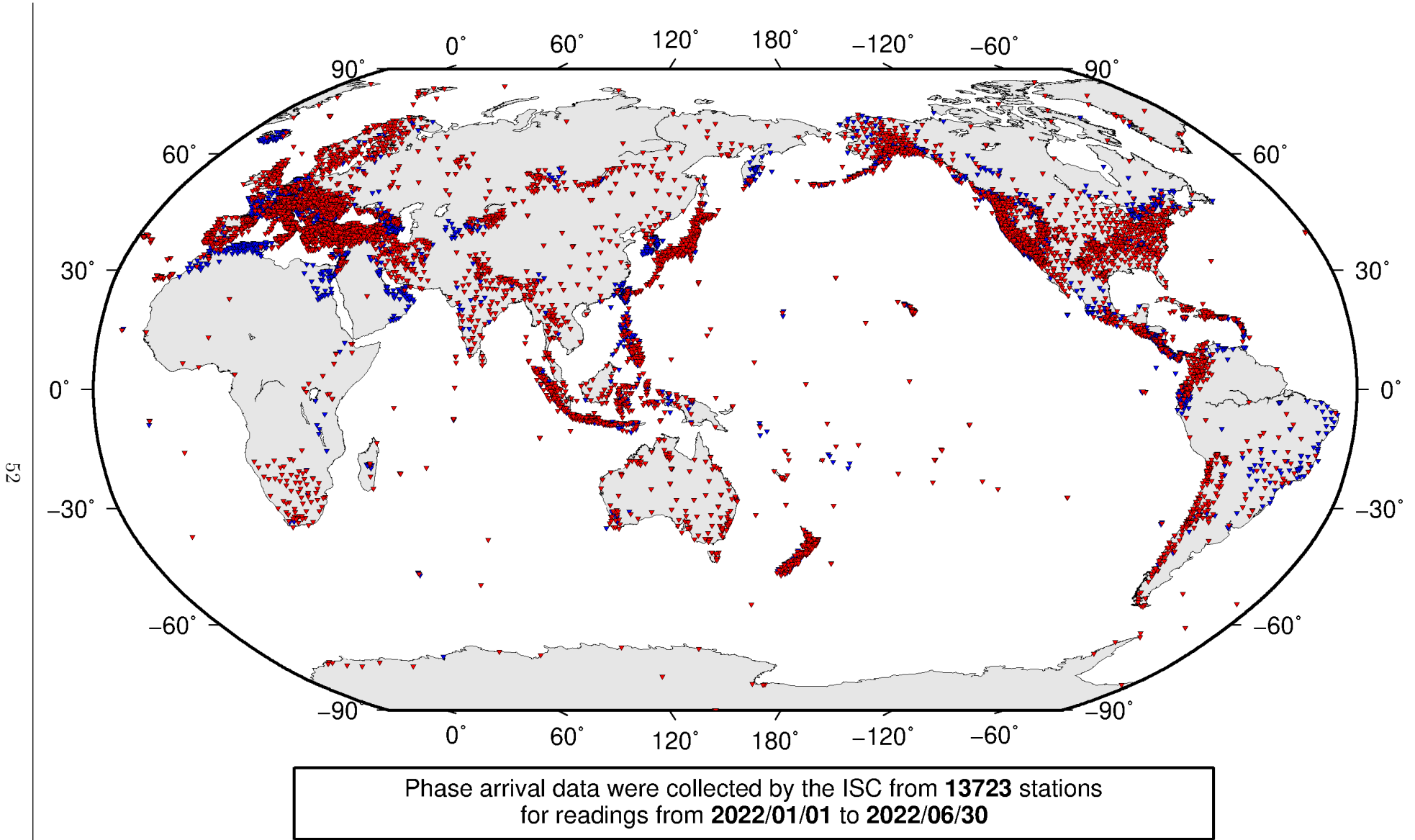


Figure 7.4: Stations contributing phase data to the ISC for readings from January 2022 to the end of June 2022. Stations in blue provided phase arrival times only; stations in red provided both phase arrival times and amplitude data.

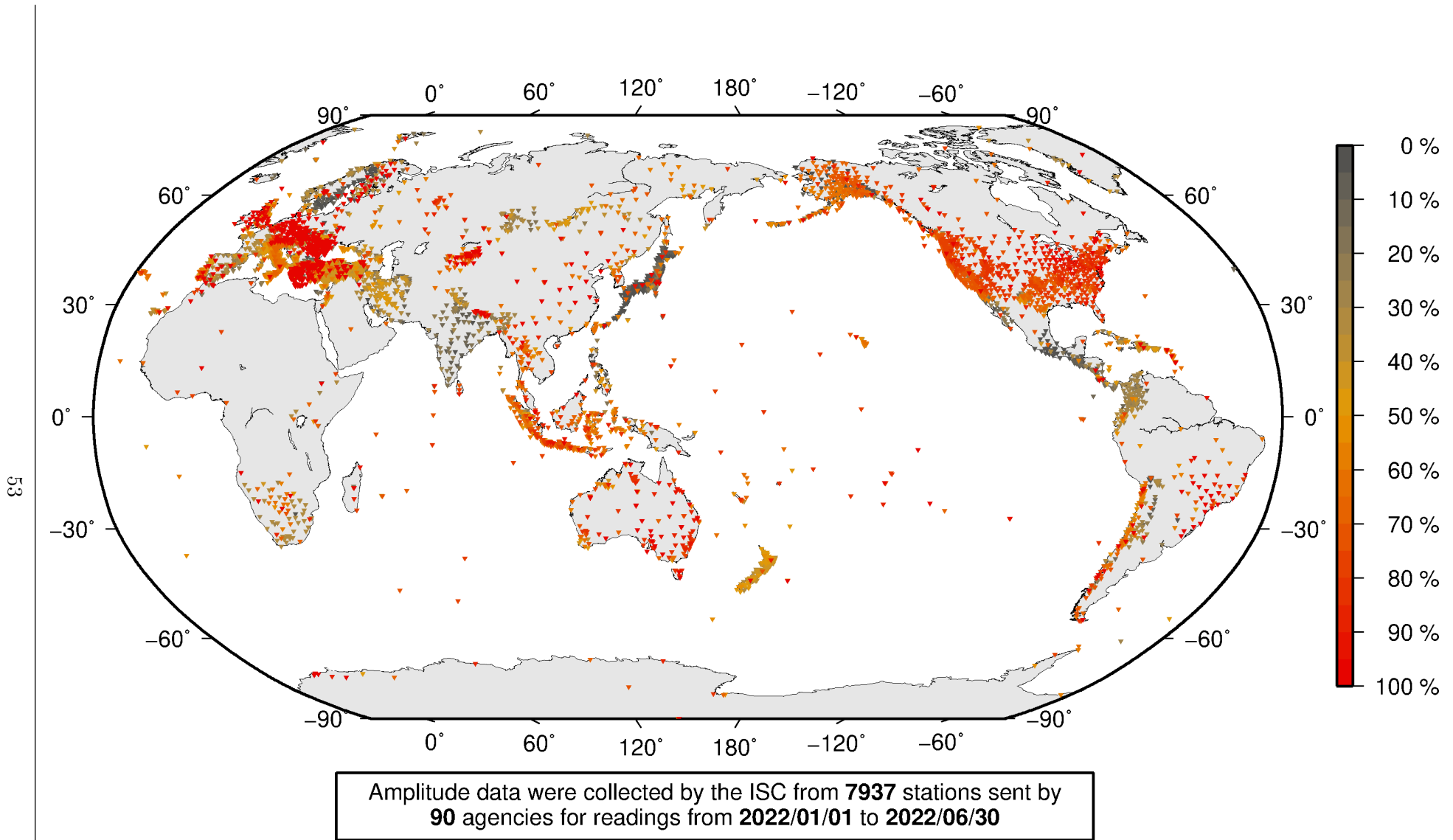
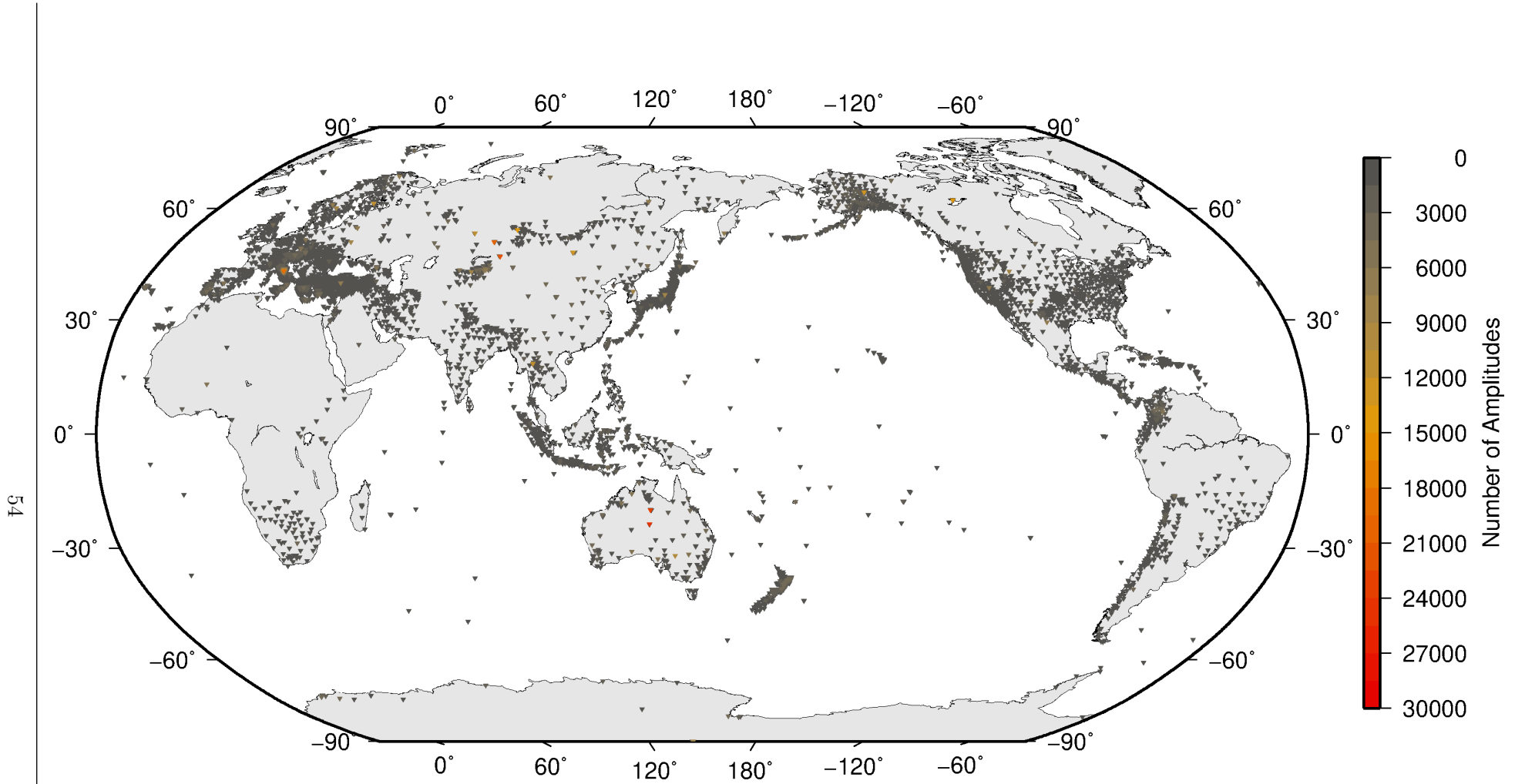


Figure 7.5: Percentage of events for which phase arrival times from each station are accompanied with amplitude and period measurements.



Amplitude data were collected by the ISC from **7937** stations sent by **90** agencies for readings from **2022/01/01** to **2022/06/30**

Figure 7.6: Number of amplitude and period measurements for each station.

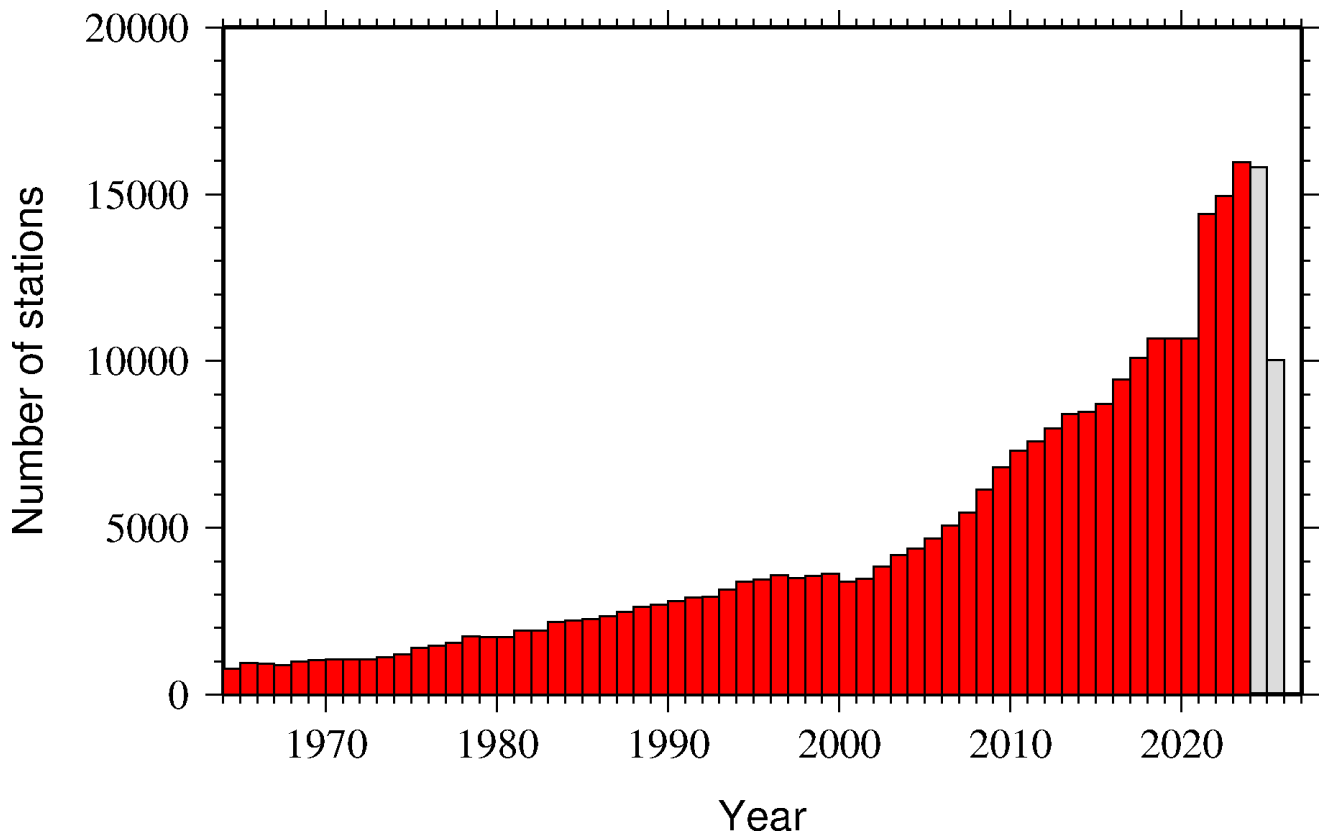


Figure 7.7: Histogram showing the number of stations reporting to the ISC each year since 1964. The data in grey covers the current period where station information is still being collected before the ISC review of events takes place and is accurate at the time of publication.

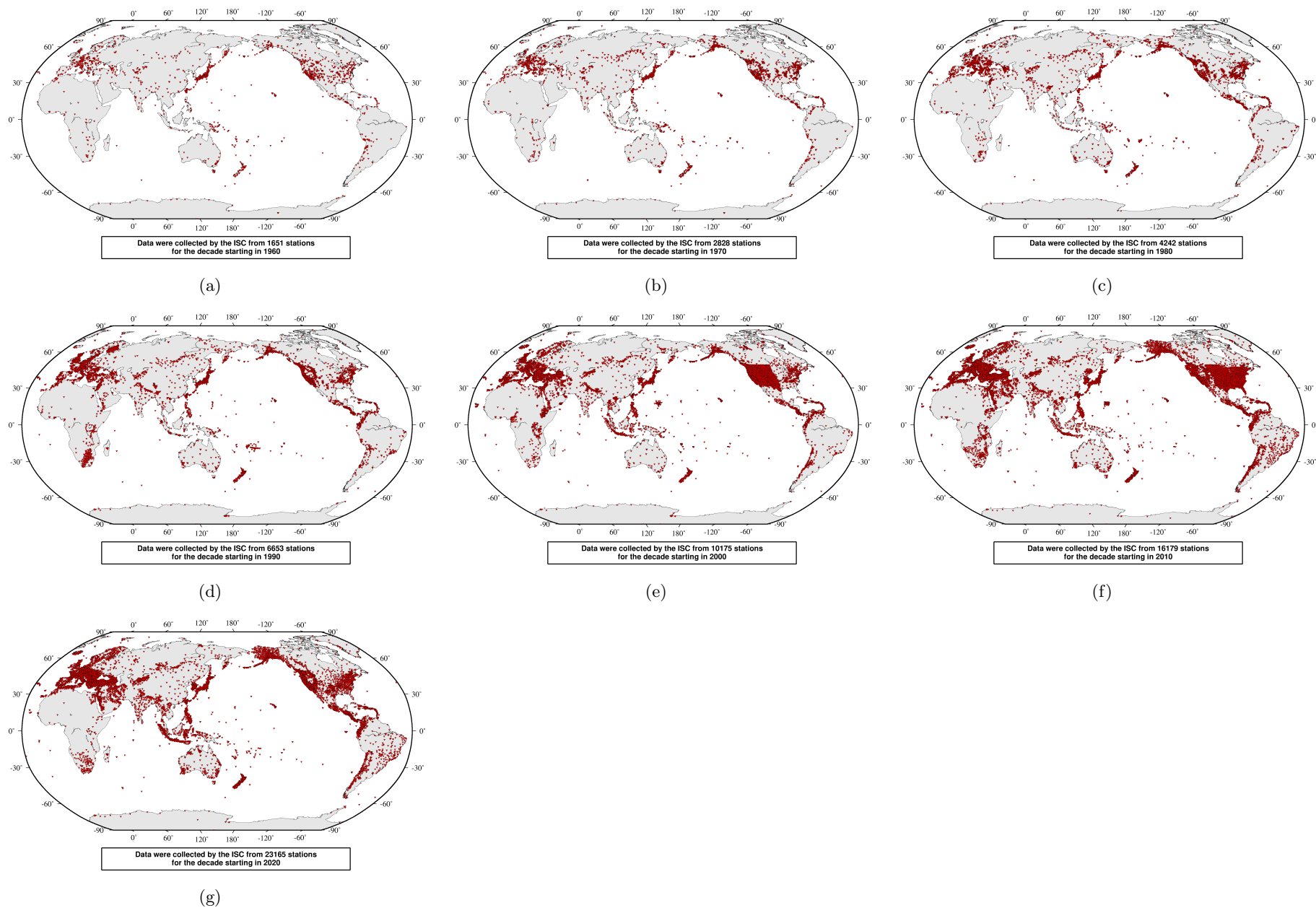


Figure 7.8: Maps showing the stations reported to the ISC for each decade since 1960. Note that the last map covers a shorter time period.

7.4 Hypocentres Collected

The ISC Bulletin groups multiple estimates of hypocentres into individual events, with an appropriate prime hypocentre solution selected. The collection of these hypocentre estimates are described in this section.

The reports containing hypocentres are summarised in Table 7.4. The number of hypocentres collected by the ISC has also increased significantly since 1964, as shown in Figure 7.9. A map of all hypocentres reported to the ISC for this summary period is shown in Figure 7.10. Where a network magnitude was reported with the hypocentre, this is also shown on the map, with preference given to reported values, first of M_W followed by M_S , m_b and M_L respectively (where more than one network magnitude was reported).

Table 7.4: Summary of the reports containing hypocentres.

Reports with hypocentres	10333
Reports of hypocentres only (no phase readings)	403
Total hypocentres received	461164
Number of duplicate hypocentres	10140 (2.2%)
Agencies determining hypocentres	166

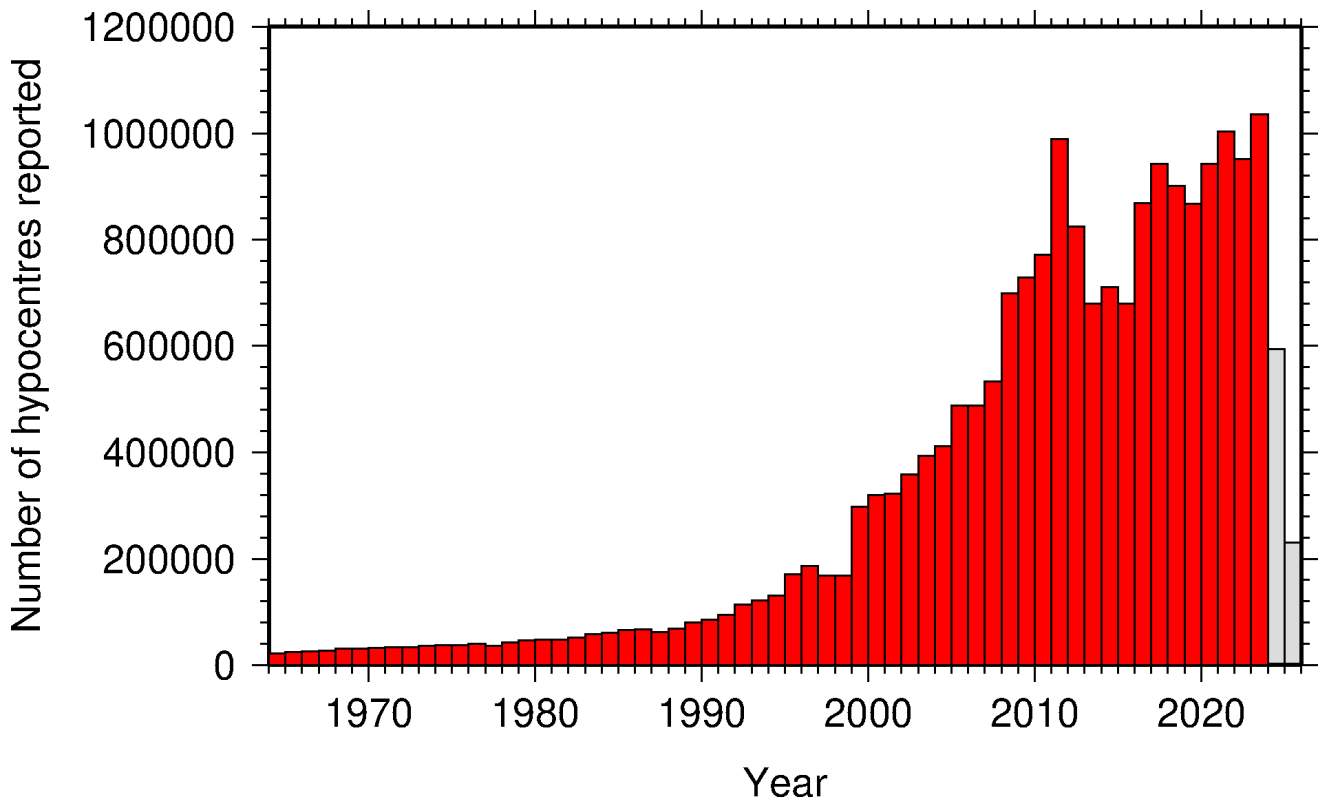


Figure 7.9: Histogram showing the number of hypocentres collected by the ISC for events each year since 1964. For each event, multiple hypocentres may be reported.

All the hypocentres that are reported to the ISC are automatically grouped into events, which form the basis of the ISC Bulletin. For this summary period 484,127 hypocentres (including ISC) were grouped into 334,144 events, the largest of these having 59 hypocentres in one event. The total number of events

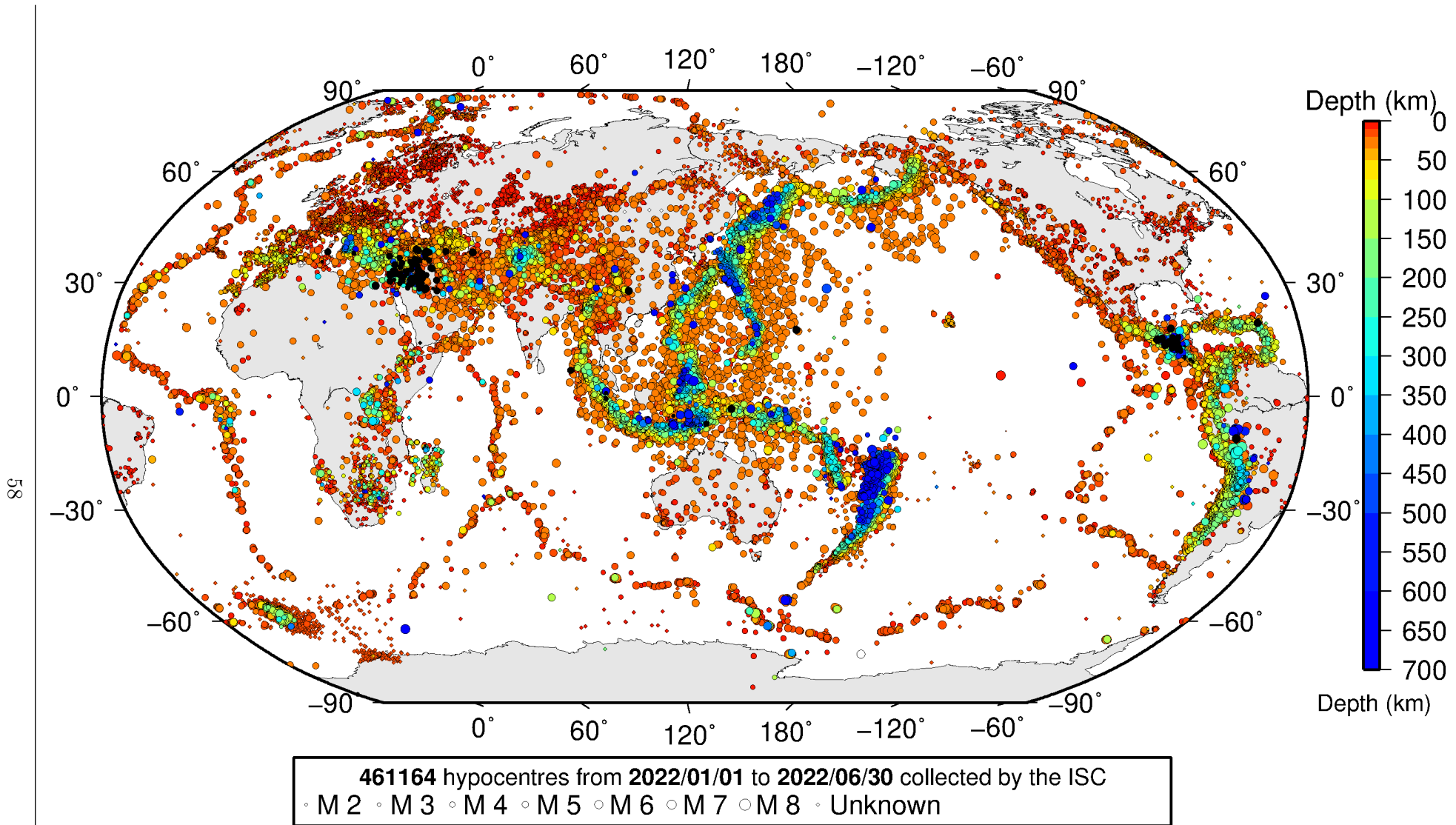


Figure 7.10: Map of all hypocenters collected by the ISC. The scatter shows the large variation of the multiple hypocenters that are reported for each event. The magnitude corresponds with the reported network magnitude. If more than one network magnitude type was reported, preference was given to values of M_W , M_S , m_b and M_L respectively. Compare with Figure 8.2

shown here is the result of an automatic grouping algorithm, and will differ from the total events in the published ISC Bulletin, where both the number of events and the number of hypocentre estimates will have changed due to further analysis. The process of grouping is detailed in Section 10.1.3. Figure 8.2 on page 72 shows a map of all prime hypocentres.

7.5 Collection of Network Magnitude Data

Data contributing agencies normally report earthquake hypocentre solutions along with magnitude estimates. For each seismic event, each agency may report one or more magnitudes of the same or different types. This stems from variability in observational practices at regional, national and global level in computing magnitudes based on a multitude of wave types. Differences in the amplitude measurement algorithm, seismogram component(s) used, frequency range, station distance range as well as the instrument type contribute to the diversity of magnitude types. Table 7.5 provides an overview of the complexity of reported network magnitudes reported for seismic events during the summary period.

Table 7.5: Statistics of magnitude reports to the ISC; M – average magnitude of estimates reported for each event.

	$M < 3.0$	$3.0 \leq M < 5.0$	$M \geq 5.0$
Number of seismic events	263624	45163	699
Average number of magnitude estimates per event	1.3	3.3	22.0
Average number of magnitudes (by the same agency) per event	1.2	2.0	3.1
Average number of magnitude types per event	1.2	2.6	12.3
Number of magnitude types	34	42	38

Table 7.6 gives the basic description, main features and scientific paper references for the most commonly reported magnitude types.

Table 7.6: Description of the most common magnitude types reported to the ISC.

Magnitude type	Description	References	Comments
M	Unspecified		Often used in real or near-real time magnitude estimations
mB	Medium-period and Broad-band body-wave magnitude	<i>Gutenberg</i> (1945a); <i>Gutenberg</i> (1945b); <i>IASPEI</i> (2005); <i>IASPEI</i> (2013); <i>Bormann et al.</i> (2009); <i>Bormann and Dewey</i> (2012)	
mb	Short-period body-wave magnitude	<i>IASPEI</i> (2005); <i>IASPEI</i> (2013); <i>Bormann et al.</i> (2009); <i>Bormann and Dewey</i> (2012)	Classical mb based on stations between 21°-100° distance

Table 7.6: continued

Magnitude type	Description	References	Comments
mb1	Short-period body-wave magnitude	<i>IDC</i> (1999) and references therein	Reported only by the IDC; also includes stations at distances less than 21°
mb1mx	Maximum likelihood short-period body-wave magnitude	<i>Ringdal</i> (1976); <i>IDC</i> (1999) and references therein	Reported only by the IDC
mbtmp	short-period body-wave magnitude with depth fixed at the surface	<i>IDC</i> (1999) and references therein	Reported only by the IDC
mbLg	Lg-wave magnitude	<i>Nuttli</i> (1973); <i>IASPEI</i> (2005); <i>IASPEI</i> (2013); <i>Bormann and Dewey</i> (2012)	Also reported as MN
Mc	Coda magnitude		
MD (Md)	Duration magnitude	<i>Bisztricsany</i> (1958); <i>Lee et al.</i> (1972)	
ME (Me)	Energy magnitude	<i>Choy and Boatwright</i> (1995)	Reported only by NEIC
MJMA	JMA magnitude	<i>Tsuboi</i> (1954)	Reported only by JMA
ML (MI)	Local (Richter) magnitude	<i>Richter</i> (1935); <i>Hutton and Boore</i> (1987); <i>IASPEI</i> (2005); <i>IASPEI</i> (2013)	
MLSn	Local magnitude calculated for Sn phases	<i>Balfour et al.</i> (2008)	Reported by PGC only for earthquakes west of the Cascadia subduction zone
MLv	Local (Richter) magnitude computed from the vertical component		Reported only by DJA and BKK
MN (Mn)	Lg-wave magnitude	<i>Nuttli</i> (1973); <i>IASPEI</i> (2005)	Also reported as mbLg
MS (Ms)	Surface-wave magnitude	<i>Gutenberg</i> (1945c); <i>Vaněk et al.</i> (1962); <i>IASPEI</i> (2005)	Classical surface-wave magnitude computed from station between 20°-160° distance
Ms1	Surface-wave magnitude	<i>IDC</i> (1999) and references therein	Reported only by the IDC; also includes stations at distances less than 20°
ms1mx	Maximum likelihood surface-wave magnitude	<i>Ringdal</i> (1976); <i>IDC</i> (1999) and references therein	Reported only by the IDC

Table 7.6: *continued*

Magnitude type	Description	References	Comments
Ms7	Surface-wave magnitude	<i>Bormann et al. (2007)</i>	Reported only by BJI and computed from records of a Chinese-made long-period seismograph in the distance range 3°-177°
MW (Mw)	Moment magnitude	<i>Kanamori (1977); Dziewonski et al. (1981)</i>	Computed according to the <i>IASPEI (2005)</i> and <i>IASPEI (2013)</i> standard formula
Mw(mB)	Proxy Mw based on mB	<i>Bormann and Saul (2008)</i>	Reported only by DJA and BKK
Mwp	Moment magnitude from P-waves	<i>Tsuboi et al. (1995)</i>	Reported only by DJA and BKK and used in rapid response
mbh	Unknown		
mbv	Unknown		
MG	Unspecified type		Contact contributor
Mm	Unknown		
msh	Unknown		
MSV	Unknown		

Table 7.7 lists all magnitude types reported, the corresponding number of events in the ISC Bulletin and the agency codes along with the number of earthquakes.

Table 7.7: *Summary of magnitude types in the ISC Bulletin for this summary period. The number of events with values for each magnitude type is listed. The agencies reporting these magnitude types are listed, together with the total number of values reported.*

Magnitude type	Events	Agencies reporting magnitude type (number of values)
MD	449	OGS (449)
M	19918	WEL (8297), MOS (5261), GFZ (2786), CATAC (2489), SNET (1571), OTT (357), BKK (341), IGQ (52), JSO (34), PRU (32), RSNC (27), OSUNB (10), INMG (5), TAN (2), GUC (1), RSPR (1)
M_mb	81	MDD (81)
mb	23602	IDC (16451), NEIC (8333), NNC (3904), GFZ (2789), VIE (2408), MOS (1281), DJA (1169), BJI (1149), KRNET (678), VAO (285), MAN (255), BGR (230), RSNC (203), AUST (175), OMAN (169), CATAC (131), BKK (118), MDD (84), CFUSG (67), MCSM (51), SFS (26), NDI (25), DSN (13), THE (11), PGC (9), SNET (6), INMG (5), OSUNB (5), PDG (5), YARS (5), CRAAG (4), OTT (4), PTWC (4), CNRM (4), DNK (4), BGS (3), IGIL (3), IGQ (2), DMN (2), GUC (1), AEIC (1), SSNC (1), ROM (1)
MB	175	NAO (104), SCB (61), SSNC (9), IPEC (1)

Table 7.7: Continued.

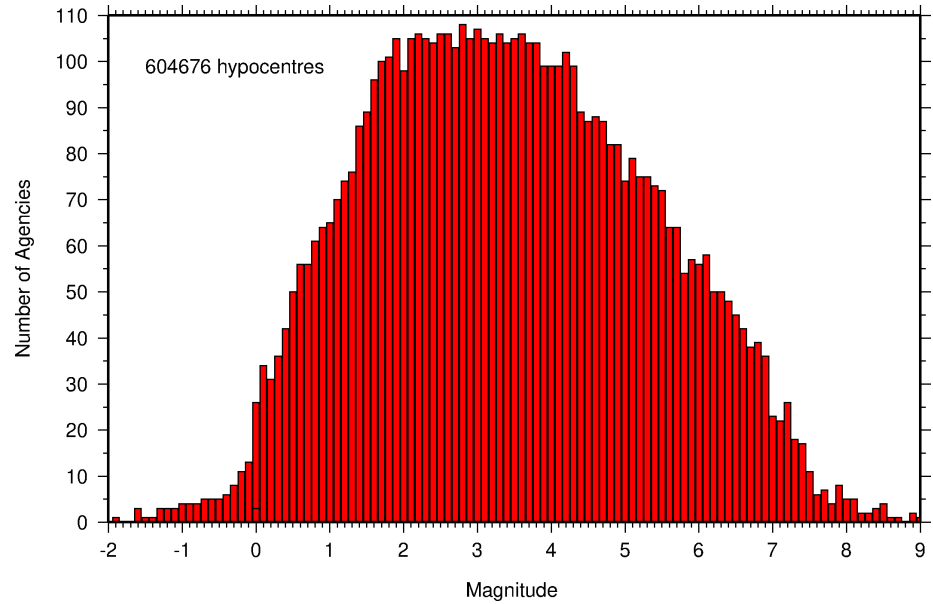
Magnitude type	Events	Agencies reporting magnitude type (number of values)
mB	2022	BJI (1124), DJA (679), WEL (288), GFZ (146), CATAAC (102), BKK (95), RSNC (38), OTT (3), OSUNB (3), SNET (2), SFS (2), IGQ (2)
mB_BB	23	BGR (23)
mb_Lg	6635	MDD (5962), NEIC (629), OTT (47)
mbR	119	VAO (119)
mbtmp	18101	IDC (18101)
Mc	15	KRSC (15)
MD	14518	RSPR (2646), SSNC (2624), LDG (2298), GCG (2266), TRN (1450), ECX (917), SDD (542), JMA (496), SOF (389), NCEDC (235), ROM (150), JSN (139), PDG (133), GRAL (120), MEX (111), PNSN (93), SLM (90), UPA (82), CFUSG (74), TUN (37), SIGU (27), HVO (17), STR (13), EAF (9), USSS (7), SNET (5), JSO (4), BUL (3), GII (3), DNK (2), HLW (2), AFAD (2), NDI (1), BUT (1), SEA (1), SJA (1)
Me	15	GFZ (14), PAS (1)
Mjma	5312	DJA (4193), SNET (1211), BKK (343), IGQ (40), RSNC (3), JSO (1)
ML	128930	ATH (11423), RSNC (11323), IDC (10311), ISK (9634), AFAD (9140), WEL (9044), ROM (7996), TAP (7377), HEL (6434), NEIC (6086), CNRM (5885), GUC (4894), VIE (4314), AZER (4209), AEIC (3303), INMG (3098), SSNC (2688), UPP (2618), KOGSR (2527), PRE (1880), LDG (1764), SFS (1648), OSPL (1571), RHSSO (1551), BER (1473), TEH (1324), MRB (1318), TXNET (1315), DNK (1217), TIR (1166), CATAAC (1160), LJU (1116), BEO (1087), ECX (1068), SJA (983), KRSZO (964), SCB (954), PGC (949), GEN (940), SKO (922), BRA (866), PDG (733), TAN (645), NIC (605), HVO (597), IGIL (560), SDD (542), SARA (480), KRSC (465), AUST (446), BUC (425), IPEC (411), MIRAS (354), OMAN (353), NDI (326), BGSi (320), MAN (316), DSN (305), GCG (304), UCC (304), BKK (299), NAO (276), YARS (257), CRAAG (257), KNET (248), BJI (221), PAS (213), EAF (189), BGS (182), PPT (168), ISN (163), REN (124), BUT (106), TIF (101), BGR (87), LVSN (87), WBNET (86), THR (77), SKHL (73), AAE (66), NAM (61), SEA (58), CUPWA (55), NCEDC (50), GFZ (44), HLW (41), KEA (40), SNET (40), USSS (36), BNS (24), JSO (23), PTWC (23), OTT (20), IGQ (18), DJA (16), SIGU (13), RISSC (9), DMN (6), UPA (5), VAO (5), RSPR (4), STR (2), BUL (1), CLL (1)
MLh	2834	THE (2726), ASGSR (105), RSNC (3)
MLhc	431	ZUR (431)
MLidc	1	SNET (1)
MLn	19	DBN (19)
MLna	3	DBN (3)
MLs	24	DBN (24)
MLSn	231	PGC (231)

Table 7.7: Continued.

Magnitude type	Events	Agencies reporting magnitude type (number of values)
ML _v	28426	WEL (9752), STR (6105), DJA (5111), CATAC (2492), RSNC (2206), SNET (1576), SFS (827), JSO (725), BKK (371), OTT (341), IGQ (107), MCSM (50), GFZ (15), OSUNB (7)
MN	344	OTT (344)
mpv	4295	NNC (4295)
MPVA	262	NOGSR (226), MOS (157)
mR	147	OSUNB (147)
MS	8175	IDC (7993), BJI (892), MOS (406), MAN (314), BGR (135), NSSP (61), GCMT (36), VIE (32), OMAN (19), KEA (17), SOME (14), DSN (9), DNK (7), INMG (5), SSNC (1), GUC (1), NDI (1), YARS (1), BGS (1), IPEC (1)
Ms(BB)	40	IGQ (33), SNET (4), RSNC (2), BKK (1)
Ms7	889	BJI (889)
Ms_20	194	NEIC (194)
MsBB	17	OTT (17)
MSH	97	CFUSG (82), SIGU (25)
MV	132173	JMA (132173)
MW	6526	GCMT (1272), SJA (977), NIED (809), GFZ (593), FUNV (535), SDD (508), UPA (507), BER (507), UCR (445), TIR (417), PGC (234), DJA (172), AFAD (169), IPGP (121), SSNC (103), JMA (90), WEL (76), AAE (71), ASIES (68), MED_RCMT (63), NDI (46), JSN (39), GCG (37), ROM (16), PRE (5), MEX (5), OSUNB (4), ECX (4), RSNC (3), AUST (1), UPSL (1)
Mw(mB)	595	WEL (280), GFZ (125), CATAC (100), BKK (92), SNET (2), SFS (2), IGQ (2)
Mwb	176	NEIC (176)
Mwc	10	NEIC (10)
MwMwp	56	CATAC (26), GFZ (18), BKK (12), IGQ (1)
Mwp	785	SARA (480), DJA (150), PTWC (147), GFZ (66), CATAC (26), BKK (13), OMAN (9), RSNC (3), THE (2), NEIC (1), ROM (1), IGQ (1)
Mwr	321	NEIC (239), GUC (106), NCEDC (20), PAS (16), SLM (11), REN (7), OTT (5)
Mws	595	GII (595)
Mww	644	NEIC (644), GUC (8)

The most commonly reported magnitude types are short-period body-wave, surface-wave, local (or Richter), moment, duration and JMA magnitude type. For a given earthquake, the number and type of reported magnitudes greatly vary depending on its size and location. The large earthquake of October 25, 2010 gives an example of the multitude of reported magnitude types for large earthquakes (Listing 7.1). Different magnitude estimates come from global monitoring agencies such as the IDC, NEIC and GCMT, a local agency (GUC) and other agencies, such as MOS and BJI, providing estimates based on

Figure 7.11: Histogram showing the number of agencies that reported network magnitude values. All magnitude types are included.



7.6 Moment Tensor Solutions

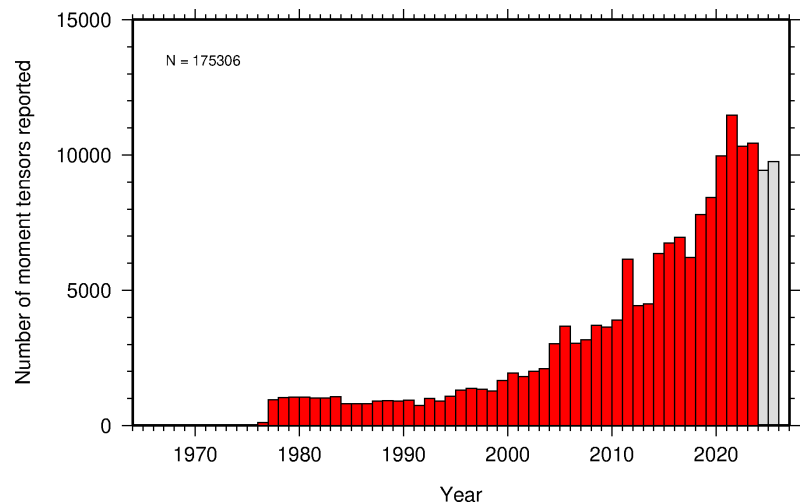
The ISC Bulletin publishes moment tensor solutions, which are reported to the ISC by other agencies. The collection of moment tensor solutions is summarised in Table 7.8. A histogram showing all moment tensor solutions collected throughout the ISC history is shown in Figure 7.12. Several moment tensor solutions from different authors and different moment tensor solutions calculated by different methods from the same agency may be present for the same event.

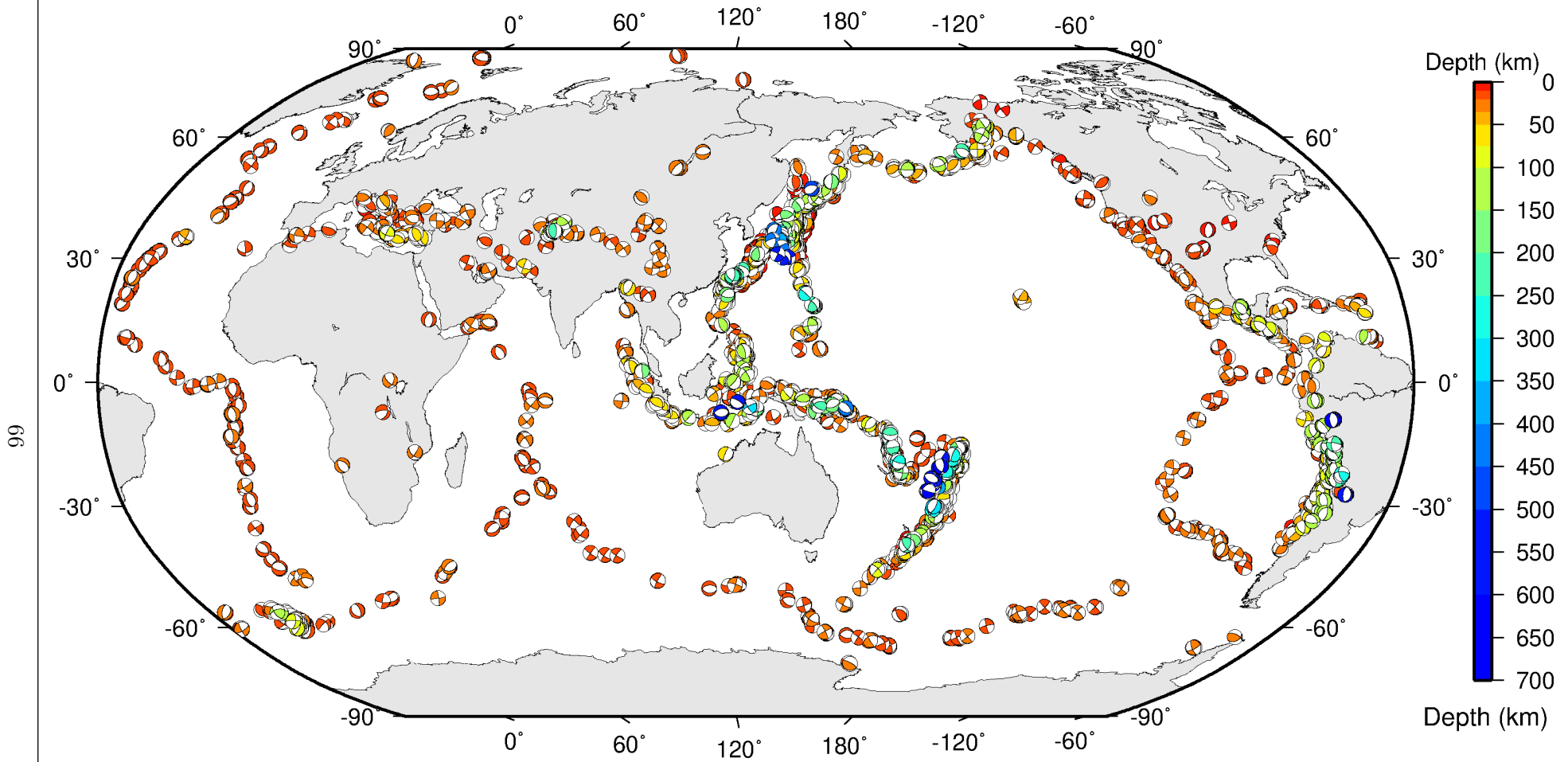
Table 7.8: Summary of reports containing moment tensor solutions.

Reports with Moment Tensors	2073
Total moment tensors received	10060
Agencies reporting moment tensors	14

The number of moment tensors for this summary period, reported by each agency, is shown in Table 7.9. The moment tensor solutions are plotted in Figure 7.13.

Figure 7.12: Histogram showing the number of moment tensors reported to the ISC since 1964. The regions in grey represent data that are still being actively collected.





ISC Bulletin: **3673** focal mechanism solutions for **2267** events from **2022/01/01** to **2022/06/30**

Figure 7.13: Map of all moment tensor solutions in the ISC Bulletin for this summary period.

Table 7.9: Summary of moment tensor solutions in the ISC Bulletin reported by each agency.

Agency	Number of moment tensor solutions
GCMT	1272
NEIC	822
NIED	809
TAN	645
GFZ	527
IPGP	241
ASIES	136
MED_RCMT	126
PNSN	93
WEL	76
UNK	63
ISC-PPSM	63
UPA	26
UCR	21
ROM	14
SLM	11
GCG	10
MEX	8
JSN	8
NCEDC	7
MOS	6
OSPL	5
OTT	5
TIR	4
ECX	4
PAS	2
UPSL	1
AUST	1

7.7 Timing of Data Collection

Here we present the timing of reports to the ISC. Please note, this does not include provisional alerts, which are replaced at a later stage. Instead, it reflects the final data sent to the ISC. The absolute timing of all hypocentre reports, regardless of magnitude, is shown in Figure 7.14. In Figure 7.15 the reports are grouped into one of six categories - from within three days of an event origin time, to over one year. The histogram shows the distribution with magnitude (for hypocentres where a network magnitude was reported) for each category, whilst the map shows the geographic distribution of the reported hypocentres.

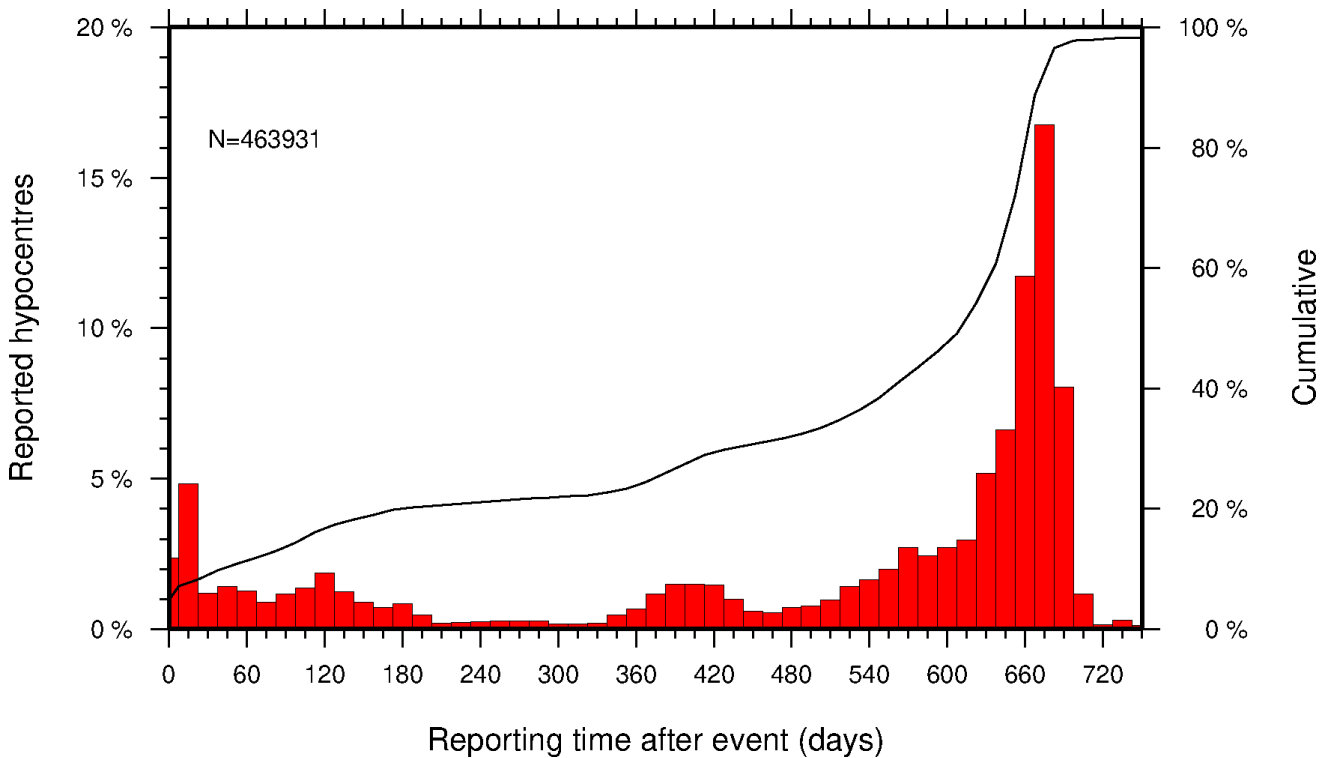


Figure 7.14: Histogram showing the timing of final reports of the hypocentres (total of N) to the ISC. The cumulative frequency is shown by the solid line.

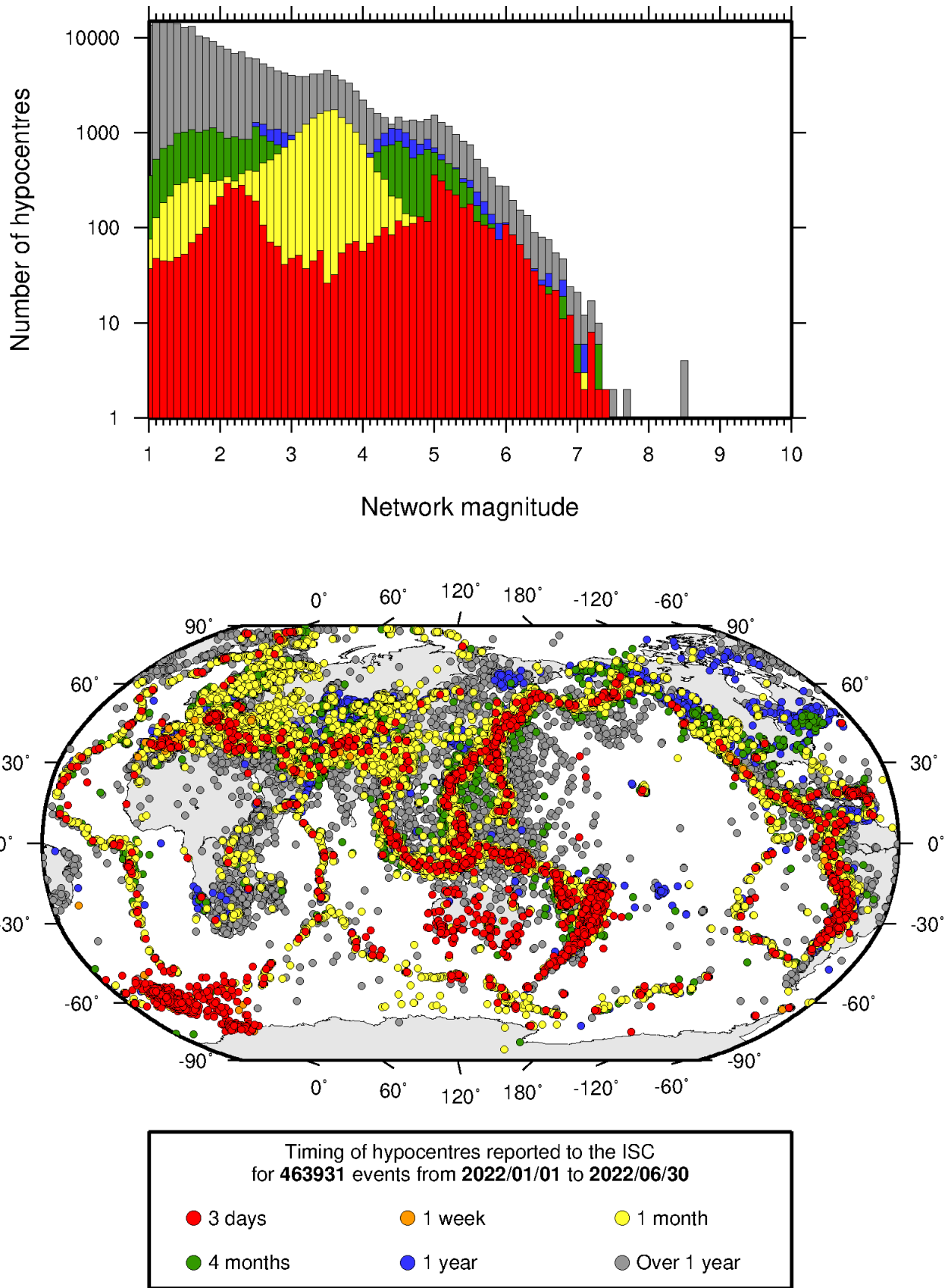


Figure 7.15: Timing of hypocentres reported to the ISC. The colours show the time after the origin time that the corresponding hypocentre was reported. The histogram shows the distribution with magnitude. If more than one network magnitude was reported, preference was given to a value of M_W followed by M_S , m_b and M_L respectively; all reported hypocentres are included on the map. Note: early reported hypocentres are plotted over later reported hypocentres, on both the map and histogram.

8

Overview of the ISC Bulletin

This chapter provides an overview of the seismic event data in the ISC Bulletin. We indicate the differences between all ISC events and those ISC events that are reviewed or located. We describe the wealth of phase arrivals and phase amplitudes and periods observed at seismic stations worldwide, reported in the ISC Bulletin and often used in the ISC location and magnitude determination. Finally, we make some comparisons of the ISC magnitudes with those reported by other agencies, and discuss magnitude completeness of the ISC Bulletin.

8.1 Events

The ISC Bulletin had 324,401 reported events in the summary period between January and June 2022. Some 90% (292,575) of the events were identified as earthquakes, the rest (10) were of anthropogenic origin (including mining and other chemical explosions, rockbursts and induced events) or of unknown origin. In this summary period 8% of the events were reviewed and 6% of the events were located by the ISC. For events that are not located by the ISC, the prime hypocentre is identified according to the rules described in Section 10.1.3.

Of the 11,668,561 reported phase observations, 36% are associated to ISC-reviewed events, and 35% are associated to events selected for ISC location. Note that all large events are reviewed and located by the ISC. Since large events are globally recorded and thus reported by stations worldwide, they will provide the bulk of observations. This explains why only a small percentage of the events in a month is reviewed although the number of phases associated to reviewed events has increased nearly exponentially in the past decades.

Figure 8.1 shows the daily number of events throughout the summary period. Figure 8.2 shows the locations of the events in the ISC Bulletin; the locations of ISC-reviewed and ISC-located events are shown in Figures 8.3 and 8.4, respectively.

Figure 8.5 shows the hypocentral depth distributions of events in the ISC Bulletin for the summary period. The vast majority of events occur in the Earth's crust. Note that the peaks at 0, 10, 35 km, and at every 50 km intervals deeper than 100 km are artifacts of analyst practices of fixing the depth to a nominal value when the depth cannot be reliably resolved.

Figure 8.6 shows the depth distribution of free-depth solutions in the ISC Bulletin. The depth of a hypocentre reported to the ISC is assumed to be determined as a free parameter, unless it is explicitly labelled as a fixed-depth solution. On the other hand, as described in Section 10.1.4, the ISC locator attempts to get a free-depth solution if, and only if, there is resolution for the depth in the data, i.e. if there is a local network and/or sufficient depth-sensitive phases are reported.

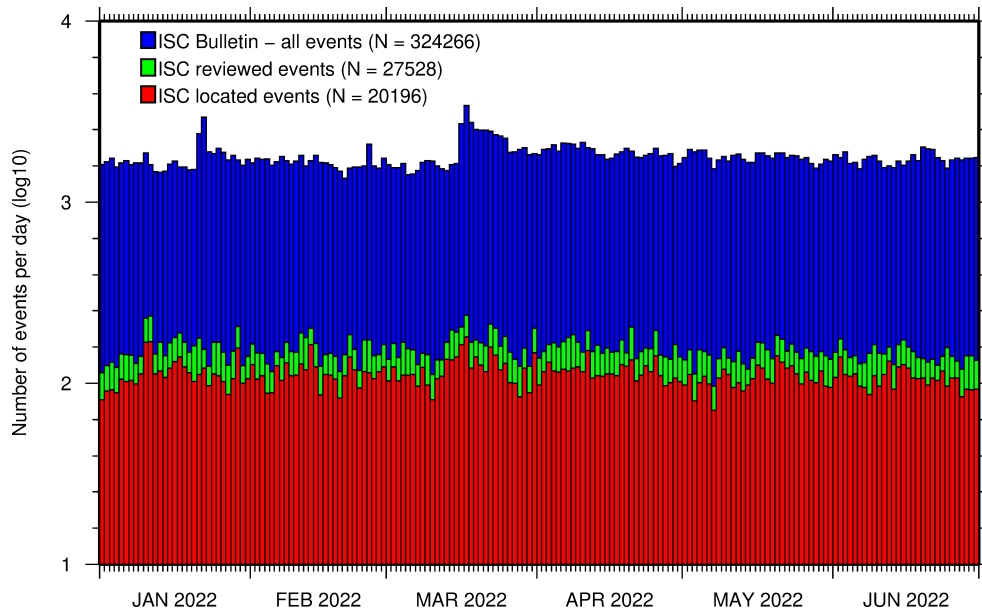


Figure 8.1: Histogram showing the number of events in the ISC Bulletin for the current summary period. The vertical scale is logarithmic.

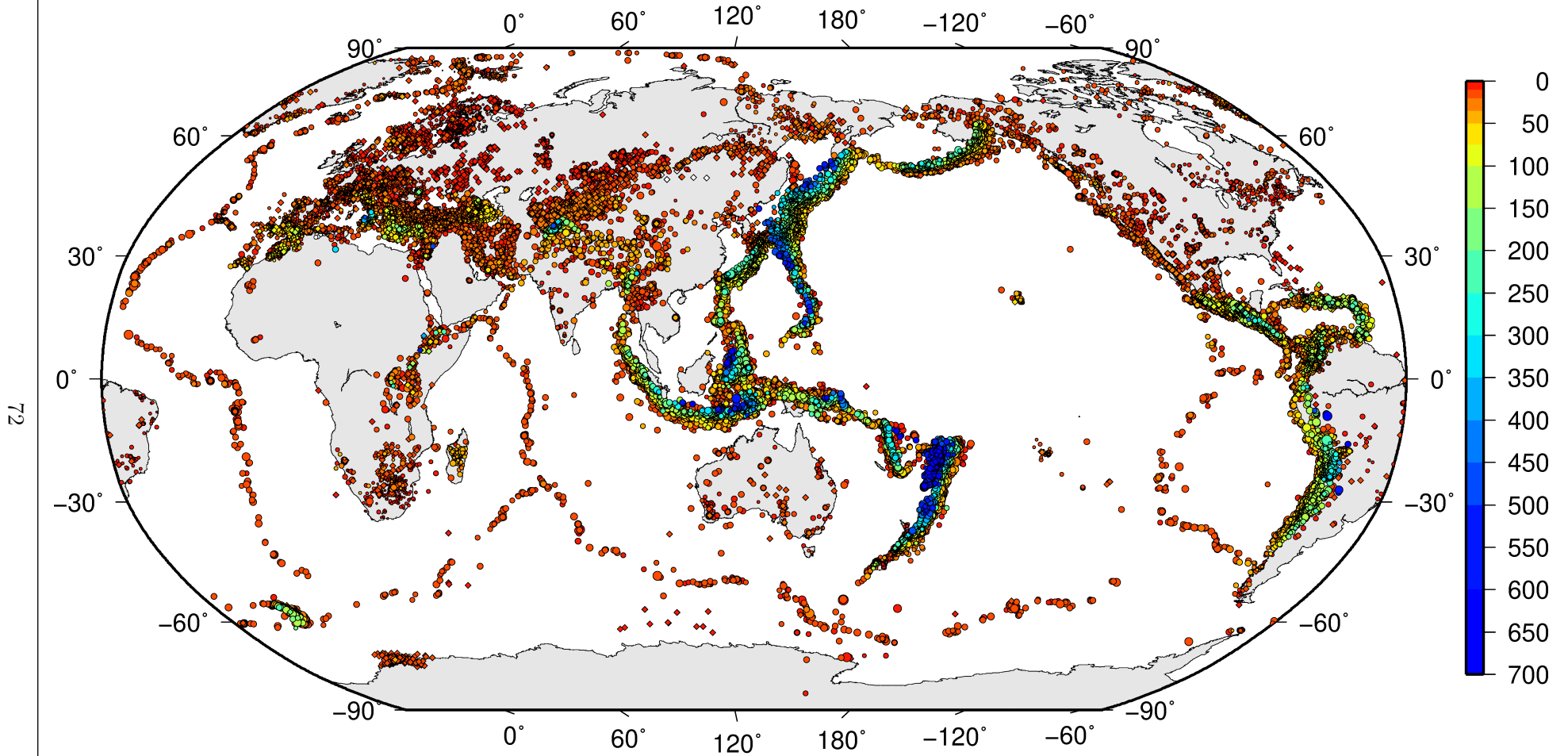
Figure 8.7 shows the depth distribution of fixed-depth solutions in the ISC Bulletin. Except for a fraction of events whose depth is fixed to a shallow depth, this set comprises mostly ISC-located events. If there is no resolution for depth in the data, the ISC locator fixes the depth to a value obtained from the ISC default depth grid file, or if no default depth exists for that location, to a nominal default depth assigned to each Flinn-Engdahl region (see details in Section 10.1.4). If during review the ISC analysts find these depth to be a poor fit, the depth will usually be fixed to a round number, preferably divisible by 50.

For events selected for ISC location, the number of stations typically increases as arrival data reported by several agencies are grouped together and associated to the prime hypocentre. Consequently, the network geometry, characterised by the secondary azimuthal gap (the largest azimuthal gap a single station closes), is typically improved. Figure 8.8 illustrates that the secondary azimuthal gap is indeed generally smaller for ISC-located events than that for all events in the ISC Bulletin. Figure 8.9 shows the distribution of the number of associated stations. For large events the number of associated stations is usually larger for ISC-located events than for any of the reported event bulletins. On the other hand, events with just a few reporting stations are rarely selected for ISC location. The same is true for the number of defining stations (stations with at least one defining phase that were used in the location). Figure 8.10 indicates that because the reported observations from multiple agencies are associated to the prime, large ISC-located events typically have a larger number of defining stations than any of the reported event bulletins.

The formal uncertainty estimates are also typically smaller for ISC-located events. Figure 8.11 shows the distribution of the area of the 90% confidence error ellipse for ISC-located events during the summary period. The distribution suffers from a long tail indicating a few poorly constrained event locations. Nevertheless, half of the events are characterised by an error ellipse with an area less than 166 km^2 , 90% of the events have an error ellipse area less than 1130 km^2 , and 95% of the events have an error ellipse area less than 2098 km^2 .

Figure 8.12 shows one of the major characteristic features of the ISC location algorithm (Bondár and

ISC Bulletin – all events

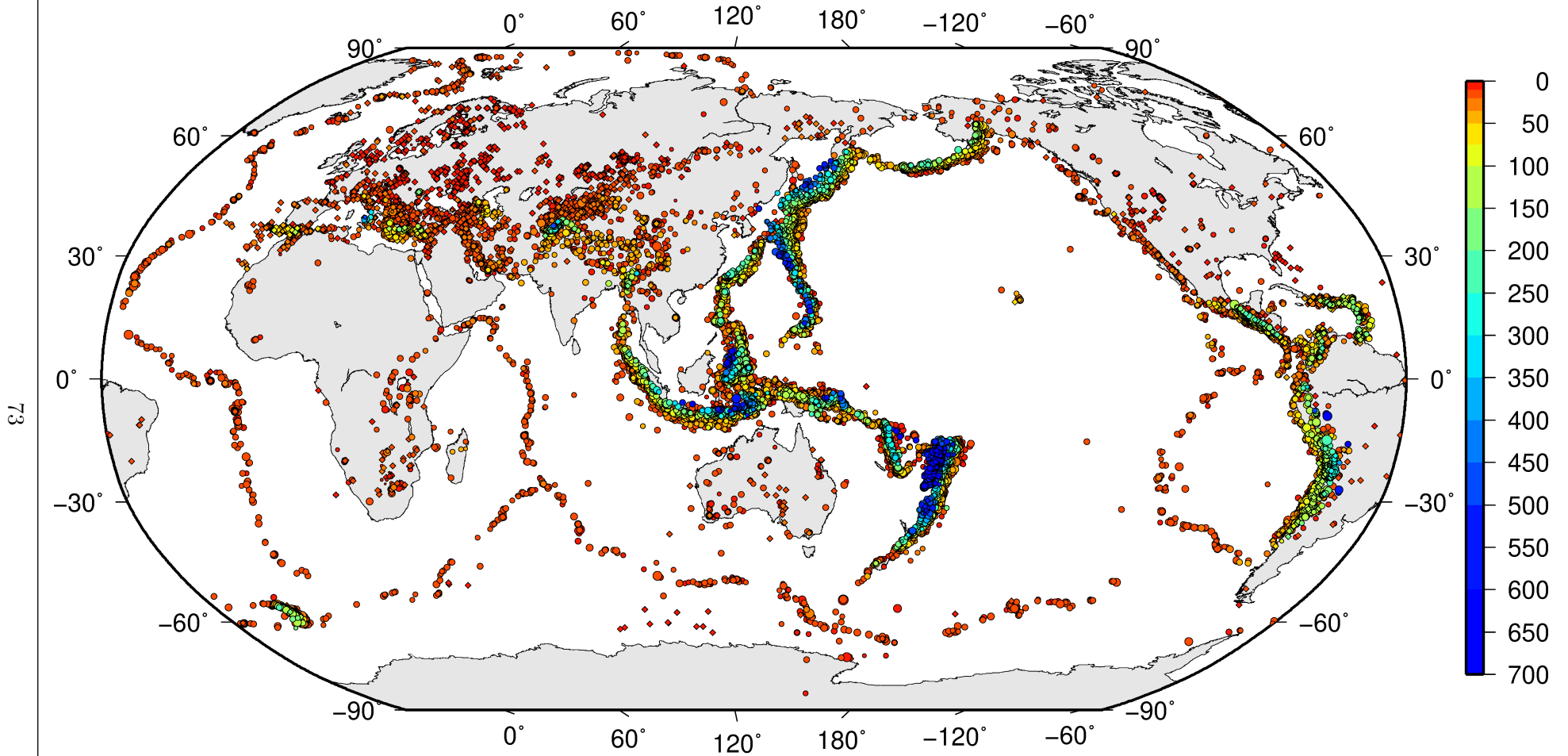


ISC Bulletin: **324266** reported events from **2022/01/01** to **2022/06/30**

◦ M 2 ◦ M 3 ◦ M 4 ◦ M 5 ◦ M 6 ◦ M 7 ◦ M 8 ◊ Unknown

Figure 8.2: Map of all events in the ISC Bulletin. Prime hypocentre locations are shown. Compare with Figure 7.10.

ISC Bulletin – reviewed events



ISC Bulletin: **27528** reviewed events from **2022/01/01** to **2022/06/30**

◦ M 2 ◦ M 3 ◦ M 4 ◦ M 5 ◦ M 6 ◦ M 7 ◦ M 8 ◦ Unknown

Figure 8.3: Map of all events reviewed by the ISC for this time period. Prime hypocentre locations are shown.

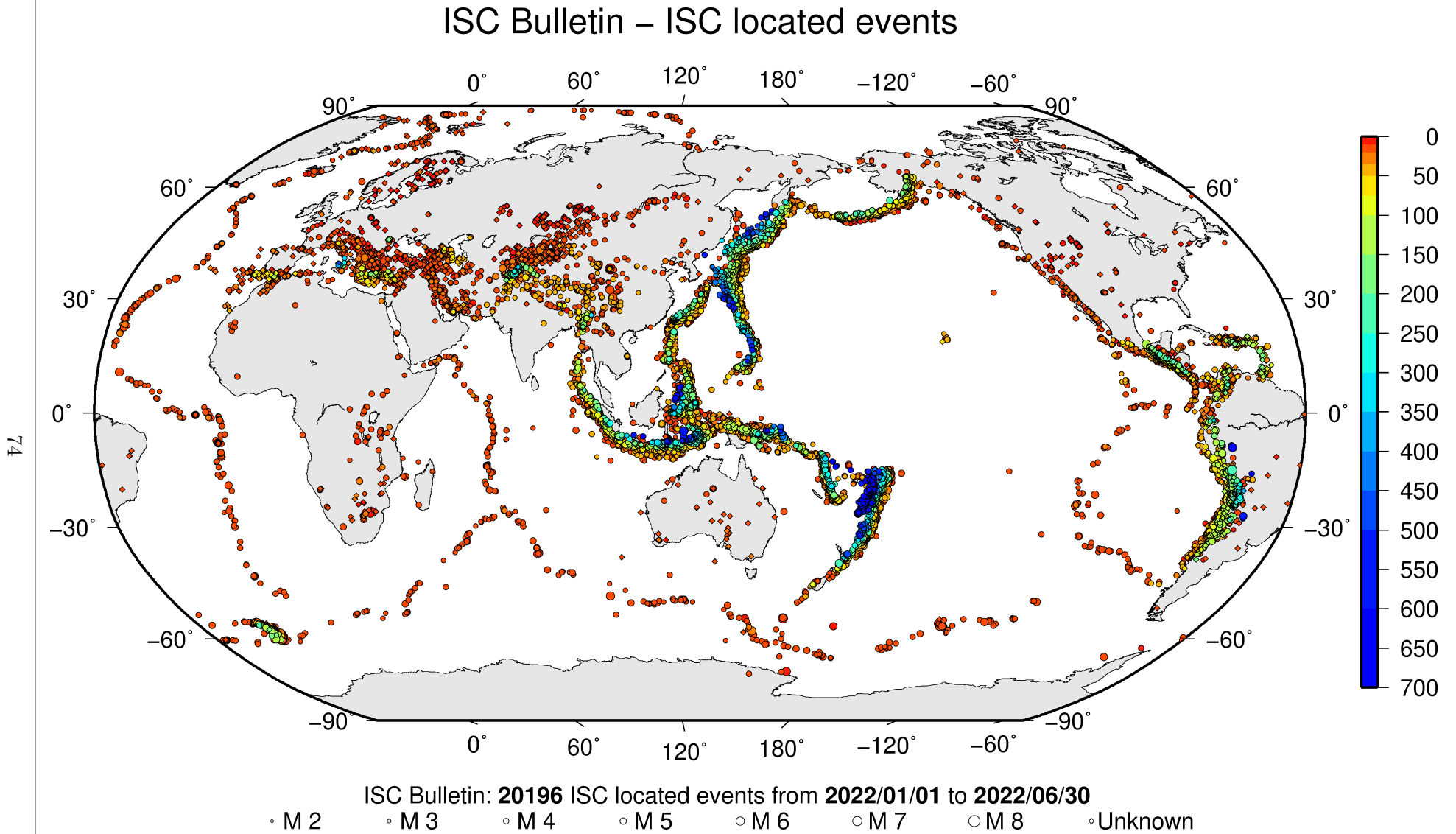


Figure 8.4: Map of all events located by the ISC for this time period. ISC determined hypocentre locations are shown.

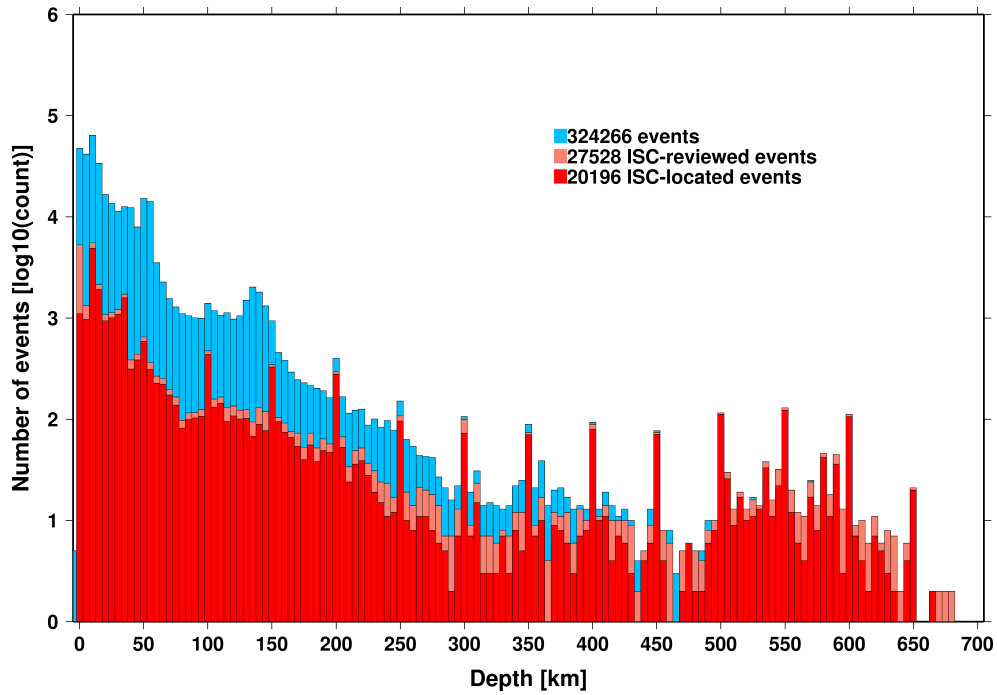


Figure 8.5: Distribution of event depths in the ISC Bulletin (blue) and for the ISC-reviewed (pink) and the ISC-located (red) events during the summary period. All ISC-located events are reviewed, but not all reviewed events are located by the ISC. The vertical scale is logarithmic.

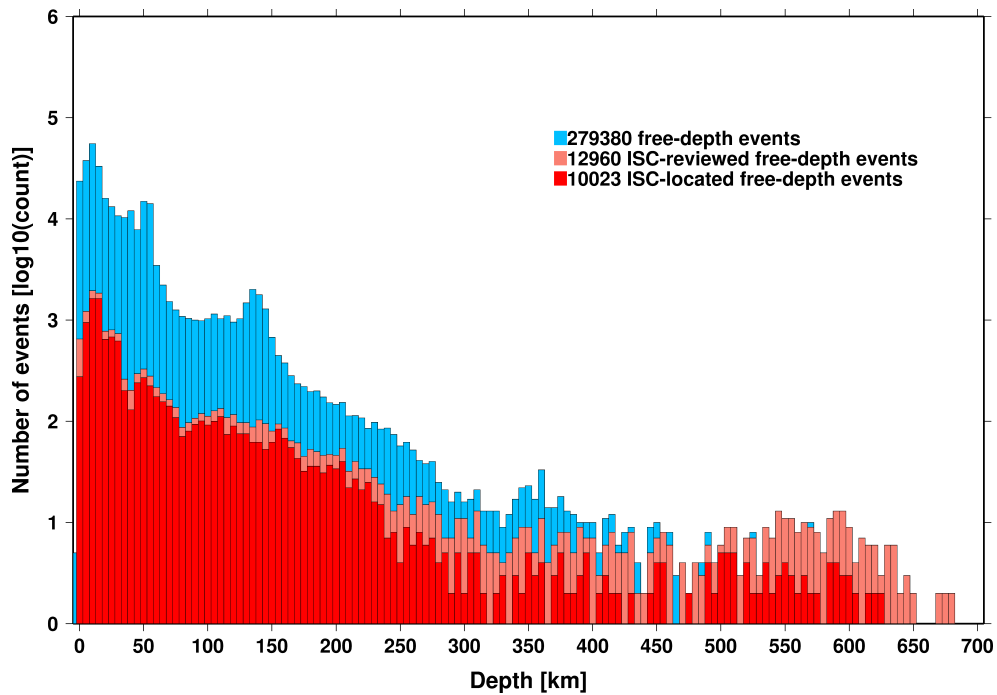


Figure 8.6: Hypocentral depth distribution of events where the prime hypocentres are reported/located with a free-depth solution in the ISC Bulletin. The vertical scale is logarithmic.

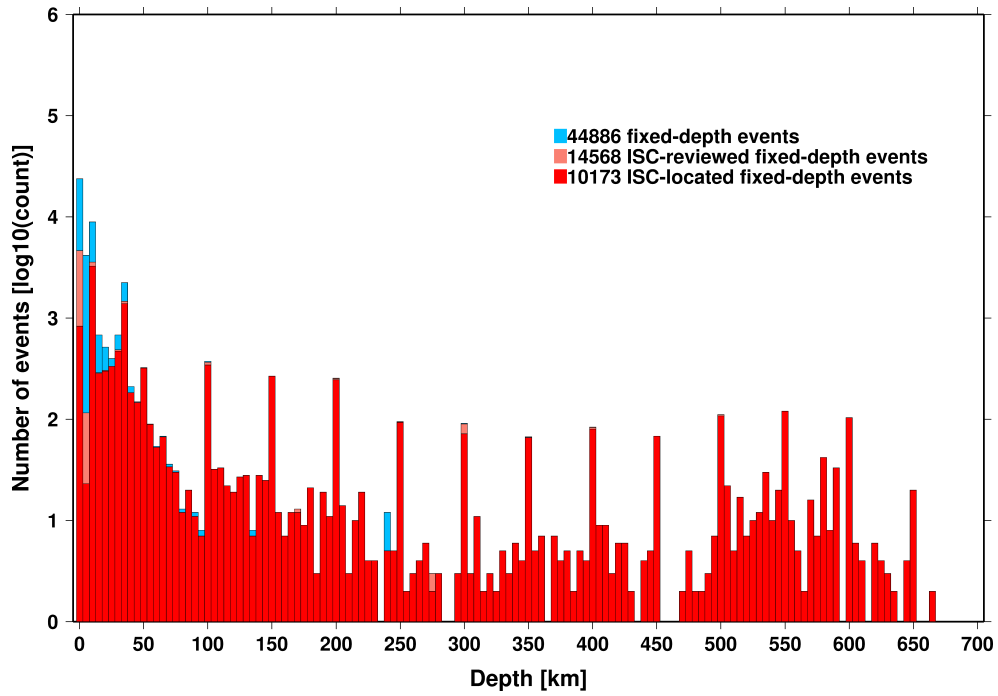


Figure 8.7: Hypocentral depth distribution of events where the prime hypocentres are reported/located with a fixed-depth solution in the ISC Bulletin. The vertical scale is logarithmic.

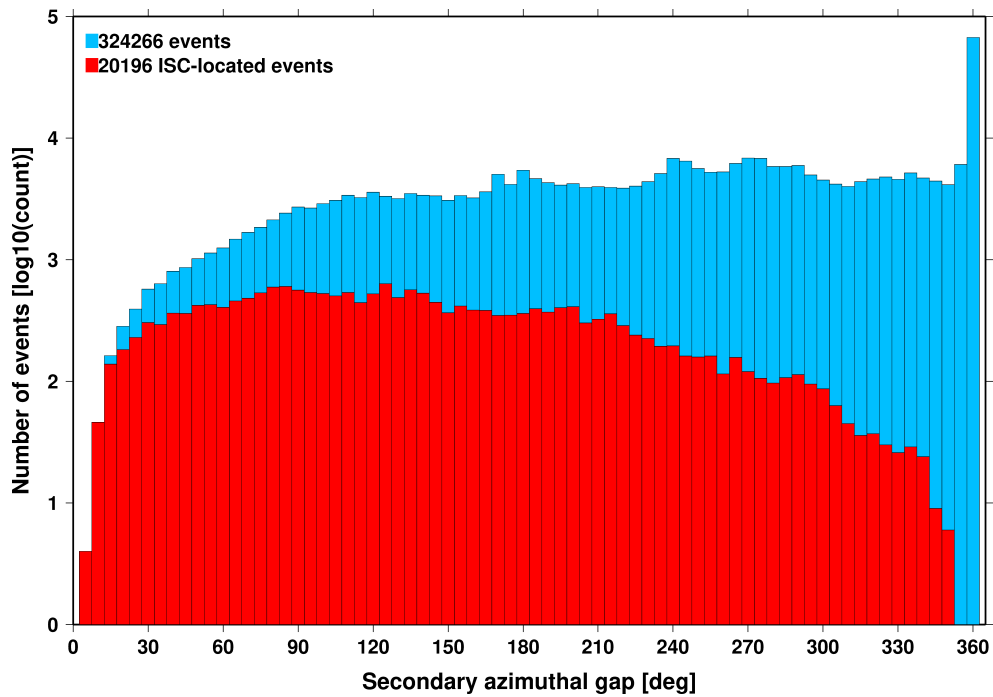


Figure 8.8: Distribution of secondary azimuthal gap for events in the ISC Bulletin (blue) and those selected for ISC location (red). The vertical scale is logarithmic.

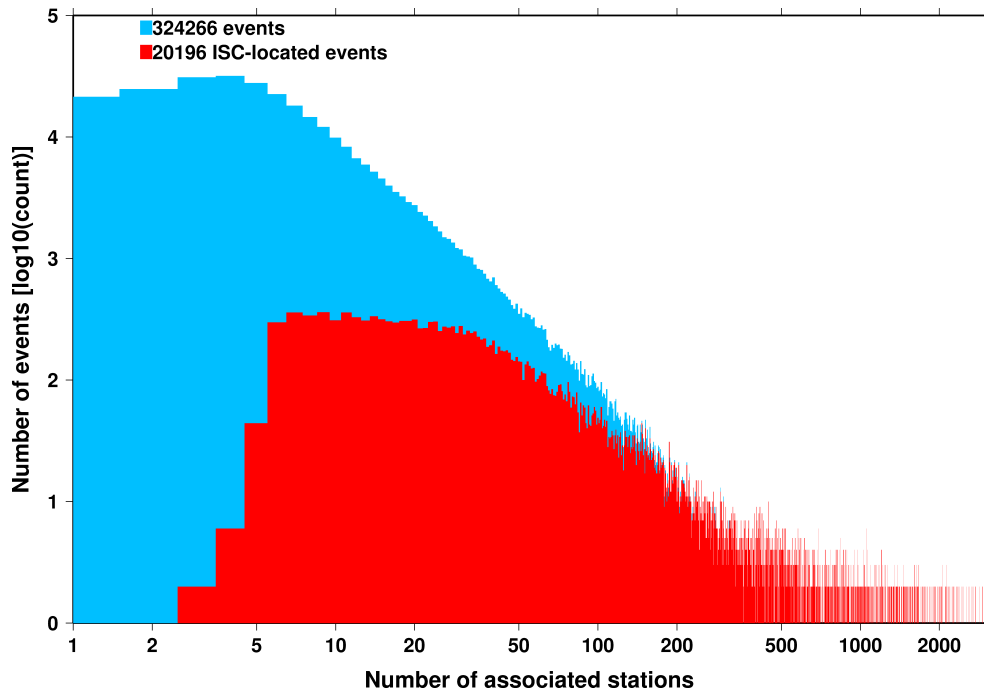


Figure 8.9: Distribution of the number of associated stations for events in the ISC Bulletin (blue) and those selected for ISC location (red). The vertical scale is logarithmic.

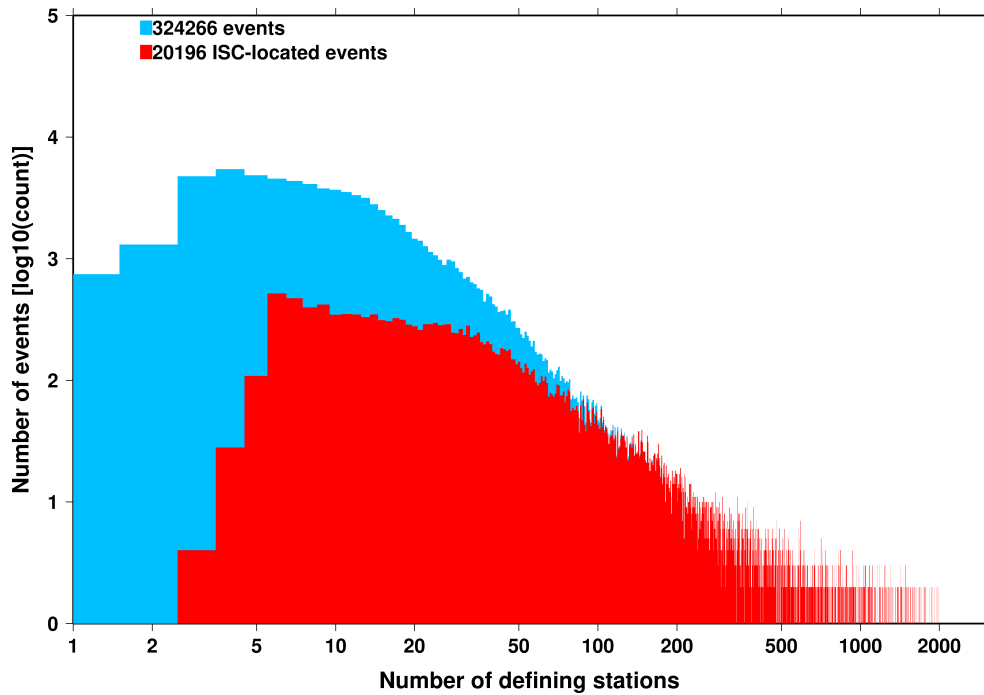


Figure 8.10: Distribution of the number of defining stations for events in the ISC Bulletin (blue) and those selected for ISC location (red). The vertical scale is logarithmic.

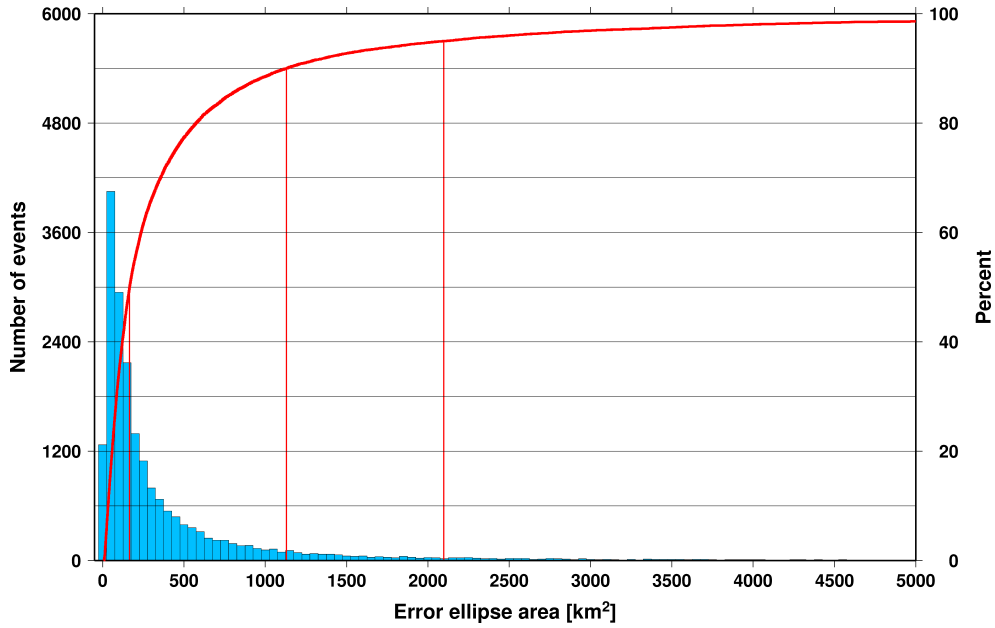


Figure 8.11: Distribution of the area of the 90% confidence error ellipse of the ISC-located events. Vertical red lines indicate the 50th, 90th and 95th percentile values.

Storchak, 2011). Because the ISC locator accounts for correlated travel-time prediction errors due to unmodelled velocity heterogeneities along similar ray paths, the area of the 90% confidence error ellipse does not decrease indefinitely with increasing number of stations, but levels off once the information carried by the network geometry is exhausted, thus providing more realistic uncertainty estimates.

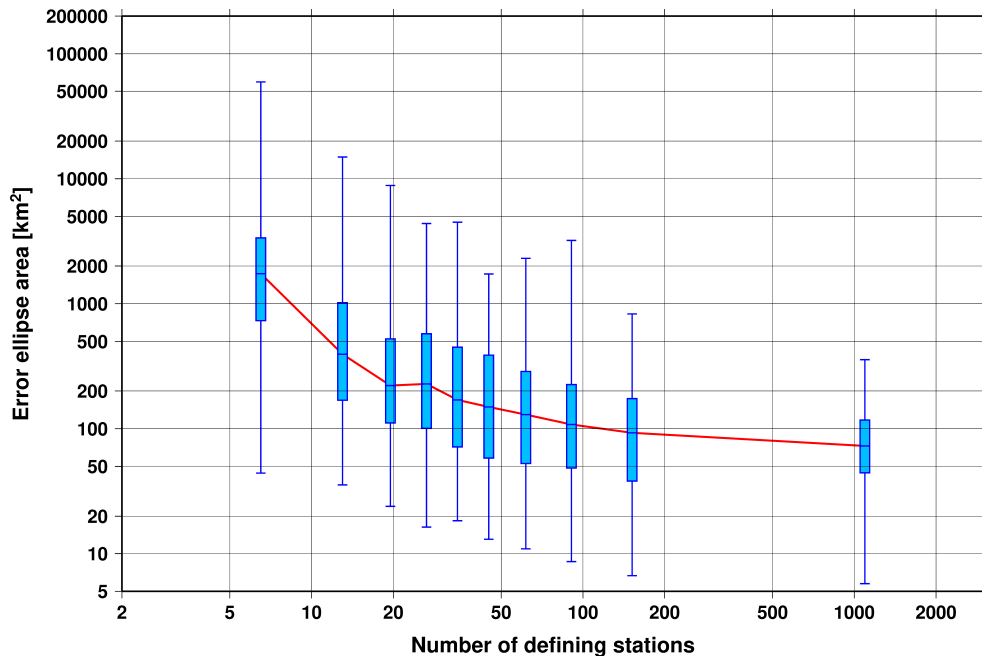


Figure 8.12: Box-and-whisker plot of the area of the 90% confidence error ellipse of the ISC-located events as a function of the number of defining stations. Each box represents one-tenth-worth of the total number of data. The red line indicates the median 90% confidence error ellipse area.

8.2 Seismic Phases and Travel-Time Residuals

The number of phases that are associated to events over the summary period in the ISC Bulletin is shown in Figure 8.13. Phase types and their total number in the ISC Bulletin is shown in the Appendix, Table 10.3. A summary of phase types is indicated in Figure 8.14.

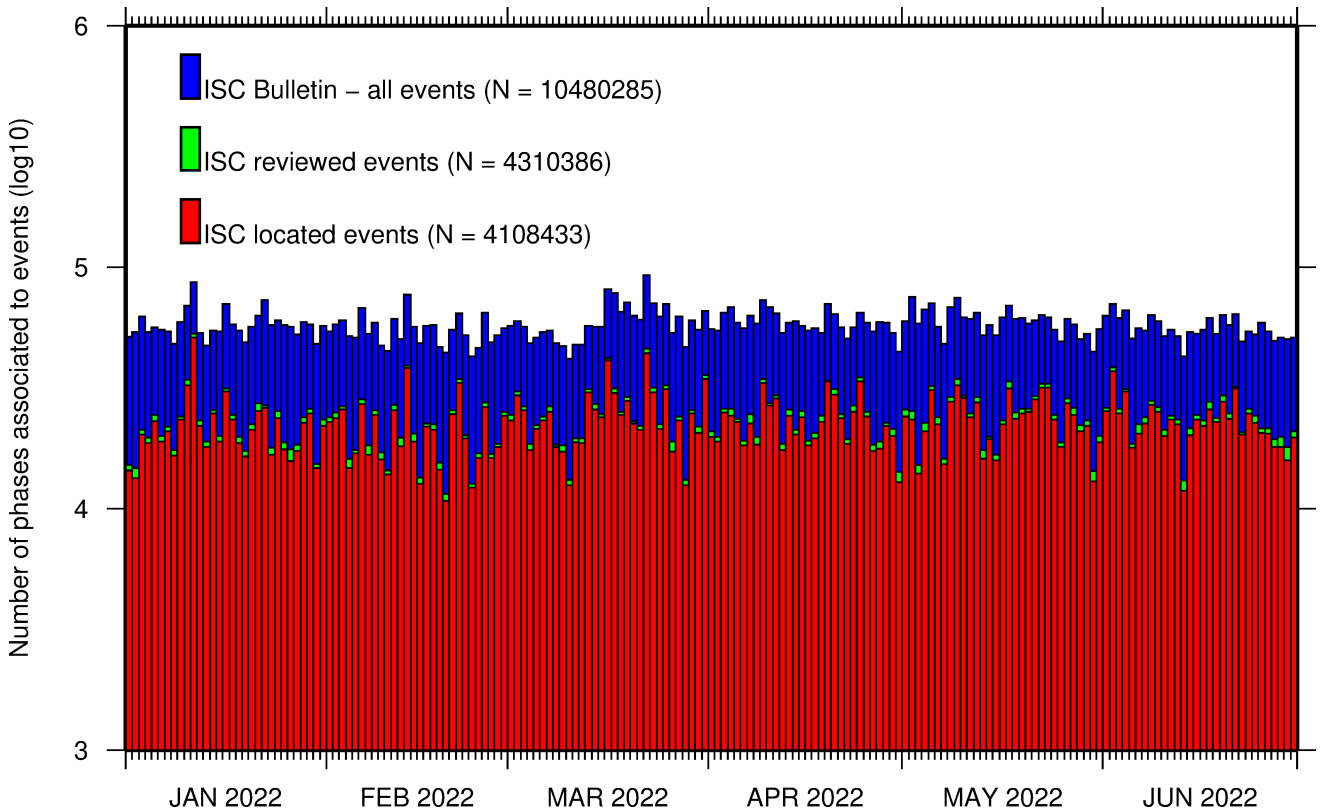


Figure 8.13: Histogram showing the number of phases (N) that the ISC has associated to events within the ISC Bulletin for the current summary period.

In computing ISC locations, the current (for events since 2009) ISC location algorithm (*Bondár and Storchak, 2011*) uses all *ak135* phases where possible. Within the Bulletin, the phases that contribute to an ISC location are labelled as *time defining*. In this section, we summarise these time defining phases.

In Figure 8.15, the number of defining phases is shown in a histogram over the summary period. Each defining phase is listed in Table 8.1, which also provides a summary of the number of defining phases per event. A pie chart showing the proportion of defining phases is shown in Figure 8.16. Figure 8.17 shows travel times of seismic waves. The distribution of residuals for these defining phases is shown for the top five phases in Figures 8.18 through 8.22.

Table 8.1: Numbers of ‘time defining’ phases within the ISC Bulletin for 20196 ISC located events.

Phase	Number of ‘defining’ phases	Number of events	Max per event	Median per event
P	1077565	14153	2476	19
Pn	696281	18672	1123	20
Sn	233281	15707	192	8
Pb	103436	8495	182	7
Pg	69626	6302	156	5
Sb	68383	7752	117	5
PKP _{df}	58286	4685	685	3
Sg	50918	5876	151	5

Table 8.1: (continued)

Phase	Number of 'defining' phases	Number of events	Max per event	Median per event
S	34206	3487	243	3
PKiKP	30503	3484	358	2
PKPbc	24419	3895	143	2
PcP	17890	3944	72	2
PKPab	17881	2774	219	2
pP	13149	1536	205	3
PP	9377	1310	162	2
Pdif	8974	1107	285	2
ScP	4809	1065	64	2
sP	4722	1102	55	2
SS	3716	893	44	2
SKSac	2796	533	115	2
PKKPbc	2477	499	94	2
pwP	2085	607	53	2
SKPbc	1117	338	51	2
pPKPdf	1041	319	61	1
PnPn	915	502	17	1
SnSn	902	502	7	1
ScS	803	342	28	1
sS	795	393	18	1
P'P'df	751	183	40	2
PKKPdf	514	237	25	1
SKiKP	501	256	16	1
SKPdf	463	166	65	1
PKKPab	451	207	30	1
pPKPab	447	163	28	1
pPKPbc	380	194	12	1
PS	315	144	19	2
sPKPdf	307	184	16	1
SKSdf	250	193	5	1
SKPab	227	126	9	1
SKKSac	199	149	11	1
P'P'bc	198	119	7	1
PnS	151	125	4	1
sPKPab	136	72	21	1
SKKPbc	129	37	16	2
PKSdf	120	66	15	1
pPKiKP	118	74	15	1
sPKPbc	112	76	13	1
SP	111	43	29	1
PcS	102	81	3	1
SKKSdf	94	89	2	1
pS	81	75	3	1
Sdif	76	58	7	1
pPdif	61	42	8	1
P'P'ab	55	40	6	1
SPn	51	18	27	1
SKKPdf	38	15	18	1
sPdif	24	17	6	1
SKKPab	23	13	4	1
PbPb	15	11	3	1
sPKiKP	12	12	1	1
sSKSac	8	8	1	1
SbSb	6	5	2	1
PKSbc	4	4	1	1
sPn	3	2	2	2
S'S'ac	2	2	1	1
SgSg	2	2	1	1
sSdif	1	1	1	1
pSKSdf	1	1	1	1
PgPg	1	1	1	1
sSKSdf	1	1	1	1
pPn	1	1	1	1
pSKSac	1	1	1	1

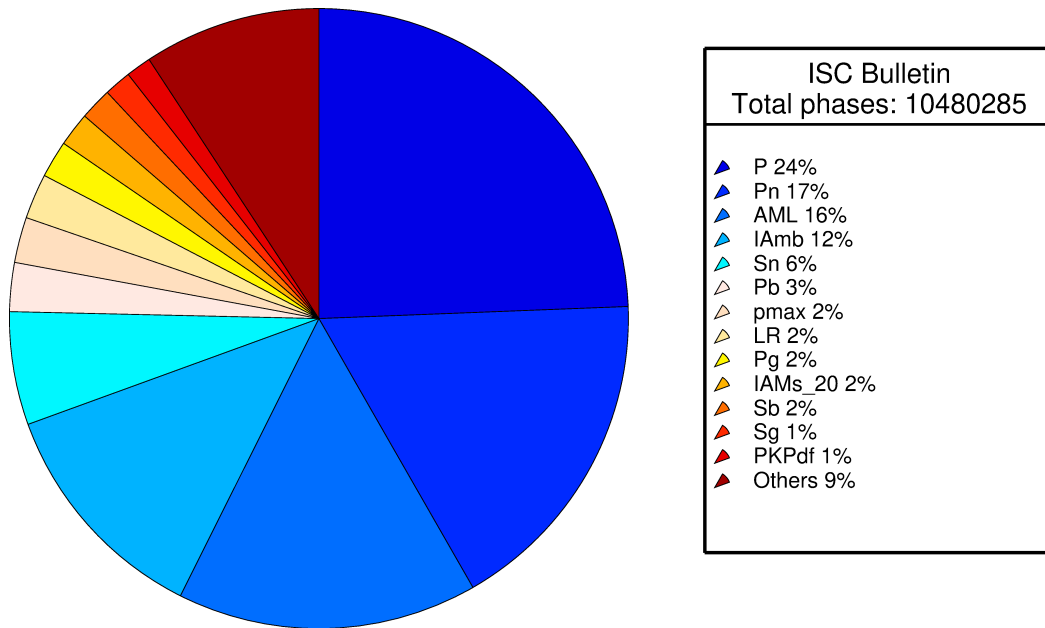


Figure 8.14: Pie chart showing the fraction of various phase types in the ISC Bulletin for this summary period.

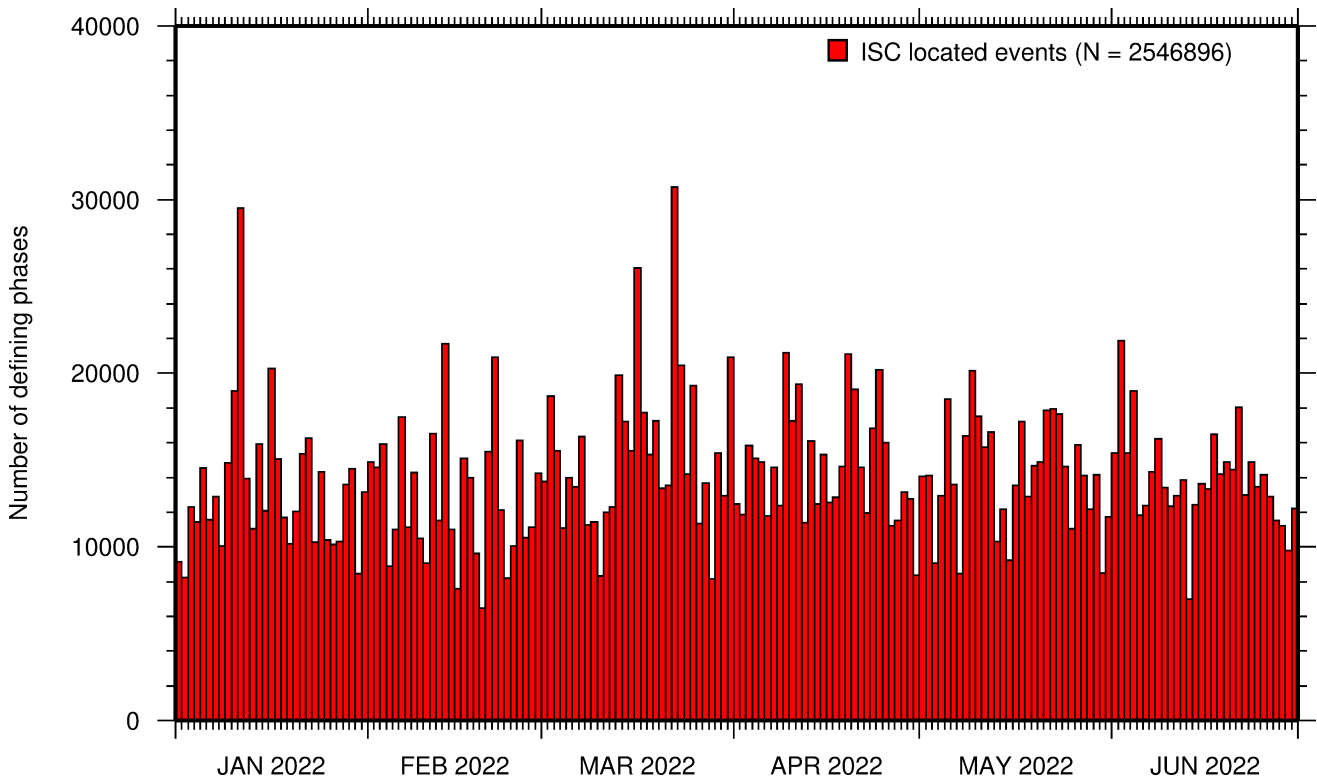


Figure 8.15: Histogram showing the number of defining phases in the ISC Bulletin, for events located by the ISC.

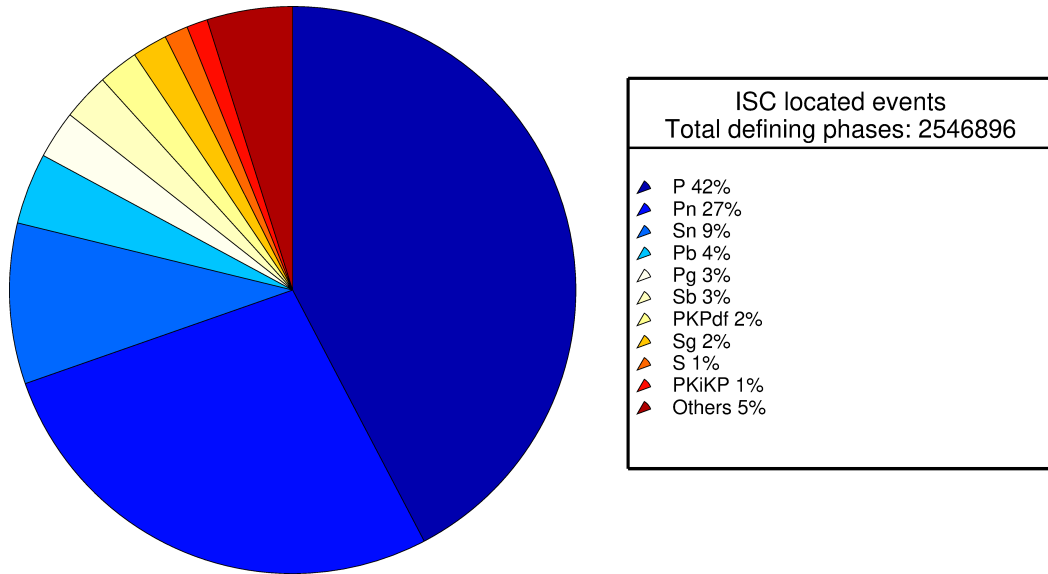


Figure 8.16: Pie chart showing the defining phases in the ISC Bulletin, for events located by the ISC. A complete list of defining phases is shown in Table 8.1.

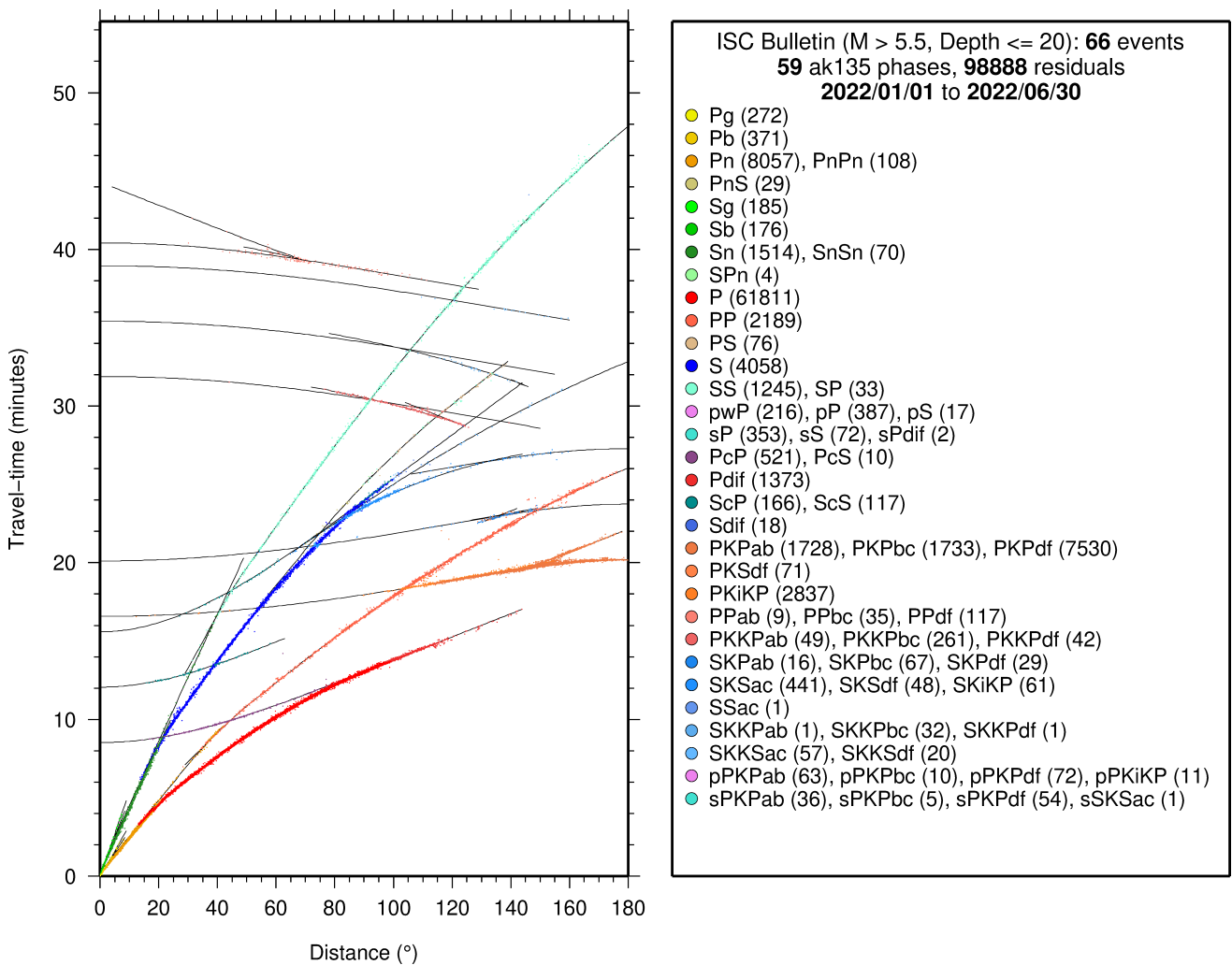


Figure 8.17: Distribution of travel-time observations in the ISC Bulletin for events with $M > 5.5$ and depth less than 20 km. The travel-time observations are shown relative to a 0 km source and compared with the theoretical ak135 travel-time curves (solid lines). The legend lists the number of each phase plotted.

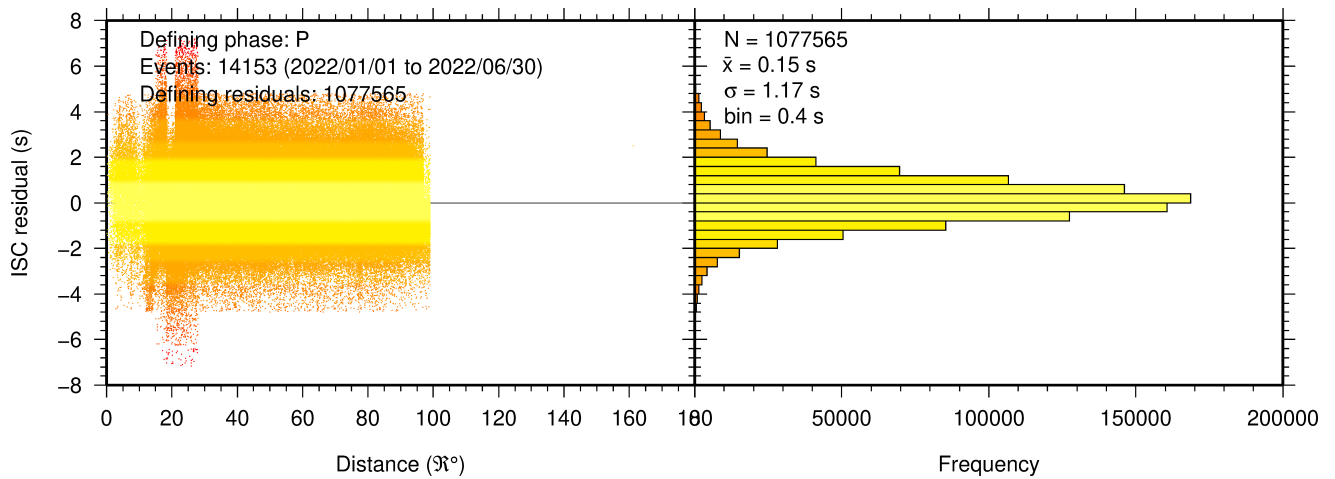


Figure 8.18: Distribution of travel-time residuals for the defining P phases used in the computation of ISC located events in the Bulletin.

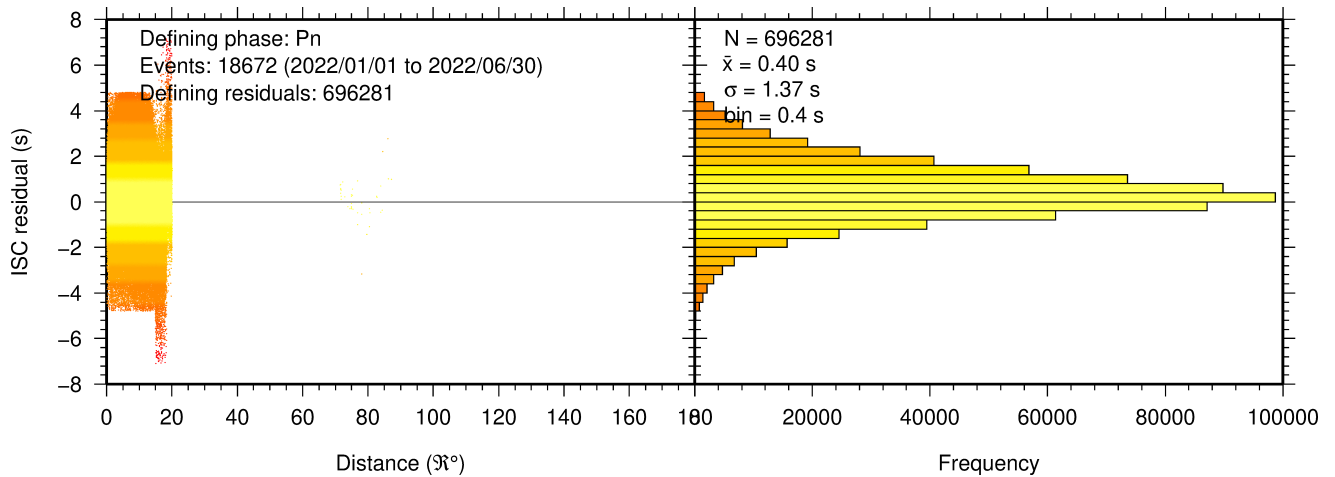


Figure 8.19: Distribution of travel-time residuals for the defining Pn phases used in the computation of ISC located events in the Bulletin.

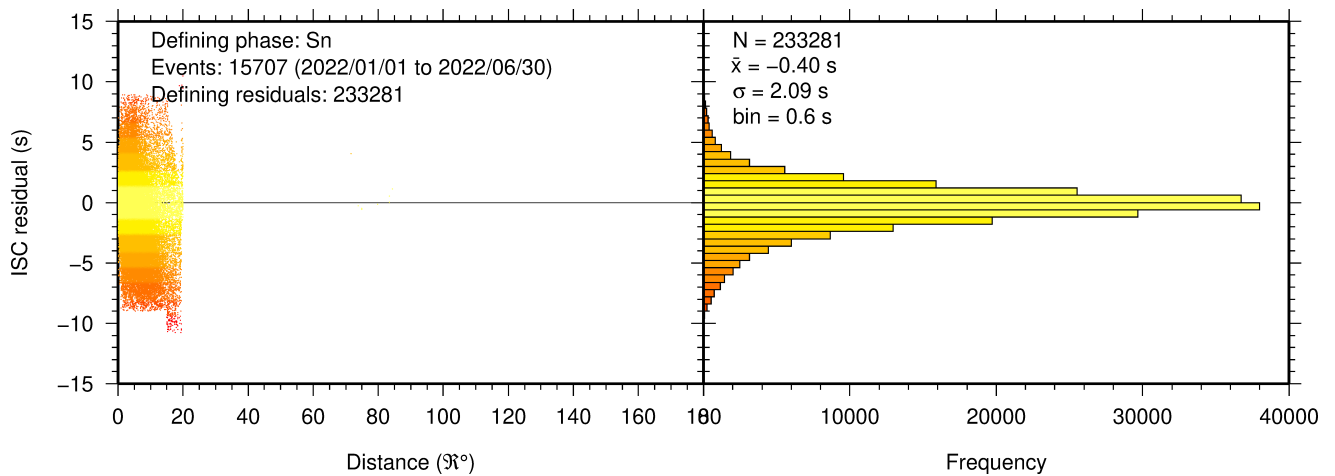


Figure 8.20: Distribution of travel-time residuals for the defining Sn phases used in the computation of ISC located events in the Bulletin.

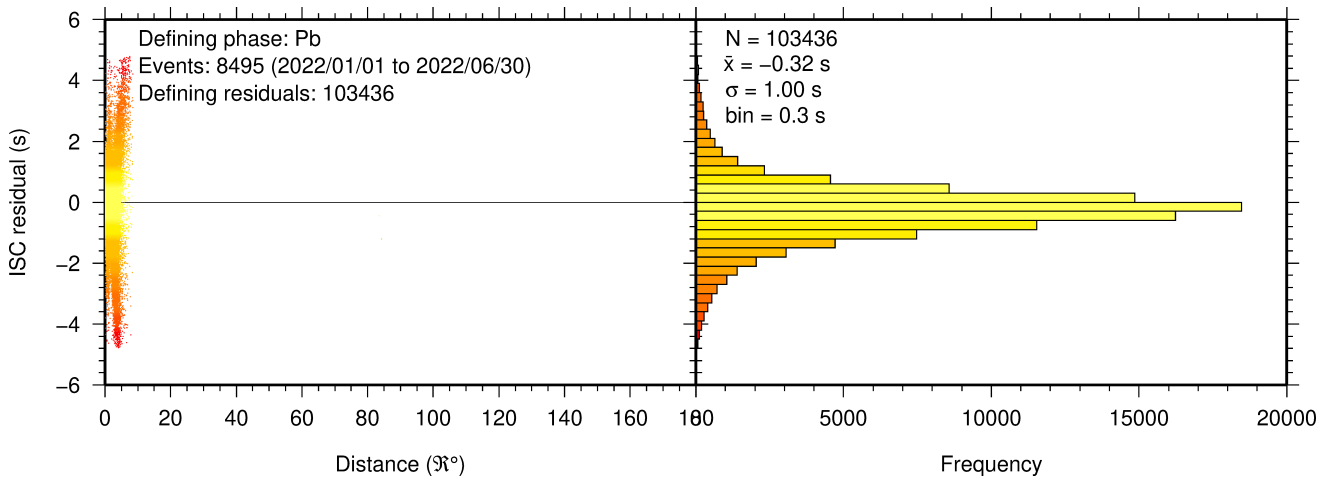


Figure 8.21: Distribution of travel-time residuals for the defining Pb phases used in the computation of ISC located events in the Bulletin.

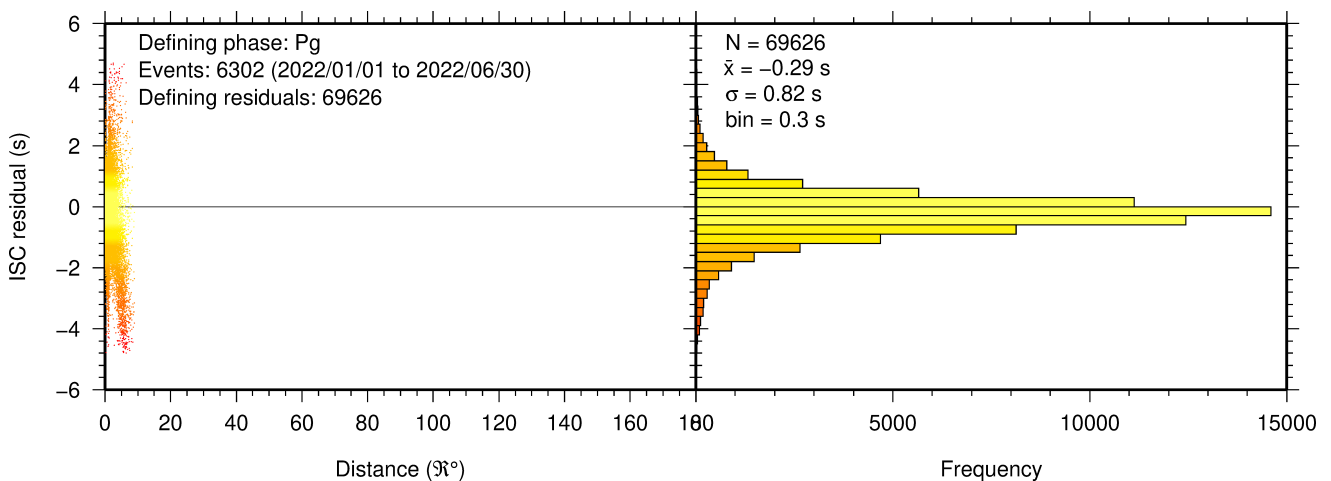
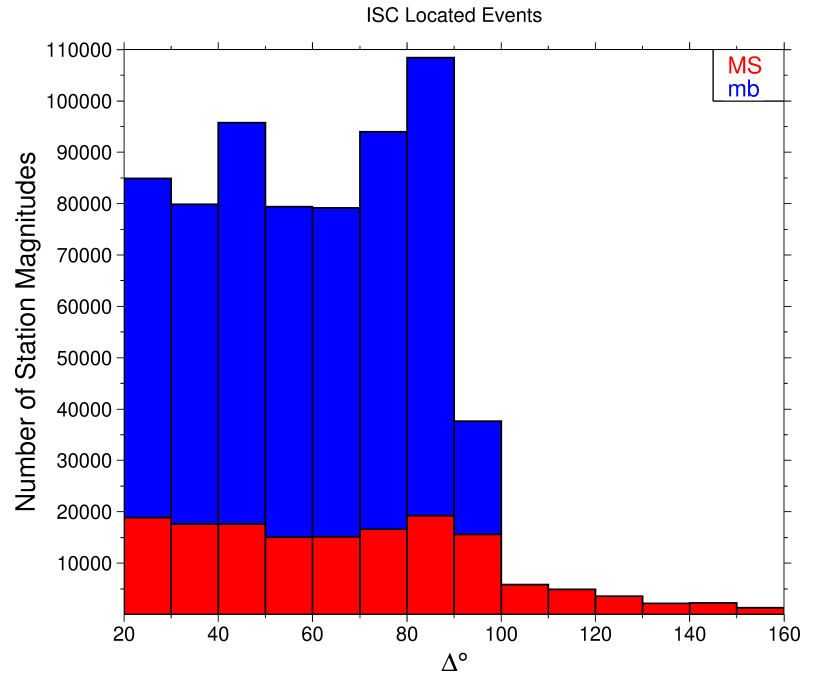


Figure 8.22: Distribution of travel-time residuals for the defining Pg phases used in the computation of ISC located events in the Bulletin.

8.3 Seismic Wave Amplitudes and Periods

The ISC Bulletin contains a variety of seismic wave amplitudes and periods measured by reporting agencies. For this Bulletin Summary, the total of collected amplitudes and periods is 4,362,526 (see Section 7.3). For the determination of the ISC magnitudes M_S and m_b , only a fraction of such data can be used. Indeed, the ISC network magnitudes are computed only for ISC located events. Here we recall the main features of the ISC procedure for M_S and m_b computation (see detailed description in Section 10.1.4). For each amplitude-period pair in a reading the ISC algorithm computes the magnitude (a reading can include several amplitude-period measurements) and the reading magnitude is assigned to the maximum A/T in the reading. If more than one reading magnitude is available for a station, the station magnitude is the median of the reading magnitudes. The network magnitude is computed then as the 20% alpha-trimmed median of the station magnitudes (at least three required). M_S is computed for shallow earthquakes (depth ≤ 60 km) only and using amplitudes and periods on all three components (when available) if the period is within 10-60 s and the epicentral distance is between 20° and 160° . m_b is computed also for deep earthquakes (depth down to 700 km) but only with amplitudes on the vertical

Figure 8.23: Distribution of the number of station magnitudes computed by the ISC Locator for *mb* (blue) and *MS* (red) versus distance.



component measured at periods ≤ 3 s in the distance range 21° - 100° .

Table 8.2 is a summary of the amplitude and period data that contributed to the computation of station and ISC *MS* and *mb* network magnitudes for this Bulletin Summary.

Table 8.2: Summary of the amplitude-period data used by the ISC Locator to compute *MS* and *mb*.

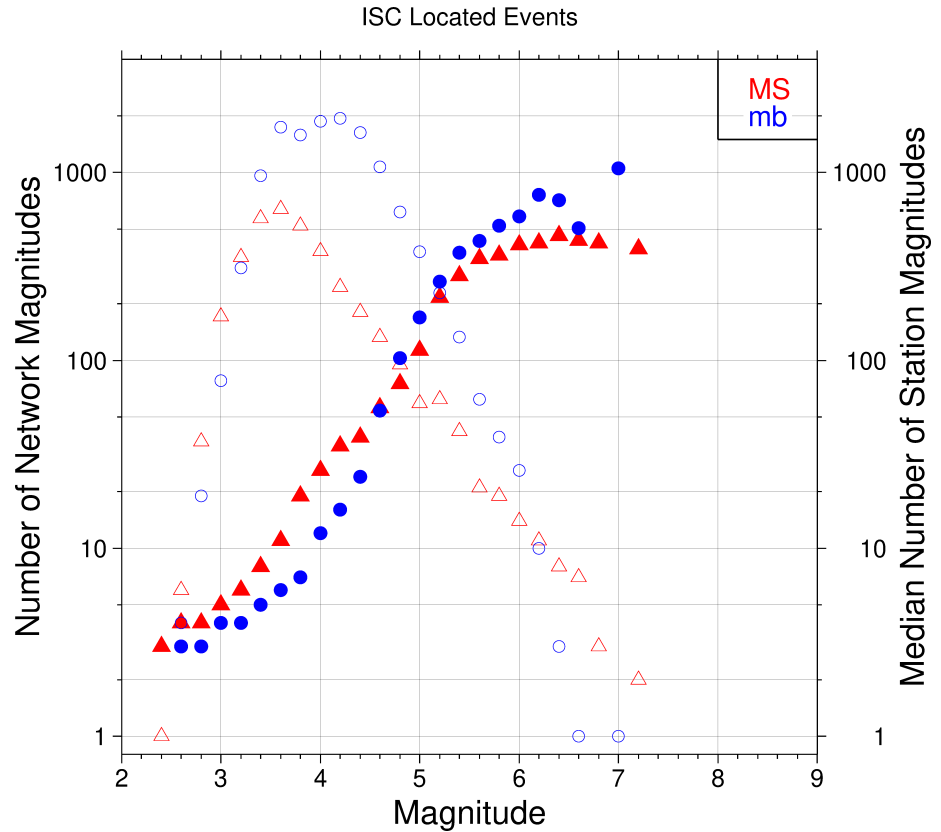
	<i>MS</i>	<i>mb</i>
Number of amplitude-period data	179141	773024
Number of readings	159085	767798
Percentage of readings in the ISC located events with qualifying data for magnitude computation	14.1	55.2
Number of station magnitudes	150030	596388
Number of network magnitudes	3736	12774

A small percentage of the readings with qualifying data for *MS* and *mb* calculation have more than one amplitude-period pair. Notably, only 14% of the readings for the ISC located (shallow) events included qualifying data for *MS* computation, whereas for *mb* the percentage is much higher at 55%. This is due to the seismological practice of reporting agencies. Agencies contributing systematic reports of amplitude and period data are listed in Appendix Table 10.4. Obviously the ISC Bulletin would benefit if more agencies included surface wave amplitude-period data in their reports.

Figure 8.23 shows the distribution of the number of station magnitudes versus distance. For *mb* there is a significant increase in the distance range 70° - 90° , whereas for *MS* most of the contributing stations are below 100° . The increase in number of station magnitude between 70° - 90° for *mb* is partly due to the very dense distribution of seismic stations in North America and Europe with respect to earthquake occurring in various subduction zones around the Pacific Ocean.

Finally, Figure 8.24 shows the distribution of network *MS* and *mb* as well as the median number of stations for magnitude bins of 0.2. Clearly with increasing magnitude the number of events is smaller

Figure 8.24: Number of network magnitudes (open symbols) and median number of stations magnitudes (filled symbols). Blue circles refer to mb and red triangles to MS. The width of the magnitude interval δM is 0.2, and each symbol includes data with magnitude in $M \pm \delta M/2$.



but with a general tendency of having more stations contributing to the network magnitude.

8.4 Completeness of the ISC Bulletin

We define the magnitude of completeness (hereafter M_C) as the lowest magnitude threshold above which all events are believed to be recorded. The Bulletin with events bigger than the defined M_C is assumed to be complete.

Until Issue 53, Volume II (July - December 2016) of the Summary of the ISC an estimation of M_C was computed only with the maximum curvature technique (*Woessner and Wiemer, 2005*). After the completion of the Rebuild Project and relocation of ISC hypocenters from data years 1964 to 2010 (*Storchak et al., 2017*), the estimate of M_C for the entire ISC Bulletin is re-computed using four catalogue based methodologies (*Adamaki, 2017*, and references therein): the previously used maximum curvature for comparison (maxC), M_C based on the b-value stability (MBS technique), the Goodness of Fit Test with a 90% level of fit (GFT90) and the modified Goodness of Fit Test (mGFT). Further details on each of these methodologies and their statistical behaviour can be found in *Leptokaropoulos et al. (2018)*.

The magnitudes of completeness of the ISC Bulletin for this Summary period is shown in Figure 8.25. How M_C varies for the ISC Bulletin over the years is shown in Figure 8.26. The step change in 1996 corresponds with the inclusion of the Prototype IDC (EIDC) Bulletin, followed by the Reviewed Event Bulletin (REB) of the IDC.

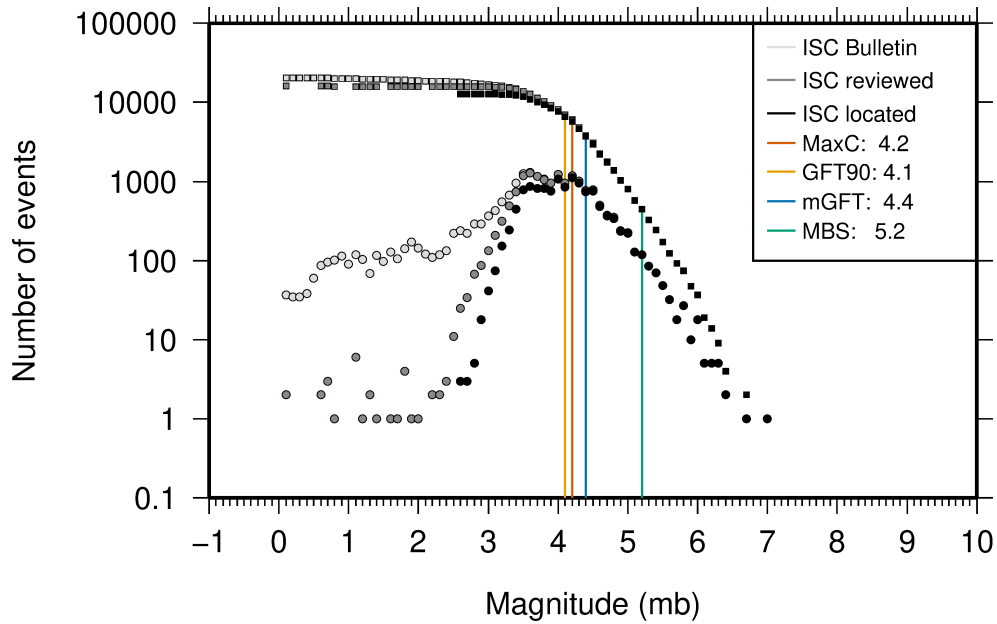


Figure 8.25: Frequency and cumulative frequency magnitude distribution for all events in the ISC Bulletin, ISC reviewed events and events located by the ISC. The magnitude of completeness (M_C) is shown for the ISC Bulletin. Note: only events with values of mb are represented in the figure.

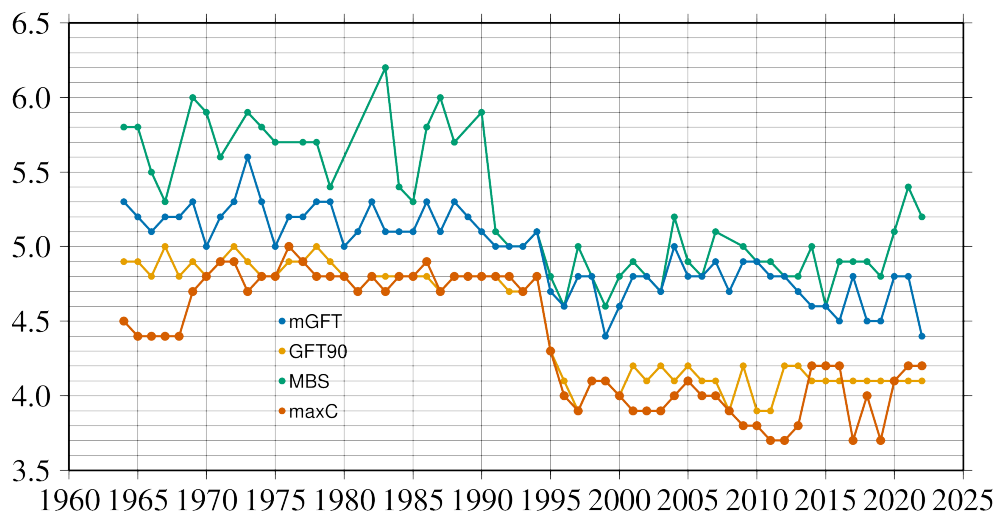


Figure 8.26: Variation of magnitude of completeness (M_C) for each year in the ISC Bulletin. Note: M_C is calculated only using those events with values of mb .

8.5 Magnitude Comparisons

The ISC Bulletin publishes network magnitudes reported by multiple agencies to the ISC. For events that have been located by the ISC, where enough amplitude data has been collected, the MS and mb magnitudes are calculated by the ISC (MS is computed only for depths ≤ 60 km). In this section, ISC magnitudes and some other reported magnitudes in the ISC Bulletin are compared.

The comparison between MS and mb computed by the ISC locator for events in this summary period is shown in Figure 8.27, where the large number of data pairs allows a colour coding of the data density. The scatter in the data reflects the fundamental differences between these magnitude scales.

Similar plots are shown in Figure 8.28 and 8.29, respectively, for comparisons of ISC mb and ISC MS with M_W from the GCMT catalogue. Since M_W is not often available below magnitude 5, these distributions are mostly for larger, global events. Not surprisingly, the scatter between mb and M_W is larger than the scatter between MS and M_W . Also, the saturation effect of mb is clearly visible for earthquakes with $M_W > 6.5$. In contrast, MS scales well with $M_W > 6$, whereas for smaller magnitudes MS appears to be systematically smaller than M_W .

In Figure 8.30 ISC values of mb are compared with all reported values of mb , values of mb reported by NEIC and values of mb reported by IDC. Similarly in Figure 8.31, ISC values of MS are compared with all reported values of MS , values of MS reported by NEIC and values of MS reported by IDC. There is a large scatter between the ISC magnitudes and the mb and MS reported by all other agencies.

The scatter decreases both for mb and MS when ISC magnitudes are compared just with NEIC and IDC magnitudes. This is not surprising as the latter two agencies provide most of the amplitudes and periods used by the ISC locator to compute MS and mb . However, ISC mb appears to be smaller than NEIC mb for $mb < 4$ and larger than IDC mb for $mb > 4$. Since NEIC does not include IDC amplitudes, it seems these features originate from observations at the high-gain, low-noise sites reported by the IDC. A good scaling is generally observed for the MS comparisons between ISC and IDC.

Figure 8.27: Comparison of ISC values of MS with mb for common event pairs.

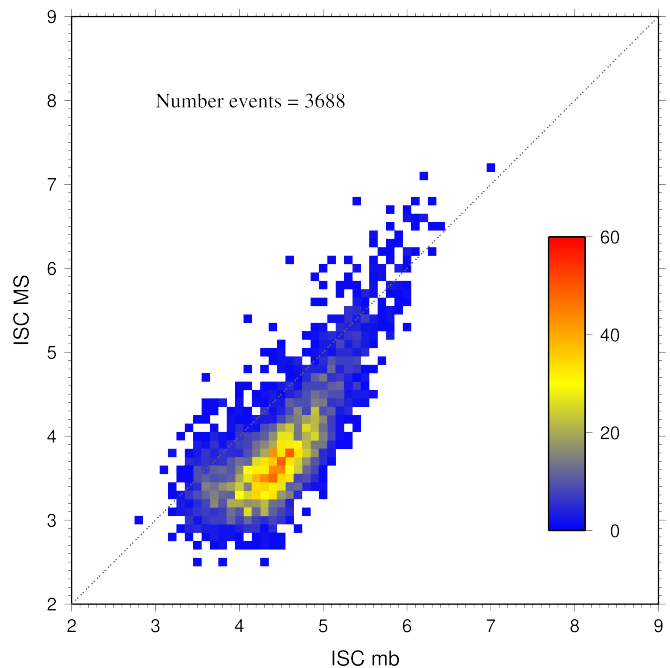


Figure 8.28: Comparison of ISC values of m_b with GCMT M_W for common event pairs.

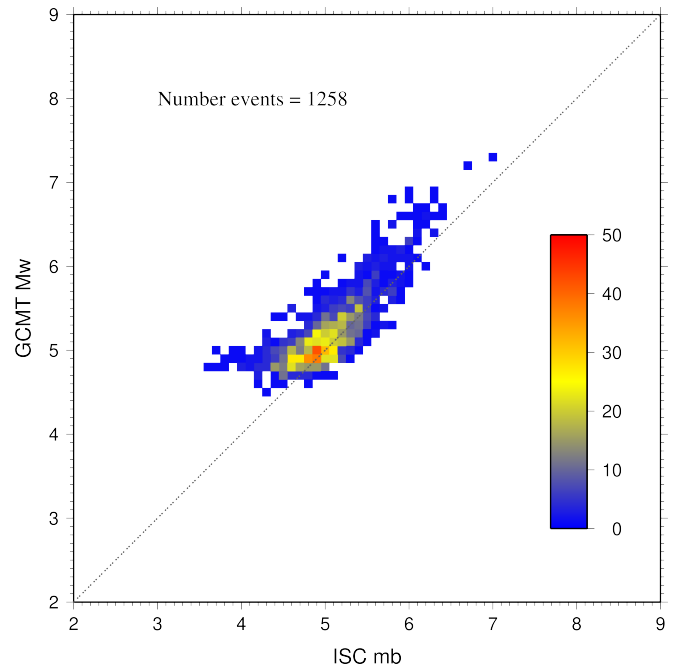
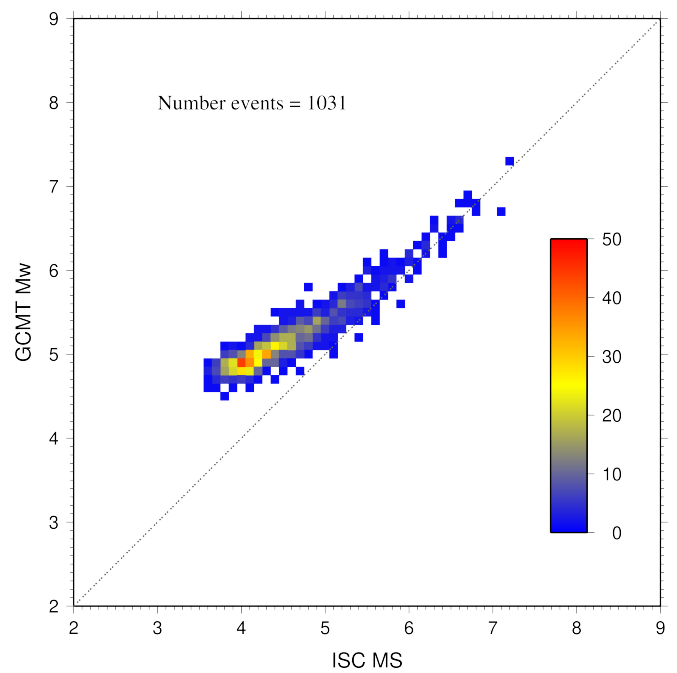


Figure 8.29: Comparison of ISC values of M_S with GCMT M_W for common event pairs.



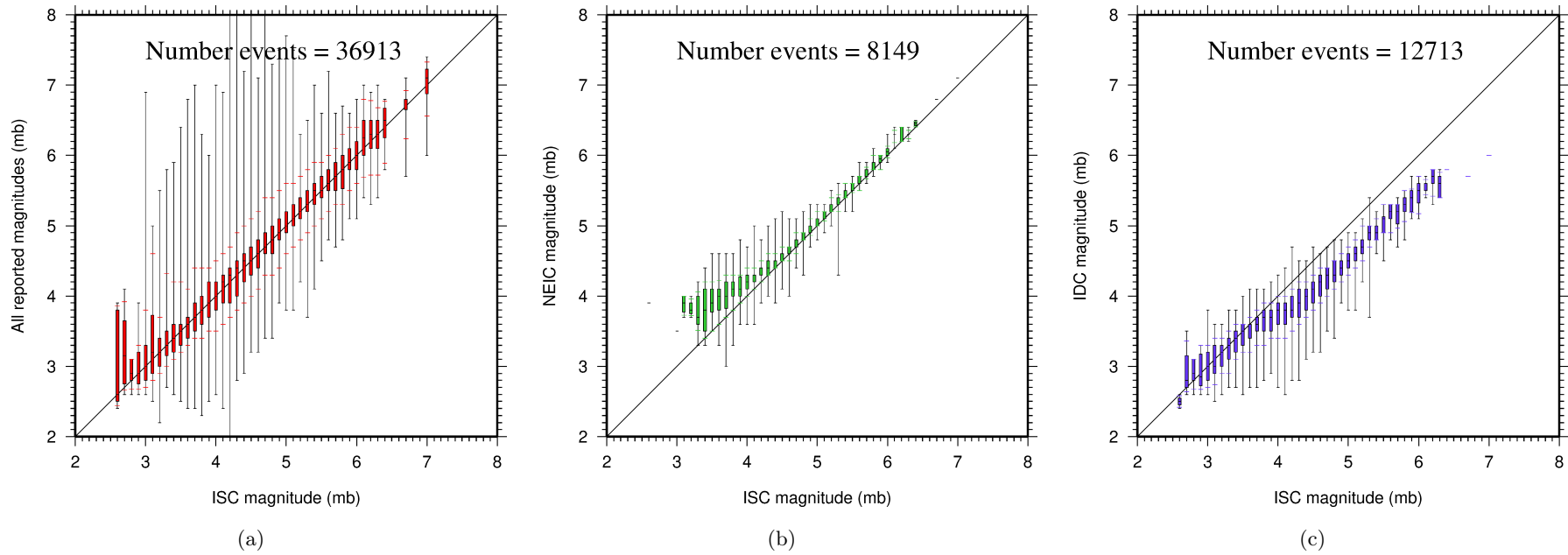


Figure 8.30: Comparison of ISC magnitude data (mb) with additional agency magnitudes (mb). The statistical summary is shown in box-and-whisker plots where the 10th and 90th percentiles are shown in addition to the max and min values. (a): All magnitudes reported; (b): NEIC magnitudes; (c): IDC magnitudes.

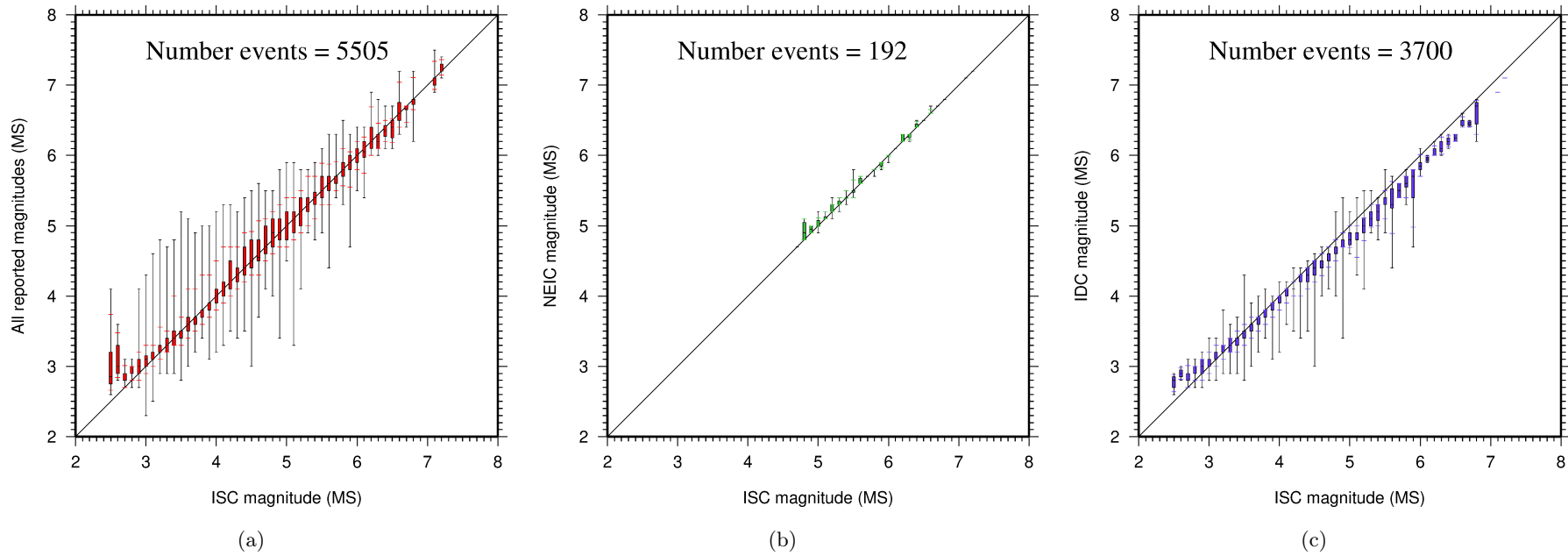


Figure 8.31: Comparison of ISC magnitude data (MS) with additional agency magnitudes (MS). The statistical summary is shown in the box-and-whisker plots where the 10th and 90th percentiles are shown in addition to the max and min values. (a): All magnitudes reported; (b): NEIC magnitudes; (c): IDC magnitudes.

9

The Leading Data Contributors

For the current six-month period, 150 agencies reported related bulletin data. Although we are grateful for every report, we nevertheless would like to acknowledge those agencies that made the most useful or distinct contributions to the contents of the ISC Bulletin. Here we note those agencies that:

- provided a comparatively large volume of parametric data (see Section 9.1),
- reported data that helped quite considerably to improve the quality of the ISC locations or magnitude determinations (see Section 9.2),
- helped the ISC by consistently reporting data in one of the standard recognised formats and in-line with the ISC data collection schedule (see Section 9.3).

We do not aim to discourage those numerous small networks who provide comparatively smaller yet still most essential volumes of regional data regularly, consistently and accurately. Without these reports the ISC Bulletin would not be as comprehensive and complete as it is today.

9.1 The Largest Data Contributors

We acknowledge the contribution of IDC, NEIC, GFZ, CLL, BJI and a few others (Figure 9.1) that reported the majority of moderate to large events recorded at teleseismic distances. The contributions of NEIC, IDC, MEX, JMA and several others are also acknowledged with respect to smaller seismic events. The contributions of JMA, RSNC, ATH, ISK, AFAD, WEL, ROM and a number of others are also acknowledged with respect to small seismic events. Note that the NEIC bulletin accumulates a contribution of all regional networks in the USA. Several agencies monitoring highly seismic regions routinely report large volumes of small to moderate magnitude events, such as those in Japan, Turkey, Italy, Greece, New Zealand, Mexico and Columbia. Contributions of small magnitude events by agencies in regions of low seismicity, such as Finland are also gratefully received.

We also would like to acknowledge contributions of those agencies that report a large portion of arrival time and amplitude data (Figure 9.2). For small magnitude events, these are local agencies in charge of monitoring local and regional seismicity. For moderate to large events, contributions of NEIC, GFZ, DJA, MOS, IDC are especially acknowledged. Notably, two agencies (NEIC, GFZ) together reported over 50% of all amplitude measurements made for teleseismically recorded events. We hope that other agencies would also be able to update their monitoring routines in the future to include the amplitude reports for teleseismic events compliant with the IASPEI standards.

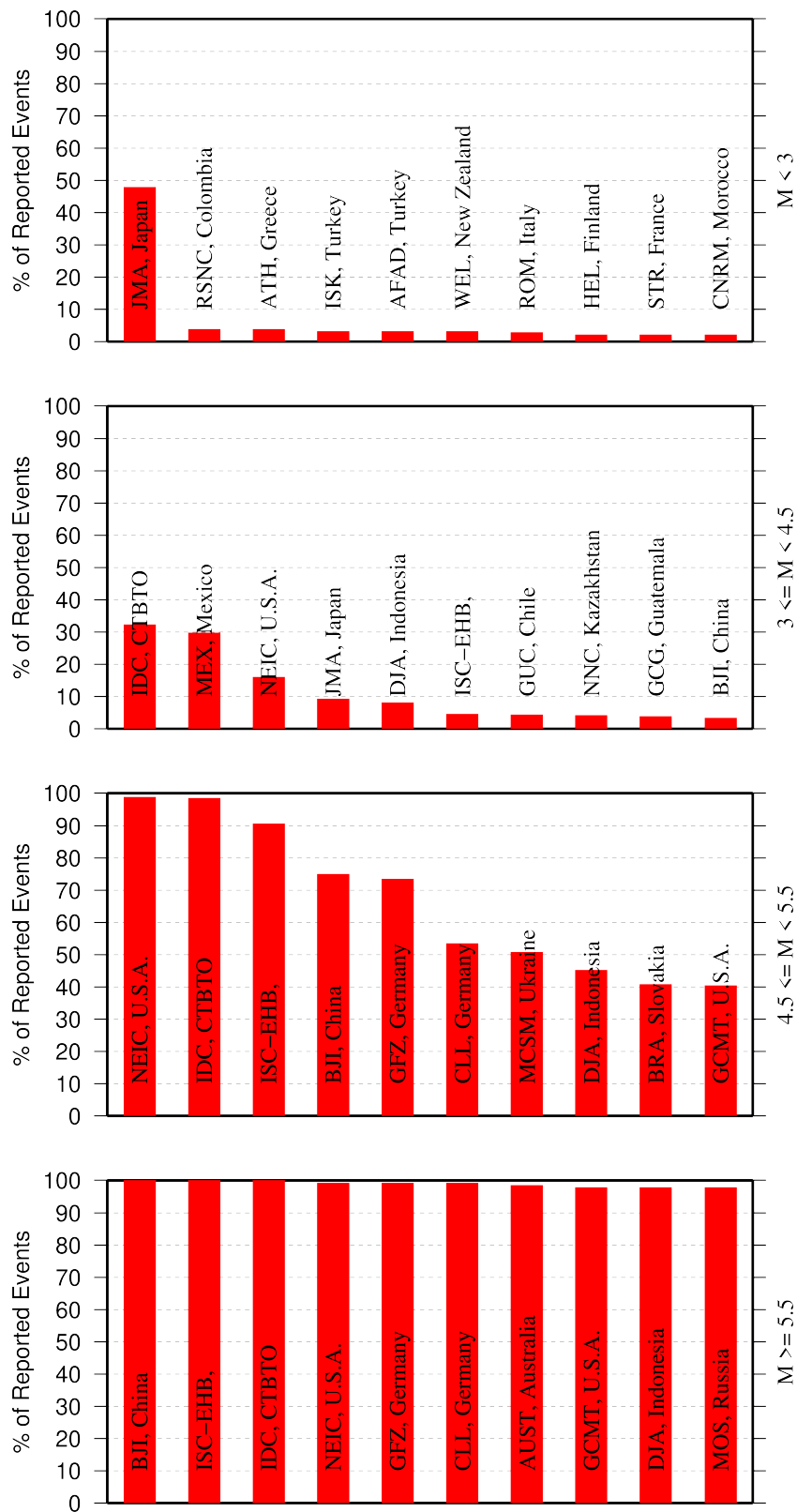


Figure 9.1: Frequency of events in the ISC Bulletin for which an agency reported at least one item of data: a moment tensor, a hypocentre, a station arrival time or an amplitude. The top ten agencies are shown for four magnitude intervals.

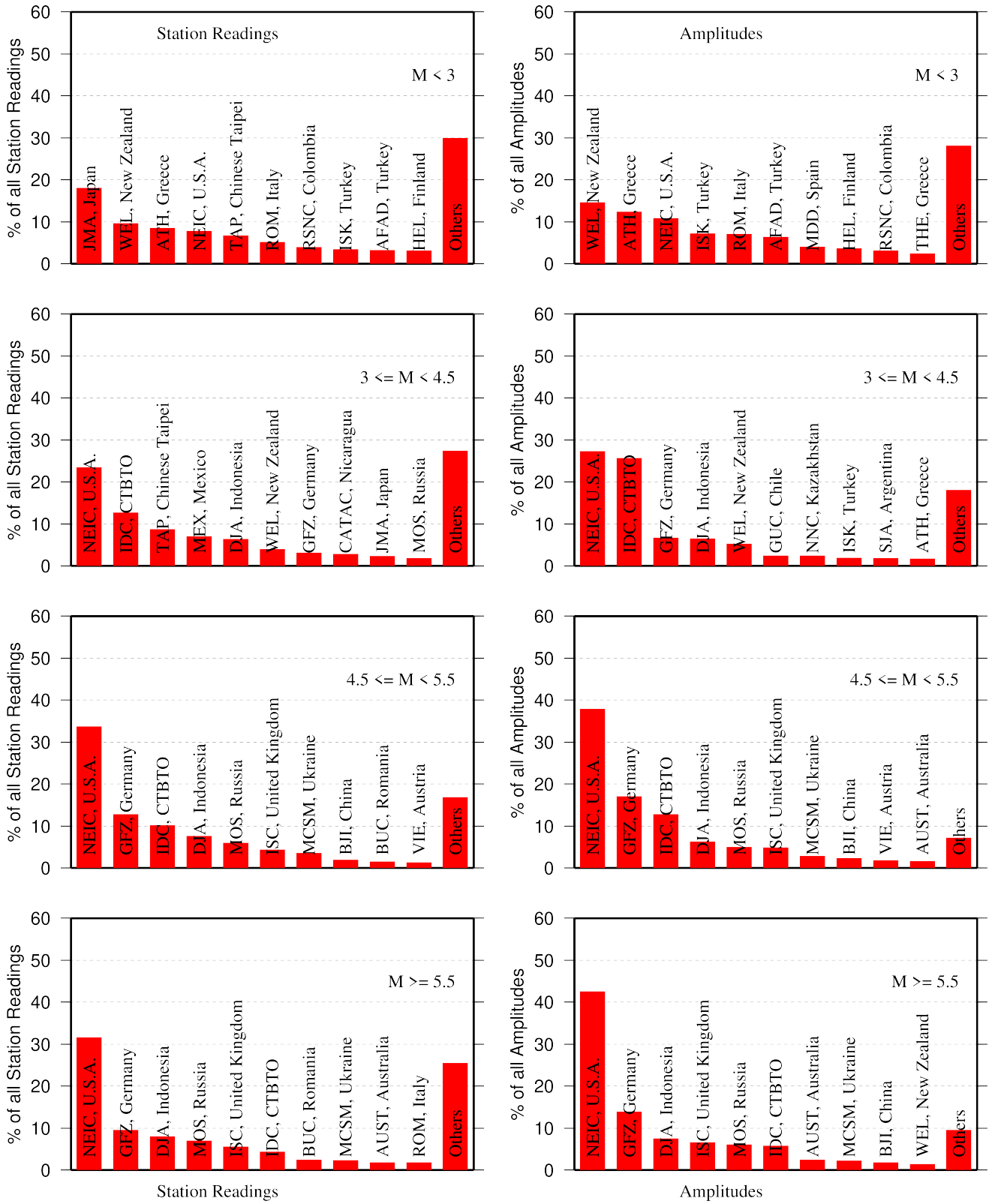


Figure 9.2: Contributions of station arrival time readings (left) and amplitudes (right) of agencies to the ISC Bulletin. Top ten agencies are shown for four magnitude intervals.

9.2 Contributors Reporting the Most Valuable Parameters

One of the main ISC duties is to re-calculate hypocentre estimates for those seismic events where a collective wealth of all station reports received from all agencies is likely to improve either the event location or depth compared to the hypocentre solution from each single agency. For areas with a sparse local seismic network or an unfavourable station configuration, readings made by other networks at teleseismic distances are very important. All events near mid-oceanic ridges as well as those in the majority of subduction zones around the world fall into this category. Hence we greatly appreciate the effort made by many agencies that report data for remote earthquakes (Figure 9.3). For some agencies, such as the IDC and the NEIC, it is part of their mission. For instance, the IDC reports almost every seismic event that is large enough to be recorded at teleseismic distance (20 degrees and beyond). This is largely because the International Monitoring System of primary arrays and broadband instruments is distributed at quiet sites around the world in order to be able to detect possible violations of the Comprehensive Nuclear-Test-Ban Treaty. The NEIC reported almost 50% of those events as their mission requires them to report events above magnitude 4.5 outside the United States of America. For other agencies reporting distant events it is an extra effort that they undertake to notify their governments and relief agencies as well as to help the ISC and academic research in general. Hence these agencies usually report on the larger magnitude events. BJI, GFZ, CLL, NAO, MCSM, BRA, VIE each reported individual station arrivals for several percent of all relevant events. We encourage other agencies to report distant events to us.

In addition to the first arriving phase we encourage reporters to contribute observations of secondary seismic phases that help constrain the event location and depth: S, Sn, Sg and pP, sP, PcP (Figure 9.4). We expect though that these observations are actually made from waveforms, rather than just predicted by standard velocity models and modern software programs. It is especially important that these arrivals are manually reviewed by an operator (as we know takes place at the IDC and NEIC), as opposed to some lesser attempts to provide automatic phase readings that are later rejected by the ISC due to a generally poor quality of unreviewed picking.

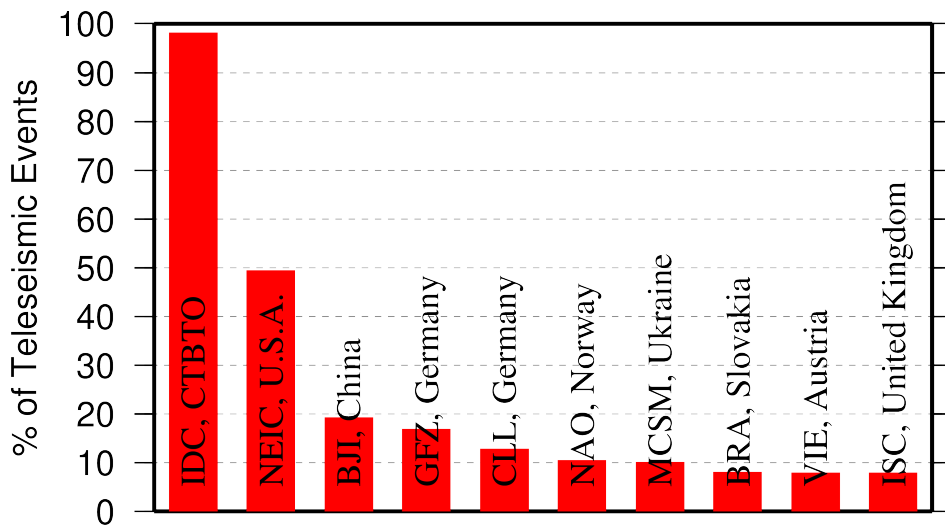


Figure 9.3: Top ten agencies that reported teleseismic phase arrivals for a large portion of ISC events.

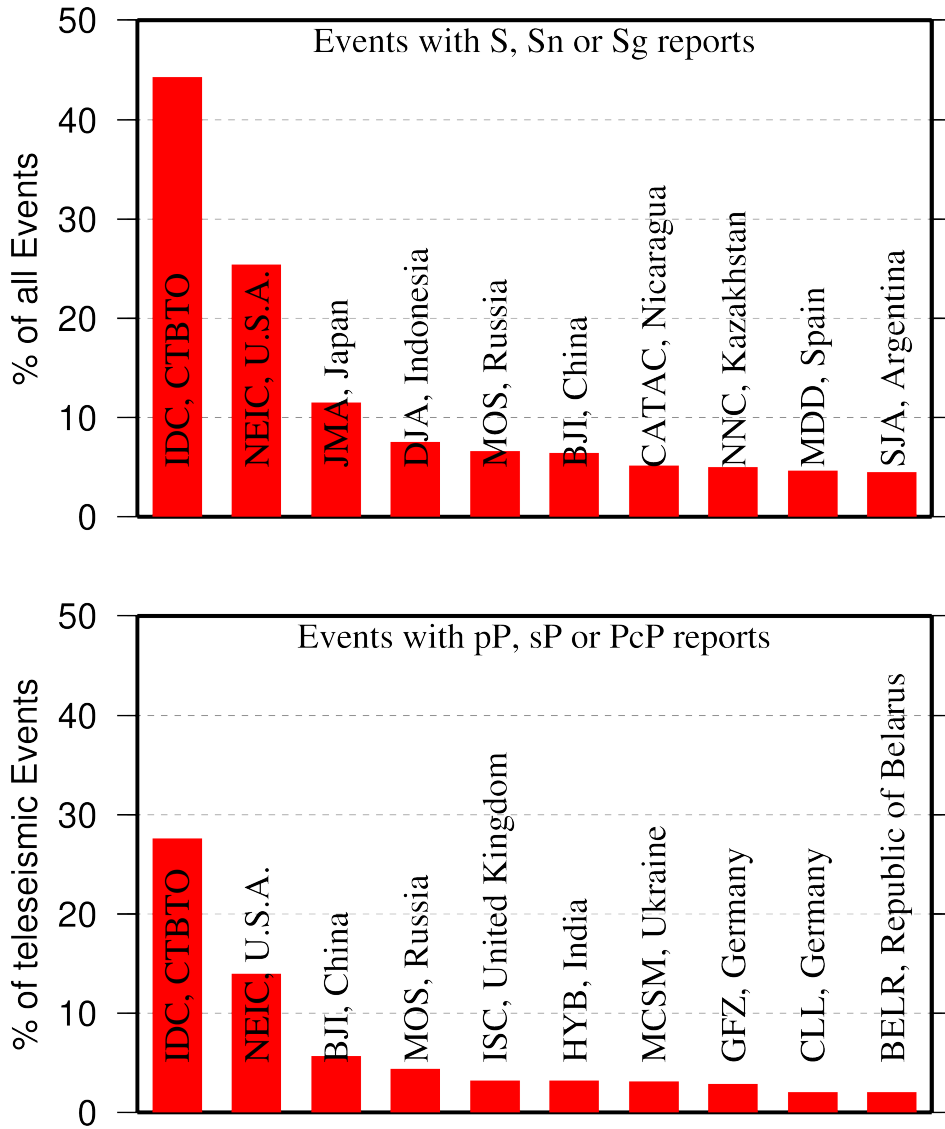


Figure 9.4: Top ten agencies that reported secondary phases important for an accurate epicentre location (top) and focal depth determination (bottom).

Another important long-term task that the ISC performs is to compute the most definitive values of M_S and m_b network magnitudes that are considered reliable due to removal of outliers and consequent averaging (using alpha-trimmed median) across the largest network of stations, generally not feasible for a single agency. Despite concern over the bias at the lower end of m_b introduced by the body wave amplitude data from the IDC, other agencies are also known to bias the results. This topic is further discussed in Section 8.5.

Notably, the IDC reports almost 100% of all events for which M_S and m_b are estimated. This is due to the standard routine that requires determination of body and surface wave magnitudes useful for discrimination purposes. NEIC, BJI, GFZ, MOS, CLL and a few other agencies (Figure 9.5) are also responsible for the majority of the amplitude and period reports that contribute towards the ISC magnitudes.

The top ten agencies that most frequently report seismic moment tensor determinations and moment magnitude are shown in Figure 9.6. The ISC calculates moment tensors, along with the earthquake source

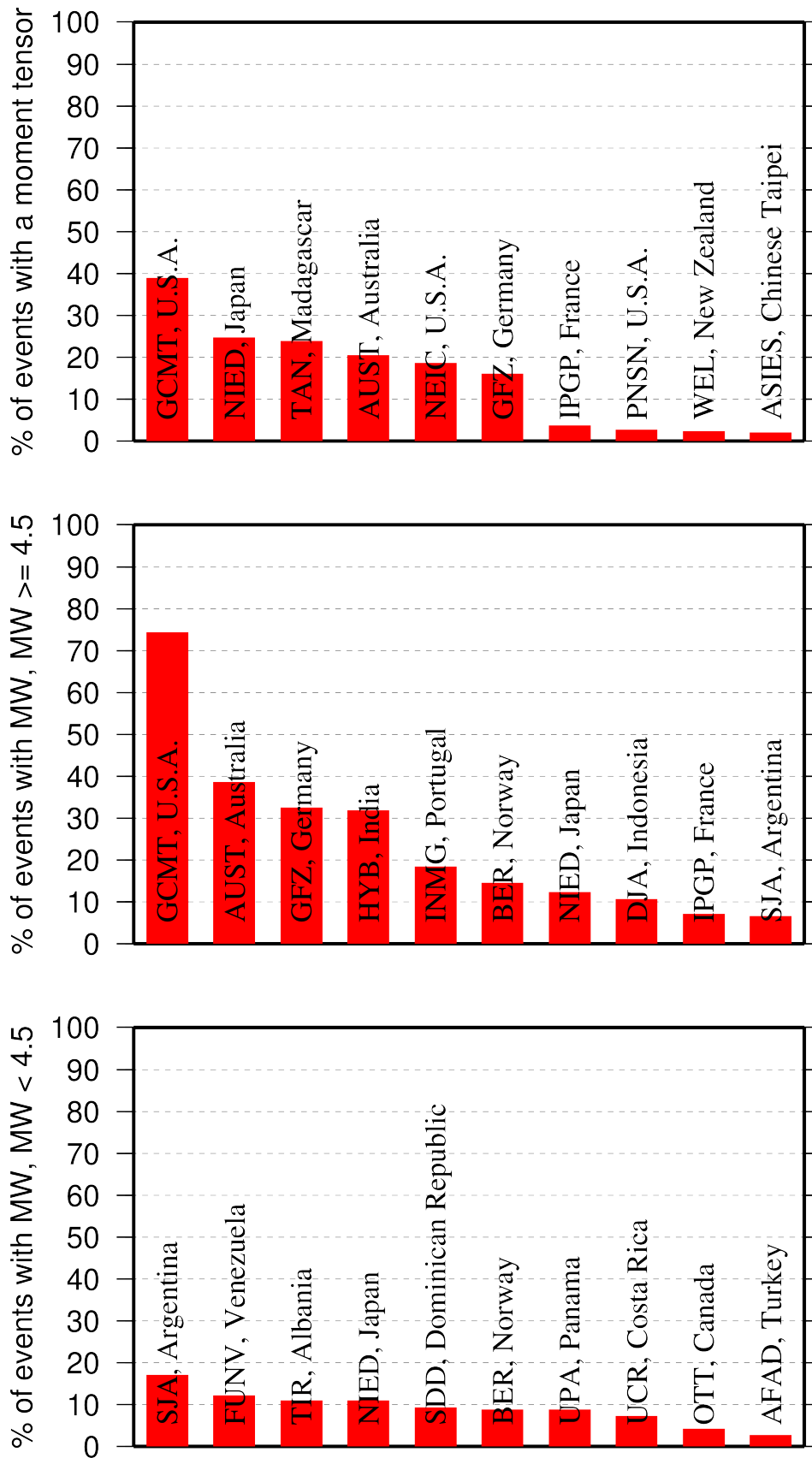


Figure 9.6: Top ten agencies that most frequently report determinations of seismic moment tensor (top) and moment magnitude (middle/bottom for M greater/smaller than 4.5).

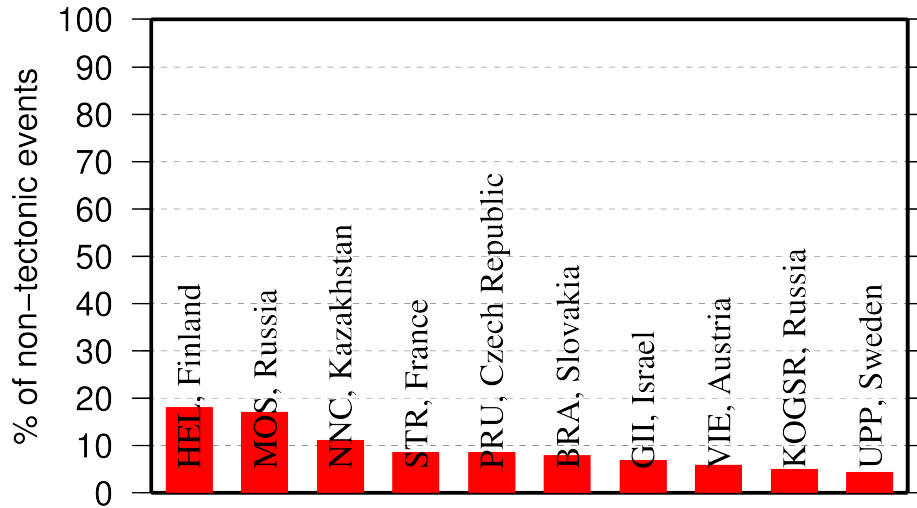


Figure 9.7: Top ten agencies that most frequently report non-tectonic seismic events to the ISC.

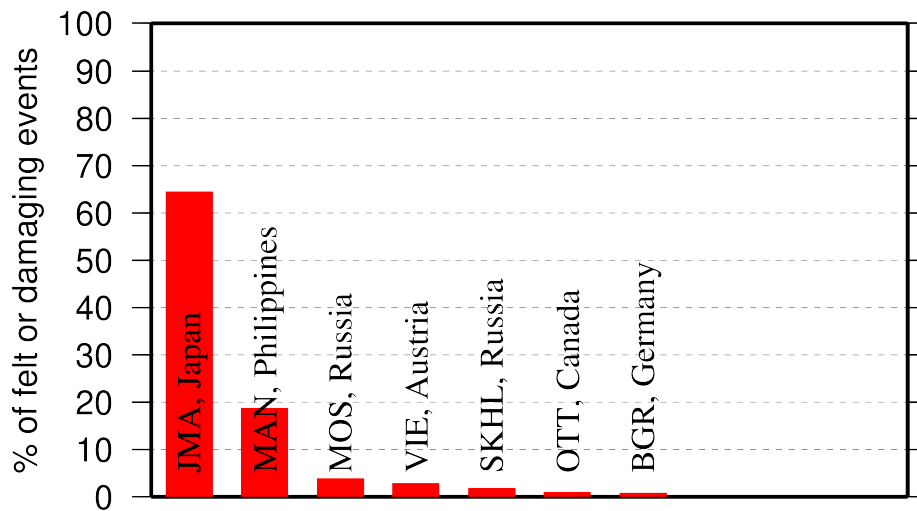


Figure 9.8: Top agencies that most frequently report macroseismic information to the ISC.

9.3 The Most Consistent and Punctual Contributors

During this six-month period, 27 agencies reported their bulletin data in one of the standard seismic formats (ISF, IMS, GSE, Nordic or QuakeML) and within the current 12-month deadline. Here we must reiterate that the ISC accepts reviewed bulletin data after a final analysis as soon as they are ready. These data, even if they arrive before the deadline, are immediately parsed into the ISC database, grouped with other data and become available to the ISC users on-line as part of the preliminary ISC Bulletin. There is no reason to wait until the deadline to send the data to the ISC. Table 9.1 lists all agencies that have been helpful to the ISC in this respect during the six-month period.

Table 9.1: Agencies that contributed reviewed bulletin data to the ISC in one of the standard international formats before the submission deadline.

Agency Code	Country	Average Delay from real time (days)
AUST	Australia	15
ZUR	Switzerland	17
WEL	New Zealand	18
IDC	Austria	28
ATH	Greece	28
IGIL	Portugal	31
PPT	French Polynesia	34
LDG	France	35
ECX	Mexico	35
BUC	Romania	37
NAO	Norway	44
KNET	Kyrgyzstan	49
BGS	United Kingdom	61
MDD	Spain	69
TIR	Albania	82
NEIC	U.S.A.	100
ISK	Turkey	109
SVSA	Portugal	126
INMG	Portugal	134
DSN	United Arab Emirates	167
BJI	China	167
KEA	Democratic People's Republic of Korea	175
VIE	Austria	250
NDI	India	288
BER	Norway	295
UCC	Belgium	321
IPEC	Czech Republic	328

10

Appendix

10.1 ISC Operational Procedures

10.1.1 Introduction

The relational database at the ISC is the primary source for the ISC Bulletin. This database is also the source for the ISC web-based search and this printed Summary. The ISC database is also mirrored at several institutions such as the Data Management Center of the Incorporated Research Institutions for Seismology (IRIS DMC), Earthquake Research Institute (ERI) of the University of Tokyo and a few others.

The database holds information about ISC events, both natural and anthropogenic. Information on each event may include hypocentre estimates, moment tensors, event type, felt and damaging reports and associated station observations reported by different agencies and grouped together per physical event.

The majority of the ISC events are small and are not reviewed by the ISC analysts. Those that are reviewed (usually magnitude greater than 3.5) may or may not include an ISC hypocentre solution and magnitude estimates. The decision depends on whether the wealth of combined information from several agencies as compared to the data of each single agency alone warrants the ISC location. The events are called ISC events regardless of whether they have been reviewed or located by the ISC or not.

All events located by the ISC are reviewed by the ISC analysts but not the other way round. Analyst review involves an examination of the integrity of all reported parametric information. It does not involve review of waveforms. Even if waveforms from all of the thousands of stations included in a typical recent month of the ISC Bulletin were freely available, it would be an unmanageable task to inspect them all.

We shall now describe briefly current processes and procedures involved in producing the Bulletin of the International Seismological Centre. These have been developed from former practices described in the Introduction to earlier issues of the ISC Bulletin to account for modern methods and technologies of data collection and analysis.

10.1.2 Data Collection

Parametric data, mainly comprising seismic event hypocentre solutions, phase arrival observations and associated magnitude data, are now mostly emailed to the ISC (seismo@isc.ac.uk) by agencies around the world. Other macroseismic and source information associated with seismic events may also be incorporated in accordance with modern standards. The process of data collection at the ISC involves the automatic parsing of these data into the ISC relational database. The ISC now has over 200 individual parsers to account for legacy and current bulletin data formats used by data reporters.

Figure 10.1 shows the 313 agencies that have reported bulletin data to the ISC, directly or via regional data centres, during the entire period of the ISC existence: these agencies are also listed in Table 10.2 of the Appendix. In Figure 10.1, corresponding countries are shown shaded in red. Please note that the continent of Antarctica appears white on the map despite a steady stream of bulletin data from Antarctic stations: the agencies that run these stations are based elsewhere.

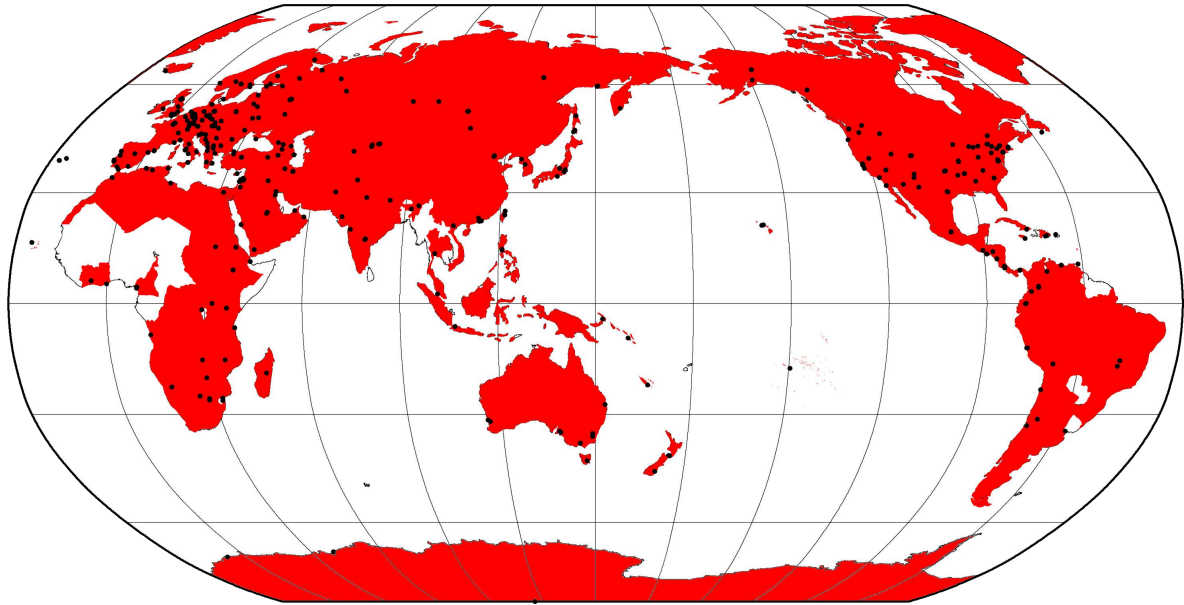


Figure 10.1: Map of 313 agencies and corresponding countries that have reported seismic bulletin data to the ISC at least once during the entire period of the ISC operations, either directly or via regional data centres. Corresponding countries are shaded in red.

10.1.3 ISC Automatic Procedures

Grouping

Grouping is the automatic process by which the many hypocentre solutions sent by the agencies reporting to the ISC for the same physical event are merged together into a single ISC event. This process possibly begins with an alert message and ends before a final review by ISC analysts. The process periodically runs through a set time interval of the input data stream, typically one day, looking for hypocentres in newly received data that are not yet grouped into an ISC event. Thus it considers only data more recent than the last data month reviewed by the ISC analysts. Immediately after grouping the seismic arrival associator is run on the same time interval, dealing with new phase arrival data not associated with any hypocentre.

The first stage of grouping gets a score where possible for each hypocentre to determine whether the reported hypocentre will be considered to be the primary estimate, or prime, for an ISC event. This score is based on the station arrival times reported in association with the hypocentre in four epicentral distance zones that characterise the networks of stations reporting:

1. Whole network
2. Local, 0 - 150 km

3. Near-regional, 3° - 10°
4. Teleseismic, 28° - 180°

For each distance zone, the azimuthal gap, the secondary azimuthal gap (the largest azimuthal gap filled by a single station), the minimum and maximum epicentral distance and number of stations are all used to calculate the value of dU , the normalised absolute deviation from best fitting uniformly distributed stations (*Bondár and McLaughlin, 2009a*). Clearly, this procedure can only use:

1. Bulletin data with hypocentres and sufficient associated seismic arrivals
2. Data for stations that are in the International Registry (IR)
3. Station data that are actually reported to ISC: CENC (China), for example, reports at most 34 stations, whilst many more may have been used to determine the hypocentre.

The hypocentres are then each considered in turn for grouping using one of two methods, the first by searching for a similar hypocentre, and the second by searching for the best fit of the reported phase arrival data that are associated with the candidate hypocentre. The method chosen for a reporter is based on feedback gained from ISC analysts.

For finding similar hypocentres, three sets of limits for origin-time difference and epicentral separation are used according to the type of bulletin data, be it alert, provisional or final. These limits are, respectively:

- ± 2 minutes and 10°
- ± 2 minutes and 4°
- ± 1 minutes and 2°

If there is no overlap with the hypocentre of an existing ISC event, a new event is formed. For each candidate hypocentre, a proximity score is otherwise calculated based on differences in time, t , and distance, s , between the candidate hypocentre and a hypocentre in an event with which it could potentially be grouped.

$$\text{Proximity score} = 2 - (dt/dt_{max}) - (ds/ds_{max})$$

where ds_{max} is the maximum distance between hypocentres and dt_{max} the maximum difference in origin time.

As long as there is no duplication of hypocentre (with the same author, origin time and location within tight limits) the candidate hypocentre together with the associated phase data is grouped with the prime hypocentre of the event and the initial dU score is used to reassess the prime hypocentre designation. Apparent duplicated hypocentre estimations, including preliminary solutions relayed by other agencies, need to be assessed to determine whether they should really be split between different events. Should there be two or more equally valid events, these can be assessed in turn and may eventually be merged together.

Grouping by fit of the associated phase arrival data is simpler. The residuals of the arrival data are calculated using ak135 travel times for all suitable prime hypocentres within the widest proximity limits given above for similar hypocentres. The hypocentre and associated phase arrival data is then grouped with the event with the best fitting prime hypocentre, which may similarly be re-designated according to the dU scores. Associations of phase arrival data are updated to be with the prime hypocentre estimate of each ISC event.

It follows that a hypocentre and associated phase arrival data submitted by a reporter will have the reported hypocentre set as the prime hypocentre in the ISC event if no other submitted hypocentre estimate is a closer match. It follows also that a hypocentre submitted without phase data can only be grouped with a similar hypocentre. Generally, early arriving data may be superseded by later arriving data: the data will still be in the ISC database but be deprecated, that is, marked as being no longer useful for further processes.

Association

Association is the automatic procedure, run routinely after grouping, that links reported phase arrivals at IR stations with the prime hypocentres of ISC events. As grouping took care of those phases associated with reported hypocentres, by associating the phases to the respective prime hypocentres of the ISC events without further checks, this procedure is only required for phase arrival observations that were sent without any association of event made for them by the reporter. Currently only 5% of arrival data is sent unassociated compared with 25% when the ISC began storing reported data directly to a database for data year 1999.

If a phase arrival is found to be very similar to another already reported, it is placed in the same event, otherwise the procedure below is followed.

For associating a phase arrival, suitable events are sought with prime hypocentre origin-times in the window 40 minutes before and 100 s after the arrival time. For each phase arrival and prime hypocentre an ak135 travel-time residual is calculated for either the reported arrival phase name or an alternative from a default list if appropriate. Possible timing errors that are multiples of 60 s (a minute) are considered if the phase arrival is at a station not known to be digitally recording. A reporting likelihood is then determined based on the reported event magnitude: a magnitude default of 3.0 is used if no magnitude is given.

A final score is calculated from the residuals, from the likelihood of the phase observations for the magnitude of the event and from the S-P misfit. A phase arrival along with all other phase arrivals in that reading for the station is then associated with the prime hypocentre with the best score. If no suitable match is found, the reading remains unassociated but may be used at some later stage.

Thresholding

Thresholding is the process determining which events are to be reviewed by the ISC analysts. In former times, before email transmission of data was convenient, all events were reviewed, with magnitudes nearly always 3.5 or above. Nowadays, data contributors are encouraged to send all their data, which

are stored in the ISC database. The overwhelming amount of data, including that for many more smaller events and from many more seismograph stations, led to the advent of ISC Comprehensive Bulletin, for all events, and the ISC Reviewed Bulletin, for selected events reviewed by ISC analysts. Thresholding has been under constant review since the start of the 1999 data year.

Several criteria are considered to decide which events merit review. Once a decision is made, whether or not an event is to be reviewed, further criteria are not considered.

In this section, M is the maximum magnitude reported by any agency for the event. The sequence of tests in the automatic decision process for reviewing events is currently:

- All events reported by the International Data Centre (IDC) of the Comprehensive Nuclear-Test-Ban Treaty Organization (CTBTO) are reviewed.
- If M is greater than or equal to 3.5, the event is reviewed.
- If M is less than 2.5, the event is not reviewed.
- If M is unknown, the number of data sources of hypocentres and phase arrivals is used. Care is taken here to avoid counting indirect reports arriving via agencies such as NEIC, which compile regional and global data:
 - If the number of hypocentre authors is greater than two and the maximum epicentral distance of arrival data is greater than 10° , the event is reviewed.
 - If the number of arrival authors is greater than two and the maximum epicentral distance of arrival data is greater than 10° , the event is reviewed.
 - Otherwise the event is not reviewed.
- If M is between 2.5 and 3.5:
 - If the number of hypocentre and seismic arrival authors is less than two, the event is not reviewed.
 - If any bulletin contributing to the event has at least ten stations within 3° and the secondary azimuthal gap (the largest azimuthal gap filled by a single station) is less than 135° , the event is not reviewed.

Location by the ISC

The automatic processes group and associate incoming data into ISC events as indicated above. These data are available to users before review by the ISC analysts but there will be no ISC hypocentre solutions for any of the events. The candidate events due for review by the ISC analysts are determined by the thresholding process, which is why many smaller events remain without an ISC hypocentre solution even after the analyst review.

Several further checks of the data are made in preparation for the analyst review, and initial trial estimates for ISC hypocentres are then generated using the accumulated data. If sufficiently robust, the

ISC hypocentre estimation will be retained and be made the prime solution for the event, but this, of course, will itself be subject to the analyst review.

It is important to note that not all reviewed events will have an ISC hypocentre. At least one of the criteria listed below must be met for an initial ISC location of a reviewed event to be made:

- All events with an IDC hypocentre, unless IDC is the only hypocentre author and there are less than six associated phases.
- Two or more reporters of data
- Phase data at epicentral distance $\geq 20^\circ$

The ISC locator also needs an initial seed location; in all events except those with eight or more reporters of data where the existing prime is used, this is calculated using a Neighbourhood Algorithm (NA) (*Sambridge, 1999; Sambridge and Kennett, 2001*). More information about the ISC location algorithm and initial seed is given in the next section.

10.1.4 ISC Location Algorithm

The ISC location algorithm is described in detail in *Bondár and Storchak (2011)* (<https://doi.org/10.1111/j.1365-246X.2011.05107.x>, Manual: www.isc.ac.uk/iscbulletin/iscloc/); here we give a short summary of the major features. Ever since the ISC came into existence in 1964, it has been committed to providing a homogeneous bulletin that benefits scientific research. Hence the location algorithm used by the ISC then, except for some minor modifications, had remained largely unchanged for 40 years (*Adams et al., 1982; Bolt, 1960*). While the ISC location procedures had served the scientific community well in the past, they could certainly be improved and a new ISC location algorithm was developed and implemented from data year 2010. Since then, the entire ISC Bulletin has been relocated with the new location algorithm as part of the Rebuild project (*Storchak et al., 2017; 2020*).

Linearised location algorithms are very sensitive to the initial starting point for the location. The old procedures made the assumption that a good initial hypocentre is available among the reported hypocentres. However, there is no guarantee that any of the reported hypocentres are close to the global minimum in the search space. Furthermore, attempting to find a free-depth solution was futile when the data had no resolving power for depth (e.g. when the first arrival is not within the inflection point of the P travel-time curve). When there was no depth resolution, the algorithm would simply pick a point on the origin time – depth trade-off curve. The old ISC locator assumed that the observational errors are independent. The recent years have seen a phenomenal growth both in the number of reported events and phases, owing to the ever-increasing number of stations worldwide. Similar ray paths will produce correlated travel-time prediction errors due to unmodelled heterogeneities in the Earth, resulting in underestimated location uncertainties and for unfavourable network geometries, location bias. Hence, accounting for correlated travel-time prediction errors becomes imperative if we want to improve (or simply maintain) location accuracy as station networks become progressively denser. Finally, publishing network magnitudes that may have been derived from a single station measurement was rather prone to producing erroneous event magnitude estimates.

To meet the challenge imposed by the ever-increasing data volume from heavily unbalanced networks a new ISC location algorithm was introduced to ensure the efficient handling of data and to further improve the location accuracy of events reviewed by the ISC. The ISC location algorithm

- Uses all ak135 (*Kennett et al.*, 1995) predicted phases (including depth phases) in the location;
- Obtains the initial hypocentre guess via the Neighbourhood Algorithm (NA) (*Sambridge*, 1999; *Sambridge and Kennett*, 2001);
- Performs iterative linearised inversion using an *a priori* estimate of the full data covariance matrix to account for correlated model errors (*Bondár and McLaughlin*, 2009b);
- Attempts a free-depth solution if and only if there is depth resolution, otherwise it fixes the depth to a region-dependent default depth;
- Scales uncertainties to 90% confidence level and calculates location quality metrics for various distance ranges;
- Obtains a depth-phase depth estimate based on reported surface reflections via depth-phase stacking (*Murphy and Barker*, 2006);
- Provides robust network magnitude estimates with uncertainties.

Seismic Phases

One of the major advantages of using the ak135 travel-time predictions (*Kennett et al.*, 1995) is that they do not suffer from the baseline difference between P, S and PKP phases compared with the Jeffreys-Bullen tables (*Jeffreys and Bullen*, 1940). Furthermore, ak135 offers an abundance of phases from the IASPEI Standard Seismic List (*Storchak et al.*, 2003; 2011) that can be used in the location, most notably the PKP branches and depth-sensitive phases. Elevation and ellipticity corrections (*Dziewonski and Gilbert*, 1976; *Engdahl et al.*, 1998; *Kennett et al.*, 1996), using the WG84 ellipsoid parameters, are added to the ak135 predictions. For depth phases, bounce point (elevation correction at the surface reflection point) and water depth (for pwP) corrections are calculated using the algorithm of *Engdahl et al.* (1998). We use the ETOPO1 global relief model (*Amante and Eakins*, 2009) to obtain the elevation or the water depth at the bounce point.

Phase picking errors are described by *a priori* measurement error estimates derived from the inspection of the distribution of ground truth residuals (residuals calculated with respect to the ground truth location) from the IASPEI Reference Event List (*Bondár and McLaughlin*, 2009a). For phases that do not have a sufficient number of observations in the ground truth database we establish *a priori* measurement errors so that the consistency of the relative weighting schema is maintained. First-arriving P-type phases (P, Pn, Pb, Pg) are picked more accurately than later phases, so their measurement error estimates are the smallest, 0.8 s. The measurement error for first-arriving S-phases (S, Sn, Sb, Sg) is set to 1.5 s. Phases traversing through or reflecting from the inner/outer core of the Earth have somewhat larger (1.3 s for PKP, PKS, PKKP, PKKS and P'P' branches as well as PKiKP, PcP and PcS, and 1.8 s for SKP, SKS, SKKP, SKKS and S'S' branches as well as SKiKP, ScP and ScS) measurement error estimates

to account for possible identification errors among the various branches. Free-surface reflections and conversions (PnPn, PbPb, PgPg, PS, PnS, PgS and SnSn, SbSb, SgSg, SP, SPn, SPg) are observed less frequently and with larger uncertainty, and therefore suffer from large, 2.5 s, measurement errors. Similarly, a measurement error of 2.8 s is assigned to the longer period and typically emergent diffracted phases (Pdif, Sdif, PKPdif). The *a priori* measurement error for the commonly observed depth phases (pP, sP, pS, sS and pwP) is set to 1.3 s, while the remaining depth phases (pPKP, sPKP, pSKS, sSKS branches and pPb, sPb, sSb, pPn, sPn, sSn) have the measurement error estimate set to 1.8 s. We set the measurement error estimate to 2.5 s for the less reliable depth phases (pPg, sPg, sSg, pPdif, pSdif, sPdif and sSdif). Note that we also allow for distance-dependent measurement errors. For instance, to account for possible phase identification errors at far-regional distances the *a priori* measurement error for Pn and P is increased from 0.8 s to 1.2 s and for Sn and S from 1.5 s to 1.8 s between 15° and 28°. The measurement errors between 40° and 180° are set to 1.3 s and 1.8 s for the prominent PP and SS arrivals respectively, but they are increased to 1.8 s and 2.5 s between 25° and 40°.

The relative weighting scheme (Figure 10.2) described above ensures that arrivals picked less reliably or prone to phase identification errors are down-weighted in the location algorithm. Since the ISC works with reported parametric data with wildly varying quality, we opted for a rather conservative set of *a priori* measurement error estimates.

Correlated Travel-Time Prediction Error Structure

Most location algorithms, either linearised or non-linear, assume that all observational errors are independent. This assumption is violated when the separation between stations is less than the scale length of local velocity heterogeneities. When correlated travel-time prediction errors are present, the data covariance matrix is no longer diagonal, and the redundancy in the observations reduces the effective number of degrees of freedom. Thus, ignoring the correlated error structure inevitably results in underestimated location uncertainty estimates. For events located by an unbalanced seismic network this may also lead to a biased location estimate. *Chang et al.* (1983) demonstrated that accounting for correlated error structure in a linearised location algorithm is relatively straightforward once an estimate of the non-diagonal data covariance matrix is available. To determine the data covariance matrix we follow the approach described by *Bondár and McLaughlin* (2009b). They assume that the similarity between ray paths is well approximated by the station separation. This simplifying assumption allows for the estimation of covariances between station pairs from a generic P variogram model derived from ground truth residuals. Because the overwhelming number of phases in the ISC Bulletin is teleseismic P, we expect that the generic variogram model will perform reasonably well anywhere on the globe.

Since in this representation the covariances depend only on station separations, the covariance matrix (and its inverse) needs to be calculated only once. We assume that different phases owing to the different ray paths they travel along as well as station pairs with a separation larger than 1000 km are uncorrelated. Hence, the data covariance matrix is a sparse, block-diagonal matrix. Furthermore, if the stations in each phase block are ordered by their nearest neighbour distance, the phase blocks themselves become block-diagonal. To reduce the computational time of inverting large matrices we exploit the inherent block-diagonal structure by inverting the covariance matrix block-by-block. The *a priori* measurement error variances are added to the diagonal of the data covariance matrix.

Depth Resolution

In principle, depth can be resolved if there is a mixture of upgoing and downgoing waves emanating from the source, that is, if there are stations covering the distance range where the vertical partial derivative of the travel-time of the first-arriving phase changes sign (local networks), or if there are phases with vertical slowness of opposite sign (depth phases). Core reflections, such as PcP, and to a lesser extent, secondary phases (S in particular) could also help in resolving the depth.

We developed a number of criteria to test whether the reported data for an event have sufficient depth resolution:

- local network: one or more stations within 0.2° with time-defining phases
- depth phases: five or more time-defining depth phases reported by at least two agencies (to reduce a chance of misinterpretation by a single inexperienced analyst)
- core reflections: five or more time-defining core reflections (PcP, ScS) reported by at least two agencies
- local/near regional S: five or more time-defining S and P pairs within 3°

We attempt a free-depth solution if any of the above criteria are satisfied; otherwise we fix the depth to a default depth dependent on the epicentre location. This will preferably be the grid depth based on the ISC default depth grid (Figure 10.3). Where no grid depth is available the default depth is set to either 10 km or 35 km based on the GRN (See Figure 10.4. A list of GRN's can be found in Section 10.2.2). The default depth grid was derived from the EHB (*Engdahl et al., 1998*) free-depth solutions, including the fixed-depth EHB earthquakes that were flagged as having reliable depth estimate (personal communication with Bob Engdahl), as well as from free-depth solutions obtained by the new locator when locating the entire ISC Bulletin data-set. As Figure 10.3 indicates, the default depth grid provides a reasonable depth estimate where seismicity is well established. Note that the depths of known anthropogenic events and landslides are fixed to the surface.

Depth-Phase Stack

While we use depth phases directly in the location, the depth-phase stacking method (*Murphy and Barker, 2006*) provides an independent means to obtain robust depth estimates. Because the depth obtained from the depth-phase stacking method implicitly depends on the epicentre itself, we perform the depth-phase stack only twice: first, with respect to the initial location in order to obtain a reasonable starting point for the depth in the grid search described in the following section; second, with respect to the final location to obtain the final estimate for the depth-phase constrained depth.

Initial Hypocentre

For poorly recorded events the reported hypocentres may exhibit a large scatter and they could suffer from large location errors, especially if they are only recorded teleseismically. In order to obtain a good

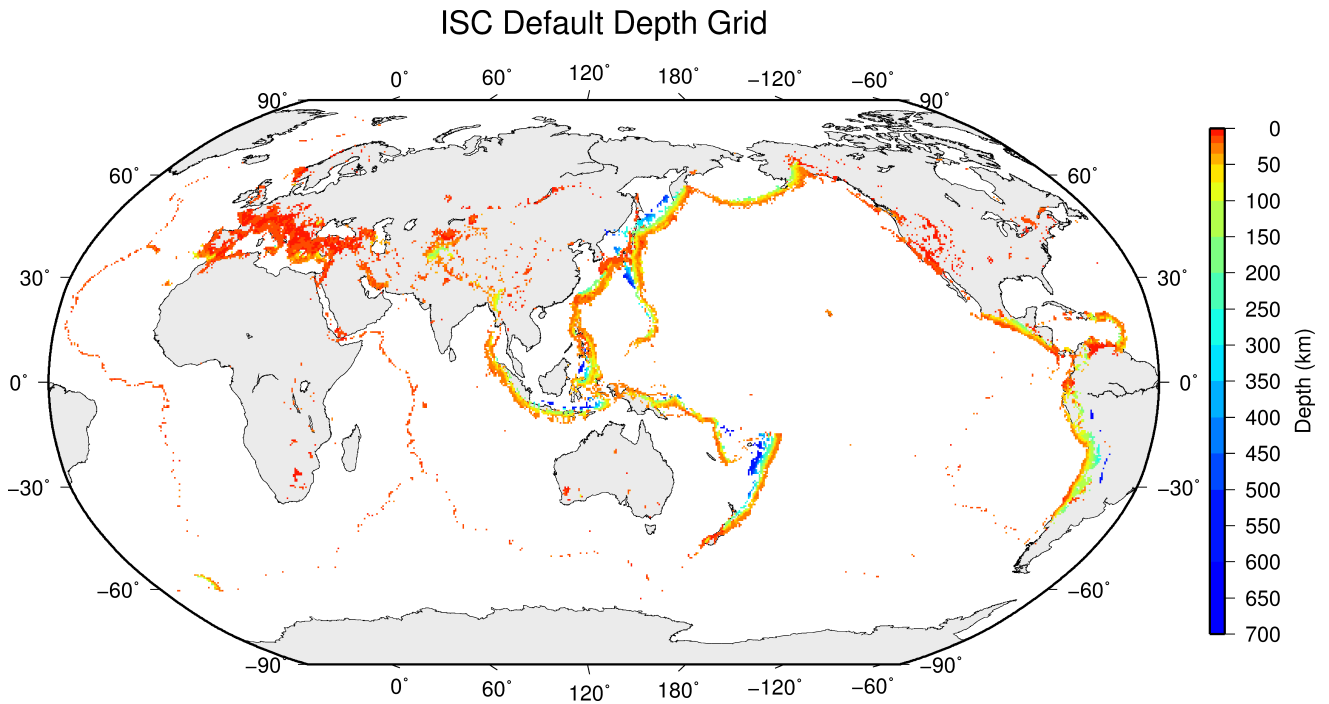


Figure 10.3: Default depths on a 0.5×0.5 degree grid derived from EHB free-depth solutions and EHB events flagged as reliable depth, as well as free-depth solutions from the entire ISC Bulletin located with the new locator.

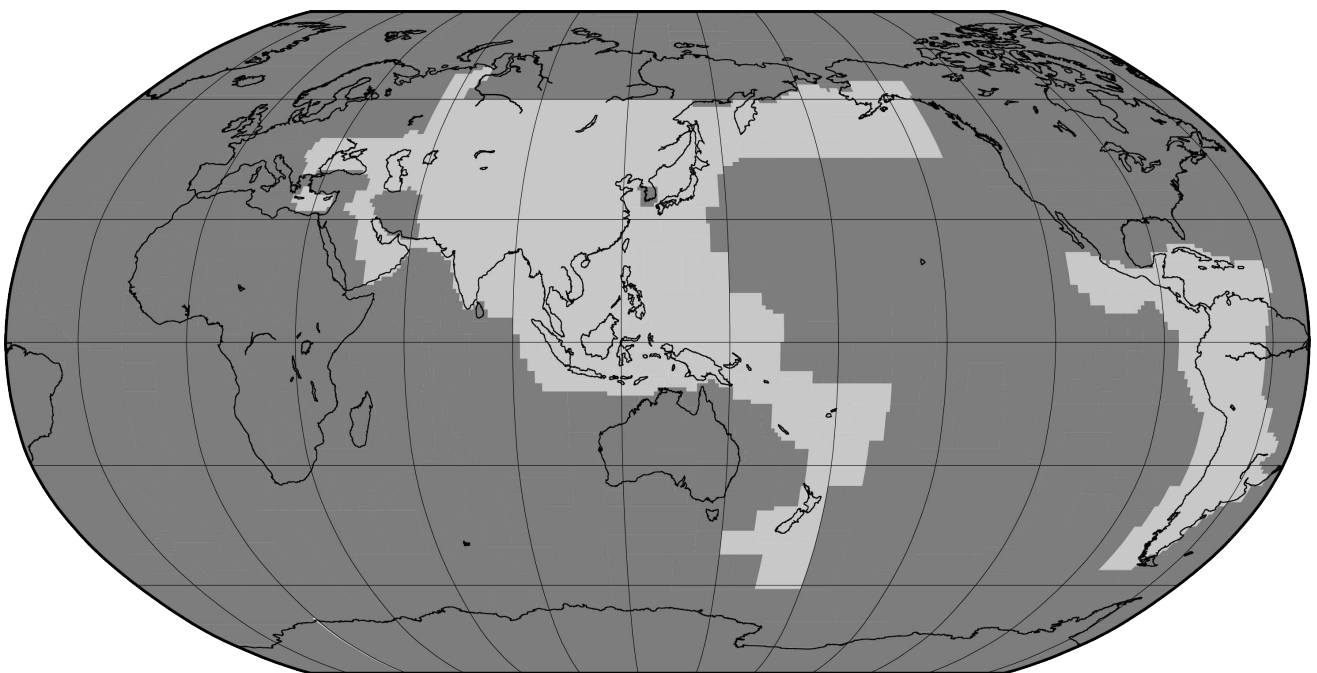


Figure 10.4: Default depths by Flinn-Engdahl geographic regions. Dark grey regions are set to 10 km and light grey to 35 km

initial hypocentre guess for the linearised location algorithm we employ the Neighbourhood Algorithm (NA) (*Sambridge, 1999; Sambridge and Kennett, 2001*). NA is a nonlinear grid search method capable of exploring a large search space and rapidly closing in on the global optimum. *Kennett (2006)* discusses in detail the NA algorithm and its use for locating earthquakes.

We perform a search around the median of reported hypocentre parameters with a generously defined search region – within a 2° radius circle around the median epicentre, 10 s around the median origin time and 150 km around the median reported depth. These default search parameters were obtained by trial-and-error runs to achieve a compromise between execution time and allowance for gross errors in the median reported hypocentre parameters. Note that if our test for depth resolution fails, we fix the depth to the region-dependent default depth. The initial hypocentre estimate will be the one with the smallest L1-norm misfit among the NA trial hypocentres. Once close to the global optimum, we proceed with the linearised location algorithm to obtain the final solution and corresponding formal uncertainties.

Iterative Linearised Location Algorithm

We adopt the location algorithm described in detail in *Bondár and McLaughlin (2009b)*. Recall that in the presence of correlated travel-time prediction errors the data covariance matrix is no longer diagonal. Using the singular value decomposition of the data covariance matrix we construct a projection matrix that orthogonalises the data set and projects redundant observations into the null space. In other words, we solve the inversion problem in the eigen coordinate system in which the transformed observations are independent.

The model covariance matrix yields the four-dimensional error ellipsoid whose projections provide the two-dimensional error ellipse and one-dimensional errors for depth and origin time. These uncertainties are scaled to the 90% confidence level. Note that since we projected the system of equations into the eigen coordinate system, the number of independent observations is less than the total number of observations. Hence, the estimated location error ellipses necessarily become larger, providing a more realistic representation of the location uncertainties. The major advantage of this approach is that the projection matrix is calculated only once for each event location.

Validation Tests

To demonstrate improvements due to the new location procedures, we located some 7,200 GT0-5 events in the IASPEI Reference Event List (*Bondár and McLaughlin, 2009a*) both with the old ISC locator (which constitutes the baseline) and with the new location algorithm. We also located the entire available (1960-2010) ISC Bulletin, including four years of the International Seismological Summary (ISS, the predecessor of the ISC) catalogue (*Villaseñor and Engdahl, 2005; 2007*).

The location of GT events demonstrated that the new ISC location algorithm provides small but consistent location improvements, considerable improvements in depth determination and significantly more accurate formal uncertainty estimates. Even using a 1-D model and a variogram model that fits teleseismic observations we could achieve realistic uncertainty estimates, as the 90% confidence error ellipses

cover the true locations 80-85% of the time. The default depth grid provides reasonable depth estimates where there is seismicity. We have shown that the location and depth accuracy obtained by the new algorithm matches or surpasses the accuracy of the original EHB Bulletin. The EHB Bulletin has since been improved and is replaced by the ISC-EHB Bulletin.

We noted above that the location improvements for the ground truth events are consistent, but minor. This is not surprising as most of the events in the IASPEI Reference Event List are very well-recorded with a small azimuthal gap and dominated by P-type phases. In these circumstances we can expect significant location improvements only for heavily unbalanced networks where large numbers of correlated ray paths conspire to introduce location bias. On the other hand, the ISC Bulletin represents a plethora of station configurations ranging from reasonable to the most unfavourable network geometries. Hence, more dramatic location improvements when locating the ISC Bulletin is expected. Although in this case we cannot measure the improvement in location accuracy due to the lack of ground truth information, we show that with the new locator we obtain significantly better clustering of event locations (Figure 10.5), thus providing an improved view of the seismicity of the Earth.

Magnitude Calculation

Currently the ISC locator calculates body and surface wave magnitudes. MS is calculated for shallow events (depth < 60 km) only. At least three station magnitudes are required for a network (mb or MS) magnitude. The network magnitude is defined as the median of the station magnitudes, and its uncertainty is defined as the standard median absolute deviation (SMAD) of the alpha-trimmed ($\alpha = 20\%$) station magnitudes.

The station magnitude is defined as the median of reading magnitudes for a station. The reading magnitude is defined as the magnitude computed from the maximal $\log(A/T)$ in a reading. Amplitude magnitudes are calculated for each reported amplitude-period pair.

Body-Wave Magnitudes

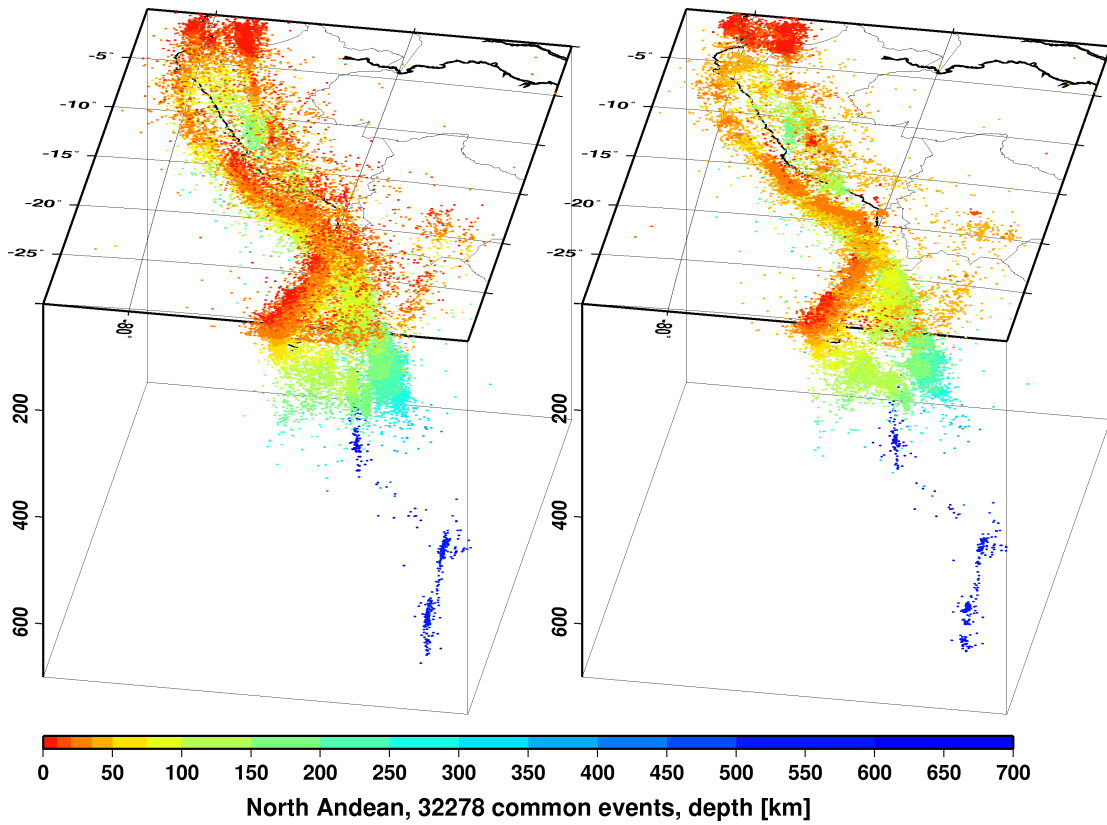
Body-wave magnitudes are calculated for each reported amplitude-period pair, provided that the phase is in the list of phases that can contribute to mb (P, pP, sP, AMB, IAmb, pmax), the station is between the epicentral distances $21 - 100^\circ$ and the period is less than 3 s.

A reading contains all parametric data reported by a single agency for an event at a station, and it may have several reported amplitude and periods. The amplitudes are measured as zero-to-peak values in nanometres. For each pair an amplitude mb is calculated.

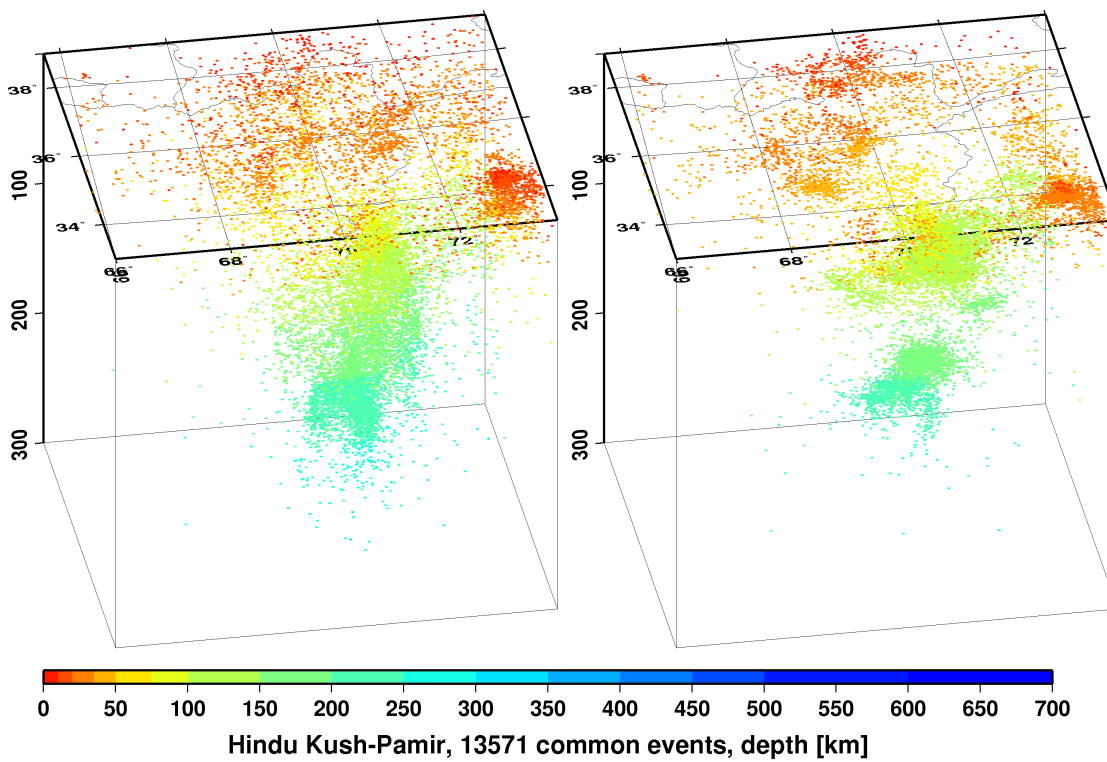
$$mb_{amp} = \log(A/T) + Q(\Delta, h) - 3 \quad (10.1)$$

If no amplitude-period pairs are reported for a reading, the body-wave magnitude is calculated using the reported \logat values for $\log(A/T)$.

$$mb_{amp} = \logat + Q(\Delta, h) - 3 \quad (10.2)$$



(a)



(b)

Figure 10.5: Comparison of seismicity maps for common events in the reviewed ISC Bulletin (old locator, left) and the located ISC Bulletin (new locator, right) for the North Andean (a) and Hindu Kush - Pamir regions (b). The events are better clustered when located with the new locator.

where the magnitude attenuation $Q(\Delta, h)$ value is calculated using the Gutenberg-Richter tables (*Gutenberg and Richter, 1956*).

For each reading the ISC locator finds the reported amplitude-period pair for which A/T is maximal:

$$mb_{rd} = \log(\max(A/T)) + Q(\Delta, h) - 3 \quad (10.3)$$

Or, if no amplitude-period pairs were reported for the reading:

$$mb_{rd} = \max(\logat) + Q(\Delta, h) - 3 \quad (10.4)$$

Several agencies may report data from the same station. The station magnitude is defined as the median of the reading magnitudes for a station.

$$mb_{sta} = \text{med}(mb_{rd}) \quad (10.5)$$

Once all station mb values are determined, the station magnitudes are sorted and the lower and upper alpha percentiles are made non-defining. The network mb and its uncertainty are then calculated as the median and the standard median absolute deviation (SMAD) of the alpha-trimmed station magnitudes, respectively.

Surface-Wave Magnitudes

Surface-wave magnitudes are calculated for each reported amplitude-period pair, provided that the phase is in the list of phases that can contribute to MS (AMS , $IAMS_{20}$, LR , MLR , M , L), the station is between the epicentral distances $20 - 160^\circ$ and the period is between $10 - 60$ s.

For each reported amplitude-period pair MS is calculated using the Prague formula (*Vaněk et al., 1962*). Amplitude MS is calculated for each component (Z , E , N) separately.

$$MS_{amp} = \log(A/T) + 1.66 * \log(\Delta) + 0.3 \quad (10.6)$$

To calculate the reading MS , the ISC locator first finds the reported amplitude-period pair for which A/T is maximal on the vertical component.

$$MS_Z = \log(\max(A_Z/T_Z)) + 1.66 * \log(\Delta) + 0.3 \quad (10.7)$$

Then it finds the $\max(A/T)$ for the E and N components for which the period measured on the horizontal components is within ± 5 s from the period measured on the vertical component.

$$MS_E = \log(\max(A_E/T_E)) + 1.66 * \log(\Delta) + 0.3 \quad (10.8)$$

$$MS_N = \log(\max(A_N/T_N)) + 1.66 * \log(\Delta) + 0.3 \quad (10.9)$$

The horizontal MS is calculated as

$$\max(A/T)h = \begin{cases} \sqrt{2(\max(A_E/T_E))^2} & \text{if } MS_N \text{ does not exist} \\ \sqrt{(\max(A_E/T_E))^2 + (\max(A_N/T_N))^2} & \text{if } MS_E \text{ and } MS_N \text{ exist} \\ \sqrt{2(\max(A_N/T_N))^2} & \text{if } MS_E \text{ does not exist} \end{cases} \quad (10.10)$$

$$MS_H = \log(\max(A/T)_H) + 1.66 * \log(\Delta) + 0.3 \quad (10.11)$$

The reading MS is defined as

$$MS = \begin{cases} (MS_Z + MS_H)/2 & \text{if } MS_Z \text{ and } MS_H \text{ exist} \\ MS_H & \text{if } MS_Z \text{ does not exist} \\ MS_Z & \text{if } MS_H \text{ does not exist} \end{cases} \quad (10.12)$$

Several agencies may report data from the same station. The station magnitude is defined as the median of the reading magnitudes for a station.

$$MS_{sta} = \text{med}(MS_{rd}) \quad (10.13)$$

Once all station MS values are determined, the station magnitudes are sorted and the lower and upper alpha percentiles are made non-defining. The network MS and its uncertainty are calculated as the median and the standard median absolute deviation (SMAD) of the alpha-trimmed station magnitudes, respectively.

10.1.5 Review Process

Typically, for each month, the ISC analysts now review approximately 10-20% of the events in the ISC database, currently 3,500-5,000 per data month. This review is done about 24 months behind real time to allow for the comprehensive collection of data from networks and data centres worldwide.

Users of the ISC Bulletin can be assured that all ISC Bulletin events with an ISC hypocentre solution have been reviewed by the ISC analysts. Not all reviewed events will end up having an ISC hypocentre solution, but events that have not been reviewed are flagged accordingly.

At the beginning of analysis of each data month, events that need to be reviewed by an analyst are flagged based on the thresholding procedure described in Section 10.1.3. These events are split into daily blocks on average consisting of 100 – 150 events. They are then analysed and if necessary edited by an analyst. After all blocks in a data month have been reviewed, they are being assessed again by a different analyst to spot any potential inconsistencies that might have been overlooked in the first run.

Analysis is done with the help of the Visual Bulletin Analysis System (VBAS) developed at the ISC. For each event it shows the reported hypocentres, magnitudes and phase arrivals as well as an ISC

solution for the hypocentre, if there is one, along with phase arrival-time residuals and error estimates. Amongst other visual aids, VBAS plots graphs of travel time curves, seismicity maps, depth distributions of reported hypocentres and station geometry.

The analysts have the capability to execute a variety of commands that can be used to merge or split events, to move phase arrivals or hypocentres from one event to another or to modify the reported phase names. There are also several commands to change the starting depth or location in the location algorithm.

The main tasks in reviewing the ISC Bulletin are to:

1. Check that the grouping of hypocentres and association of phase arrivals is appropriate.
2. Check that the depth and location is appropriate for the region and reported phase arrivals.
3. Check that no data are missing for an event, given the region and magnitude, and that included data are appropriate.
4. Examine the phase arrival-time residuals to check that the ISC hypocentre solution is appropriate.
5. Look for outliers in the observations and for misassociated phases.
6. Check that the station azimuthal coverage for ISC hypocentres is at least 45 deg.

As well as examining each event closely, it is also important to scan the hypocentres and phase arrivals of adjacent events, close in time and space, to ensure that there is uniformity in the composition of the events. In some cases, two events should be merged into one event, as apparent in some other case. In other cases, one apparent event needs to be split into two events, when the automatic grouping has erroneously created one event with more than one reported hypocentre out of the observations for two real events that are distinct but closely occurring.

Misassociated phase arrivals are returned to the unassociated data stream, if not immediately placed by the analyst in another event where they belong. These unassociated phases are then available to be associated with some other event if the time and location is appropriate. The analysts also check that no phase is associated to more than one event.

Towards the end of the monthly analysis, the ISC 'Search' procedure runs, attempting to build events from the remaining set of unassociated phase arrivals. The algorithm is based on the methodology of *Engdahl and Gunst* (1966). Candidate events are validated or rejected by attempting to find ISC hypocentres for them using the ISC locator. The surviving events are then reviewed. Those events with phase arrival observations reported by stations from at least two networks are added to the ISC Bulletin if the solutions meet the standards set by the ISC analysts. These events have only an ISC determination of hypocentre.

At the end of analysis for a data month, a set of final checks is run for quality control, with the results reviewed by an analyst and the defects rectified. These are checks for inconsistencies and errors to ensure the general integrity of the ISC Bulletin.

10.1.6 Probabilistic Point Source Model (ISC-PPSM)

From data month January 2019 we have begun routinely calculating the earthquake moment tensor, source time function (STF) and depth for moderate magnitude (M_W 5.8 – 7.2) earthquakes. The resulting catalogue is referred to as ISC-PPSM (International Seismological Centre - Probabilistic Point Source Model). This point source calculation is performed using a Bayesian inversion technique based on the methods proposed by *Stähler and Sigloch* (2014; 2016). There are three main purposes of the ISC-PPSM catalogue:

1. Quantifying the uncertainties in the earthquake moment tensor.
2. Providing new constraints on the earthquake STF, along with full error estimation.
3. Adding new depth resolution, especially for relatively shallow (< 40 km depth) moderate magnitude earthquakes, where surface reflected depth phases are subsumed into the earthquake STF.

The first purpose is motivated by the range of moment tensor solutions that can be reported by different agencies or methods for the same earthquake (e.g., *Lentas et al.* (2019)). It is clear that given the variability in the data and methods these different earthquake mechanisms may not be reconciled in all cases. Instead, we aim to quantify the full range of plausible earthquake mechanisms for a given event.

The second role of the ISC-PPSM catalogue is to provide new parameterised estimates of the earthquake STF. By parameterising the STF, we allow the range of plausible STFs to be assessed, but also reduce the sensitivity to near source reverberations (such as water depth phases). It is hoped that this will provide a new resource for full waveform tomographic studies, as well as earthquake physics studies.

Thirdly, and of most significance to the wider ISC operations, ISC-PPSM offers new depth resolution for remote shallow moderate magnitude earthquakes, where the depth of an ISC hypocentre would otherwise be fixed to a default or grid depth (e.g., Section 10.1.4 and *Bondár and Storchak* (2011)). As ISC-PPSM solves for both the earthquake depth and STF, the tradeoffs between depth and STF length are directly addressed. In cases where no free depth solution is possible, the ISC-PPSM depth can be fixed to by an analyst during the review process.

To allow the ISC-PPSM depth to be used in the main ISC review process, we calculate preliminary ISC-PPSM results ahead of the review process. For the preliminary ISC-PPSM result, the earthquake latitude and longitude are fixed to the USGS-PDE epicenter. After the main ISC review process, we recalculate the ISC-PPSM solution at the location of the reviewed ISC epicenter. After checking that the revised ISC-PPSM depths are consistent with any earthquake depths that were fixed to preliminary ISC-PPSM, we publish the revised ISC-PPSM solution. If the depths are not consistent to within 1 km, we relocate the ISC hypocentre at the revised ISC-PPSM depth.

10.1.7 ISC Standard Waveform Download

The ISC uses publicly available waveforms for: determining the accuracy of station polarities, picking depth phase arrivals (i.e. pP), calculating amplitude measurements, picking phases at under-reported stations and to distribute waveforms associated with the IASPEI Reference Events List (Ground Truth

events, see Section 10.2.5). These tasks supplement ISC products in accordance with the ISC Data Collection Policy and have required the ISC to develop and expand the capacity to download and store waveforms. This activity is performed on an event by event basis, and the methodology detailed here, started in 2021 and has continued to the present.

Station Availability

In order to determine which waveforms are available to be downloaded for each event we first create a database of stations registered with FDSN which are accessible through the FDSN web services. This database has been populated from 1964 – Present and is updated on a monthly basis. We store the following information in this database where available:

- Avid - a unique identifier for every entry in the database
- IR - station code of matching stations in the Intl. Registry of Seismograph Stations
- Sta - FDSN station code
- Net - FDSN network code
- Starttime - start time of the Net/Sta/Location epoch
- Endtime - end time of the Net/Sta/Location epoch
- Lat - latitude of the station
- Lon - longitude of the station
- Location - FDSN location code
- Channel - FDSN channel
- Source - FDSN data centre the data was obtained from
- Resp - response file location, where a response file is downloaded where available

Thus the start and end times from the station availability database for each event informs which stations are operational and are candidates for downloading. Stations are excluded based on the distance from the event and its reported magnitude for both P and S waves. This uses an empirically derived relationship based on the maximum distance of P and S phases reported to the ISC (Fig. 10.6).

Waveform Download Procedure

Events are selected for waveform download based on a magnitude threshold of 3.5 or if they match other thresholding criteria (see Section 10.1.3). For each event waveform download is applied at all stations identified as being operational in the database and within the correct distance range. We choose which waveforms to download from a station based on the availability of 3 components (despite generally only downloading the vertical component) and by channel code:

1	BH?
2	HH?
3	CH?
4	DH?
5	SH?
6	EH?

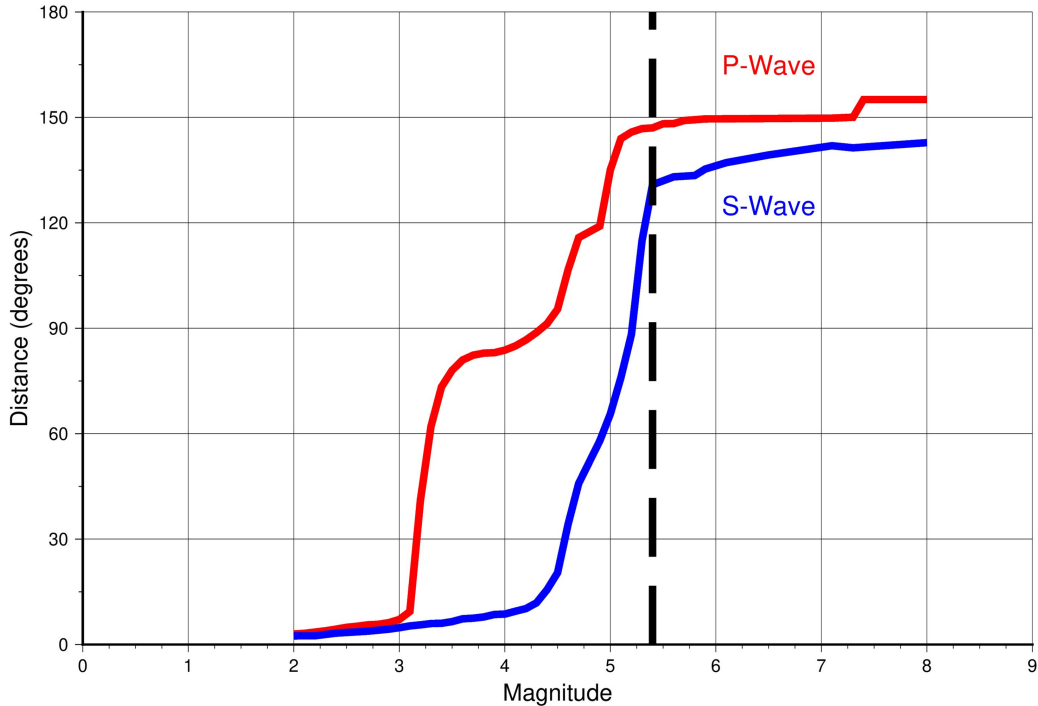


Figure 10.6: Plot showing an empirical relationship between maximum station distance and event magnitude reported to the ISC. The black line shows the magnitude for which global coverage is expected for both P and S waves.

Raw waveforms are saved for each event from 120 seconds before the predicted P arrival based on the ak135 velocity model to 780 seconds after the predicted surface wave arrival time based on *Willmore* (1979). All successfully downloaded waveforms are stored locally and indexed in a database along with a signal to noise value for the expected P wave arrival time. This download is performed twice for a given month; once about 1-2 months behind real-time and again about 22 months behind real-time. This download strategy accounts for new events being added during the interim period as well as allowing time for waveforms to be made available.

10.1.8 Automatic amplitude and Period Measurements for ISC Magnitudes Estimations

Earthquake magnitude is a fundamental seismological parameter that describes event size and the amount of released energy. Among standard magnitude scales, teleseismic short-period body-wave (*mb*) and surface-wave (*MS*) magnitudes are the most widely used and historically significant. Seismic networks and observatories routinely estimate these magnitudes and report them to the ISC; however, differences in processing procedures (e.g. *Havskov et al.*, 2024) can produce heterogeneous datasets and introduce biases in magnitude determination. To improve the consistency of ISC recomputed magnitudes, we implemented an automatic procedure to measure body and surface-wave amplitudes and periods for standard *mb* and *MS* calculations using broadband waveform data globally available via the International Federation of Digital Seismograph Networks (FDSN) web-services. The procedure relies on the IASPEI Magnitude Working Group (WG) guidelines (*Bormann and Dewey*, 2012; *IASPEI*, 2013) and is currently applied to events with $M \geq 4.5$. Its goal is to provide uniform, reliable, and reproducible earthquake magnitude estimates.

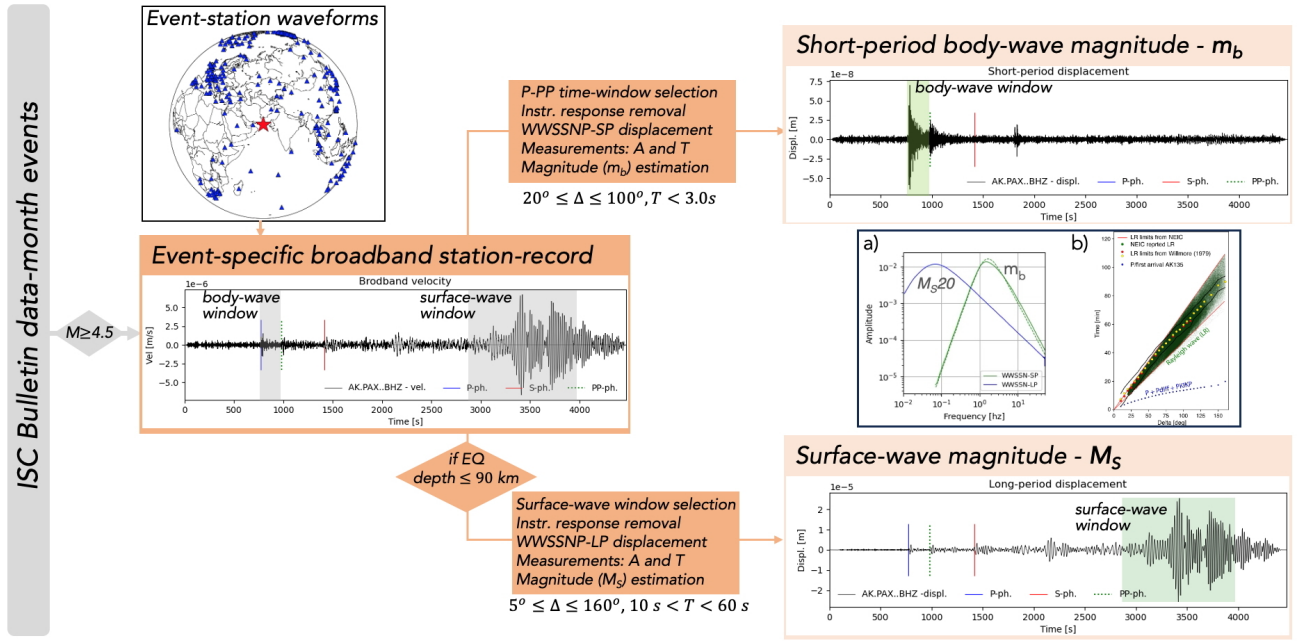


Figure 10.7: Outline of the automated amplitude and period measurement workflow. The workflow is illustrated with an example event and its station waveforms; the time windows in which body and surface-wave amplitude/period measurements are performed are highlighted by green rectangles. a) The displacement amplitude-frequency responses of the standard WWSSN short-period (SP) and long-period (LP) instruments used for teleseismic body-wave (m_b) and surface-wave (M_S) amplitude and periods measurements. b) LR-wave amplitude arrival times (green dots) reported by NEIC plotted versus epicentral distance. Red lines delimit the empirically defined surface-wave time window (start and end).

Definition and Formulations

Two main magnitude categories targeted in the implementation are defined as follows:

1. Teleseismic short-period body-wave magnitude – m_b

Estimated for earthquakes globally from recordings at stations at teleseismic distances.

$$m_b = \log_{10} \left(\frac{A}{T} \right) + Q(\Delta, h) - 3.0 \quad \text{for } 20^\circ \leq \Delta \leq 100^\circ \text{ and } T < 3s, \quad (10.14)$$

where A is the vertical component of the P-wave ground displacement in nm measured as the maximum trace-amplitude in the P-wave train window before the PP phase on a waveform filtered according to the response of the World-Wide Standardized Seismograph Network short-period seismograph (WWSSN-SP; Fig. 10.7a), and $Q(\Delta, h)$ represents the attenuation function for P-waves recorded at an epicentral distance Δ ($^\circ$) from an earthquake with a focal depth h (km) as introduced by *Gutenberg and Richter* (1956) and available in (*IASPEI*, 2013).

2. Surface-wave magnitude – M_S

Estimated for shallow earthquakes with depths ≤ 60 km, we expand and adapt the *IASPEI* (2013) formulation for MS_{20} .

$$M_S = \log_{10} \left(\frac{A}{T} \right) + 1.66 \log_{10} \Delta + 0.3 \quad \text{for } 20^\circ \leq \Delta \leq 160^\circ \text{ and } 18s \leq T \leq 22s, \quad (10.15)$$

where A is the vertical component ground displacement in nm measured as the maximum of the surface-wave amplitude, in the defined period range, on a waveform that has been filtered according to the response of the WWSSN long-period seismograph (WWSSN-LP; Fig. 10.7a), by allowing measurements for a broader periods' interval, between 10 and 60 s, in line with long-standing ISC procedures.

The Rayleigh (LR) surface-wave time windows, within which the peak amplitude is measured, are defined from empirically derived arrival-time versus epicentral-distance relations based on LR amplitude timings reported by the National Earthquake Information Center (NEIC) in the ISC Bulletin (Fig. 10.7b). These relations delimit the start and end of the expected LR window for amplitude measurements (Fig. 10.7c). Tests show that this method better captures regional variations in surface-wave propagation than the intervals reported in *Willmore* (1979).

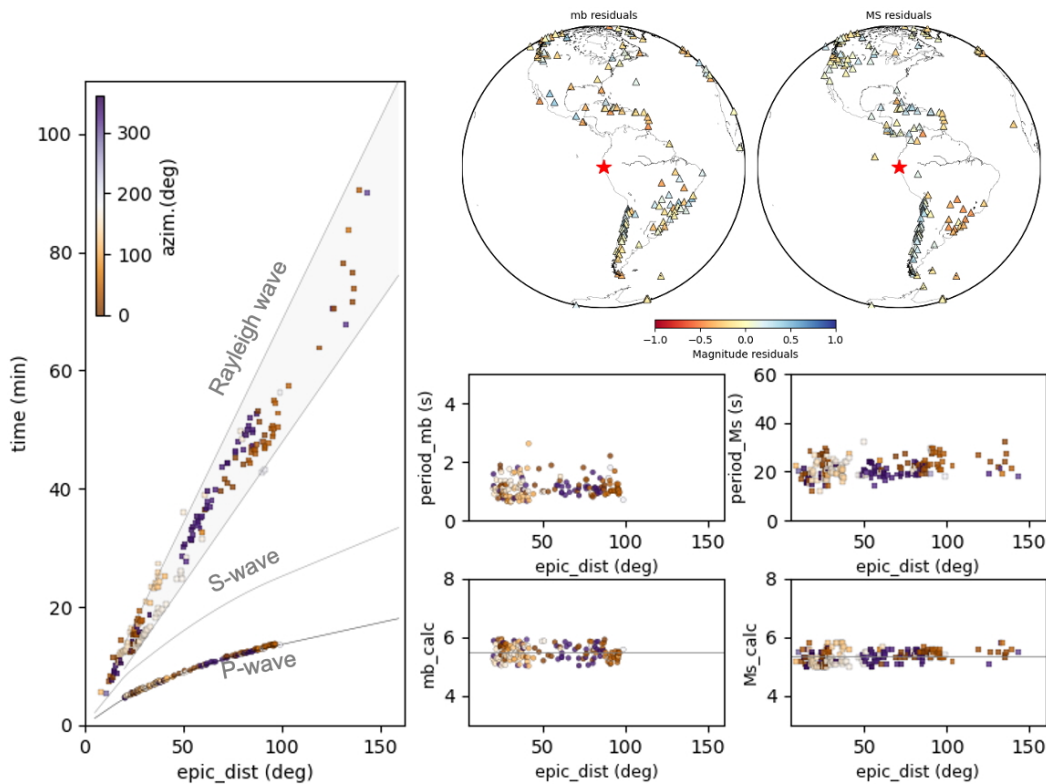


Figure 10.8: Example of the automatic amplitude and period measurements for the 2022/10/05, 08:26:19.68, M_w 5.9 (GCMT) event in the Peru-Ecuador border region (ISC event ID 624850030, event is available in the ISC online Bulletin [here](#).)

Implementation Procedure

The IASPEI Magnitude WG guidelines are transformed into an automated procedure for systematic measurement of the amplitudes and periods for ISC body and surface-wave magnitudes. The procedure can be summarised as follows:

- Selecting BHZ component waveforms from the ISC waveform-download database for events with $M \geq 4.5$ and selecting stations according to epicentral distance and P and/or S-phase arrivals reported in the ISC Bulletin.

- Data processing: Perform data-integrity checks and pre-processing (demeaning, detrending, re-sampling); Estimate broadband traces proportional to ground velocity and displacement; Convert traces to short and long-period traces by deconvolving the instrument response (*IASPEI*, 2013) to remove instrumental sensitivity and apply the standardised WWSSN responses.
- Amplitude A and period T measurements for stations satisfying the epicentral distance conditions of each magnitude type after (waveform and spectral-base) signal-to-noise ratio (SNR) checks.

A preliminary pre-processing step of duplicate removal (overlapping phase arrivals from event-pairs at globally distributed stations) was implemented to address the issue of the space and time complexity of global earthquake occurrence and provide a cleaner dataset for the ISC Bulletin before the review. The ISC automated amplitude and period measurements scheme provides event station-specific measurements (see Fig. 10.8 for an event output example) that are then included in the ISC Bulletin and are integrated into standard ISC operations, including ISC magnitude estimations (see previous section on page 113 and *Bondár and Storchak*, 2011).

10.1.9 The use of Network Code for Arrivals at the ISC and in ISCLoc

The ISC has implemented the use of the IASPEI station coding standard ADSL (**A**gency **D**eployment **S**tation **L**ocation) from data year 2021.

This allows the use of many additional stations and complements the increasing usage of reporting formats, such as QuakeML, where more extensive station information is a requirement. As of 2024, 27 agencies report data to the ISC, in a format that includes a network code (this is the equivalent of deployment in ADSL standard). Currently we use stations that are included in the FDSN registry, <https://www.fdsn.org/>, in addition to the International Station Registry (IR) which is hosted by the ISC, both are the equivalent of Agency in ADSL. Any agencies established in the future will be able to fit within this framework as required. To ensure users can utilise all station information contained within the ISC Bulletin, station coordinates and agency/network codes are included in ISF 2.1. It also allows for greater attribution of the data reported in the ISC Bulletin.

Figure 10.9 shows the location of FDSN registered stations (1848) that are not in or very near to an IR registered station that the ISC has arrivals for 2021. These are counted in a similar way to the IR, that is, the new stations are positions that are at least 2 km from any other station. The number would be much higher if multiple networks and channels were included in the count.

Figure 10.10 shows a step change in secondary azimuthal gaps of the ISC hypocentres from 2021 onwards, this improvement is a direct result of the switch to ADSL.

All the programs used by the ISC, the locator ISCLoc, database and public search tools have all had to be changed to deal with network codes.

Details of all stations used in the ISC Bulletin can be found here <https://www.isc.ac.uk/stations/>.

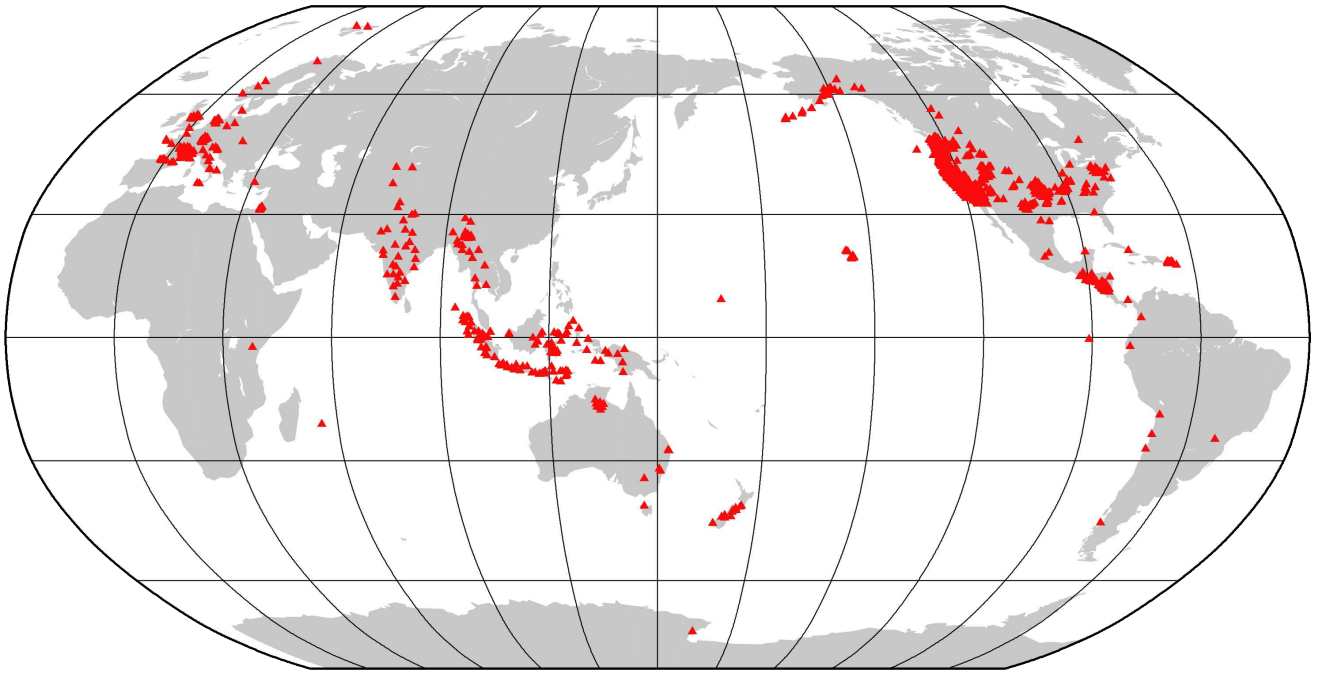


Figure 10.9: Non-IR registered stations in the ISC Bulletin 2021

ISC Hypocentre Median Secondary Gaps

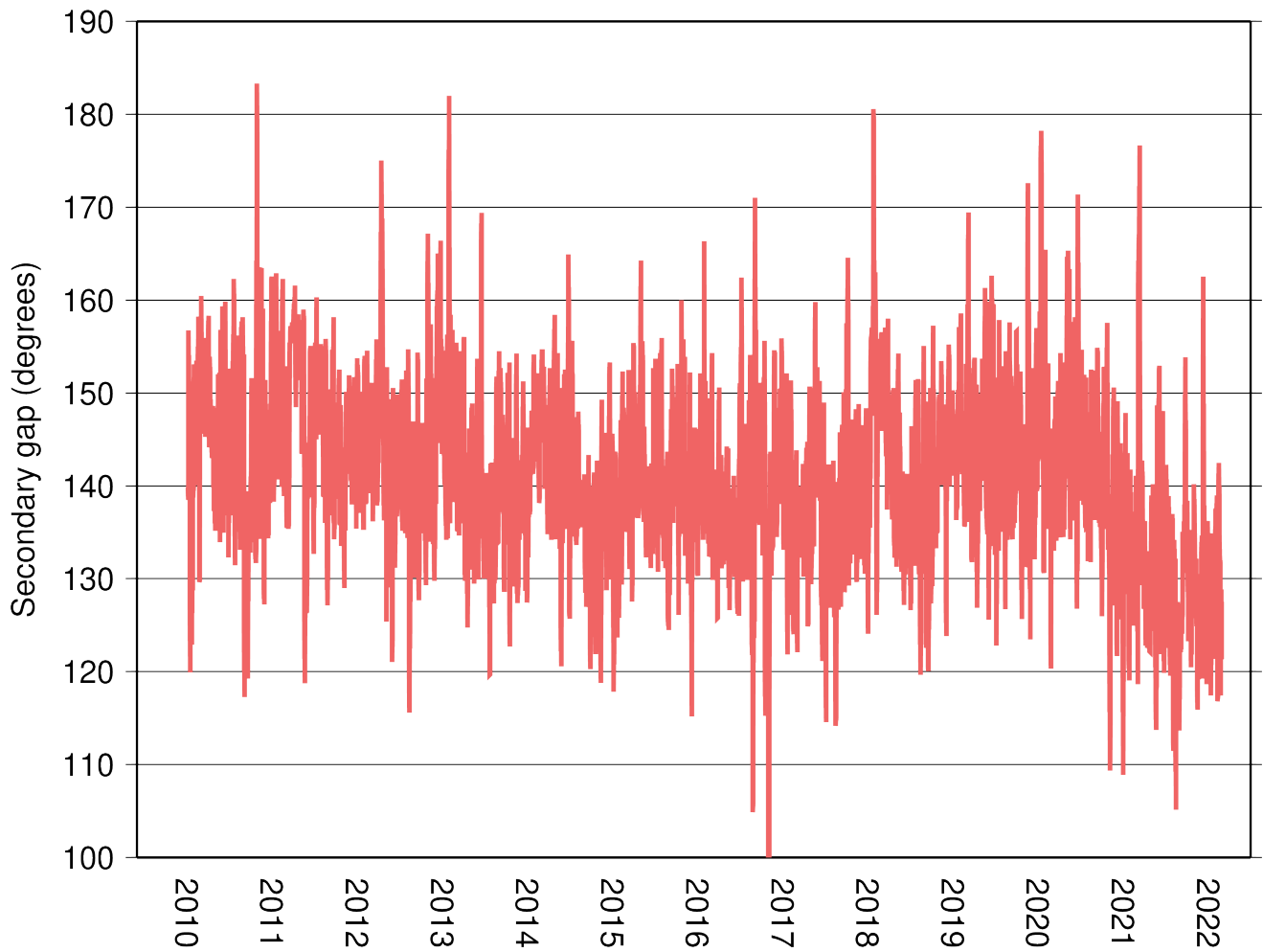


Figure 10.10: Secondary gap of ISC hypocentres

10.1.10 History of Operational Changes

The following operational changes are listed here for historical archiving purpose. Some of them have effectively become irrelevant as a result of further changes.

- From data-month January 2001 onwards, both P and S groups of arrival times are used in location.
- From data-month September 2002 onwards, the printed ISC Bulletins have been generated directly from the ISC Relational Database.
- From data-month October 2002, a new location program ISCloc has been used in operations. Also, the IASPEI standard phase list has now been adopted by the ISC. Please see Section 10.2.1 for details.
- From data-month January 2003 onwards, an updated regionalisation scheme has been adopted (*Young et al.*, 1996).
- From data-month January 2006 the ISC hypocentres are computed using the *ak135* earth velocity model (*Kennett et al.*, 1995) and then reviewed by ISC seismologists. The ISC still produces the hypocentre solutions based on Jeffreys-Bullen travel time tables (agency code ISCJB), yet these solutions are no longer reviewed.

The ISC is re-computing the entire ISC Bulletin as part of the Rebuild Project using *ak135* and the new location program (Section 10.1.4) in order to assure homogeneity and consistency of the data in the ISC Bulletin.

- From data-month January 2009, a new location program (*Bondár and Storchak*, 2011) has been used in operations. The new program uses all predicted *ak135* phases and accounts for correlated model errors. An overview of the location algorithm is provided in this volume (Section 10.1.4).
- As of February 2020, the ISC Bulletin for the period 1964-2010 has been completely rebuilt (*Storchak et al.*, 2017; 2020): all ISC hypocentres and magnitude have been recalculated using the algorithm by *Bondár and Storchak* (2011); many new previously unavailable datasets added based on extensive international correspondence with networks, data centres, temporary deployment managers and individual researchers; the Bulletin has been cleaned from phantom and poorly constrained events; many station readings have been added or corrected.
- From data-month April 2016 onwards, depth sensitive phases (P, pP, sP, pwP, PcP, ScP) and polarities for events with $M > 4.8$ and depth > 28 km are manually picked at 30° to 90° distance and integrated into the ISC Bulletin and other ISC products to improve depth determination.
- The depth of shallow moderate magnitude earthquakes (M_w 5.8 - 7.2) have been informed by waveform derived depths calculated using the ISC-PPSM methodology, which has been applied since data month January 2019 (see Section 10.1.6).
- From data-month January 2021 the ISC Bulletin will be using data from stations with network codes (see Section 10.1.9).

- From data-month May 2022, the ISC complements the mb and MS readings from reporting agencies with automatic readings of amplitude and periods of body- and surface-waves from waveforms freely available. This procedure supports the mb and MS re-computation by ISCloc by following, in many aspects, the IASPEI guidelines on magnitude computation (see Section 10.1.8).

10.2 IASPEI Standards

10.2.1 Standard Nomenclature of Seismic Phases

The following list of seismic phases was approved by the IASPEI Commission on Seismological Observation and Interpretation (CoSOI) and adopted by IASPEI on 9th July 2003. More details can be found in *Storchak et al. (2003)* and *Storchak et al. (2011)*. Ray paths for some of these phases are shown in Figures 10.11–10.16.

Crustal Phases

Pg	At short distances, either an upgoing P wave from a source in the upper crust or a P wave bottoming in the upper crust. At larger distances also, arrivals caused by multiple P-wave reverberations inside the whole crust with a group velocity around 5.8 km/s.
Pb	Either an upgoing P wave from a source in the lower crust or a P wave bottoming in the lower crust (alt: P*)
Pn	Any P wave bottoming in the uppermost mantle or an upgoing P wave from a source in the uppermost mantle
PnPn	Pn free-surface reflection
PgPg	Pg free-surface reflection
PmP	P reflection from the outer side of the Moho
PmPN	PmP multiple free surface reflection; <i>N</i> is a positive integer. For example, PmP2 is PmPPmP.
PmS	P to S reflection/conversion from the outer side of the Moho
Sg	At short distances, either an upgoing S wave from a source in the upper crust or an S wave bottoming in the upper crust. At larger distances also, arrivals caused by superposition of multiple S-wave reverberations and SV to P and/or P to SV conversions inside the whole crust.
Sb	Either an upgoing S wave from a source in the lower crust or an S wave bottoming in the lower crust (alt: S*)
Sn	Any S wave bottoming in the uppermost mantle or an upgoing S wave from a source in the uppermost mantle
SnSn	Sn free-surface reflection
SgSg	Sg free-surface reflection
SmS	S reflection from the outer side of the Moho
SmSN	SmS multiple free-surface reflection; <i>N</i> is a positive integer. For example, SmS2 is SmSSmS.
SmP	S to P reflection/conversion from the outer side of the Moho
Lg	A wave group observed at larger regional distances and caused by superposition of multiple S-wave reverberations and SV to P and/or P to SV conversions inside the whole crust. The maximum energy travels with a group velocity of approximately 3.5 km/s
Rg	Short-period crustal Rayleigh wave

Mantle Phases

P	A longitudinal wave, bottoming below the uppermost mantle; also an upgoing longitudinal wave from a source below the uppermost mantle
PP	Free-surface reflection of P wave leaving a source downward

PS	P, leaving a source downward, reflected as an S at the free surface. At shorter distances the first leg is represented by a crustal P wave.
PPP	Analogous to PP
PPS	PP which is converted to S at the second reflection point on the free surface; travel time matches that of PSP
PSS	PS reflected at the free surface
PcP	P reflection from the core-mantle boundary (CMB)
PcS	P converted to S when reflected from the CMB
PcPN	PcP reflected from the free surface $N - 1$ times; N is a positive integer. For example PcP2 is PcPPcP.
Pz+P	(alt: PzP) P reflection from outer side of a discontinuity at depth z ; z may be a positive numerical value in km. For example, P660+P is a P reflection from the top of the 660 km discontinuity.
Pz-P	P reflection from inner side of a discontinuity at depth z . For example, P660-P is a P reflection from below the 660 km discontinuity, which means it is precursory to PP.
Pz+S	(alt:PzS) P converted to S when reflected from outer side of discontinuity at depth z
Pz-S	P converted to S when reflected from inner side of discontinuity at depth z
PScS	P (leaving a source downward) to ScS reflection at the free surface
Pdif	P diffracted along the CMB in the mantle (old: Pdif)
S	Shear wave, bottoming below the uppermost mantle; also an upgoing shear wave from a source below the uppermost mantle
SS	Free-surface reflection of an S wave leaving a source downward
SP	S, leaving a source downward, reflected as P at the free surface. At shorter distances the second leg is represented by a crustal P wave.
SSS	Analogous to SS
SSP	SS converted to P when reflected from the free surface; travel time matches that of SPS
SPP	SP reflected at the free surface
ScS	S reflection from the CMB
ScP	S converted to P when reflected from the CMB
ScSN	ScS multiple free-surface reflection; N is a positive integer. For example ScS2 is ScSScS.
Sz+S	S reflection from outer side of a discontinuity at depth z ; z may be a positive numerical value in km. For example S660+S is an S reflection from the top of the 660 km discontinuity. (alt: SzS)
Sz-S	S reflection from inner side of discontinuity at depth z . For example, S660-S is an S reflection from below the 660 km discontinuity, which means it is precursory to SS.
Sz+P	(alt: SzP) S converted to P when reflected from outer side of discontinuity at depth z
Sz-P	S converted to P when reflected from inner side of discontinuity at depth z
ScSP	ScS to P reflection at the free surface
Sdif	S diffracted along the CMB in the mantle (old: Sdif)
Core Phases	
PKP	Unspecified P wave bottoming in the core (alt: P')
PKPab	P wave bottoming in the upper outer core; ab indicates the retrograde branch of the PKP caustic (old: PKP2)
PKPbc	P wave bottoming in the lower outer core; bc indicates the prograde branch of the PKP caustic (old: PKP1)
PKPdf	P wave bottoming in the inner core (alt: PKIKP)
PKPpre	A precursor to PKPdf due to scattering near or at the CMB (old: PKhKP)
PKPdif	P wave diffracted at the inner core boundary (ICB) in the outer core
PKS	Unspecified P wave bottoming in the core and converting to S at the CMB
PKSab	PKS bottoming in the upper outer core
PKSbc	PKS bottoming in the lower outer core
PKSdf	PKS bottoming in the inner core

P'P'	Free-surface reflection of PKP (alt: PKPPKP)
P'N	PKP reflected at the free surface $N - 1$ times; N is a positive integer. For example, P'3 is P'P'P'. (alt: PKPN)
P'z-P'	PKP reflected from inner side of a discontinuity at depth z outside the core, which means it is precursory to P'P'; z may be a positive numerical value in km
P'S'	(alt: PKPSKS) PKP converted to SKS when reflected from the free surface; other examples are P'PKS, P'SKP
PS'	P (leaving a source downward) to SKS reflection at the free surface (alt: PSKS)
PKKP	Unspecified P wave reflected once from the inner side of the CMB
PKKPab	PKKP bottoming in the upper outer core
PKKPbc	PKKP bottoming in the lower outer core
PKKPdf	PKKP bottoming in the inner core
PNKP	P wave reflected $N - 1$ times from inner side of the CMB; N is a positive integer.
PKKPpre	A precursor to PKKP due to scattering near the CMB
PKiKP	P wave reflected from the inner core boundary (ICB)
PKNIKP	P wave reflected $N - 1$ times from the inner side of the ICB
PKJKP	P wave traversing the outer core as P and the inner core as S
PKKS	P wave reflected once from inner side of the CMB and converted to S at the CMB
PKKSab	PKKS bottoming in the upper outer core
PKKSbc	PKKS bottoming in the lower outer core
PKKSdf	PKKS bottoming in the inner core
PcPP'	PcP to PKP reflection at the free surface; other examples are PcPS', PcSP', PcSS', PcPSKP, PcSSKP. (alt: PcPPKP)
SKS	unspecified S wave traversing the core as P (alt: S')
SKSac	SKS bottoming in the outer core
SKSdf	SKS bottoming in the inner core (alt: SKIKS)
SPdifKS	SKS wave with a segment of mantle side Pdif at the source and/or the receiver side of the ray path (alt: SKPdifS)
SKP	Unspecified S wave traversing the core and then the mantle as P
SKPab	SKP bottoming in the upper outer core
SKPbc	SKP bottoming in the lower outer core
SKPdf	SKP bottoming in the inner core
S'S'	Free-surface reflection of SKS (alt: SKSSKS)
S'N	SKS reflected at the free surface $N - 1$ times; N is a positive integer
S'z-S'	SKS reflected from inner side of discontinuity at depth z outside the core, which means it is precursory to S'S'; z may be a positive numerical value in km.
S'P'	(alt: SKSPKP) SKS converted to PKP when reflected from the free surface; other examples are S'SKP, S'PKS.
S'P	(alt: SKSP) SKS to P reflection at the free surface
SKKS	Unspecified S wave reflected once from inner side of the CMB
SKKSac	SKKS bottoming in the outer core
SKKSdf	SKKS bottoming in the inner core
SNKS	S wave reflected $N - 1$ times from inner side of the CMB; N is a positive integer.
SKiKS	S wave traversing the outer core as P and reflected from the ICB
SKJKS	S wave traversing the outer core as P and the inner core as S
SKKP	S wave traversing the core as P with one reflection from the inner side of the CMB and then continuing as P in the mantle
SKKPab	SKKP bottoming in the upper outer core
SKKPbc	SKKP bottoming in the lower outer core
SKKPdf	SKKP bottoming in the inner core
ScSS'	ScS to SKS reflection at the free surface; other examples are ScPS', ScSP', ScPP', ScSSKP, ScPSKP. (alt: ScSSKS)

Near-source Surface reflections (Depth Phases)

pPy	All P-type onsets (<i>Py</i>), as defined above, which resulted from reflection of an upgoing P wave at the free surface or an ocean bottom. WARNING: The character <i>y</i> is only a wild card for any seismic phase, which could be generated at the free surface. Examples are pP, pPKP, pPP, pPcP, etc.
sPy	All <i>Py</i> resulting from reflection of an upgoing S wave at the free surface or an ocean bottom; for example, sP, sPKP, sPP, sPcP, etc.
pSy	All S-type onsets (<i>Sy</i>), as defined above, which resulted from reflection of an upgoing P wave at the free surface or an ocean bottom; for example, pS, pSKS, pSS, pScP, etc.
sSy	All <i>Sy</i> resulting from reflection of an upgoing S wave at the free surface or an ocean bottom; for example, sSn, sSS, sScS, sSdif, etc.
pwPy	All <i>Py</i> resulting from reflection of an upgoing P wave at the ocean's free surface
pmPy	All <i>Py</i> resulting from reflection of an upgoing P wave from the inner side of the Moho

Surface Waves

L	Unspecified long-period surface wave
LQ	Love wave
LR	Rayleigh wave
G	Mantle wave of Love type
GN	Mantle wave of Love type; <i>N</i> is integer and indicates wave packets traveling along the minor arcs (odd numbers) or major arc (even numbers) of the great circle
R	Mantle wave of Rayleigh type
RN	Mantle wave of Rayleigh type; <i>N</i> is integer and indicates wave packets traveling along the minor arcs (odd numbers) or major arc (even numbers) of the great circle
PL	Fundamental leaking mode following P onsets generated by coupling of P energy into the waveguide formed by the crust and upper mantle SPL S wave coupling into the PL waveguide; other examples are SSPL, SSSPL.

Acoustic Phases

H	A hydroacoustic wave from a source in the water, which couples in the ground
HPg	H phase converted to Pg at the receiver side
HSg	H phase converted to Sg at the receiver side
HRg	H phase converted to Rg at the receiver side
I	An atmospheric sound arrival which couples in the ground
IPg	I phase converted to Pg at the receiver side
ISg	I phase converted to Sg at the receiver side
IRg	I phase converted to Rg at the receiver side
T	A tertiary wave. This is an acoustic wave from a source in the solid earth, usually trapped in a low-velocity oceanic water layer called the SOFAR channel (SOund Fixing And Ranging).
TPg	T phase converted to Pg at the receiver side
TSg	T phase converted to Sg at the receiver side
TRg	T phase converted to Rg at the receiver side

Amplitude Measurement Phases

The following set of amplitude measurement names refers to the IASPEI Magnitude Standard (see http://www.iaspei.org/commissions/commission-on-seismological-observation-and-interpretation/Summary_WG_recommendations_20130327.pdf), compliance to which is indicated by the presence of leading letter I. The absence of leading letter I indicates that a measurement is non-standard. Letter A indicates a measurement in *nm* made on a displacement seismogram, whereas letter V indicates a measurement in *nm/s* made on a velocity seismogram.

IAML	Displacement amplitude measured according to the IASPEI standard for local magnitude <i>ML</i>
IAMs_20	Displacement amplitude measured according to IASPEI standard for surface-wave magnitude <i>MS(20)</i>

IVMs_BB	Velocity amplitude measured according to IASPEI standard for broadband surface-wave magnitude $MS(BB)$
IAmb	Displacement amplitude measured according to IASPEI standard for short-period teleseismic body-wave magnitude mb
IVmB_BB	Velocity amplitude measured according to IASPEI standard for broadband teleseismic body-wave magnitude $mB(BB)$
AX_IN	Displacement amplitude of phase of type X (e.g., PP, S, etc), measured on an instrument of type IN (e.g., SP - short-period, LP - long-period, BB - broadband)
VX_IN	Velocity amplitude of phase of type X and instrument of type IN (as above)
A	Unspecified displacement amplitude measurement
V	Unspecified velocity amplitude measurement
AML	Displacement amplitude measurement for nonstandard local magnitude
AMs	Displacement amplitude measurement for nonstandard surface-wave magnitude
Amb	Displacement amplitude measurement for nonstandard short-period body-wave magnitude
AmB	Displacement amplitude measurement for nonstandard medium to long-period body-wave magnitude
END	Time of visible end of record for duration magnitude

Unidentified Arrivals

x	unidentified arrival (old: i, e, NULL)
rx	unidentified regional arrival (old: i, e, NULL)
tx	unidentified teleseismic arrival (old: i, e, NULL)
Px	unidentified arrival of P type (old: i, e, NULL, (P), P?)
Sx	unidentified arrival of S type (old: i, e, NULL, (S), S?)

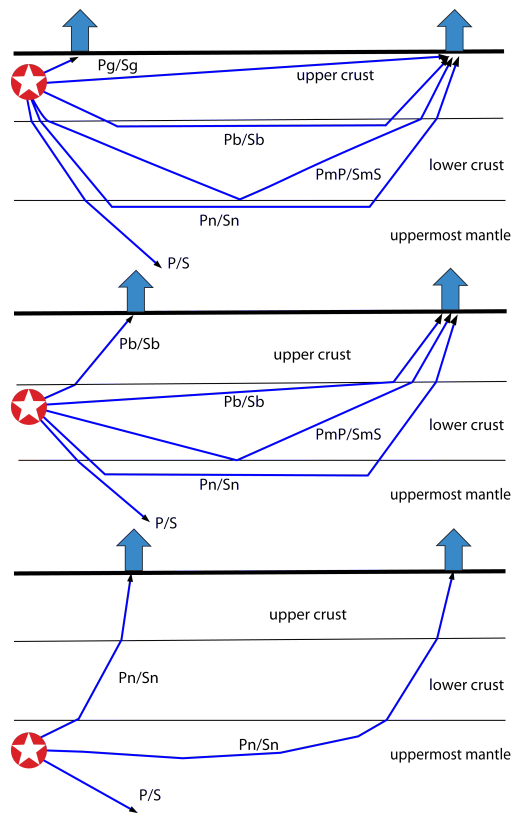


Figure 10.11: Seismic ‘crustal phases’ observed in the case of a two-layer crust in local and regional distance ranges ($0^\circ < D < \text{about } 20^\circ$) from the seismic source in the: upper crust (top); lower crust (middle); and uppermost mantle (bottom).

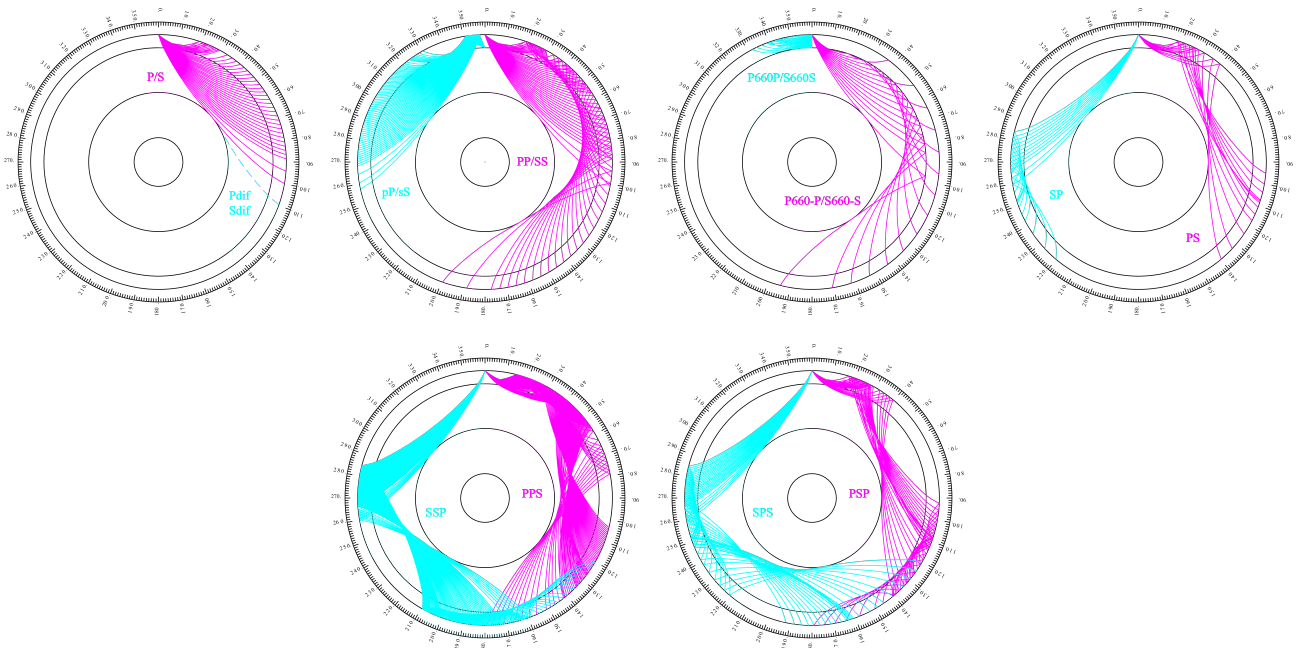


Figure 10.12: Mantle phases observed at the teleseismic distance range $D > \text{about } 20^\circ$.

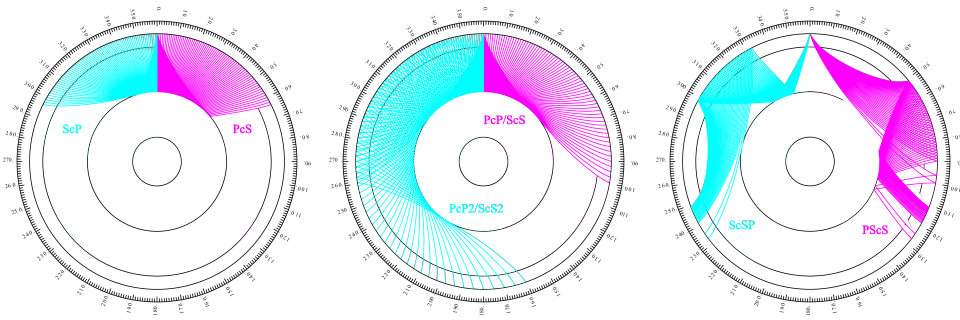


Figure 10.13: Reflections from the Earth's core.

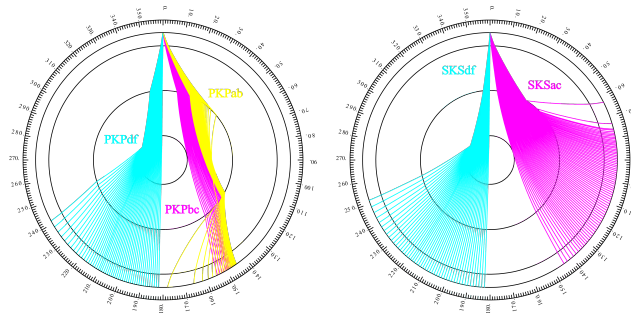


Figure 10.14: Seismic rays of direct core phases.

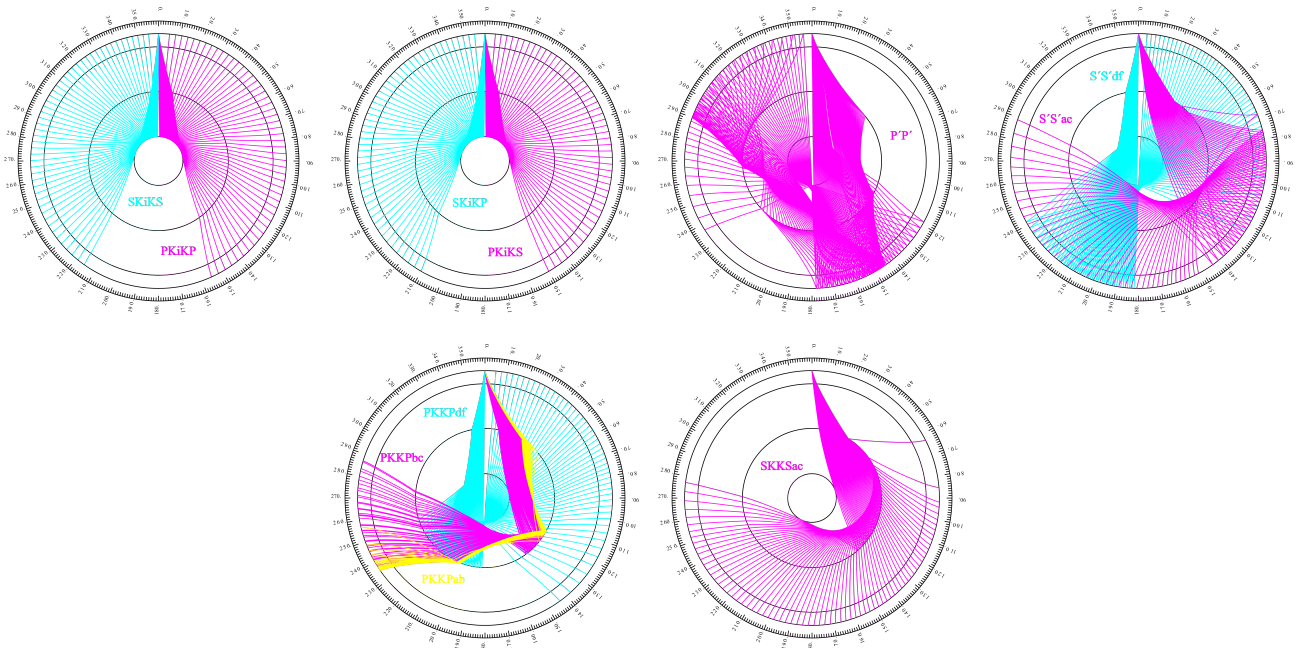


Figure 10.15: Seismic rays of single-reflected core phases.

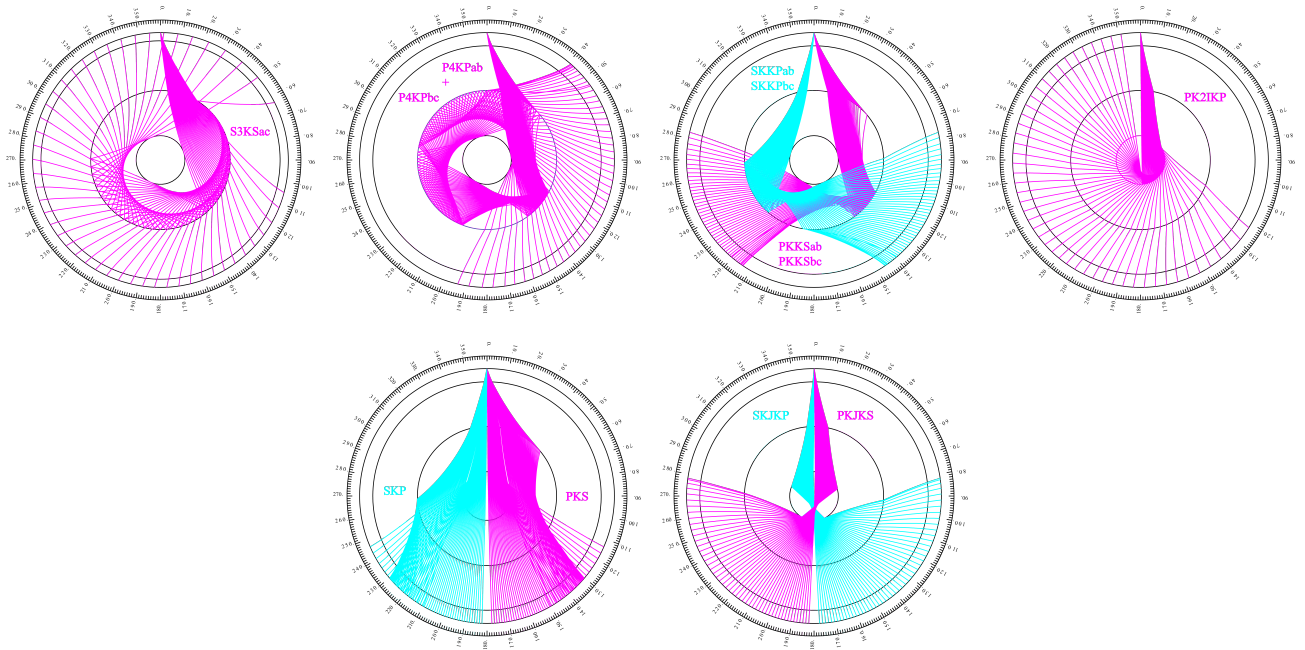


Figure 10.16: Seismic rays of multiple-reflected and converted core phases.

10.2.2 Flinn-Engdahl Regions

The Flinn-Engdahl regions were first proposed by *Flinn and Engdahl* (1965), with the standard defined by *Flinn et al.* (1974). The latest version of the schema, published by *Young et al.* (1996), divides the Earth into 50 seismic regions (Figure 10.17), which are further subdivided producing a total of 754 geographical regions (listed below). The geographic regions are numbered 1 to 757 with regions 172, 299 and 550 no longer in use. The boundaries of these regions are defined at one-degree intervals.

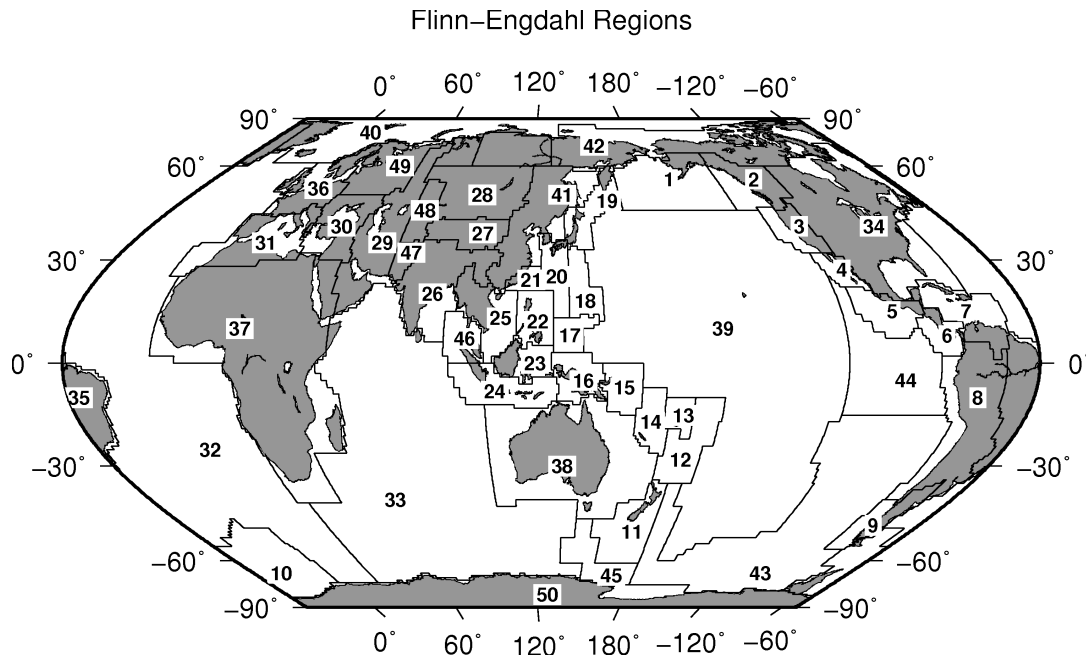


Figure 10.17: Map of all Flinn-Engdahl seismic regions.

Seismic Region 1

Alaska-Aleutian Arc

- 1. Central Alaska
- 2. Southern Alaska
- 3. Bering Sea
- 4. Komandorsky Islands region
- 5. Near Islands
- 6. Rat Islands
- 7. Andeanof Islands
- 8. Pribilof Islands
- 9. Fox Islands
- 10. Unimak Island region
- 11. Bristol Bay
- 12. Alaska Peninsula
- 13. Kodiak Island region
- 14. Kenai Peninsula
- 15. Gulf of Alaska
- 16. South of Aleutian Islands
- 17. South of Alaska

Seismic Region 2

Eastern Alaska to Vancouver Island

- 18. Southern Yukon Territory

- 19. Southeastern Alaska
- 20. Off coast of southeastern Alaska
- 21. West of Vancouver Island
- 22. Queen Charlotte Islands region
- 23. British Columbia
- 24. Alberta
- 25. Vancouver Island region
- 26. Off coast of Washington
- 27. Near coast of Washington
- 28. Washington-Oregon border region
- 29. Washington

Seismic Region 3

California-Nevada Region

- 30. Off coast of Oregon
- 31. Near coast of Oregon
- 32. Oregon
- 33. Western Idaho
- 34. Off coast of northern California
- 35. Near coast of northern California
- 36. Northern California
- 37. Nevada
- 38. Off coast of California

- 39. Central California
- 40. California-Nevada border region
- 41. Southern Nevada
- 42. Western Arizona
- 43. Southern California
- 44. California-Arizona border region
- 45. California-Baja California border region
- 46. Western Arizona-Sonora border region

Seismic Region 4

Lower California and Gulf of California

- 47. Off west coast of Baja California
- 48. Baja California
- 49. Gulf of California
- 50. Sonora
- 51. Off coast of central Mexico
- 52. Near coast of central Mexico

Seismic Region 5

Mexico-Guatemala Area

- 53. Revilla Gigedo Islands region

- 54. Off coast of Jalisco
- 55. Near coast of Jalisco
- 56. Near coast of Michoacan
- 57. Michoacan
- 58. Near coast of Guerrero
- 59. Guerrero
- 60. Oaxaca
- 61. Chiapas
- 62. Mexico-Guatemala border region
- 63. Off coast of Mexico
- 64. Off coast of Michoacan
- 65. Off coast of Guerrero
- 66. Near coast of Oaxaca
- 67. Off coast of Oaxaca
- 68. Off coast of Chiapas
- 69. Near coast of Chiapas
- 70. Guatemala
- 71. Near coast of Guatemala
- 730. Northern East Pacific Rise

Seismic Region 6

Central America

- 72. Honduras
- 73. El Salvador
- 74. Near coast of Nicaragua
- 75. Nicaragua
- 76. Off coast of central America
- 77. Off coast of Costa Rica
- 78. Costa Rica
- 79. North of Panama
- 80. Panama-Costa Rica border region
- 81. Panama
- 82. Panama-Colombia border region
- 83. South of Panama

Seismic Region 7

Caribbean Loop

- 84. Yucatan Peninsula
- 85. Cuba region
- 86. Jamaica region
- 87. Haiti region
- 88. Dominican Republic region
- 89. Mona Passage
- 90. Puerto Rico region
- 91. Virgin Islands
- 92. Leeward Islands
- 93. Belize
- 94. Caribbean Sea
- 95. Windward Islands
- 96. Near north coast of Colombia
- 97. Near coast of Venezuela
- 98. Trinidad
- 99. Northern Colombia
- 100. Lake Maracaibo
- 101. Venezuela
- 731. North of Honduras

Seismic Region 8

Andean South America

- 102. Near west coast of Colombia
- 103. Colombia
- 104. Off coast of Ecuador
- 105. Near coast of Ecuador
- 106. Colombia-Ecuador border region
- 107. Ecuador
- 108. Off coast of northern Peru
- 109. Near coast of northern Peru
- 110. Peru-Ecuador border region
- 111. Northern Peru
- 112. Peru-Brazil border region
- 113. Western Brazil
- 114. Off coast of Peru
- 115. Near coast of Peru
- 116. Central Peru
- 117. Southern Peru
- 118. Peru-Bolivia border region
- 119. Northern Bolivia
- 120. Central Bolivia
- 121. Off coast of northern Chile
- 122. Near coast of northern Chile
- 123. Northern Chile
- 124. Chile-Bolivia border region
- 125. Southern Bolivia
- 126. Paraguay
- 127. Chile-Argentina border region
- 128. Jujuy Province
- 129. Salta Province
- 130. Catamarca Province
- 131. Tucuman Province
- 132. Santiago del Estero Province
- 133. Northeastern Argentina
- 134. Off coast of central Chile
- 135. Near coast of central Chile
- 136. Central Chile
- 137. San Juan Province
- 138. La Rioja Province
- 139. Mendoza Province
- 140. San Luis Province
- 141. Cordoba Province
- 142. Uruguay

Seismic Region 9

Extreme South America

- 143. Off coast of southern Chile
- 144. Southern Chile
- 145. Southern Chile-Argentina border region
- 146. Southern Argentina

Seismic Region 10

Southern Antilles

- 147. Tierra del Fuego

- 148. Falkland Islands region
- 149. Drake Passage
- 150. Scotia Sea
- 151. South Georgia Island region
- 152. South Georgia Rise
- 153. South Sandwich Islands region
- 154. South Shetland Islands
- 155. Antarctic Peninsula
- 156. Southwestern Atlantic Ocean
- 157. Weddell Sea
- 732. East of South Sandwich Islands

Seismic Region 11

New Zealand Region

- 158. Off west coast of North Island
- 159. North Island
- 160. Off east coast of North Island
- 161. Off west coast of South Island
- 162. South Island
- 163. Cook Strait
- 164. Off east coast of South Island
- 165. North of Macquarie Island
- 166. Auckland Islands region
- 167. Macquarie Island region
- 168. South of New Zealand

Seismic Region 12

Kermadec-Tonga-Samoa Area

- 169. Samoa Islands region
- 170. Samoa Islands
- 171. South of Fiji Islands
- 172. West of Tonga Islands (REGION NOT IN USE)
- 173. Tonga Islands
- 174. Tonga Islands region
- 175. South of Tonga Islands
- 176. North of New Zealand
- 177. Kermadec Islands region
- 178. Kermadec Islands
- 179. South of Kermadec Islands

Seismic Region 13

Fiji Area

- 180. North of Fiji Islands
- 181. Fiji Islands region
- 182. Fiji Islands

Seismic Region 14

Vanuatu (New Hebrides)

- 183. Santa Cruz Islands region
- 184. Santa Cruz Islands
- 185. Vanuatu Islands region
- 186. Vanuatu Islands
- 187. New Caledonia
- 188. Loyalty Islands
- 189. Southeast of Loyalty Islands

Seismic Region 15

Bismarck and Solomon Islands

- 190. New Ireland region
- 191. North of Solomon Islands
- 192. New Britain region
- 193. Bougainville-Solomon Islands region
- 194. D'Entrecasteaux Islands region
- 195. South of Solomon Islands

Seismic Region 16

New Guinea

- 196. Irian Jaya region
- 197. Near north coast of Irian Jaya
- 198. Ninigo Islands region
- 199. Admiralty Islands region
- 200. Near north coast of New Guinea
- 201. Irian Jaya
- 202. New Guinea
- 203. Bismarck Sea
- 204. Aru Islands region
- 205. Near south coast of Irian Jaya
- 206. Near south coast of New Guinea
- 207. Eastern New Guinea region
- 208. Arafura Sea

Seismic Region 17

Caroline Islands to Guam

- 209. Western Caroline Islands
- 210. South of Mariana Islands

Seismic Region 18

Guam to Japan

- 211. Southeast of Honshu
- 212. Bonin Islands region
- 213. Volcano Islands region
- 214. West of Mariana Islands
- 215. Mariana Islands region
- 216. Mariana Islands

Seismic Region 19

Japan-Kurils-Kamchatka

- 217. Kamchatka Peninsula
- 218. Near east coast of Kamchatka Peninsula
- 219. Off east coast of Kamchatka Peninsula
- 220. Northwest of Kuril Islands
- 221. Kuril Islands
- 222. East of Kuril Islands
- 223. Eastern Sea of Japan
- 224. Hokkaido region
- 225. Off southeast coast of Hokkaido
- 226. Near west coast of eastern Honshu

- 227. Eastern Honshu

- 228. Near east coast of eastern Honshu

- 229. Off east coast of Honshu

- 230. Near south coast of eastern Honshu

Seismic Region 20

Southwestern Japan and Ryukyu Islands

- 231. South Korea
- 232. Western Honshu
- 233. Near south coast of western Honshu
- 234. Northwest of Ryukyu Islands
- 235. Kyushu
- 236. Shikoku
- 237. Southeast of Shikoku
- 238. Ryukyu Islands
- 239. Southeast of Ryukyu Islands
- 240. West of Bonin Islands
- 241. Philippine Sea

Seismic Region 21

Taiwan

- 242. Near coast of southeastern China
- 243. Taiwan region
- 244. Taiwan
- 245. Northeast of Taiwan
- 246. Southwestern Ryukyu Islands
- 247. Southeast of Taiwan

Seismic Region 22

Philippines

- 248. Philippine Islands region
- 249. Luzon
- 250. Mindoro
- 251. Samar
- 252. Palawan
- 253. Sulu Sea
- 254. Panay
- 255. Cebu
- 256. Leyte
- 257. Negros
- 258. Sulu Archipelago
- 259. Mindanao
- 260. East of Philippine Islands

Seismic Region 23

Borneo-Sulawesi

- 261. Borneo
- 262. Celebes Sea
- 263. Talaud Islands
- 264. North of Halmahera
- 265. Minahassa Peninsula, Sulawesi

- 266. Northern Molucca Sea

- 267. Halmahera

- 268. Sulawesi

- 269. Southern Molucca Sea

- 270. Ceram Sea

- 271. Buru

- 272. Seram

Seismic Region 24

Sunda Arc

- 273. Southwest of Sumatera
- 274. Southern Sumatera
- 275. Java Sea
- 276. Sunda Strait
- 277. Jawa
- 278. Bali Sea
- 279. Flores Sea
- 280. Banda Sea
- 281. Tanimbar Islands region
- 282. South of Jawa
- 283. Bali region
- 284. South of Bali
- 285. Sumbawa region
- 286. Flores region
- 287. Sumba region
- 288. Savu Sea
- 289. Timor region
- 290. Timor Sea
- 291. South of Sumbawa
- 292. South of Sumba
- 293. South of Timor

Seismic Region 25

Myanmar and Southeast Asia

- 294. Myanmar-India border region
- 295. Myanmar-Bangladesh border region
- 296. Myanmar
- 297. Myanmar-China border region
- 298. Near south coast of Myanmar
- 299. Southeast Asia (REGION NOT IN USE)
- 300. Hainan Island
- 301. South China Sea
- 733. Thailand
- 734. Laos
- 735. Kampuchea
- 736. Vietnam
- 737. Gulf of Tongking

Seismic Region 26

India-Xizang-Szechwan-Yunnan

- 302. Eastern Kashmir
- 303. Kashmir-India border region
- 304. Kashmir-Xizang border region
- 305. Western Xizang-India border

- region
- 306. Xizang
- 307. Sichuan
- 308. Northern India
- 309. Nepal-India border region
- 310. Nepal
- 311. Sikkim
- 312. Bhutan
- 313. Eastern Xizang-India border region
- 314. Southern India
- 315. India-Bangladesh border region
- 316. Bangladesh
- 317. Northeastern India
- 318. Yunnan
- 319. Bay of Bengal

Seismic Region 27

Southern Xinjiang to Gansu

- 320. Kyrgyzstan-Xinjiang border region
- 321. Southern Xinjiang
- 322. Gansu
- 323. Western Nei Mongol
- 324. Kashmir-Xinjiang border region
- 325. Qinghai

Seismic Region 28

Alma-Ata to Lake Baikal

- 326. Southwestern Siberia
- 327. Lake Baykal region
- 328. East of Lake Baykal
- 329. Eastern Kazakhstan
- 330. Lake Issyk-Kul region
- 331. Kazakhstan-Xinjiang border region
- 332. Northern Xinjiang
- 333. Tuva-Buryatia-Mongolia border region
- 334. Mongolia

Seismic Region 29

Western Asia

- 335. Ural Mountains region
- 336. Western Kazakhstan
- 337. Eastern Caucasus
- 338. Caspian Sea
- 339. Northwestern Uzbekistan
- 340. Turkmenistan
- 341. Iran-Turkmenistan border region
- 342. Turkmenistan-Afghanistan border region
- 343. Turkey-Iran border region
- 344. Iran-Armenia-Azerbaijan border region

- 345. Northwestern Iran
- 346. Iran-Iraq border region
- 347. Western Iran
- 348. Northern and central Iran
- 349. Northwestern Afghanistan
- 350. Southwestern Afghanistan
- 351. Eastern Arabian Peninsula
- 352. Persian Gulf
- 353. Southern Iran
- 354. Southwestern Pakistan
- 355. Gulf of Oman
- 356. Off coast of Pakistan

Seismic Region 30

Middle East-Crimea-Eastern Balkans

- 357. Ukraine-Moldova-Southwestern Russia region
- 358. Romania
- 359. Bulgaria
- 360. Black Sea
- 361. Crimea region
- 362. Western Caucasus
- 363. Greece-Bulgaria border region
- 364. Greece
- 365. Aegean Sea
- 366. Turkey
- 367. Turkey-Georgia-Armenia border region
- 368. Southern Greece
- 369. Dodecanese Islands
- 370. Crete
- 371. Eastern Mediterranean Sea
- 372. Cyprus region
- 373. Dead Sea region
- 374. Jordan-Syria region
- 375. Iraq

Seismic Region 31

Western Mediterranean Area

- 376. Portugal
- 377. Spain
- 378. Pyrenees
- 379. Near south coast of France
- 380. Corsica
- 381. Central Italy
- 382. Adriatic Sea
- 383. Northwestern Balkan Peninsula
- 384. West of Gibraltar
- 385. Strait of Gibraltar
- 386. Balearic Islands
- 387. Western Mediterranean Sea
- 388. Sardinia
- 389. Tyrrhenian Sea
- 390. Southern Italy
- 391. Albania
- 392. Greece-Albania border region

- 393. Madeira Islands region
- 394. Canary Islands region
- 395. Morocco
- 396. Northern Algeria
- 397. Tunisia
- 398. Sicily
- 399. Ionian Sea
- 400. Central Mediterranean Sea
- 401. Near coast of Libya

Seismic Region 32

Atlantic Ocean

- 402. North Atlantic Ocean
- 403. Northern Mid-Atlantic Ridge
- 404. Azores Islands region
- 405. Azores Islands
- 406. Central Mid-Atlantic Ridge
- 407. North of Ascension Island
- 408. Ascension Island region
- 409. South Atlantic Ocean
- 410. Southern Mid-Atlantic Ridge
- 411. Tristan da Cunha region
- 412. Bouvet Island region
- 413. Southwest of Africa
- 414. Southeastern Atlantic Ocean
- 738. Reykjanes Ridge
- 739. Azores-Cape St. Vincent Ridge

Seismic Region 33

Indian Ocean

- 415. Eastern Gulf of Aden
- 416. Socotra region
- 417. Arabian Sea
- 418. Lakshadweep region
- 419. Northeastern Somalia
- 420. North Indian Ocean
- 421. Carlsberg Ridge
- 422. Maldives Islands region
- 423. Laccadive Sea
- 424. Sri Lanka
- 425. South Indian Ocean
- 426. Chagos Archipelago region
- 427. Mauritius-Reunion region
- 428. Southwest Indian Ridge
- 429. Mid-Indian Ridge
- 430. South of Africa
- 431. Prince Edward Islands region
- 432. Crozet Islands region
- 433. Kerguelen Islands region
- 434. Broken Ridge
- 435. Southeast Indian Ridge
- 436. Southern Kerguelen Plateau
- 437. South of Australia
- 740. Owen Fracture Zone region
- 741. Indian Ocean Triple Junction
- 742. Western Indian-Antarctic Ridge

**Seismic Region 34
Eastern North America**

- 438. Saskatchewan
- 439. Manitoba
- 440. Hudson Bay
- 441. Ontario
- 442. Hudson Strait region
- 443. Northern Quebec
- 444. Davis Strait
- 445. Labrador
- 446. Labrador Sea
- 447. Southern Quebec
- 448. Gaspé Peninsula
- 449. Eastern Quebec
- 450. Anticosti Island
- 451. New Brunswick
- 452. Nova Scotia
- 453. Prince Edward Island
- 454. Gulf of St. Lawrence
- 455. Newfoundland
- 456. Montana
- 457. Eastern Idaho
- 458. Hebgen Lake region, Montana
- 459. Yellowstone region
- 460. Wyoming
- 461. North Dakota
- 462. South Dakota
- 463. Nebraska
- 464. Minnesota
- 465. Iowa
- 466. Wisconsin
- 467. Illinois
- 468. Michigan
- 469. Indiana
- 470. Southern Ontario
- 471. Ohio
- 472. New York
- 473. Pennsylvania
- 474. Vermont-New Hampshire region
- 475. Maine
- 476. Southern New England
- 477. Gulf of Maine
- 478. Utah
- 479. Colorado
- 480. Kansas
- 481. Iowa-Missouri border region
- 482. Missouri-Kansas border region
- 483. Missouri
- 484. Missouri-Arkansas border region
- 485. Missouri-Illinois border region
- 486. New Madrid region, Missouri
- 487. Cape Girardeau region, Missouri
- 488. Southern Illinois
- 489. Southern Indiana

- 490. Kentucky
- 491. West Virginia
- 492. Virginia
- 493. Chesapeake Bay region
- 494. New Jersey
- 495. Eastern Arizona
- 496. New Mexico
- 497. Northwestern Texas-Oklahoma border region
- 498. Western Texas
- 499. Oklahoma
- 500. Central Texas
- 501. Arkansas-Oklahoma border region
- 502. Arkansas
- 503. Louisiana-Texas border region
- 504. Louisiana
- 505. Mississippi
- 506. Tennessee
- 507. Alabama
- 508. Western Florida
- 509. Georgia
- 510. Florida-Georgia border region
- 511. South Carolina
- 512. North Carolina
- 513. Off east coast of United States
- 514. Florida Peninsula
- 515. Bahama Islands
- 516. Eastern Arizona-Sonora border region
- 517. New Mexico-Chihuahua border region
- 518. Texas-Mexico border region
- 519. Southern Texas
- 520. Near coast of Texas
- 521. Chihuahua
- 522. Northern Mexico
- 523. Central Mexico
- 524. Jalisco
- 525. Veracruz
- 526. Gulf of Mexico
- 527. Bay of Campeche

**Seismic Region 35
Eastern South America**

- 528. Brazil
- 529. Guyana
- 530. Suriname
- 531. French Guiana

**Seismic Region 36
Northwestern Europe**

- 532. Eire
- 533. United Kingdom
- 534. North Sea
- 535. Southern Norway
- 536. Sweden

- 537. Baltic Sea
- 538. France
- 539. Bay of Biscay
- 540. The Netherlands
- 541. Belgium
- 542. Denmark
- 543. Germany
- 544. Switzerland
- 545. Northern Italy
- 546. Austria
- 547. Czech and Slovak Republics
- 548. Poland
- 549. Hungary

**Seismic Region 37
Africa**

- 550. Northwest Africa (REGION NOT IN USE)
- 551. Southern Algeria
- 552. Libya
- 553. Egypt
- 554. Red Sea
- 555. Western Arabian Peninsula
- 556. Chad region
- 557. Sudan
- 558. Ethiopia
- 559. Western Gulf of Aden
- 560. Northwestern Somalia
- 561. Off south coast of northwest Africa
- 562. Cameroon
- 563. Equatorial Guinea
- 564. Central African Republic
- 565. Gabon
- 566. Congo
- 567. Zaire
- 568. Uganda
- 569. Lake Victoria region
- 570. Kenya
- 571. Southern Somalia
- 572. Lake Tanganyika region
- 573. Tanzania
- 574. Northwest of Madagascar
- 575. Angola
- 576. Zambia
- 577. Malawi
- 578. Namibia
- 579. Botswana
- 580. Zimbabwe
- 581. Mozambique
- 582. Mozambique Channel
- 583. Madagascar
- 584. South Africa
- 585. Lesotho
- 586. Swaziland
- 587. Off coast of South Africa
- 743. Western Sahara
- 744. Mauritania

745. Mali
746. Senegal-Gambia region
747. Guinea region
748. Sierra Leone
749. Liberia region
750. Cote d'Ivoire
751. Burkina Faso
752. Ghana
753. Benin-Togo region
754. Niger
755. Nigeria

Seismic Region 38

Australia

588. Northwest of Australia
589. West of Australia
590. Western Australia
591. Northern Territory
592. South Australia
593. Gulf of Carpentaria
594. Queensland
595. Coral Sea
596. Northwest of New Caledonia
597. New Caledonia region
598. Southwest of Australia
599. Off south coast of Australia
600. Near coast of South Australia
601. New South Wales
602. Victoria
603. Near southeast coast of Australia
604. Near east coast of Australia
605. East of Australia
606. Norfolk Island region
607. Northwest of New Zealand
608. Bass Strait
609. Tasmania region
610. Southeast of Australia

Seismic Region 39

Pacific Basin

611. North Pacific Ocean
612. Hawaiian Islands region
613. Hawaiian Islands
614. Eastern Caroline Islands region
615. Marshall Islands region
616. Enewetak Atoll region
617. Bikini Atoll region
618. Gilbert Islands region
619. Johnston Island region
620. Line Islands region
621. Palmyra Island region
622. Kiritimati region
623. Tuvalu region
624. Phoenix Islands region
625. Tokelau Islands region
626. Northern Cook Islands

627. Cook Islands region
628. Society Islands region
629. Tubuai Islands region
630. Marquesas Islands region
631. Tuamotu Archipelago region
632. South Pacific Ocean

Seismic Region 40

Arctic Zone

633. Lomonosov Ridge
634. Arctic Ocean
635. Near north coast of Kalaallit Nunaat
636. Eastern Kalaallit Nunaat
637. Iceland region
638. Iceland
639. Jan Mayen Island region
640. Greenland Sea
641. North of Svalbard
642. Norwegian Sea
643. Svalbard region
644. North of Franz Josef Land
645. Franz Josef Land
646. Northern Norway
647. Barents Sea
648. Novaya Zemlya
649. Kara Sea
650. Near coast of northwestern Siberia
651. North of Severnaya Zemlya
652. Severnaya Zemlya
653. Near coast of northern Siberia
654. East of Severnaya Zemlya
655. Laptev Sea

Seismic Region 41

Eastern Asia

656. Southeastern Siberia
657. Priamurye-Northeastern China border region
658. Northeastern China
659. North Korea
660. Sea of Japan
661. Primorye
662. Sakhalin Island
663. Sea of Okhotsk
664. Southeastern China
665. Yellow Sea
666. Off east coast of southeastern China

Seismic Region 42

Northeastern Asia, Northern Alaska to Greenland

667. North of New Siberian Islands
668. New Siberian Islands
669. Eastern Siberian Sea

670. Near north coast of eastern Siberia
671. Eastern Siberia
672. Chukchi Sea
673. Bering Strait
674. St. Lawrence Island region
675. Beaufort Sea
676. Northern Alaska
677. Northern Yukon Territory
678. Queen Elizabeth Islands
679. Northwest Territories
680. Western Kalaallit Nunaat
681. Baffin Bay
682. Baffin Island region

Seismic Region 43

Southeastern and Antarctic Pacific Ocean

683. Southeastcentral Pacific Ocean
684. Southern East Pacific Rise
685. Easter Island region
686. West Chile Rise
687. Juan Fernandez Islands region
688. East of North Island
689. Chatham Islands region
690. South of Chatham Islands
691. Pacific-Antarctic Ridge
692. Southern Pacific Ocean
756. Southeast of Easter Island

Seismic Region 44

Galapagos Area

693. Eastcentral Pacific Ocean
694. Central East Pacific Rise
695. West of Galapagos Islands
696. Galapagos Islands region
697. Galapagos Islands
698. Southwest of Galapagos Islands
699. Southeast of Galapagos Islands
757. Galapagos Triple Junction region

Seismic Region 45

Macquarie Loop

700. South of Tasmania
701. West of Macquarie Island
702. Balleny Islands region

Seismic Region 46

Andaman Islands to Sumatera

703. Andaman Islands region
704. Nicobar Islands region
705. Off west coast of northern Sumatera
706. Northern Sumatera
707. Malay Peninsula

708. Gulf of Thailand

**Seismic Region 47
Baluchistan**

709. Southeastern Afghanistan
710. Pakistan
711. Southwestern Kashmir
712. India-Pakistan border region

**Seismic Region 48
Hindu Kush and Pamir**

713. Central Kazakhstan
714. Southeastern Uzbekistan

715. Tajikistan
716. Kyrgyzstan
717. Afghanistan-Tajikistan border region
718. Hindu Kush region
719. Tajikistan-Xinjiang border region
720. Northwestern Kashmir

**Seismic Region 49
Northern Eurasia**
721. Finland
722. Norway-Murmansk border re-

723. Finland-Karelia border region
724. Baltic States-Belarus-Northwestern Russia
725. Northwestern Siberia
726. Northern and central Siberia

**Seismic Region 50
Antarctica**

727. Victoria Land
728. Ross Sea
729. Antarctica

10.2.3 IASPEI Magnitudes

The ISC publishes a diversity of magnitude data. Although trying to be as complete and specific as possible, preference is now given to magnitudes determined according to standard procedures recommended by the Working Group on Magnitude Measurements of the IASPEI Commission on Seismological Observation and Interpretation (CoSOI). So far, such standards have been agreed upon for the local magnitude ML , the local-regional mb_Lg , and for two types each of body-wave (mb and mB_BB) and surface-wave magnitudes (Ms_20 and Ms_BB). With the exception of ML , all other standard magnitudes are measured on vertical-component records only. BB stands for direct measurement on unfiltered velocity broadband records in a wide range of periods, provided that their passband covers at least the period range within which mB_BB and Ms_BB are supposed to be measured. Otherwise, a deconvolution has to be applied prior to the amplitude and period measurement so as to assure that this specification is met. In contrast, mb_Lg , mb and Ms_20 are based on narrowband amplitude measurements around periods of 1 s and 20 s, respectively.

ML is consistent with the original definition of the local magnitude by *Richter* (1935) and mB_BB in close agreement with the original definition of medium-period body-wave magnitude mB measured in a wide range of periods between some 2 to 20 s and calibrated with the *Gutenberg and Richter* (1956) Q-function for vertical-component P waves. Similarly, Ms_BB is best tuned to the unbiased use of the IASPEI (1967) recommended standard magnitude formula for surface-wave amplitudes in a wide range of periods and distances, as proposed by its authors *Vaněk et al.* (1962). In contrast, mb and Ms_20 are chiefly based on measurement standards defined by US agencies in the 1960s in conjunction with the global deployment of the World-Wide Standard Seismograph Network (WWSSN), which did not include medium or broadband recordings. Some modifications were made in the 1970s to account for IASPEI recommendations on extended measurement time windows for mb . Although not optimal for calibrating narrow-band spectral amplitudes measured around 1 s and 20 s only, mb and Ms_20 use the same original calibrations functions as mB_BB and Ms_BB . But mb and Ms_20 data constitute by far the largest available magnitude data sets. Therefore they continue to be used, with appreciation for their advantages (e.g., mb is by far the most frequently measured teleseismic magnitude and often the only available and reasonably good magnitude estimator for small earthquakes) and their shortcomings (see Section 3.2.5.2 of Chapter 3 in NMSOP-2).

Abbreviated descriptions of the standard procedures for ML , mb_Lg , mb , mB_BB and Ms_BB are summarised below. For more details, including also the transfer functions of the simulation filters to be used, see http://www.iaspei.org/commissions/commission-on-seismological-observation-and-interpretation/Summary_WG_recommendations_20130327.pdf.

All amplitudes used in the magnitude formulas below are in most circumstances to be measured as one-half the maximum deflection of the seismogram trace, peak-to-adjacent-trough or trough-to-adjacent-peak, where the peak and trough are separated by one crossing of the zero-line: this measurement is sometimes described as “one-half peak-to-peak amplitude.” The periods are to be measured as twice the time-intervals separating the peak and adjacent-trough from which the amplitudes are measured. The amplitude-phase arrival-times are to be measured and reported too as the time of the zero-crossing between the peak and adjacent-trough from which the amplitudes are measured. The issue of amplitude and period measuring procedures, and circumstances under which alternative procedures are acceptable or preferable, is discussed further in Section 5 of IS 3.3 and in Section 3.2.3.3 of Chapter 3 of NMSOP-2.

Amplitudes measured according to recommended IASPEI standard procedures should be reported with the following ISF “phase names”: IAMB, IAMs_20, IAML, IAMB_Lg, IVmB_BB and IVMs_BB. “I” stands for “International” or “IASPEI”, “A” for displacement amplitude, measured in nm, and “V” for velocity amplitude, measured in nm/s. Although the ISC will calculate standard surface-wave magnitudes only for earthquakes shallower than 60 km, contributing agencies or stations are encouraged to report standard amplitude measurements of IAMs_20 and IVMs_BB for deeper earthquakes as well.

Note that the commonly known classical calibration relationships have been modified in the following to be consistent with displacements measured in nm, and velocities in nm/s, which is now common with high-resolution digital data and analysis tools. With these general definitions of the measurement parameters, where R is hypocentral distance in km (typically less than 1000 km), Δ is epicentral distance in degrees and h is hypocentre depth in km, the standard formulas and procedures read as follows:

ML :

$$ML = \log_{10}(A) + 1.11 \log_{10} R + 0.00189R - 2.09 \quad (10.16)$$

for crustal earthquakes in regions with attenuative properties similar to those of southern California, and with A being the maximum trace amplitude in nm that is measured on output from a horizontal-component instrument that is filtered so that the response of the seismograph/filter system replicates that of a Wood-Anderson standard seismograph (but with a static magnification of 1). For the normalised simulated response curve and related poles and zeros see Figure 1 and Table 1 in IS 3.3 of NMSOP-2.

Equation (10.16) is an expansion of that of *Hutton and Boore (1987)*. The constant term in equation (10.16), -2.09 , is based on an experimentally determined static magnification of the Wood-Anderson of 2080 (see *Uhrhammer and Collins (1990)*), rather than the theoretical magnification of 2800 that was specified by the seismograph’s manufacturer. The formulation of equation (10.16) assures that reported ML amplitude data are not affected by uncertainty in the static magnification of the Wood-Anderson seismograph.

For seismographic stations containing two horizontal components, amplitudes are measured indepen-

dently from each horizontal component and each amplitude is treated as a single datum. There is no effort to measure the two observations at the same time, and there is no attempt to compute a vector average. For crustal earthquakes in regions with attenuative properties that are different from those of coastal California and for measuring magnitudes with vertical-component seismographs the constants in the above equation have to be re-determined to adjust for the different regional attenuation and travel paths as well as for systematic differences between amplitudes measured on horizontal and vertical seismographs.

mb_Lg :

$$mb_Lg = \log_{10}(A) + 0.833 \log_{10} R + 0.434\gamma(R - 10) - 0.87 \quad (10.17)$$

where A = “sustained ground-motion amplitude” in nm, defined as the third largest amplitude in the time window corresponding to group velocities of 3.6 to 3.2 km/s, in the period (T) range 0.7 s to 1.3 s; R = epicentral distance in km, γ = coefficient of attenuation in km^{-1} . γ is related to the quality factor Q through the equation $\gamma = \pi/(QUT)$, where U is group velocity and T is the wave period of the L_g wave. γ is a strong function of crustal structure and should be determined specifically for the region in which the mb_Lg is to be used. A and T are measured on output from a vertical-component instrument that is filtered so that the frequency response of the seismograph/filter system replicates that of a WWSSN short-period seismograph (see Figure 1 and Table 1 in IS 3.3 of NMSOP-2). Arrival times with respect to the origin of the seismic disturbance are used, along with epicentral distance, to compute group velocity U .

mb :

$$mb = \log_{10}(A/T) + Q(\Delta, h) - 3.0 \quad (10.18)$$

where A = vertical component P-wave ground amplitude in nm measured at distances $20^\circ \leq \Delta \leq 100^\circ$ and calculated from the maximum trace-amplitude with $T < 3$ s in the entire P-phase train (time spanned by P, pP, sP, and possibly PcP and their codas, and ending preferably before PP). A and T are measured on output from an instrument that is filtered so that the frequency response of the seismograph/filter system replicates that of a WWSSN short-period seismograph (see Figure 1 and Table 1 in IS 3.3 of NMSOP-2). A is determined by dividing the maximum trace amplitude by the magnification of the simulated WWSSN-SP response at period T .

$Q(\Delta, h)$ = attenuation function for PZ (P-waves recorded on vertical component seismographs) established by *Gutenberg and Richter* (1956) in the tabulated or algorithmic form as used by the U.S. Geological Survey/National Earthquake Information Center (USGS/NEIC) (see Table 2 in IS 3.3 and program description PD 3.1 in NMSOP-2);

mB_BB :

$$mB_BB = \log_{10}(Vmax/2\pi) + Q(\Delta, h) - 3.0 \quad (10.19)$$

where $Vmax$ = vertical component ground velocity in nm/s at periods between $0.2 \text{ s} < T < 30 \text{ s}$,

measured in the range $20^\circ \leq \Delta \leq 100^\circ$. $Vmax$ is calculated from the maximum trace-amplitude in the entire P-phase train (see *mb*), as recorded on a seismogram that is proportional to velocity at least in the period range of measurements. $Q(\Delta, h)$ = attenuation function for PZ established by *Gutenberg and Richter* (1956) (see 10.18). Equation (10.18) differs from the equation for *mB* of *Gutenberg and Richter* (1956) by virtue of the $\log_{10}(Vmax/2\pi)$ term, which replaces the classical $\log_{10}(A/T)_{max}$ term. Contributors should continue to send observations of A and T to ISC.

Ms_20:

$$Ms_{20} = \log_{10}(A/T) + 1.66 \log_{10} \Delta + 0.3 \quad (10.20)$$

where A = vertical-component ground displacement in nm at $20^\circ \leq \Delta \leq 160^\circ$ epicentral distance measured from the maximum trace amplitude of a surface-wave phase having a period T between 18 s and 22 s on a waveform that has been filtered so that the frequency response of the seismograph/filter replicates that of a WWSSN long-period seismograph (see Figure 1 and Table 1 in IS 3.3 of NMSOP-2). A is determined by dividing the maximum trace amplitude by the magnification of the simulated WWSSN-LP response at period T . Equation (10.20) is formally equivalent to the *Ms* equation proposed by *Vaněk et al.* (1962) but is here applied to vertical motion measurements in a narrow range of periods.

Ms_BB:

$$Ms_{BB} = \log_{10}(Vmax/2\pi) + 1.66 \log_{10} \Delta + 0.3 \quad (10.21)$$

where $Vmax$ = vertical-component ground velocity in nm/s associated with the maximum trace-amplitude in the surface-wave train at periods between $3 \text{ s} < T < 60 \text{ s}$ as recorded at distances $2^\circ \leq \Delta \leq 160^\circ$ on a seismogram that is proportional to velocity in that range of considered periods. Equation (10.21) is based on the *Ms* equation proposed by *Vaněk et al.* (1962), but is here applied to vertical motion measurements and is used with the $\log_{10}(Vmax/2\pi)$ term replacing the $\log_{10}(A/T)_{max}$ term of the original. As for *mB_BB*, observations of A and T should be reported to ISC.

Mw:

$$Mw = (\log_{10} M_0 - 9.1) / 1.5 \quad (10.22)$$

Moment magnitude Mw is calculated from data of the scalar seismic moment M_0 (when given in Nm), or

$$Mw = (\log_{10} M_0 - 16.1) / 1.5 \quad (10.23)$$

its CGS equivalent when M_0 is in dyne·cm.

Please note that the magnitude nomenclature used in this Section uses the IASPEI standards as the reference. However, the magnitude type is typically written in plain text in most typical data reports and so it is in this document. Moreover, writing magnitude types in plain text allows us to reproduce

the magnitude type as stored in the database and provides a more direct identification of the magnitude type reported by different agencies. A short description of the common magnitude types available in this Summary is given in table 7.6.

10.2.4 The IASPEI Seismic Format (ISF)

The ISF is the IASPEI approved standard format for the exchange of parametric seismological data (hypocentres, magnitudes, phase arrivals, moment tensors etc.) and is one of the formats used by the ISC. It was adopted as standard in August 2001 and is an extension of the International Monitoring System 1.0 (IMS1.0) standard, which was developed for exchanging data used to monitor the Comprehensive Nuclear-Test-Ban Treaty. An example of the ISF is shown in Listing 10.1.

Bulletins which use the ISF are comprised of origin and arrival information, provided in a series of data blocks. These include: a bulletin title block; an event title block; an origin block; a magnitude sub-block; an effect block; a reference block; and a phase block.

Within these blocks an important extension of the IMS1.0 standard is the ability to add additional comments and thus provide further parametric information. The ISF comments are distinguishable within the open parentheses required for IMS1.0 comments by beginning with a hash mark (#) followed by a keyword identifying the type of formatted comment. Each additional line required in the ISF comment begins with the hash (within the comment parentheses) followed by blank spaces at least as long as the keyword. Optional lines within the comment are signified with a plus sign (+) instead of a hash mark. The keywords include **PRIME** (to designate a prime origin of a hypocentre); **CENTROID** (to indicate the centroid origin); **MOMTENS** (moment tensor solution); **FAULT_PLANE** (fault plane solution); **PRINAX** (principal axes); **PARAM** (an origin parameter e.g. hypocentre depth given by a depth phase).

The ISC has now moved to ISF 2.1 as the default format for searches, this provides more detail primarily for the identification of arrivals. An essential change with the implemented use of network codes from data year 2021.

The full documentation for the ISF 1 and 2.1 is maintained at the ISC and can be downloaded from:

www.isc.ac.uk/standards/isf/download/isf21.pdf

www.isc.ac.uk//standards/isf/download/isf.pdf

The documentation for the IMS1.0 standard can be downloaded from:

www.isc.ac.uk/standards/isf/download/ims1_0.pdf

10.2.5 Ground Truth (GT) Events

Accurate locations are crucial in testing Earth models derived from body and surface wave tomography as well as in location calibration studies. ‘Ground Truth’ (GT) events are well-established source locations and origin times. A database of IASPEI reference events (GT earthquakes and explosions) is hosted at the ISC (www.isc.ac.uk). A full description of GT selection criteria can be found in *Gallacher et al.* (2025).

The events are coded by category GT0, GT1, GT2 or GT5, where the epicentre of a GT X event is known to within X km to a 95% confidence level. A map of all IASPEI reference events is shown in Figure 10.18 and the types of event are categorised in Figure 10.19. GT0 are explosions with independently known locations and origin times. GT1 and GT2 are typically explosions, mine blasts or rock bursts either associated to explosion phenomenology located upon overhead imagery with seismically determined origin times, or precisely located by in-mine seismic networks. GT1-2 events are assumed to be shallow, but depth is unknown.

The database consists of nuclear explosions of GT0–5 quality, adopted from the Nuclear Explosion Database (*Bennett et al.*, 2010); GT0–5 chemical explosions, rock bursts, mine-induced events inherited from the reference event set by *Bondár et al.* (2004); GT5 events which have been identified using the method of *Gallacher et al.* (2025):

- Five or more stations within 150 km from the epicentre
- One or more stations within 10 km **OR** five or more stations reporting both P & S phases
- CPQ ≥ 0.4
- A secondary azimuthal gap $\leq 210^\circ$
- Event recorded at distances $\geq 2^\circ$
- Semi-major axis of the error ellipse ≤ 5 km
- A resolved event depth of 35 km or shallower

where CPQ is the Cyclic Polygon Quotient defined as the ratio between the area of the polygon created by connecting the event station azimuths on a unitary circle and the area of the unitary circle:

$$CPQ = \frac{\left| \sum_{i=1}^{n-1} x_i y_{i+1} + x_n y_1 - \sum_{i=1}^{n-1} x_{i+1} y_i - x_1 y_n \right|}{2\pi}, \quad (10.24)$$

where x and y are the cartesian coordinates of the event to station azimuths ($esazi_i$) ordered from 0 to 360 degrees and the subscript refers to the number of the vertex in clockwise order and n is the total number of stations. The cartesian coordinates are found using $x = \cos(esazi_i)$ and $y = \sin(esazi_i)$ with a radius of 1.

The seismological community is invited to participate in this project by nominating seismic events for the reference event database. Submitters may be contacted for further confirmation and for arrival time

data. The IASPEI Reference Event List will be periodically published both in written and electronic form with proper acknowledgement of all submitters.

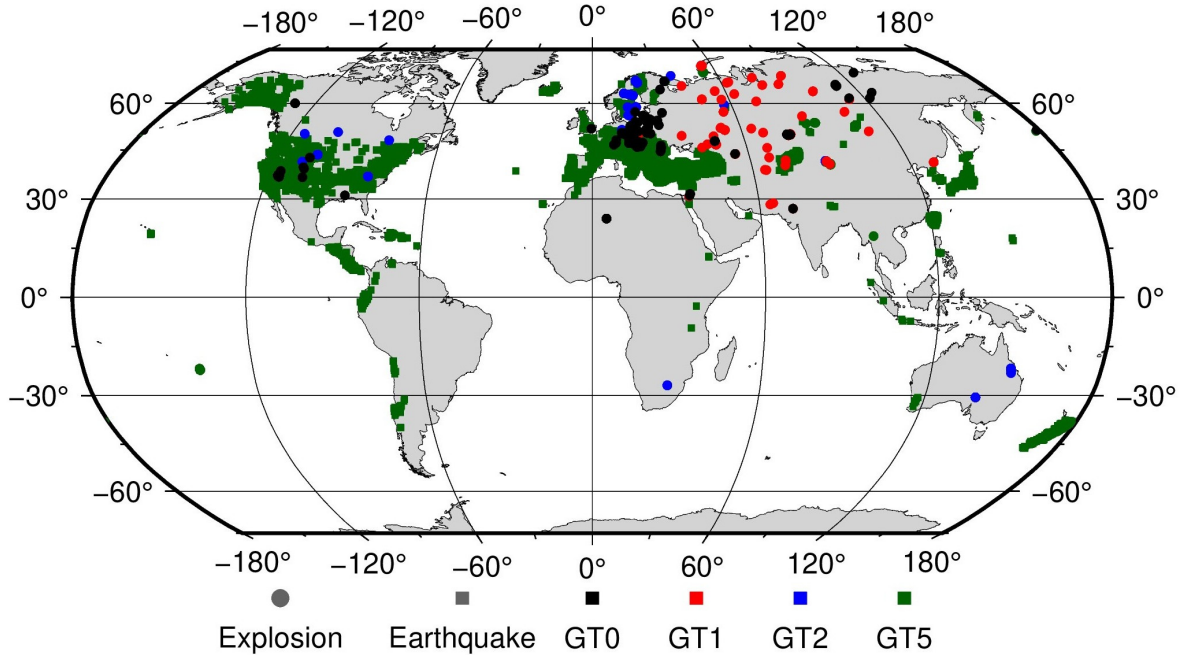


Figure 10.18: Map of all IASPEI Reference Events as of January 2023.

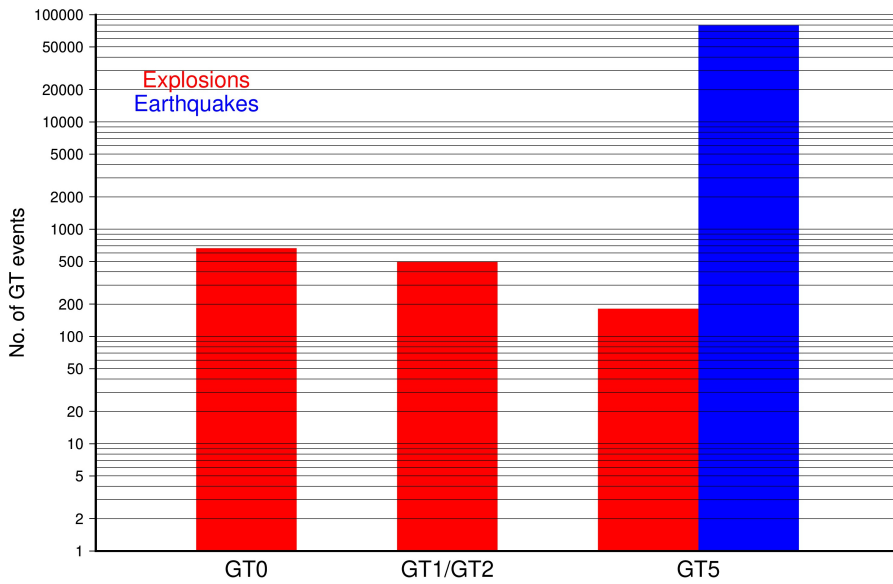


Figure 10.19: Histogram showing the event types within the IASPEI Reference Event list as of January 2023.

10.2.6 Nomenclature of Event Types

The nomenclature of event types currently used in the ISC Bulletin takes its origin from the IASPEI International Seismic Format (ISF).

Event type codes are composed of a leading character that generally indicates the confidence with which the type of the event is asserted and a trailing character that generally gives the type of the event. The leading and trailing characters may be used in any combination.

The **leading** characters are:

- s = suspected
- k = known
- f = felt (implies known)
- d = damaging (implies felt and known)

The **trailing** characters are:

- c = meteoritic event
- e = earthquake
- h = chemical explosion
- i = induced event
- l = landslide
- m = mining explosion
- n = nuclear explosion
- r = rock burst
- x = experimental explosion

A chemical explosion might be for mining or experimental purposes, and it is conceivable that other types of event might be assigned two or more different event type codes. This is deliberate, and matches the ambiguous identification of events in existing databases.

In addition, the code **uk** is used for events of unknown type and **ls** is used for known landslides.

The frequency of the different event types designated in the ISC Bulletin since 1964 is indicated in Figure 10.20.

There are currently plans to revise this nomenclature as part of the joint IASPEI Commission on Seismological Observation and Interpretation (CoSOI) and FDSN working group.

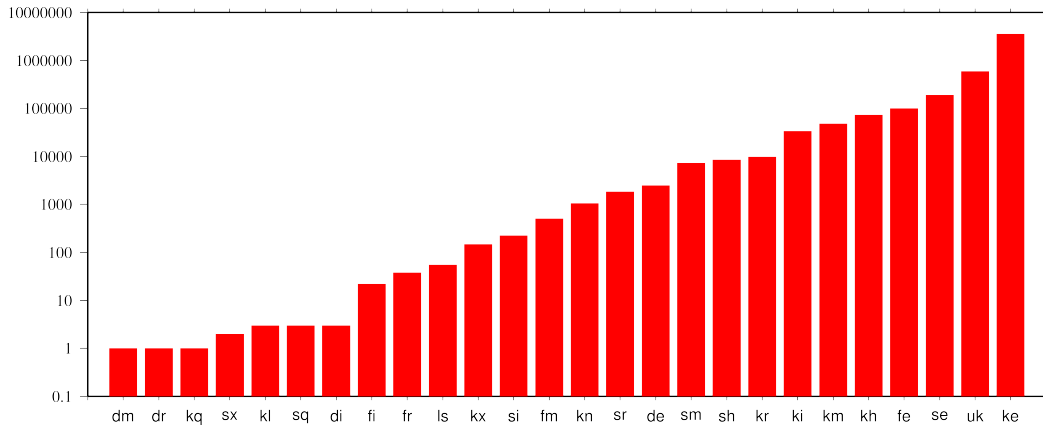


Figure 10.20: Event types in the ISC Bulletin

10.3 Tables

Table 10.2: Listing of all 399 agencies that have directly reported to the ISC. The 151 agencies highlighted in bold have reported data to the ISC Bulletin for the period of this Bulletin Summary.

Agency Code	Agency Name
AAA	Alma-ata, Kazakhstan
AAE	University of Addis Ababa, Ethiopia
AAM	University of Michigan, USA
ADE	Primary Industries and Resources SA, Australia
ADH	Observatorio Afonso Chaves, Portugal
AEIC	Alaska Earthquake Information Center, USA
AFAD	Disaster and Emergency Management Presidency, Turkey
AFAR	The Afar Depression: Interpretation of the 1960-2000 Earthquakes, Israel
AFUA	University of Alabama, USA
ALG	Algiers University, Algeria
ANDRE	, USSR
ANF	USArray Array Network Facility, USA
ANT	Antofagasta, Chile
ARE	Instituto Geofisico del Peru, Peru
ARO	Observatoire Géophysique d'Arta, Djibouti
ASGSR	Altay-Sayan Branch, Geophysical Survey, Russian Academy of Sciences, Russia
ASIES	Institute of Earth Sciences, Academia Sinica, Chinese Taipei
ASL	Albuquerque Seismological Laboratory, USA
ASM	University of Asmara, Eritrea
ATA	The Earthquake Research Center Ataturk University, Turkey
ATH	National Observatory of Athens, Greece
AUST	Geoscience Australia, Australia
AVETI	, USSR
AWI	Alfred Wegener Institute for Polar and Marine Research, Germany
AZER	Republican Seismic Survey Center of Azerbaijan National Academy of Sciences, Azerbaijan
BCIS	Bureau Central International de Sismologie, France
BDF	Observatório Sismológico da Universidade de Brasília, Brazil

Table 10.2: Continued.

Agency Code	Agency Name
BELR	Centre of Geophysical Monitoring of the National Academy of Sciences of Belarus, Republic of Belarus
BEO	Republicki seizmoloski zavod, Serbia
BER	University of Bergen, Norway
BERK	Berkheimer H, Germany
BGR	Bundesanstalt für Geowissenschaften und Rohstoffe, Germany
BGS	British Geological Survey, United Kingdom
BGSI	Botswana Geoscience Institute, Botswana
BHUJ2	Study of Aftershocks of the Bhuj Earthquake by Japanese Research Team, Japan
BIAK	Biak earthquake aftershocks (17-Feb-1996), USA
BJI	China Earthquake Networks Center, China
BKK	Thai Meteorological Department, Thailand
BNS	Erdbebenstation, Geologisches Institut der Universität, Köl, Germany
BOG	Universidad Javeriana, Colombia
BRA	Geophysical Institute, Slovak Academy of Sciences, Slovakia
BRG	Seismological Observatory Berggießhübel, TU Bergakademie Freiberg, Germany
BRK	Berkeley Seismological Laboratory, USA
BRS	Brisbane Seismograph Station, Australia
BUC	National Institute for Earth Physics, Romania
BUD	Geodetic and Geophysical Research Institute, Hungary
BUEE	Earth & Environment, USA
BUG	Institute of Geology, Mineralogy & Geophysics, Germany
BUL	Goetz Observatory, Zimbabwe
BUT	Montana Bureau of Mines and Geology, USA
BYKL	Baykal Regional Seismological Centre, GS SB RAS, Russia
CADCG	Central America Data Centre, Costa Rica
CAN	Australian National University, Australia
CANSK	Canadian and Scandinavian Networks, Sweden
CAR	Instituto Sismologico de Caracas, Venezuela
CASC	Central American Seismic Center, Costa Rica
CATAC	Central American Tsunami Advisory Center, Nicaragua
CENT	Centennial Earthquake Catalog, USA
CERI	Center for Earthquake Research and Information, USA
CFUSG	Inst. of Seismology and Geodynamics, V.I. Vernadsky Crimean Federal University, Republic of Crimea
CLL	Geophysikalisches Observatorium Collm, Germany
CNG	Seismographic Station Changalane, Mozambique
CNRM	Centre National de Recherche, Morocco
COSMOS	Consortium of Organizations for Strong Motion Observations, USA
CRAAG	Centre de Recherche en Astronomie, Astrophysique et Géophysique, Algeria
CSC	University of South Carolina, USA
CSEM	Centre Sismologique Euro-Méditerranéen (CSEM/EMSC), France
CUPWA	Curtin University, Australia
DAGSR	Dagestan Branch, Geophysical Survey, Russian Academy of Sciences, Russia
DASA	Defense Atomic Support Agency, USA

Table 10.2: Continued.

Agency Code	Agency Name
DBN	Koninklijk Nederlands Meteorologisch Instituut, Netherlands
DDA	General Directorate of Disaster Affairs, Turkey
DHMR	Yemen National Seismological Center, Yemen
DIAS	Dublin Institute for Advanced Studies, Ireland
DJA	Badan Meteorologi, Klimatologi dan Geofisika, Indonesia
DMN	National Seismological Centre, Nepal, Nepal
DNAG	, USA
DNK	Geological Survey of Denmark and Greenland, Denmark
DSN	Dubai Seismic Network, United Arab Emirates
DUSS	Damascus University, Syria, Syria
EAF	East African Network, Unknown
EAGLE	Ethiopia-Afar Geoscientific Lithospheric Experiment, Unknown
EBR	Observatori de l'Ebre, Spain
EBSE	Ethiopian Broadband Seismic Experiment, Unknown
ECGS	European Center for Geodynamics and Seismology, Luxembourg
ECX	Centro de Investigación Científica y de Educación Superior de Ensenada, Mexico
EFATE	OBS Experiment near Efate, Vanuatu, USA
EHB	Engdahl, van der Hilst and Buland, USA
EIDC	Experimental (GSETT3) International Data Center, USA
EKA	Eskdalemuir Array Station, United Kingdom
ENT	Geological Survey and Mines Department, Uganda
EPSI	Reference events computed by the ISC for EPSI project, United Kingdom
ERDA	Energy Research and Development Administration, USA
EST	Geological Survey of Estonia, Estonia
EUROP	, Unknown
EVBIB	Data from publications listed in the ISC Event Bibliography, Unknown
FBR	Fabra Observatory, Spain
FCIAR	Federal Center for Integrated Arctic Research, Russia
FDF	Fort de France, Martinique
FIA0	Finessa Array, Finland
FOR	Unknown Historical Agency, Unknown - historical agency
FUBES	Earth Science Dept., Geophysics Section, Germany
FUNV	Fundación Venezolana de Investigaciones Sismológicas, Venezuela
FUR	Geophysikalisches Observatorium der Universität München, Germany
GBZT	Marmara Research Center, Turkey
GCG	INSIVUMEH, Guatemala
GCMT	The Global CMT Project, USA
GDNRW	Geologischer Dienst Nordrhein-Westfalen, Germany
GEN	Dipartimento per lo Studio del Territorio e delle sue Risorse (RSNI), Italy
GEOAZ	UMR Géoazur, France
GEOMR	GEOMAR, Germany
GFZ	Helmholtz Centre Potsdam GFZ German Research Centre For Geosciences, Germany
GII	The Geophysical Institute of Israel, Israel
GOM	Observatoire Volcanologique de Goma, Democratic Republic of the Congo

Table 10.2: Continued.

Agency Code	Agency Name
GRAL	National Council for Scientific Research, Lebanon
GSDM	Geological Survey Department Malawi, Malawi
GSET2	Group of Scientific Experts Second Technical Test 1991, April 22 - June 2, Unknown
GTFE	German Task Force for Earthquakes, Germany
GUC	Centro Sismológico Nacional, Universidad de Chile, Chile
HAN	Hannover, Germany
HDC	Observatorio Vulcanológico y Sismológico de Costa Rica, Costa Rica
HEL	Institute of Seismology, University of Helsinki, Finland
HFS	Hagfors Observatory, Sweden
HFS1	Hagfors Observatory, Sweden
HFS2	Hagfors Observatory, Sweden
HIMNT	Himalayan Nepal Tibet Experiment, USA
HKC	Hong Kong Observatory, Hong Kong
HLUG	Hessisches Landesamt für Umwelt und Geologie, Germany
HLW	National Research Institute of Astronomy and Geophysics, Egypt
HNR	Ministry of Mines, Energy and Rural Electrification, Solomon Islands
HON	Pacific Tsunami Warning Center - NOAA, USA
HRVD	Harvard University, USA
HRVD_LR	Department of Geological Sciences, Harvard University, USA
HVO	Hawaiian Volcano Observatory, USA
HYB	National Geophysical Research Institute, India
HYD	National Geophysical Research Institute, India
IAG	Instituto Andaluz de Geofísica, Spain
IAGMA	Institute of Astronomy and Geophysics, Mongolian Academy of Sciences, Mongolia
IASBS	Institute for Advanced Studies in Basic Sciences, Iran
IASPEI	IASPEI Working Group on Reference Events, USA
ICE	Instituto Costarricense de Electricidad, Costa Rica
IDC	International Data Centre, CTBTO, Austria
IDG	Institute of Dynamics of Geosphere, Russian Academy of Sciences, Russia
IEC	Institute of the Earth Crust, SB RAS, Russia
IEPN	Institute of Environmental Problems of the North, Russian Academy of Sciences, Russia
IFREE	Institute For Research on Earth Evolution, Japan
IGGSL	Seismology Lab, Institute of Geology & Geophysics, Chinese Academy of Sciences, China
IGIL	Instituto Dom Luiz, University of Lisbon, Portugal
IGKR	Institute of Geology, Komi Science Centre, Ural Branch, Russian Academy of Sciences, Russia
IGKRC	Institute of Geology, Karelian Research Centre, Russian Academy of Sciences, Russia
IGQ	Servicio Nacional de Sismología y Vulcanología, Ecuador
IGS	Institute of Geological Sciences, United Kingdom
INAM	Instituto Nacional de Meteorología e Geofísica - INAMET, Angola
INDEPTH3	International Deep Profiling of Tibet and the Himalayas, USA
INET	Instituto Nicaragüense de Estudios Territoriales - INETER, Nicaragua

Table 10.2: Continued.

Agency Code	Agency Name
INMG	Instituto Português do Mar e da Atmosfera, I.P., Portugal
INMGC	Instituto Nacional de Meteorologia e Geofísica, Cape Verde
IPEC	The Institute of Physics of the Earth (IPEC), Czech Republic
IPER	Institute of Physics of the Earth, Academy of Sciences, Moscow, Russia
IPGP	Institut de Physique du Globe de Paris, France
IPRG	Institute for Petroleum Research and Geophysics, Israel
IRIS	IRIS Data Management Center, USA
IRSM	Institute of Rock Structure and Mechanics, Czech Republic
ISC	International Seismological Centre, United Kingdom
ISC-PPSM	International Seismological Centre Probabilistic Point Source Model, United Kingdom
ISK	Kandilli Observatory and Earthquake Research Institute, Turkey
ISN	Iraqi Meteorological and Seismology Organisation, Iraq
ISS	International Seismological Summary, United Kingdom
IST	Institute of Physics of the Earth, Technical University of Istanbul, Turkey
ISU	Institute of Seismology, Academy of Sciences, Republic of Uzbekistan, Uzbekistan
ITU	Faculty of Mines, Department of Geophysical Engineering, Turkey
JEN	Geodynamisches Observatorium Moxa, Germany
JMA	Japan Meteorological Agency, Japan
JOH	Bernard Price Institute of Geophysics, South Africa
JSN	Jamaica Seismic Network, Jamaica
JSO	Jordan Seismological Observatory, Jordan
KBC	Institut de Recherches Géologiques et Minières, Cameroon
KEA	Korea Earthquake Administration, Democratic People's Republic of Korea
KEW	Kew Observatory, United Kingdom
KHC	Institute of Geophysics, Czech Academy of Sciences, Czech Republic
KISR	Kuwait Institute for Scientific Research, Kuwait
KLM	Malaysian Meteorological Service, Malaysia
KMA	Korea Meteorological Administration, Republic of Korea
KMGRS	Kavkazskie Mineralnye Vody Branch, Geophysical Survey, RAS, Russia
KNET	Kyrgyz Seismic Network, Kyrgyzstan
KOGRS	Kola Branch, Geophysical Survey, Russian Academy of Sciences, Russia
KRAR	Krasnoyarsk Scientific Research Inst. of Geology and Mineral Resources, Russia, Russia
KRL	Geodätisches Institut der Universität Karlsruhe, Germany
KRNET	Institute of Seismology, Academy of Sciences of Kyrgyz Republic, Kyrgyzstan
KRSC	Kamchatka Branch of the Geophysical Survey of the RAS, Russia
KRSZO	HUN-REN Inst of Earth Physics and Space Science, Kövesligethy Radó Seismo Obs, Hungary
KSA	Observatoire de Ksara, Lebanon
KUK	Geological Survey Department of Ghana, Ghana
LAO	Large Aperture Seismic Array, USA
LDG	Laboratoire de Détection et de Géophysique/CEA, France

Table 10.2: Continued.

Agency Code	Agency Name
LDN	University of Western Ontario, Canada
LDO	Lamont-Doherty Earth Observatory, USA
LED	Landeserdbebendienst Baden-Württemberg, Germany
LEDBW	Landeserdbebendienst Baden-Württemberg, Germany
LER	Besucherbergwerk Binweide Station, Germany
LIB	Tripoli, Libya
LIC	Station Géophysique de Lamto, Ivory Coast
LIM	Lima, Peru
LIS	Instituto de Meteorologia, Portugal
LIT	Geological Survey of Lithuania, Lithuania
LJU	Slovenian Environment Agency, Slovenia
LPA	Universidad Nacional de La Plata, Argentina
LPZ	Observatorio San Calixto, Bolivia
LRSM	Long Range Seismic Measurements Project, Unknown
LSZ	Geological Survey Department of Zambia, Zambia
LVSN	Latvian Seismic Network, Latvia
MAN	Philippine Institute of Volcanology and Seismology, Philippines
MAT	The Matsushiro Seismological Observatory, Japan
MATSS	, USSR
MCO	Macao Meteorological and Geophysical Bureau, Macao, China
MCSM	Main Centre for Special Monitoring, Ukraine
MDD	Instituto Geográfico Nacional, Spain
MED_RCMT	MedNet Regional Centroid - Moment Tensors, Italy
MERI	Maharashtra Engineering Research Institute, India
MES	Messina Seismological Observatory, Italy
MEX	Instituto de Geofísica de la UNAM, Mexico
MIRAS	Mining Institute of the Ural Branch of the Russian Academy of Sciences, Russia
MNH	Institut für Angewandte Geophysik der Universität München, Germany
MOLD	Institute of Geophysics and Geology, Moldova
MOS	Geophysical Survey of Russian Academy of Sciences, Russia
MOZ	Direcção Nacional de Geologia, Mozambique
MOZAR	, Mozambique
MPSN	Mesopotamian Seismological Network, Iraq
MRB	Institut Cartogràfic i Geològic de Catalunya, Spain
MSI	Messina Seismological Observatory, Italy
MSSP	Micro Seismic Studies Programme, PINSTECH, Pakistan
MSUGS	Michigan State University, Department of Geological Sciences, USA
MUN	Mundaring Observatory, Australia
NAI	University of Nairobi, Kenya
NAM	The Geological Survey of Namibia, Namibia
NAO	Stiftelsen NORSAR, Norway
NCEDC	Northern California Earthquake Data Center, USA
NDI	National Centre for Seismology of the Ministry of Earth Sciences of India, India
NEGSR	North East (Magadan) Branch, Geophysical Survey, Russian Academy of Sciences, Russia
NEIC	National Earthquake Information Center, USA
NEIS	National Earthquake Information Service, USA

Table 10.2: Continued.

Agency Code	Agency Name
NER	North Eastern Regional Seismological Centre, Magadan, GS RAS, Russia
NIC	Cyprus Geological Survey Department, Cyprus
NIED	National Research Institute for Earth Science and Disaster Resilience, Japan
NK	National Center for Earthquake Engineering and Seismology, USSR
NNC	National Nuclear Center, Kazakhstan
NOGSR	North Ossetia (Alania) Branch, Geophysical Survey, Russian Academy of Sciences, Russia
NOU	IRD Centre de Nouméa, New Caledonia
NSSC	National Syrian Seismological Center, Syria
NSSP	National Survey of Seismic Protection, Armenia
OBGSR	Central (Obninsk) Branch, Geophysical Survey, Russian Academy of Sciences, Russia
OGAUC	Centro de Investigação da Terra e do Espaço da Universidade de Coimbra, Portugal
OGS	Istituto Nazionale di Oceanografia e di Geofisica Sperimentale (OGS), Italy
OGSO	Ohio Geological Survey, USA
OMAN	Sultan Qaboos University, Oman
ORF	Orfeus Data Center, Netherlands
OSPL	Observatorio Sismológico Politecnico Loyola, Dominican Republic
OSUB	Osservatorio Sismologico Universita di Bari, Italy
OSUNB	Observatory Seismological of the University of Brasilia, Brazil
OTT	Canadian Hazards Information Service, Natural Resources Canada, Canada
PAL	Palisades, USA
PAS	California Institute of Technology, USA
PDA	Universidade dos Açores, Portugal
PDG	Institute of Hydrometeorology and Seismology of Montenegro, Montenegro
PEK	Peking, China
PGC	Pacific Geoscience Centre, Canada
PJWWP	Private Observatory of Pawel Jacek Wiejacz, D.Sc., Poland
PLV	Institute of Geophysics, Viet Nam Academy of Science and Technology, Viet Nam
PMEL	Pacific seismicity from hydrophones, USA
PMR	Alaska Tsunami Warning Center,, USA
PNNL	Pacific Northwest National Laboratory, USA
PNSN	Pacific Northwest Seismic Network, USA
PPT	Laboratoire de Géophysique/CEA, French Polynesia
PRE	Council for Geoscience, South Africa
PRU	Institute of Geophysics, Czech Academy of Sciences, Czech Republic
PTO	Instituto Geofísico da Universidade do Porto, Portugal
PTWC	Pacific Tsunami Warning Center, USA
QCP	Manila Observatory, Philippines
QUE	Pakistan Meteorological Department, Pakistan

Table 10.2: Continued.

Agency Code	Agency Name
QUI	Escuela Politécnica Nacional, Ecuador
RAB	Rabaul Volcanological Observatory, Papua New Guinea
RBA	Université Mohammed V, Morocco
RCSFM	Republican Center of Seismic Forecasting Monitoring, Min. Emergency Situations, Uzbekistan
REN	MacKay School of Mines, USA
REY	Icelandic Meteorological Office, Iceland
RHSSO	Republic Hydrometeorological Service, Seismological Observatory, Banja Luka, Bosnia and Herzegovina
RISSC	Laboratory of Research on Experimental and Computational Seimology, Italy
RMIT	Royal Melbourne Institute of Technology, Australia
ROC	Odenbach Seismic Observatory, USA
ROM	Istituto Nazionale di Geofisica e Vulcanologia, Italy
RRLJ	Regional Research Laboratory Jorhat, India
RSMAC	Red Sísmica Mexicana de Apertura Continental, Mexico
RSNC	Red Sismológica Nacional de Colombia, Colombia
RSPR	Red Sísmica de Puerto Rico, USA
RYD	King Saud University, Saudi Arabia
SAA	Seismological Association of Australia, Australia
SAGSR	Sakhalin Branch, Geophysical Survey, Russian Academy of Sciences, Russia
SAPSE	Southern Alps Passive Seismic Experiment, New Zealand
SAR	Sarajevo Seismological Station, Bosnia and Herzegovina
SARA	SARA Electronic Instrument s.r.l., Italy
SBDV	, USSR
SCB	Observatorio San Calixto, Bolivia
SCEDC	Southern California Earthquake Data Center, USA
SCSIO	Key Laboratory of Ocean and Marginal Sea Geology, South China Sea, China
SDD	Universidad Autonoma de Santo Domingo, Dominican Republic
SEA	Geophysics Program AK-50, USA
SET	Setif Observatory, Algeria
SFS	Real Instituto y Observatorio de la Armada, Spain
SGS	Saudi Geological Survey, Saudi Arabia
SHL	Central Seismological Observatory, India
SIGU	Subbotin Institute of Geophysics, National Academy of Sciences, Ukraine
SIK	Seismic Institute of Kosovo, Unknown
SIO	Scripps Institution of Oceanography, USA
SJA	Instituto Nacional de Prevención Sísmica, Argentina
SJS	Instituto Costarricense de Electricidad, Costa Rica
SKHL	Sakhalin Experimental and Methodological Seismological Expedition, GS RAS, Russia
SKL	Sakhalin Complex Scientific Research Institute, Russia
SKO	Seismological Observatory Skopje, North Macedonia
SLC	Salt Lake City, USA
SLM	Saint Louis University, USA

Table 10.2: Continued.

Agency Code	Agency Name
SLUB	Seismological Laboratory of University of Basrah, Iraq
SNET	Servicio Nacional de Estudios Territoriales, El Salvador
SNM	New Mexico Institute of Mining and Technology, USA
SNSN	Saudi National Seismic Network, Saudi Arabia
SOF	National Institute of Geophysics, Geology and Geography, Bulgaria
SOMC	Seismological Observatory of Mount Cameroon, Cameroon
SOME	Seismological Experimental Methodological Expedition, Kazakhstan
SPA	USGS - South Pole, Antarctica
SPGM	Service de Physique du Globe, Morocco
SPITAK	, Armenia
SRI	Stanford Research Institute, USA
SSN	Sudan Seismic Network, Sudan
SSNC	Servicio Sismológico Nacional Cubano, Cuba
SSS	Centro de Estudios y Investigaciones Geotecnicas del San Salvador, El Salvador
STK	Stockholm Seismological Station, Sweden
STR	EOST / RéNaSS, France
STU	Stuttgart Seismological Station, Germany
SVSA	Sistema de Vigilância Sismológica dos Açores, Portugal
SYO	National Institute of Polar Research, Japan
SZGRF	Seismologisches Zentralobservatorium Gräfenberg, Germany
TAC	Estación Central de Tacubaya, Mexico
TAN	Antananarivo, Madagascar
TANZANIA	Tanzania Broadband Seismic Experiment, USA
TAP	Central Weather Bureau (CWB), Chinese Taipei
TAU	University of Tasmania, Australia
TEH	Tehran University, Iran
TEIC	Center for Earthquake Research and Information, USA
THE	Department of Geophysics, Aristotle University of Thessaloniki, Greece
THR	International Institute of Earthquake Engineering and Seismology (IIEES), Iran
TIF	Institute of Earth Sciences/ National Seismic Monitoring Center, Georgia
TIR	Institute of Geosciences, Polytechnic University of Tirana, Albania
TRN	The Seismic Research Centre, Trinidad and Tobago
TTG	Titograd Seismological Station, Montenegro
TUL	Oklahoma Geological Survey, USA
TUN	Institut National de la Météorologie, Tunisia
TVA	Tennessee Valley Authority, USA
TXNET	Texas Seismological Network, University of Texas at Austin, USA
TZN	University of Dar Es Salaam, Tanzania
UAF	Department of Geosciences, USA
UATDG	The University of Arizona, Department of Geosciences, USA
UAV	Red Sismológica de Los Andes Venezolanos, Venezuela

Table 10.2: Continued.

Agency Code	Agency Name
UCB	University of Colorado, Boulder, USA
UCC	Royal Observatory of Belgium, Belgium
UCDES	Department of Earth Sciences, United Kingdom
UCR	Sección de Sismología, Vulcanología y Exploración Geofísica, Costa Rica
UCSC	Earth & Planetary Sciences, USA
UESG	School of Geosciences, United Kingdom
UGN	Institute of Geonics AS CR, Czech Republic
ULE	University of Leeds, United Kingdom
UNAH	Universidad Nacional Autonoma de Honduras, Honduras
UPA	Universidad de Panama, Panama
UPIES	Institute of Earth- and Environmental Science, Germany
UPP	University of Uppsala, Sweden
UPSL	University of Patras, Department of Geology, Greece
UREES	Department of Earth and Environmental Science, USA
USAEC	United States Atomic Energy Commission, USA
USCGS	United States Coast and Geodetic Survey, USA
USGS	United States Geological Survey, USA
UTEP	Department of Geological Sciences, USA
UUSS	The University of Utah Seismograph Stations, USA
UVC	Universidad del Valle, Colombia
UWMDG	University of Wisconsin-Madison, Department of Geoscience, USA
VAO	Instituto Astronomico e Geofísico, Brazil
VIE	Bundesanstalt für Geologie, Geophysik, Klimatologie und Meteorologie, Austria
VMGSR	Voronezh Crystalline Massif Branch, Geophysical Survey, RAS, Russia
VSI	University of Athens, Greece
VUW	Victoria University of Wellington, New Zealand
WAR	Institute of Geophysics, Polish Academy of Sciences, Poland
WASN	, USA
WBNET	Institute of Geophysics, Czech Academy of Sciences, Czech Republic
WEL	Institute of Geological and Nuclear Sciences, New Zealand
WES	Weston Observatory, USA
WUSTL	Washington University Earth and Planetary Sciences, USA
YAGSR	Yakut (Saha) Branch, Geophysical Survey, Russian Academy of Sciences, Russia
YARS	Yakutiya Regional Seismological Center, GS SB RAS, Russia
ZAG	Seismological Survey of the Republic of Croatia, Croatia
ZEMSU	, USSR
ZUR	Swiss Seismological Service (SED), Switzerland
ZUR_RMT	Zurich Moment Tensors, Switzerland

Table 10.3: Phases reported to the ISC. These include phases that could not be matched to an appropriate ak135 phases. Those agencies that reported at least 10% of a particular phase are also shown.

Reported Phase	Total	Agencies reporting
P	4520393	
S	2052470	JMA (20%), TAP (12%)
AML	1215410	ROM (42%), WEL (19%)
IAmb	600033	NEIC (82%), ISC (16%)
NULL	595775	IDC (33%), NEIC (32%), AEIC (17%)
IAML	579870	NEIC (44%), AFAD (19%)
Pg	333856	STR (20%), ISK (18%)
Pn	261637	NEIC (28%), ISK (19%)
Sg	261447	STR (21%), ZAG (12%), ISK (11%)
IAMs_20	125446	NEIC (63%), ISC (36%)
Sn	108883	MDD (18%), NEIC (11%), IDC (11%)
pmax	108733	MOS (68%), BJI (32%)
LR	107681	IDC (94%)
SG	57598	HEL (62%), PRU (27%)
PG	55055	HEL (65%), PRU (20%), IPEC (13%)
Lg	51367	NNC (40%), SOME (22%), KRSZO (15%), IDC (14%)
PKP	44260	IDC (39%), VIE (16%), DJA (11%)
L	43203	BJI (97%)
IVmb_Lg	39559	MDD (100%)
AMS	37363	ISC (83%)
AMB	35406	ISC (86%)
IAMB_Lg	28871	NEIC (100%)
T	26558	IDC (99%)
A	23872	TEH (39%), JMA (37%), SKHL (24%)
smax	23254	HEL (70%), MOS (21%)
PN	21900	HEL (43%), MOS (41%)
pP	20175	BJI (22%), ISC1 (18%), IDC (14%)
PKPbc	17366	IDC (67%)
SN	17010	HEL (93%)
MSG	15861	HEL (100%)
PcP	15066	IDC (62%), ISC1 (11%)
END	14674	SSNC (95%)
PKIKP	14014	MOS (96%)
MLR	13416	MOS (100%)
IAMB_BB	12974	ISC (100%)
PP	12700	IDC (19%), BJI (17%), BELR (17%)
SB	11972	HEL (100%)
x	11271	TRN (50%), NDI (32%), CLL (11%)
PB	8955	HEL (100%)
PKPdf	8680	NEIC (42%), INMG (18%)
SS	8469	MOS (32%), BELR (28%), BJI (18%)
PKPab	6363	IDC (47%), INMG (17%), BRA (11%)
sP	6304	BJI (57%), ISC1 (28%)
PKiKP	5138	IDC (35%), VIE (27%), BELR (18%)
(Sg)	4184	OGS (100%)
SPEC	4096	AFAD (100%)
PPP	3959	MOS (48%), BELR (45%)
ScP	3830	IDC (80%)
SSS	3402	BELR (59%), MOS (30%)
(Pg)	3394	OGS (100%)
AmB	3063	NEIC (75%)
I	2986	IDC (100%)
Amb	2765	NEIC (71%), RSNC (19%)
LRM	2758	BELR (100%)
*PP	2627	MOS (100%)
Smax	2572	BYKL (100%)
PKKPbc	2526	IDC (98%)
LQ	2491	BELR (62%), PPT (30%)
Pmax	2274	BYKL (98%)
PKP2	2245	MOS (100%)
PKhKP	1939	IDC (100%)
pPKP	1853	VIE (49%), IDC (22%), BJI (16%)
Pdiff	1605	VIE (38%), IDC (34%), BRA (12%)
SKS	1546	BELR (43%), BJI (36%)
IVmb_VC	1504	MDD (100%)
sS	1478	BJI (64%), BELR (26%)
PKPBC	1222	PRU (100%)
SKPbc	1171	IDC (97%)
PKKP	931	VIE (55%), IDC (29%)
SKSac	828	BER (39%), HYB (31%), CLL (11%)

Table 10.3: (continued)

Reported Phase	Total	Agencies reporting
IVmB_BB	782	BER (75%), SSNC (19%)
PKPPKP	778	IDC (98%)
IVMs_BB	753	BER (86%)
PS	749	MOS (37%), BELR (27%), CLL (21%)
ScS	638	BJI (60%), HYB (22%), IDC (12%)
Px	638	MAN (92%)
SKP	623	IDC (41%), VIE (21%), BELR (20%)
PPMZ	586	BJI (100%)
PKPAB	585	PRU (100%)
AMP	579	BER (93%)
Pdif	548	INMG (22%), BJI (17%), NEIC (15%), CLL (13%)
Amp	542	BRG (100%)
SKKS	537	BELR (68%), BJI (30%)
PKHKP	537	MOS (100%)
pPKPbc	503	IDC (69%), BGR (24%)
tx	489	INMG (97%)
LH	474	CLL (100%)
e	473	BRA (100%)
*SS	465	MOS (100%)
SME	456	BJI (100%)
SMN	454	BJI (100%)
SP	450	PRU (20%), MOS (20%), ISC1 (16%), BELR (12%), BER (12%)
PKPDF	447	PRU (99%)
pPKiKP	435	BELR (43%), VIE (38%)
*SP	421	MOS (100%)
max	413	BYKL (100%)
p	395	LVSN (57%), ROM (33%)
sPKP	368	BJI (80%), BELR (12%)
H	363	IDC (100%)
LV	355	CLL (100%)
PPS	337	CLL (43%), BELR (36%), LPA (14%)
PDIFF	294	PRU (64%), IPEC (31%)
AMWP	283	NEIC (100%)
PKS	282	BELR (71%), BJI (28%)
PKKPab	266	IDC (92%)
Lm	263	CLL (100%)
PKP2bc	240	IDC (100%)
pPKPdf	212	BER (26%), CLL (17%), ISC1 (13%), AWI (12%)
SKKPbc	205	IDC (98%)
SKKP	191	BELR (53%), VIE (38%)
SA	189	BGS (98%)
SKKSac	187	HYB (70%), CLL (26%)
SSSS	187	CLL (100%)
s	173	LVSN (93%)
BAZ-Pn	158	BER (100%)
SmS	158	BGR (77%), ZUR (23%)
P3KPbc	157	IDC (100%)
SKPdf	154	CLL (45%), BER (27%), BGR (12%)
PKPpre	151	NEIC (63%), PRU (28%)
BAZ-P	149	BER (100%)
Sb	145	BYKL (72%), CLL (21%)
PmP	143	BGR (66%), ZUR (34%)
PKKS	142	BELR (95%)
LmH	137	CLL (100%)
pPP	137	LPA (62%), CLL (34%)
Pb	135	BYKL (78%)
PCP	121	LPA (74%), PRU (14%)
pPKPab	120	CLL (54%), IDC (37%)
P'P'	115	VIE (98%)
IAMLA	113	BGS (99%)
PcS	107	BJI (94%)
SKIKS	106	LPA (100%)
SKIKP	105	LPA (99%)
PKIKS	103	LPA (100%)
SKPab	102	IDC (63%), ISC1 (32%)
LmV	99	CLL (100%)
P4KPbc	96	IDC (100%)
SCS	84	LPA (100%)
(S)	79	CFUSG (100%)
BAZ-Sn	78	BER (100%)
PKP2ab	72	IDC (100%)

Table 10.3: (continued)

Reported Phase	Total	Agencies reporting
pPdif	70	VIE (94%)
(P)	69	CFUSG (88%), NERS (12%)
Sdif	68	CLL (69%), BELR (22%)
sPKiKP	67	BELR (91%)
(SG)	62	NERS (100%)
PPPP	59	CLL (98%)
PKSdf	56	BER (89%), CLL (11%)
Pn_2	56	ATH (100%)
sPP	53	CLL (100%)
sSKS	48	BELR (98%)
K	46	TRN (100%)
PSP	46	LPA (100%)
BAZ	45	DNK (58%), BER (36%)
SKSdf	45	HYB (76%), CLL (18%)
AMPG	45	MEX (100%)
PSKS	45	CLL (100%)
m	43	SIGU (100%)
PKKPdf	39	AWI (31%), CLL (28%), INMG (18%), LJU (13%)
PKPdif	39	CLL (97%)
rx	38	SKHL (63%), INMG (21%), SVSA (16%)
PKPmax	37	CLL (100%)
IAmbA	36	BGS (100%)
(sP)	35	CLL (100%)
PKP1	33	PPT (100%)
AMSG	33	MEX (100%)
Lmax	32	CLL (100%)
R2	32	CLL (100%)
e1	30	BRA (100%)
SKiKP	30	IDC (70%), BELR (17%)
SKPa	30	NAO (100%)
IAMLHF	28	BER (100%)
sSS	27	CLL (93%)
pPdif	27	BELR (48%), HYB (30%), CLL (19%)
Rg	27	IDC (74%), NDI (26%)
Plp	26	CLL (100%)
PgPg	25	BYKL (100%)
BAZ-Sg	23	BER (100%)
pPcP	23	IDC (83%), CLL (17%)
(PKPab)	23	CLL (100%)
SH	22	SYO (100%)
(PG)	20	NERS (100%)
(pP)	20	CLL (100%)
sPdif	19	CLL (47%), BELR (47%)
SDIFF	19	LPA (84%), IPEC (16%)
SPP	19	BELR (53%), CLL (42%)
sPPP	16	CLL (100%)
P3KP	16	IDC (100%)
PKPPKPdf	16	CLL (100%)
PKPlp	16	CLL (100%)
sPdif	16	VIE (100%)
Pm	15	SIGU (100%)
Sm	15	SIGU (100%)
(PKiKP)	15	CLL (100%)
E	15	YARS (93%)
(PP)	14	CLL (100%)
BAZ-PKPa	14	BER (100%)
SCP	14	PRU (100%)
sPKPdf	13	CLL (54%), LJU (23%), AWI (15%)
BAZ-Pg	13	BER (100%)
SX	13	NERS (100%)
(SSSS)	12	CLL (100%)
SgSg	12	BYKL (100%)
(SS)	12	CLL (100%)
ASPG	11	TIR (55%), BER (45%)
P*	11	BJI (36%), BGR (36%), MOS (27%)
ATSG	11	TIR (55%), BER (45%)
ASSG	11	TIR (55%), BER (45%)
ATPG	11	TIR (55%), BER (45%)
(PKPdf)	11	CLL (100%)
AP	10	MOS (100%)
(Pn)	10	CLL (80%), OGS (20%)

Table 10.3: (continued)

Reported Phase	Total	Agencies reporting
(S)	10	CFUSG (100%)
sPKPbc	10	BGR (80%), CLL (20%)
pS	10	IPEC (40%), LJU (30%)
sPS	9	CLL (100%)
SKKSdf	9	CLL (100%)
PSPS	9	CLL (100%)
PSSrev	9	CLL (100%)
sSSS	8	CLL (100%)
sSdif	8	BELR (50%), CLL (50%)
sSKSac	8	CLL (88%), HYB (12%)
Sx	8	CLL (100%)
X	8	SYO (38%), NERS (38%), QCP (12%), JMA (12%)
PPPrev	8	CLL (100%)
(P)	8	CFUSG (100%)
PX	8	NERS (100%)
SKPPKpdf	7	CLL (100%)
PSS	7	CLL (100%)
Pn_0	7	ATH (100%)
SKKSacre	7	CLL (100%)
S*	7	BJI (71%), BGR (29%)
(PKPbc)	7	CLL (100%)
Sdif	7	VIE (71%), LJU (29%)
SKSP	7	CLL (100%)
LG	7	BJI (57%), MOS (43%)
P4	7	SSNC (100%)
BAZ-PKPd	6	BER (100%)
sSSSS	6	CLL (100%)
(Sn)	6	CLL (83%), OGS (17%)
Pe	6	BRA (100%)
sPKPab	6	CLL (100%)
(Pdif)	6	CLL (100%)
sPPS	6	CLL (100%)
pPn	6	CNRM (83%), HYB (17%)
Sg_2	6	ATH (100%)
pdif	6	INMG (100%)
PSPSrev	6	CLL (100%)
(pPKPab)	5	CLL (100%)
(PKPdif)	5	CLL (100%)
pSKKSac	5	CLL (100%)
(SSS)	5	CLL (100%)
Pn_4	5	ATH (100%)
Sg_1	5	ATH (100%)
SKKpdf	5	CLL (100%)
PPlp	4	CLL (100%)
pPKKPbc	4	CLL (100%)
(PcP)	4	CLL (100%)
(PPS)	4	CLL (100%)
(SKPdf)	4	CLL (100%)
SKSSKSac	4	CLL (100%)
(PSKS)	4	CLL (100%)
sSKKSac	4	CLL (100%)
S4	4	SSNC (100%)
pScP	4	IDC (100%)
PKPbc(2)	4	CLL (100%)
(sPP)	3	CLL (100%)
sSKKSacr	3	CLL (100%)
Sglp	3	CLL (100%)
r	3	BRG (100%)
Sg_3	3	ATH (100%)
(PX)	3	NERS (100%)
PKSbc	3	CLL (100%)
Pg_3	3	ATH (100%)
SPS	3	CLL (100%)
pPKKPdf	3	LJU (100%)
PPmax	3	CLL (100%)
(SP)	3	CLL (100%)
pPPS	3	CLL (100%)
P4KP	3	IDC (100%)
(PPP)	3	CLL (100%)
SSSrev	3	CLL (100%)
(pPKPdf)	3	CLL (100%)

Table 10.3: (continued)

Reported Phase	Total	Agencies reporting
PA	3	TIR (100%)
?	2	PPT (100%)
PKPdf(2)	2	CLL (100%)
((S))	2	CFUSG (100%)
(Sdif)	2	CLL (100%)
sPcP	2	CLL (100%)
sPPPP	2	CLL (100%)
pSKSac	2	CLL (100%)
pPKPPKpd	2	CLL (100%)
(2	CFUSG (100%)
SSrev	2	CLL (100%)
RG	2	NDI (50%), IPEC (50%)
PKPPKPab	2	AWI (100%)
(pPPP)	2	CLL (100%)
(sPKPdf)	2	CLL (100%)
pPPPrev	2	CLL (100%)
pPPP	2	CLL (100%)
PPKPab	2	INMG (100%)
Pn_3	2	ATH (100%)
P5KP	2	NAO (100%)
M	2	LJU (100%)
PKPc	2	PJWWP (100%)
PKPab(2)	2	CLL (100%)
SDIF	2	PRU (100%)
(PS)	2	CLL (100%)
SKSbc	2	AWI (100%)
pSKKPbc	1	CLL (100%)
IAMS	1	GCG (100%)
(sS)	1	CLL (100%)
PKiKpf	1	CLL (100%)
(sSS)	1	CLL (100%)
(PKKPdf)	1	CLL (100%)
sPSPS	1	CLL (100%)
pSdiff	1	CLL (100%)
sPKPdffp	1	CLL (100%)
PPPmax	1	CLL (100%)
pPS	1	CLL (100%)
pPmax	1	CLL (100%)
sSKPPKpd	1	CLL (100%)
MSN	1	HEL (100%)
SKPPKPbc	1	CLL (100%)
AMSN	1	MEX (100%)
pSKPbc	1	CLL (100%)
PKiKpc	1	PJWWP (100%)
sSPS	1	CLL (100%)
(SKSac)	1	CLL (100%)
OPKIKP	1	SYO (100%)
(pPdif)	1	CLL (100%)
Ss	1	SSNC (100%)
)Pn)	1	CLL (100%)
sPKSdf	1	CLL (100%)
KP	1	INMG (100%)
S'S'ac	1	HYB (100%)
NP	1	MOS (100%)
V	1	CLL (100%)
(sPdif)	1	CLL (100%)
PKPdfmax	1	CLL (100%)
(sPPP)	1	CLL (100%)
(sSSS)	1	CLL (100%)
(sPKiKP)	1	CLL (100%)
BAZ-SKPa	1	BER (100%)
KIKP	1	LPA (100%)
SG2	1	HEL (100%)
PKPaf	1	BER (100%)
(pPKiKP)	1	CLL (100%)
SPSrev	1	CLL (100%)
sPmax	1	CLL (100%)
SSPprev	1	CLL (100%)
pPKPdffp	1	CLL (100%)
(PPPP)	1	CLL (100%)
pSKPab	1	CLL (100%)

Table 10.3: (continued)

Reported Phase	Total	Agencies reporting
SKPPKP	1	CLL (100%)
CJZ	1	PRU (100%)
(PKP)	1	CLL (100%)
OP	1	SYO (100%)
pPPPP	1	CLL (100%)
(SKPbc)	1	CLL (100%)
AGL	1	INMG (100%)
pPKPmax	1	CLL (100%)
SMZ	1	BJI (100%)
sPKPPKPd	1	CLL (100%)
(SX)	1	NERS (100%)
pP.	1	MAN (100%)
sSKPbc	1	CLL (100%)
pPKiK	1	BELR (100%)
PPPPmax	1	CLL (100%)
SKPd	1	NAO (100%)
sSSP	1	CLL (100%)
(sSdif)	1	CLL (100%)
pPKKPab	1	CLL (100%)
SKPb	1	NAO (100%)
Sr	1	MEX (100%)
SS(2)	1	LPA (100%)
PPPPrev	1	CLL (100%)
SKPbcf	1	CLL (100%)
N	1	MOS (100%)
(PSSrev)	1	CLL (100%)
SSmax	1	CLL (100%)
sSKSdf	1	CLL (100%)
PKiKp	1	SYO (100%)
SGM	1	NERS (100%)
PKPpB	1	WAR (100%)
PcPPKPre	1	CLL (100%)
(SKSdf)	1	CLL (100%)
4	1	HEL (100%)
Pn_1	1	ATH (100%)
PKPabmax	1	CLL (100%)
(SKPab)	1	CLL (100%)
PKKSbc	1	CLL (100%)
(SKKSac)	1	CLL (100%)
P(2)	1	CLL (100%)
pPcPPKPr	1	CLL (100%)

Table 10.4: Reporters of amplitude data

Agency	Number of reported amplitudes	Number of amplitudes in ISC located events	Number used for ISC <i>mb</i>	Number used for ISC <i>MS</i>
NEIC	851849	620085	216974	37873
IDC	562611	532755	132243	74510
ROM	511358	22454	0	0
GFZ	319878	317441	146232	0
AUST	253348	24172	9499	0
WEL	249070	27654	0	0
DJA	224173	168868	35142	0
ISC	216162	72560	33475	19261
ATH	121776	11065	0	0
AFAD	108734	8960	0	0
MOS	94933	91673	36610	9509
RSNC	83054	19188	2936	0
BJI	80659	78399	19836	26289
ISK	77408	13851	0	0
NNC	71518	21363	111	0
VIE	64292	33728	12368	0
INMG	54284	26284	2900	5
THE	52559	15989	0	0
MCSM	43719	41934	17902	0
MDD	41063	12062	0	0
GUC	37790	8240	0	0
SOME	36052	12350	2613	0
HEL	32354	1606	0	0
SVSA	29580	581	96	0
TXNET	22300	983	0	0
JSO	19421	4818	703	0
SSNC	19123	1110	0	0
JMA	17703	17631	0	0
DMN	14884	11561	2265	0
LDG	14804	1731	0	0
MRB	14658	201	0	0
SJA	13578	12584	0	0
PRU	12674	5390	279	3008
AWI	12199	5151	1496	0
BER	9496	2616	0	0
TEH	9237	4426	0	0
TIR	9146	3616	324	22
SKHL	8797	3448	0	0
PRE	8616	551	0	0
DNK	8427	3869	2838	17
PPT	8015	5861	384	0
NDI	7910	5849	1156	239
BELR	7760	4301	811	921
PDG	6872	2712	0	0
KRSZO	6523	606	0	0
NIC	6462	1583	0	0

Table 10.4: Continued.

Agency	Number of reported amplitudes	Number of amplitudes in ISC located events	Number used for ISC <i>mb</i>	Number used for ISC <i>MS</i>
LJU	6291	360	0	2
BKK	6165	3485	0	0
ZUR	6159	463	0	0
OSPL	6023	1285	0	0
BGS	5862	3529	2490	317
ECX	5565	530	0	0
BYKL	5282	1852	0	0
BUC	5114	1795	0	0
BGR	4725	4621	3095	0
CLL	4705	4494	309	1456
MIRAS	3651	83	0	0
YARS	3373	480	0	0
SDD	3196	1085	0	0
UCC	3045	2825	2347	0
KNET	2920	1080	0	0
SKO	2759	816	0	0
BRA	2752	1476	1190	0
SCB	2666	340	0	0
NAO	2245	1899	1216	0
EAF	2020	100	0	0
IPEC	1995	502	0	0
BGSI	1978	520	0	0
MAN	1674	1569	0	0
WBNET	1568	0	0	0
CFUSG	1308	1052	0	0
ASGSR	1287	609	0	0
NERS	1061	103	0	0
GCG	970	794	0	0
IGIL	961	496	124	111
KEA	799	525	0	86
THR	696	640	0	0
ISN	575	522	0	0
BRG	542	305	0	0
AAE	490	24	0	0
SIGU	292	130	0	0
NAM	282	55	0	0
FCIAR	263	200	48	0
WAR	233	217	0	161
LVSN	226	40	0	0
MEX	79	79	0	0
HYB	42	42	0	8
PJWWP	11	10	0	0
UPA	8	1	0	0

11

Glossary of ISC Terminology

- ADSL

An acronym for Agency.Deployment.Station.Location, a method of describing a seismic station. Allowing station coordinates to be distinguished by many more parameters.

- Agency/ISC data contributor

An academic or government institute, seismological organisation or company, geological/meteorological survey, station operator or author that reports or contributed data in the past to the ISC or one of its predecessors. Agencies may contribute data to the ISC directly, or indirectly through other ISC data contributors.

- Agency code

A unique, maximum eight-character code for a data reporting agency (e.g. NEIC, GFZ, BUD) or author (e.g. ISC, ISC-EHB, IASPEI). Often the agency code is the commonly used acronym of the reporting institute.

- Arrival

A phase pick at a station is characterised by a phase name and an arrival time.

- Associated phase

Associated phase arrival or amplitude measurements represent a collection of observations belonging to (i.e. generated by) an event. The complete set of observations are associated to the prime hypocentre.

- Azimuthal gap/Secondary azimuthal gap

The azimuthal gap for an event is defined as the largest angle between two stations with defining phases when the stations are ordered by their event-to-station azimuths. The secondary azimuthal gap is the largest azimuthal gap a single station closes.

- BAAS

Seismological bulletins published by the British Association for the Advancement of Science (1913-1917) under the leadership of H.H. Turner. These bulletins are the predecessors of the ISS Bulletins and include reports from stations distributed worldwide.

- Bulletin

An ordered list of event hypocentres, uncertainties, focal mechanisms, network magnitudes, as well as phase arrival and amplitude observations associated to each event. An event bulletin may list all the reported hypocentres for an event. The convention in the ISC Bulletin is that the preferred (prime) hypocentre appears last in the list of reported hypocentres for an event.

- Catalogue

An ordered list of event hypocentres, uncertainties and magnitudes. An event catalogue typically lists only the preferred (prime) hypocentres and network magnitudes.
- CoSOI/IASPEI

Commission on Seismological Observation and Interpretation, a commission of IASPEI that prepares and discusses international standards and procedures in seismological observation and interpretation.
- Defining/Non-defining phase

A defining phase is used in the location of the event (time-defining) or in the calculation of the network magnitude (magnitude-defining). Non-defining phases are not used in the calculations because they suffer from large residuals or could not be identified.
- Direct/Indirect report

A data report sent (e-mailed) directly to the ISC, or indirectly through another ISC data contributor.
- Duplicates

Nearly identical phase arrival time data reported by one or more agencies for the same station. Duplicates may be created by agencies reporting observations from other agencies, or several agencies independently analysing the waveforms from the same station.
- Event

A natural (e.g. earthquake, landslide, asteroid impact) or anthropogenic (e.g. explosion) phenomenon that generates seismic waves and its source can be identified by an event location algorithm.
- Grouping

The ISC algorithm that organises reported hypocentres into groups of events. Phases associated to any of the reported hypocentres will also be associated to the preferred (prime) hypocentre. The grouping algorithm also attempts to associate phases that were reported without an accompanying hypocentre to events.
- Ground Truth

An event with a hypocentre known to certain accuracy at a high confidence level. For instance, GT0 stands for events with exactly known location, depth and origin time (typically explosions); GT5 stands for events with their epicentre known to 5 km accuracy at the 95% confidence level, while their depth and origin time may be known with less accuracy.
- Ground Truth database

On behalf of IASPEI, the ISC hosts and maintains the IASPEI Reference Event List, a bulletin of ground truth events.

- IASPEI

International Association of Seismology and Physics of the Earth Interior, www.iaspei.org.

- International Registry of Seismograph Stations (IR)

Registry of seismographic stations, jointly run by the ISC and the World Data Center for Seismology, Denver (NEIC). The registry provides and maintains unique five-letter codes for stations participating in the international parametric and waveform data exchange.

- ISC Bulletin

The comprehensive bulletin of the seismicity of the Earth stored in the ISC database and accessible through the ISC website. The bulletin contains both natural and anthropogenic events. Currently the ISC Bulletin spans more than 60 years (1960-to date) and it is constantly extended by adding both recent and past data. Eventually the ISC Bulletin will contain all instrumentally recorded events since 1900.

- ISC Governing Council

According to the ISC Bye-laws: The Governing Council of the ISC is the forum of the Formal Representatives of all Members of the ISC.

- ISC-located events

A subset of the events selected for ISC review are located by the ISC. The rules for selecting an event for location are described in Section 10.1.3; ISC-located events are denoted by the author ISC.

- ISC Member

An academic or government institute, seismological organisation or company, geological/meteorological survey, station operator, national/international scientific organisation that contribute to the ISC budget by paying membership fees. ISC members have voting rights in the ISC Governing Council.

- ISC-PPSM

ISC-PPSM (ISC - Probabilistic Point Source Model) is a catalogue of probabilistic point source models, comprising an earthquake depth, moment tensor and source time function, calculated at the ISC to address shallow moderate magnitude earthquake depths and moment tensor uncertainties, as well as adding new constraints on earthquake source time functions.

- ISC-reviewed events

A subset of the events reported to the ISC are selected for ISC analyst review. These events may or may not be located by the ISC. The rules for selecting an event for review are described in Section 10.1.3. Non-reviewed events are explicitly marked in the ISC Bulletin by the comment following the prime hypocentre "Event not reviewed by the ISC".

- ISF

International Seismic Format (www.isc.ac.uk/standards/isf). A standard bulletin format approved by IASPEI. The ISC Bulletin is presented in this format at the ISC website.

- ISS

International Seismological Summary (1918-1963). These bulletins are the predecessors of the ISC Bulletin and represent the major source of instrumental seismological data before the digital era. The ISS contains regionally and teleseismically recorded events from several hundreds of globally distributed stations.

- Network magnitude

The event magnitude reported by an agency or computed by the ISC locator. An agency can report several network magnitudes for the same event and also several values for the same magnitude type. The network magnitude obtained with the ISC locator is defined as the median of station magnitudes of the same magnitude type.

- Phase

A maximum eight-character code for a seismic, infrasonic, or hydroacoustic phase. During the ISC processing, reported phases are mapped to standard IASPEI phase names. Amplitude measurements are identified by specific phase names to facilitate the computation of body-wave and surface-wave magnitudes.

- Prime hypocentre

The preferred hypocentre solution for an event from a list of hypocentres reported by various agencies or calculated by the ISC.

- Reading

Parametric data that are associated to a single event and reported by a single agency from a single station. A reading typically includes one or more phase names, arrival time and/or amplitude/period measurements.

- Report/Data report

All data that are reported to the ISC are parsed and stored in the ISC database. These may include event bulletins, focal mechanisms, moment tensor solutions, macroseismic descriptions and other event comments, as well as phase arrival data that are not associated to events. Every single report sent to the ISC can be traced back in the ISC database via its unique report identifier.

- Shide Circulars

Collections of station reports for large earthquakes occurring in the period 1899-1912. These reports were compiled through the efforts of J. Milne. The reports are mainly for stations of the British Empire equipped with Milne seismographs. After Milne's death, the Shide Circulars were replaced by the Seismological Bulletins of the BAAS.

- Station code

A maximum five-character code for a seismic station.

12

Acknowledgements

We thank our colleagues at the Morocco's National Centre for Scientific and Technical Research (CNRST) for kindly accepting our invitation and preparing an article for this issue of the Summary.

We are also grateful to the developers of the Generic Mapping Tools (GMT) suite of software (Wessel et al., 2019) that was used extensively for producing the figures.

Finally, we thank the ISC Member Institutions, Data Contributors, Funding Agencies (including NSF Award 2414178 and Royal Society Award INT004) and Sponsors for supporting the long-term operation of the ISC.

References

- Adamaki, A. (2017), Seismicity Analysis Using Dense Network Data : Catalogue Statistics and Possible Foreshocks Investigated Using Empirical and Synthetic Data, Ph.D. thesis, Uppsala University, urn:nbn:se:uu:diva-328057.
- Adams, R. D., A. A. Hughes, and D. M. McGregor (1982), Analysis procedures at the International Seismological Centre, *Physics of the Earth and Planetary Interiors*, *30*, 85–93.
- Amante, C., and B. W. Eakins (2009), ETOPO1 1 arc-minute global relief model: procedures, data sources and analysis, *NOAA Technical Memorandum NESDIS NGDC-24*, NOAA.
- Balfour, N., R. Baldwin, and A. Bird (2008), Magnitude calculations in Antelope 4.10, *Analysis Group Note of Geological Survey of Canada*, pp. 1–13.
- Bennett, T. J., V. Oancea, B. W. Barker, Y.-L. Kung, M. Bahavar, B. C. Kohl, J. . Murphy, and I. K. Bondár (2010), The nuclear explosion database NEDB: a new database and web site for accessing nuclear explosion source information and waveforms, *Seismological Research Letters*, *81*, <https://doi.org/10.1785/gssr1.81.1.12>.
- Bisztricsany, E. A. (1958), A new method for the determination of the magnitude of earthquakes, *Geofiz. Kozl*, pp. 69–76.
- Bolt, B. A. (1960), The revision of earthquake epicentres, focal depths and origin time using a high-speed computer, *Geophysical Journal of the Royal Astronomical Society*, *3*, 434–440.
- Bondár, I., and K. McLaughlin (2009a), A new ground truth data set for seismic studies, *Seismological Research Letters*, *80*, 465–472.
- Bondár, I., and K. McLaughlin (2009b), Seismic location bias and uncertainty in the presence of correlated and non-Gaussian travel-time errors, *Bulletin of the Seismological Society of America*, *99*, 172–193.
- Bondár, I., and D. Storchak (2011), Improved location procedures at the International Seismological Centre, *Geophysical Journal International*, *186*, 1220–1244.
- Bondár, I., E. R. Engdahl, X. Yang, H. A. A. Ghalib, A. Hofstetter, V. Kirchenko, R. Wagner, I. Gupta, G. Ekström, E. Bergman, H. Israelsson, and K. McLaughlin (2004), Collection of a reference event set for regional and teleseismic location calibration, *Bulletin of the Seismological Society of America*, *94*, 1528–1545.
- Bormann, P., and J. W. Dewey (2012), The new IASPEI standards for determining magnitudes from digital data and their relation to classical magnitudes, IS 3.3, *New Manual of Seismological Observatory Practice 2 (NMSOP-2)*, P. Bormann (Ed.), pp. 1–44, https://doi.org/10.2312/GFZ.NMSOP-2_IS_3.3, <https://doi.org/10.2312/GFZ.NMSOP-2>.
- Bormann, P., and J. Saul (2008), The new IASPEI standard broadband magnitude mB, *Seism. Res. Lett*, *79*(5), 698–705.
- Bormann, P., R. Liu, X. Ren, R. Gutdeutsch, D. Kaiser, and S. Castellaro (2007), Chinese national network magnitudes, their Relation to NEIC magnitudes and recommendations for new IASPEI magnitude standards, *Bulletin of the Seismological Society of America*, *97*(1B), 114–127, <https://doi.org/10.1785/0120060078>.
- Bormann, P., R. Liu, Z. Xu, R. Ren, and S. Wendt (2009), First application of the new IASPEI teleseismic magnitude standards to data of the China National Seismographic Network, *Bulletin of the Seismological Society of America*, *99*, 1868–1891, <https://doi.org/10.1785/0120080010>.

- Chang, A. C., R. H. Shumway, R. R. Blandford, and B. W. Barker (1983), Two methods to improve location estimates - preliminary results, *Bulletin of the Seismological Society of America*, *73*, 281–295.
- Choy, G. L., and J. L. Boatwright (1995), Global patterns of radiated seismic energy and apparent stress, *J. Geophys. Res.*, *100*(B9), 18,205–18,228.
- Dziewonski, A. M., and F. Gilbert (1976), The effect of small, aspherical perturbations on travel times and a re-examination of the correction for ellipticity, *Geophysical Journal of the Royal Astronomical Society*, *44*, 7–17.
- Dziewonski, A. M., T.-A. Chou, and J. H. Woodhouse (1981), Determination of earthquake source parameters from waveform data for studies of global and regional seismicity, *J. Geophys. Res.*, *86*, 2825–2852.
- Engdahl, E. R., and R. H. Gunst (1966), Use of a high speed computer for the preliminary determination of earthquake hypocentres, *Bulletin of the Seismological Society of America*, *56*, 325–336.
- Engdahl, E. R., and A. Villaseñor (2002), Global seismicity: 1900-1999, *International Handbook of Earthquake Engineering and Seismology, International Geophysics series*, *81A*, 665–690.
- Engdahl, E. R., D. Di Giacomo, B. Sakarya, C. G. Gkarlaoui, J. Harris, and D. A. Storchak (2020), ISC-EHB 1964-2016, an Improved Data Set for Studies of Earth Structure and Global Seismicity, *Earth and Space Science*, *7*(1), <https://doi.org/10.1029/2019EA000897>.
- Engdahl, E. R., R. van der Hilst, and R. Buland (1998), Global teleseismic earthquake relocation with improved travel times and procedures for depth determination, *Bulletin of the Seismological Society of America*, *88*, 722–743.
- Flinn, E. A., and E. R. Engdahl (1965), Proposed basis for geographical and seismic regionalization, *Reviews of Geophysics*, *3*(1), 123–149.
- Flinn, E. A., E. R. Engdahl, and A. R. Hill (1974), Seismic and geographical regionalization, *Bulletin of the Seismological Society of America*, *64*, 771–993.
- Gallacher, R., T. Garth, J. Harris, I. Bondár, K. McLaughlin, and D. A. Storchak (2025), Revising the Seismic Ground Truth Reference Event Identification Criteria, *Seismica*, *4*(1), <https://doi.org/10.26443/seismica.v4i1.1536>.
- Garth, T., K. Sigloch, and D. Storchak (2023), ISC-PPSM: Assessing moment tensor resolution, and addressing shallow earthquake depth resolution, in *XXVIII General Assembly of the International Union of Geodesy and Geophysics (IUGG)*, Berlin, <https://doi.org/10.57757/IUGG23-2916>.
- Gutenberg, B. (1945a), Amplitudes of P, PP and S and magnitude of shallow earthquakes, *Bulletin of the Seismological Society of America*, *35*, 57–69.
- Gutenberg, B. (1945b), Magnitude determination of deep-focus earthquakes, *Bulletin of the Seismological Society of America*, *35*, 117–130.
- Gutenberg, B. (1945c), Amplitudes of surface waves and magnitudes of shallow earthquakes, *Bulletin of the Seismological Society of America*, *35*, 3–12.
- Gutenberg, B., and C. F. Richter (1956), Magnitude and Energy of earthquakes, *Ann. Geof.*, *9*, 1–5.
- Havskov, J., L. Ottemöller, and F. Gkika (2024), Magnitude mb: Reducing Processing-Related Variability, *Seismological Research Letters*, *95*(4), 2118–2123.
- Hutton, L. K., and D. M. Boore (1987), The ML scale in southern California, *Bulletin of the Seismological Society of America*, *77*, 2074–2094.
- IASPEI (2005), Summary of Magnitude Working group recommendations on standard procedures for determining earthquake magnitudes from digital data, http://download.iaspei.org/commissions/CSOI/summary_of_WG_recommendations_2005.pdf.
- IASPEI (2013), Summary of magnitude working group recommendations on standard procedures for determining earthquake magnitudes from digital data, http://download.iaspei.org/commissions/CSOI/Summary_WG_recommendations_20130327.pdf.
- IDC (1999), IDC processing of seismic, hydroacoustic and infrasonic data, *IDC Documentation*.

- Jeffreys, H., and K. E. Bullen (1940), *Seismological Tables*, British Association for the Advancement of Science.
- Kanamori, H. (1977), The energy release in great earthquakes, *J. Geophys. Res.*, *82*, 2981–2987.
- Kennett, B. L. N. (2006), Non-linear methods for event location in a global context, *Physics of the Earth and Planetary Interiors*, *158*, 45–64.
- Kennett, B. L. N., E. R. Engdahl, and R. Buland (1995), Constraints on seismic velocities in the Earth from traveltimes, *Geophysical Journal International*, *122*, 108–124.
- Kennett, B. L. N., E. R. Engdahl, and R. Buland (1996), Ellipticity corrections for seismic phases, *Geophysical Journal International*, *127*, 40–48.
- Lee, W. H. K., R. Bennet, and K. Meagher (1972), A method of estimating magnitude of local earthquakes from signal duration, *U.S. Geol. Surv.*, Open-File Rep.
- Lentas, K., D. D. Giacomo, J. Harris, and D. A. Storchak (2019), The ISC Bulletin as a comprehensive source of earthquake source mechanisms, *Earth System Science Data*, *11*(2), 565–578, <https://doi.org/10.5194/essd-11-565-2019>.
- Leptokaropoulos, K. M., A. K. Adamaki, R. G. Roberts, C. G. Gkarlaouni, and P. M. Paradisopoulou (2018), Impact of magnitude uncertainties on seismic catalogue properties, *Geophysical Journal International*, *213*(2), 940–951, <https://doi.org/10.1093/gji/ggy023>.
- Murphy, J. R., and B. W. Barker (2006), Improved focal-depth determination through automated identification of the seismic depth phases pP and sP, *Bulletin of the Seismological Society of America*, *96*, 1213–1229.
- NMSOP-2 (2012), *New Manual of Seismological Observatory Practice (NMSOP-2)*, IASPEI, GFZ, German Research Centre for Geosciences, Potsdam, urn:nbn:de:kobv:b103-NMSOP-2, <https://doi.org/10.2312/GFZ.NMSOP-2>.
- Nuttli, O. W. (1973), Seismic wave attenuation and magnitude relations for eastern North America, *J. Geophys. Res.*, *78*, 876–885.
- Richter, C. F. (1935), An instrumental earthquake magnitude scale, *Bulletin of the Seismological Society of America*, *25*, 1–32.
- Ringdal, F. (1976), Maximum-likelihood estimation of seismic magnitude, *Bulletin of the Seismological Society of America*, *66*(3), 789–802.
- Sambridge, M. (1999), Geophysical inversion with a neighbourhood algorithm, *Geophysical Journal International*, *138*, 479–494.
- Sambridge, M., and B. L. N. Kennett (2001), Seismic event location: non-linear inversion using a neighbourhood algorithm, *Pure and Applied Geophysics*, *158*, 241–257.
- Storchak, D. A., J. Schweitzer, and P. Bormann (2003), The IASPEI standard seismic phases list, *Seismological Research Letters*, *74*(6), 761–772.
- Storchak, D. A., J. Schweitzer, and P. Bormann (2011), Seismic phase names: IASPEI Standard, in *Encyclopedia of Solid Earth Geophysics*, edited by H.K. Gupta, pp. 1162–1173, Springer.
- Storchak, D. A., J. Harris, L. Brown, K. Lieser, B. Shumba, R. Verney, D. Di Giacomo, and E. I. M. Korgor (2017), Rebuild of the Bulletin of the International Seismological Centre (ISC), part 1: 1964–1979, *Geoscience Letters*, *4*(32), <https://doi.org/10.1186/s40562-017-0098-z>.
- Storchak, D. A., J. Harris, L. Brown, K. Lieser, B. Shumba, and D. Di Giacomo (2020), Rebuild of the Bulletin of the International Seismological Centre (ISC)-part 2: 1980–2010, *Geoscience Letters*, *7*(18), <https://doi.org/10.1186/s40562-020-00164-6>.
- Stähler, S., and K. Sigloch (2014), Fully probabilistic seismic source inversion—Part 1: Efficient parameterisation, *Solid Earth*, *5*(2), 1055–1069, <https://doi.org/10.5194/se-5-1055-2014>.
- Stähler, S., and K. Sigloch (2016), Fully probabilistic seismic source inversion—Part 2: Modelling errors and station covariances, *Solid Earth*, *7*(6), 1521–1536, <https://doi.org/10.5194/se-7-1521-2016>.

- Tsuboi, C. (1954), Determination of the Gutenberg-Richter's magnitude of earthquakes occurring in and near Japan, *Zisin (J. Seism. Soc. Japan), Ser. II*(7), 185–193.
- Tsuboi, S., K. Abe, K. Takano, and Y. Yamanaka (1995), Rapid determination of Mw from broadband P waveforms, *Bulletin of the Seismological Society of America*, 85(2), 606–613.
- Uhrhammer, R. A., and E. R. Collins (1990), Synthesis of Wood-Anderson Seismograms from Broadband Digital Records, *Bulletin of the Seismological Society of America*, 80(3), 702–716.
- Vaněk, J., A. Zapotek, V. Karnik, N. V. Kondorskaya, Y. V. Riznichenko, E. F. Savarensky, S. L. Solov'yov, and N. V. Shebalin (1962), Standardization of magnitude scales, *Izvestiya Akad. SSSR., Ser. Geofiz.*(2), 153–158, Pages 108–111 in the English translation.
- Villaseñor, A., and E. R. Engdahl (2005), A digital hypocenter catalog for the International Seismological Summary, *Seismological Research Letters*, 76, 554–559.
- Villaseñor, A., and E. R. Engdahl (2007), Systematic relocation of early instrumental seismicity: Earthquakes in the International Seismological Summary for 1960–1963, *Bulletin of the Seismological Society of America*, 97, 1820–1832.
- Weston, J., E. Engdahl, J. Harris, D. Di Giacomo, and D. Storchack (2018), ISC-EHB: Reconstruction of a robust earthquake dataset, *Geophys. J. Int.*, 214(1), 474–484, <https://doi.org/10.1093/gji/ggy155>.
- Willmore, P. L. (Ed.) (1979), *Manual of Seismological Observatory Practice*, 165 pp. pp., Boulder, Colorado, USA, Report SE-20.
- Woessner, J., and S. Wiemer (2005), Assessing the quality of earthquake catalogues: estimating the magnitude of completeness and its uncertainty, *Bulletin of the Seismological Society of America*, 95(2), <https://doi.org/10.1785/0120040007>.
- Young, J. B., B. W. Presgrave, H. Aichele, D. A. Wiens, and E. A. Flinn (1996), The Flinn-Engdahl regionalisation scheme: the 1995 revision, *Physics of the Earth and Planetary Interiors*, 96, 223–297.



www.gaiacode.com

The World's First Hybrid Seismometer from Gaiacode

With the newly designed PICO three component broadband feedback instrument Gaiacode is introducing the first hybrid seismometer in the world. Small, lightweight, versatile and easy to install, PICO sets a new standard for all seismic measurements at higher frequencies, without compromising the performance in the longer period teleseismic band.

Suited for rapid deployments in temporary installations, PICO can also be used in array configurations or in more permanent networks.



What is a hybrid seismometer?

Typically, the output of seismic instruments is proportional either to the velocity or the acceleration of ground motions. Seismometers with velocity outputs are mostly used for measuring weak motions like seismic waves stemming from earthquakes at regional or teleseismic distances. On the other hand, instruments with acceleration output record strong motions and are commonly called accelerometers.

PICO's hybrid response combines the best of both worlds, by simultaneously providing two analogue outputs: one proportional to the velocity, the other to the acceleration of the ground motion. This approach has the advantage that over the whole passband both the rich information content of a typical acceleration response can be recorded without losing the sensitivity of a velocity proportional weak motion signal.

How do we get the hybrid response of the PICO?

Gaiacode achieves this unique response characteristic by adding specially designed circuitry to the mechanical side of the PICO before its signal gets processed in its feedback loop. Adding such circuitry allows us also to remotely change the low frequency cutoff (3dB) points without having to physically remove the seismometer from the installation. We offer eight different responses with low frequency cutoff points between 120 sec and 1 sec.

The instruments are delivered with a Gaiacode designed rotatable, waterproof connector (<https://www.gaiacode.com/news/item/95-a-new-type-of-connector>). Its position can be adjusted over a wide range of angles up to 270 degrees. This flexibility allows for easy installation even in postholes or other tight locations.



SARA electronic instruments s.r.l. your reliable and friendly partner in earthquake monitoring and geophysical exploration.



Since 2000 SARA is specialized in the design and production of instruments and software for applied geophysics, seismological and structural monitoring, devices with high technological content and best price-quality ratio.



Broad band seismometers
- Observatory grade
- Compact
- Borehole



DoReMi
digital telemetry
exploration
seismograph.



Strong motion
AceBox



Modal analysis
Digital Array



Seismic stations
VelBox



GEOEXPLORER

Processing software suite to perform fast and reliable quality data check and analysis of elasto-mechanical properties of soil before construction or before deploying a seismic station.

- MASW
- HVSr
- REFRACT
- MARW
- DH
- SSV

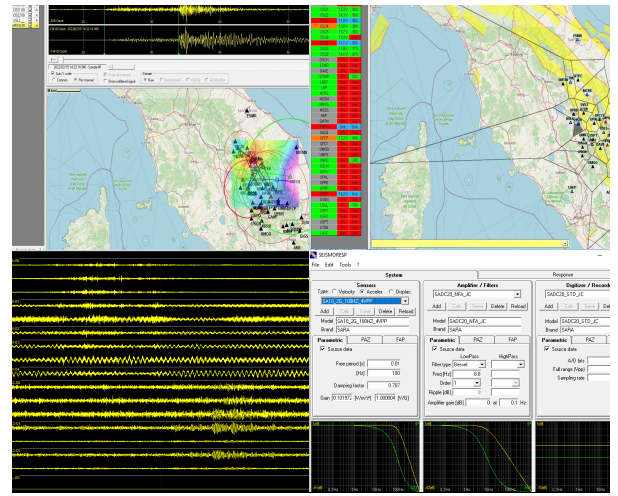
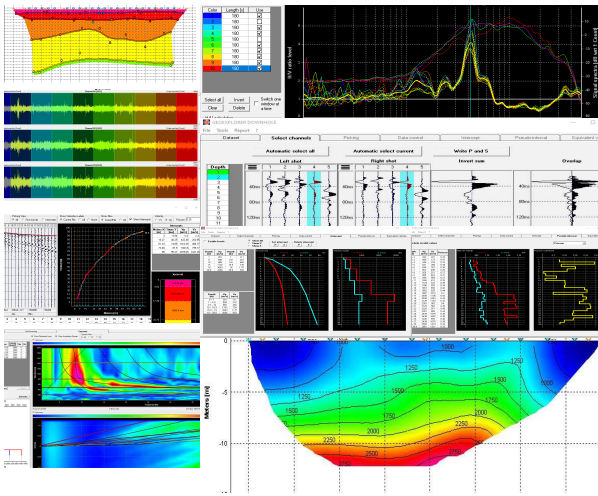


SEISMOWIN

Modules for earthquakes, seismic and microseismic monitoring.

Capable to:

- Handle hundreds of channels
- Maintain and design networks
- Locate and analyse earthquakes
- Calculate transfer functions
- Plot all events location
- Monitor stations status of health
- Send alerts
- And more...



Via Angelo Morettini, 11 06128 Perugia
 +39 075 5051014
 www.sara.pg.it - info@sara.pg.it



PERFECTLY PAIRED



arolla + **nair^{slim}**
VE series broadband seismometer GMS series recorder / digitiser

The **arolla** broadband seismometer features a compact and lightweight design, yet it is rugged and versatile, making it an ideal choice for many applications. Weak-motion, broadband seismometers have the highest sensitivity among seismometers over long periods, and are able to pick up even small tremors at great distances.

The culmination of years of experience designing reliable, high-precision, low-noise seismic equipment enabled the creation of **arolla**.

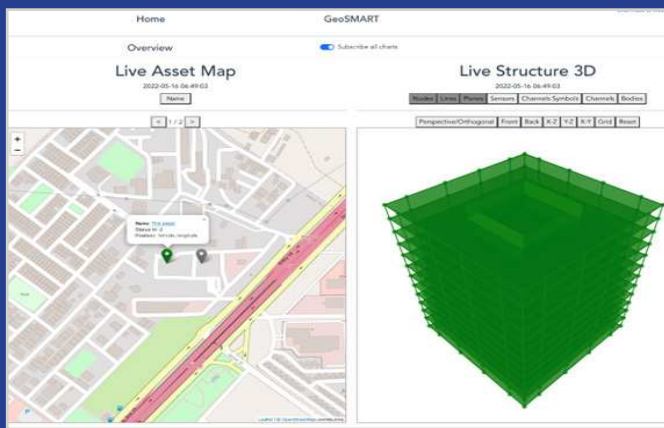
Best paired with **arolla** is **nair^{slim}**—GeoSIG’s latest generation seismic recorder that offers highest performance, excellent operational flexibility and enhanced connectivity. GeoSIG’s **nair^{slim}** is a self-contained instrument that acquires and processes data in real time. It boasts an impressive 146db (0.01-30Hz), making it suitable for weak motion precision recording. A set comprising **arolla** and **nair^{slim}** is fully compatible with existing GeoSIG systems that may already be in place. Also, its simple upgrade path makes **nair^{slim}** “future proof.”

A winning combination: **arolla** and **nair^{slim}**!

GeoSIG
swiss made to measure 



GeoSIG
swiss made to measure



GeoSMART Offers Peak Performance

GeoSMART is an innovative graphical application that provides **tools** for realtime structural health monitoring for civil engineering structures. GeoSMART, with its “smart” features, can **monitor** and display the status of a structure that is equipped with GeoSIG measuring instruments. GeoSMART is S2HM in a Box; it has been designed to meet fundamental engineering requirements with respect to **structural health** monitoring applications.

Main Features of GeoSMART

- ◆ Support for any type of sensor such as acceleration, velocity, displacement, tilt, wind, temperature, strain, and many more.
- ◆ User-friendly web-interface for an intuitive experience.
- ◆ 3D representation of any structure with live status.
- ◆ Interactive zoom, rotate, pan, visibility and projection.
- ◆ Multiple structures on live interactive map.
- ◆ Real-time continuous data acquisition and processing.
- ◆ Storage and direct download of all data and graphics.
- ◆ Data export for long-term storage.
- ◆ Sliding window-based continuous frequency analyses: Amplitude, Spectrogram and Response Spectra.
- ◆ Rigid body motions in translations and rotations.
- ◆ Interpolations for non-instrumented areas.
- ◆ Interstorey drift ratios and torsion.
- ◆ Exceedance of predefined threshold levels or curves.
- ◆ Plot of archive data and statistical information.
- ◆ Live screen indicators and HTML formatted emails.
- ◆ Individualised notifications to users / user groups.
- ◆ Customisable messages such as action plans.
- ◆ Reports including actual images of plotted graphics.
- ◆ Hardware relays to start or shutdown any process.
- ◆ Advanced user accessible powerful database.
- ◆ API to fetch and externally manipulate the stored data.

GeoSIG Ltd | Wiesenstrasse 39
8952 Schlieren, Switzerland
T: +41 44 810 2150 | F: +41 44 810 2350
www.geosig.com

For more information, contact us at info@geosig.com



